Universidad del País Vasco Euskal Herriko Unibertsitatea

BILBOKO INGENIARITZA ESKOLA
ESCUELA DE INGENIERÍA DE BILBAO

SUSTAINABLE LIMESTONE AND EAF AGGREGATE CONCRETES THROUGH PARTICLE PACKING MODELS (PPMs) AND LIFE CYCLE ASSESSMENT (LCA)

VERONICA GARCIA CORTES

Supervisors:

Dr. José Tomás San-José Lombera

Dr. David García Estévez

April 2020, Bilbao

Universidad del País Vasco Euskal Herriko Unibertsitatea

BILBOKO INGENIARITZA ESKOLA
ESCUELA DE INGENIERÍA DE BILBAO

SUSTAINABLE LIMESTONE AND EAF AGGREGATE CONCRETES THROUGH PARTICLE PACKING MODELS (PPMs) AND LIFE CYCLE ASSESSMENT (LCA)

VERONICA GARCIA CORTES

Supervisors:

Dr. José Tomás San-José Lombera

Dr. David García Estévez

April 2020, Bilbao

tecnalia

Agradecimientos

Realizar una tesis doctoral requiere un gran trabajo y esfuerzo personal durante varios años, que sería muy difícil superar sin el apoyo y ayuda de muchas personas. Por ello, me gustaría agradecer a todas las personas que han estado cerca durante estos 4 años y han hecho posible este trabajo.

En primer lugar, agradecer a mis directores, Tomás y David. Gracias por darme la oportunidad de realizar la presente Tesis Doctoral, por confiar en mí y por vuestro apoyo tanto moral como técnico durante todo el proceso. Asimismo, agradecer también a Javier Jesús Gonzalez y Juan Antonio Polanco por sus consejos y todo el conocimiento prestado.

A todas las personas que forman parte de la división de Building Technologies de Tecnalia, por darme la oportunidad de formarme como investigadora en un entorno industrial, desde el primer día me recibisteis con los brazos abiertos y estaré siempre agradecida. Especial mención a las personas del área Cement-Based Products del que he formado parte, sin vuestro apoyo emocional y técnico esta tesis no hubiese sido posible. Y también a todas las personas que me han ayudado en el laboratorio haciendo las horas más agradables.

I want to thank Professor Will Hansen for accepting me as a member of his team during my time at the University of Michigan, being kind whenever I needed help and providing me with valuable knowledge. Of course, thanks also to all the people who made my stay in Ann Arbor so memorable. I wish also to acknowledge the European Commission and the members of the SUPERCONCRE EU project (Grant agreement ID: 645704) for its support in part of the development of this thesis.

Agradecer al Gobierno Vasco, en especial al departamento de educación, por la financiación aportada a través de la convocatoria de ayuda para el Programa Predoctoral de Formación de Personal de Investigador no Doctor 2016. Al ministerio español MCI, AEI, EU y CEDER (RTI2018-097079-494-B-C31) y la Universidad del País Vasco (PGA19/61) por los fondos adicionales. Y al grupo de investigación del Gobierno Vasco (IT1314-19).

Mi agradecimiento también a las empresas que han contribuido suministrando los materiales empleados en la tesis, Hormigones y Morteros Agote (Hormor), Cementos Rezola (FYM HeilderbergCement Group), Grupo Amantegui. Y también a aquellas que han aportado los datos necesarios para evaluar el impacto ambiental, Hormigones y Morteros Agote (Hormor), Grupo Amantegui y Prefabricados Alberdi.

Finalmente, agradezco a mi familia por estar siempre ahí y haberme apoyado para lograr mis objetivos tanto en lo personal como durante toda mi carrera universitaria, sin

vosotros esto no hubiese sido posible. También a mis amigos, los de siempre y los que han aparecido en el camino, mil gracias por aguantarme y darme tanto ánimo durante estos últimos años. Y por supuesto a mi compañero de viaje, has sido mi gran motor para conseguir esto, te quiero.

Abstract

In view of the current concern about environmental problems, the depletion of natural resources, the lack of space in landfills and climate change among others, initiatives such as the valorisation of waste and industrial by-products in cement-based products are currently a priority that will lead to sustainable development in the construction sector.

As a result of this approach, the use of slags from the Electric Arc Furnace (EAF) as aggregates in the concrete has been proved to be successful for multiple applications avoiding the use of natural aggregates. Hence, the range of aggregates available for designing concretes is continuously growing.

The morphology of granular materials strongly depends on their physical properties and the processing operations to which they have been exposed. In particular, the EAF slag possess a cavernous structure which difficult the concrete mix design according to the conventional methods. Thus, the growing need to manufacture a more sustainable concrete with the available materials taking advantage of all the natural resources and including waste or by-products from other industries, requires the optimization of the concrete mix design considering the properties of the components and reducing the environmental and economic impact.

The main objective of this thesis is to design economic and environmentally sustainable concrete mixes made with natural limestone (NL) aggregates and electric arc furnace (EAF) aggregate through a particle packing density perspective without compromising their compressive strength and workability.

In order to verify the potential of particle packing theories to design more economical and environmentally sustainable NL aggregate and EAF aggregate concrete mixes, two traditional optimal curves and two current discrete packing models were validated with experimental packing results to demonstrate its feasibility in the prediction of the most compacted structure. Several (17) NL and EAF aggregate concrete mixes were then designed by varying the aggregate proportion and the content of cement paste to analyse the effect of aggregate packing density on the fresh and hardened concrete properties. Finally, the economic and environmental impact of the different concrete mixes were assessed to evaluate the potential of the particle packing methods in the development of more sustainable concrete.

It was concluded that the concrete mixtures designed by maximizing the coarse aggregates content in the range of the maximum packing density present the highest compressive strength and workability and the low environmental and economic impact. In addition, due to the higher compressive strength and the low contribution of aggregate in the concrete environmental impact, the EAF aggregate concrete contributes to a greater reduction of the environmental and economic impact.

Table of Contents

TABLE OF CONTENTS

Agradecimientos ..... **i**

Abstract ..... **iii**

Table of Contents ..... **v**

Acronyms ..... **xi**

1 Introduction **3**

1.1 Scope 3

1.2 Objectives 4

1.3 Structure of the thesis 5

2 Concrete overview **9**

2.1 Introduction 9

2.2 Cement 11

2.2.1 Introduction 11

2.2.2 Cement manufacturing process 11

2.2.3 Types of cements 14

2.2.4 Supplementary Cementitious Materials (SCM) 14

2.3 Fillers 16

2.4 Aggregates 17

2.4.1 Introduction 17

2.4.2 Aggregates classification 18

2.4.3 Aggregate consumption 24

2.4.4 Aggregate properties 26

2.4.5 Aggregate gradation 27

2.5 Admixtures 29

2.6 Water 30

2.7 Mix-design methods 31

2.7.1 Standard mix design methods 33

2.7.2 Particle packing optimization methods 38

2.7.3 Paste demand 50

2.8 Concrete manufacturing process 57
2.8.1 Mixing process 57
2.8.2 Transport to work site 59
2.8.3 Placing and compacting 59
2.9 Summary and conclusions 60
2.10 References 61
3 Concrete environmental and economic assessment 73
3.1 Introduction 73
3.2 Environmental impacts 76
3.3 Economic impacts 79
3.4 Assessment methods 80
3.4.1 Life Cycle Assessment (LCA) approach 80
3.4.2 Environmental Product Declarations (EPD) 88
3.4.3 Product Environmental Footprint (PEF) 89
3.4.4 LCI of concrete industries 89
3.4.5 Review of environmental assessment methods and tools 91
3.4.6 Environmental and economic indicators 94
3.4.7 LCA of concrete made with alternative aggregates 95
3.5 Multiple-Criteria Decision Methods (MCDM) 95
3.5.1 Analytic Hierarchy Process (AHP) 97
3.5.2 Technique for Order of Preference by Similarity to Ideal Solution (TOPSIS) 98
3.5.3 The Preference Ranking Organization Method for Enrichment of Evaluations (PROMEHTEE) 98
3.5.4 Elimination and Choice Expressing Reality (ELECTRE) 99
3.5.5 Integrated Value Model for Sustainable Assessment (MIVES) 99
3.6 Integration of LCA and MCDM methods 99
3.7 Summary and conclusions 102
3.8 References 103
4 Optimization of concrete granular compacity 113
4.1 Introduction 113
4.2 Methodology and materials 114

4.2.1 Overall methodological approach 114
4.2.2 Materials 117
4.2.3 Dry packing of aggregates 122
4.2.4 Wet packing of aggregates 126
4.2.5 Wet packing of cement 128
4.2.6 Theoretical models 129
4.2.7 Equipment 136
4.3 Experimental packing density of aggregates with different morphologies .. 137
4.3.1 Individual aggregate fractions 138
4.3.2 Cement packing density 144
4.3.3 Mixing of aggregate fractions 145
4.4 Comparison of theoretical model and experimental test results 162
4.4.1 Natural limestone aggregates 162
4.4.2 Electric arc furnace (EAF) aggregates 171
4.5 Conclusions 180
4.6 References 182
5 Concrete mix design 187
5.1 Introduction 187
5.2 Methodology and materials 188
5.2.1 Overall methodological approach 188
5.2.2 Materials 190
5.2.3 Determination of aggregate specific surface area 190
5.2.4 Cement-paste characterization 191
5.2.5 Concrete mix design and characterization techniques 192
5.3 Determination of cement-paste content 198
5.4 Effect of packing density on cement-paste compressive strength and workability 201
5.5 Compressive strength and dry aggregate compacity of NL aggregate concretes 203
5.6 Funk and Dinger curves for cement-content reduction in concrete mix design 210
5.7 Effect of paste content on different aggregate proportions 215

5.8 Conclusions 221
5.9 References 222
6 Environmental and economic impact of NL and EAF aggregate concretes 229
6.1 Introduction 229
6.2 Life cycle Assessment (LCA) approach 231
6.2.1 Goal and scope definition 231
6.2.2 Life Cycle Inventory (LCI) 234
6.2.3 Environmental impact assessment (LCIA) 247
6.3 Economic assessment 248
6.4 Global environmental and economic index 249
6.5 Comparative LCA of aggregates 250
6.5.1 Natural aggregates 250
6.5.2 EAF aggregates 253
6.5.3 Recycled aggregates 259
6.5.4 Comparison 263
6.6 Concrete assessment 265
6.6.1 SUPERCONCRETE tool 266
6.6.2 Sensitive analysis of EAF aggregates transport distance 271
6.6.3 Economic and environmental impact. Global index 272
6.7 Conclusions 276
6.8 References 278
7 Conclusions and Future Perspectives 285
7.1 Conclusions 285
7.2 Afterthoughts: Future Perspectives 287
Annex 1. Additional information of Chapter 4. 291
A- Calibration process of vibration-table acceleration 291
B- Deviations of the theoretical models from the experimental packing density ... 296
Natural limestone aggregates 296
Electric Arc Furnace (EAF) aggregates 303
Annex 2. Additional information of Chapter 6 314
A- NL aggregate data: 314

B- EAF aggregates data 317
C- RCA aggregates 319
D- Environmental impact of concrete mixes. 321
List of Figures 329
List of Tables 333
Curriculum Vitae 337

Acronyms

3-P	3-parameter Packing Model
A&A	Andreasen and Andersen model
AAC	Alkali-activated Cements
ABS	Air-cooled Blast furnace Slag
ADP-E	Abiotic depletion potential (Resource use, minerals and metals)
ADP-F	Abiotic depletion potential-fossil fuels (Resource use, energy carries)
AGM	Aim and Goff Model
AHP	Analytic Hierarchy Process
AP	Acidification potential
BOF	Basic Oxygen Furnace
C&DW	Construction & Demolition Waste
CA	Coarse Aggregate
CAS	Concurrent algorithm-based simulation
CCS	Carbon Capture Storage
CIPM	Compaction-Interaction Packing Model
CLAS	Concrete Life Cycle Assessment System
CPM	Compressible Packing Model
CSD	Commission on Sustainable Development
D-C	Compacted by means of a tamping rod packing
D-C26	Compaction by vibration (26 Hz) and compression (10kPa)
D-C33	Compaction by vibration (33 Hz) and compression (10kPa)
DEM	Discrete element method
D-L	Loose packing
EAF	Electric Arc Furnace
EAF	Electric Arc Furnace
EAFS	Electric Arc Furnace Slag
EI	Environmental Impact
ELCD	European Life Cycle Database
ELECTRE	Elimination and Choice Expressing Reality
EP	Eutrophication potential
EPD	Environmental Product Declaration
EPfw	Eutrophication, aquatic freshwater
EPmw	Eutrophication, aquatic marine
EPt	Eutrophication, terrestrial
ERs	Environmental Reports
ET	Ecotoxicity (freshwater)
FA	Fine Aggregate
FM	Fineness Modulus or Furnas Model
FU	Funtional Unit

GBFS	Granulated Blast Furnace Slag
GDP	Gross Domestic Product
GGBFS	Ground Granulated Blast Furnace Slag
GHG	Greenhouse Gas
GWP	Global warming potential (climate change)
HTc	Human toxicity, cancer effects
HTn-c	Human toxicity, non-cancer effects
IR	Ionising radiation, human health
LCA	Life Cycle Assessment
LCI	Life Cycle Inventory
LCIA	Life Cycle Impact Assessment
LFS	Ladle Furnace slag
LMPM	Linear-Mixture Packing Model
LPM	Linear Packing density Model
LU	Land use
MA	Medium size aggregate
MCDM	Multiple-Criteria Decision Methods
MFT	Mortar film thickness
MIVES	Integrated Value Model for Sustainable Assessment
MLPM	Modified Linear Packing Model
MPM	Mixture Packing Model
MRA	Mixed Recycled Aggregate
MTM	Modified Toufar Model
NL	Natural Limestone
ODP	Ozone depletion potential
OPC	Ordinary Portland Cement
PCR	Product Category Rules
PD	Packing Density
PEF	Product Environmental Footprint
Pe-NRe	Total non-renewable primary energy consumption
Pe-Re	Total renewable primary energy consumption
PFT	Paste film thickness
PM	Particle matter/Respiratory inorganics
POCP	Photochemical ozone creation potential
PPM	Particle Packing Model
PROMEHTEE	The Preference Ranking Organization Method for Enrichment of Evaluations
RA	Recycled Aggregate
RAC	Recycled Aggregate Concrete
RCA	Recycled Concrete Aggregate
R-GB	Glass Marbles

R-S	Rounded Siliceous aggregates
RSA	Random sequential addition
R-WTB	White Tumbled Boulder
SCC	Self-Compacting Concrete
SCM	Supplementary Cementitious Materials
SSA	Specific Surface Area
SSD	Saturated Surface Dry density
SSM	Solid Suspension Model
TOPSIS	Technique for Order of Preference by Similarity to Ideal solution
TPM	Theory of Particle Mixtures
W/C	Water-to-Cement ratio
W/S	Water to Solid ratio
WFT	Water Film Thickness
WS	Water scarcity

1

Introduction

CONTENT

1 Introduction 3

1.1 Scope 3

1.2 Objectives 4

1.3 Structure of the thesis 5

1 Introduction

In Chapter 1, the scope of the problem that will be treated in this thesis, the objectives, and an outline of their development will be presented.

1.1 Scope

The growing trend towards a circular economy in the construction sector focuses attention on waste minimisation and the recovery of products, materials and resources so that they remain in the circular economy for as long as possible. Among all construction industry materials, concrete (33 billion tons/year) is used more than any other, causing a significant environmental impact, not only due to CO_2 emissions, but also because of the substantial volume of raw materials that are consumed and the waste that is generated during its life cycle.

The high volume of aggregates within the concrete mix (60-80%), converts it into a potential receptor of large quantities of granular recycled materials. In this research line, successful substitutions of natural aggregate by Electric Arc Furnace (EAF) aggregates have been reported in several studies on multiples applications, in response to current problems arising from limited landfill space and pressure on natural resources.

Thus, the growing need to manufacture a more sustainable concrete with the available materials taking advantage of all the natural resources and including waste or by-products from other industries, requires the optimization of the concrete mix design considering the properties of the components and reducing the environmental and economic impact.

Most of the available mix-design methods for concrete are limited by the type of materials (generally they are only useful for conventional concrete components) and few of them consider the morphological aspects of the aggregate and the environmental and economic impact.

The aim of this research is to explore the current mix design methods to design ecological and economic concrete mixes made with Natural Limestone (NL) aggregates and EAF aggregates, while maintaining both the fresh and the hardened concrete properties at similar levels to those obtained through conventional methods. With this end in sight, the particulate packing approach to aggregate mix design appears to be a promising alternative for a twofold reason. First, a more compacted aggregate structure will require less cement paste to fill the voids, reducing the cement content and consequently the environmental and economic impacts of the concrete. Second, the morphology (shape, texture and size) of the aggregate is inherently covered in the

packing density measurements, which helps to optimize a compact aggregate structure from which higher compressive strength and longer durability may be expected.

The use of alternative aggregate from waste or other industries will not always lead to more sustainable concretes. Therefore, both the environmental and the economic impacts will also be evaluated through objective methods, such as life cycle assessment (LCA). This challenge has been addressed in the SUPERCONCRETE project (645704 - SUPERCONCRETE 2014) that has mainly been focused on theoretical models for the next-generation concretes, including low-carbon concrete, high-class concrete, and fibre-reinforced cementitious composites. SUPERCONCRETE also includes the characterization and impact inventory of some alternative materials, through a simple evaluation tool, to arrive at a sustainability index that is intended to support decision makers when selecting the most suitable concrete mix.

1.2 Objectives

The main objective of this study is to design economic and environmentally sustainable concrete mixes made with Natural Limestone (NL) aggregates and Electric Arc Furnace (EAF) aggregate from a particle packing density perspective.

To obtain the principle objective, the following partial objectives are proposed:

- Identify a suitable method for proportioning the NL and the EAF aggregate for maximum packing density. This objective will be pursued through two investigative paths:
    - Analysis and validation of the applicability of ideal grading curves, specifically Fuller and Funk and Dinger, for NL and EAF aggregate mix design through maximum packing density.
    - Analysis and validation of the applicability of discrete particle packing models (PPM), specifically the Compressible Packing Model (CPM) and the 3-parameter packing model (3-P), to predict the packing density of NL and EAF aggregates by comparing them with the experimental results.
- Studying aggregate mix designs from the perspective of maximum packing density, examining the fresh and the hardened properties of both NL and EAF aggregate concrete.
- Assessing the maximum packing density perspective and its potential to reduce the cement content of NL and EAF aggregate concrete mixes and to predict suitable results without compromising performance properties.
- Providing reliable data on the production of NL and EAF aggregates, to overcome the absence of a Life Cycle Inventory (LCI) at a regional scale, to perform the life cycle assessment (LCA).

- Assessing and comparing the environmental impact of NL aggregates and EAF aggregate production through LCA.
- Determine the environmental and the economic impact of the designed concrete mixtures to evaluate the potential of the particle packing method in the development of more sustainable concretes.

1.3 Structure of the thesis

The present thesis is composed of a total of 8 chapters (see Fig. 1.1). In each one, a series of observations and conclusions are presented at the end. The content of each chapter is briefly described below:

The background to the problem and the strategy developed in the thesis for its successful resolution are discussed in this first chapter.

The concepts, theories and methods and the state of the art related to the scope of this thesis will be spread out across the following two chapters:

- In Chapter 2, some background on concrete constituents and their effect on concrete properties will be given, placing emphasis on the use of different aggregates and the influence of particle characteristics on packing density. Furthermore, a literature survey on the mix design methodologies and approaches will be included in this chapter, focusing on particle packing optimization methods.

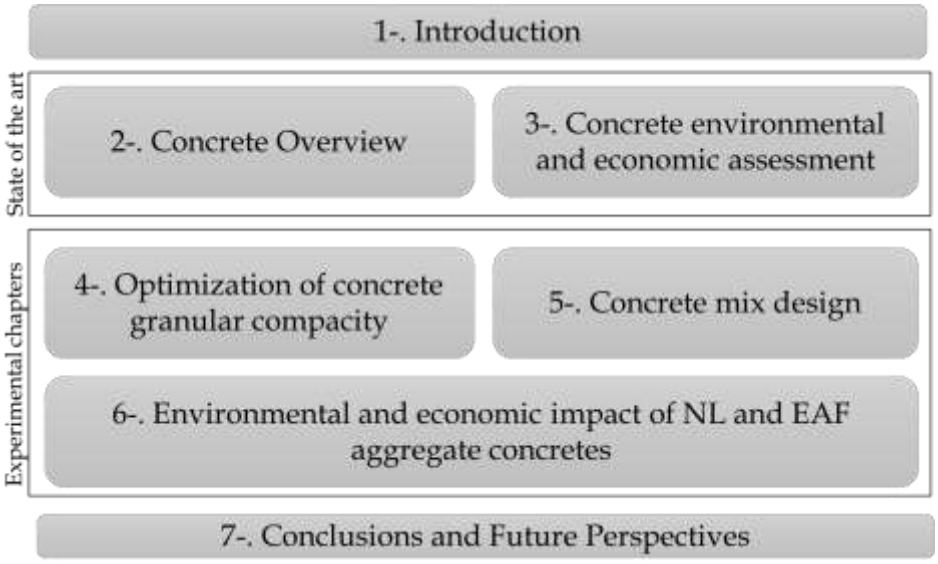

Fig. 1.1. Structure of the thesis.

- In Chapter 3, an overview of the environmental impact of concrete will be provided, including common strategies to reduce the environmental impact of concrete and the available methodologies, and research into assessing the

environmental impact in combination with other criteria such as economic and functional aspects.

The experimental work reported in this thesis will be presented in three chapters:

- In Chapter 4, the study of aggregate particle packing density will be presented. It contains the characterization of the materials, the results of the experimental packing density of the NL and EAF aggregates and a comparison of traditional and current packing density models.
- In Chapter 5, the concrete mix designs incorporating NL and EAF aggregates and based on particle packing methods will be reported. A discussion, in this chapter, will examine the influence of aggregate packing density on the fresh and the hardened properties of the concrete mix, designed with different amounts of cement and different aggregate mixes, based on the results of chapter 4.
- In Chapter 6, the environmental and economic impacts of the NL and EAF aggregate concrete mixes designed in Chapter 5 will be assessed. In this chapter, the feasibility of the concrete mixes, designed through particle packing methods in the previous chapter, will be analysed to reduce the environmental and economic impacts.

Finally, a summary of the most relevant contributions of the thesis and some research areas for future study will be reported in Chapter

2

Concrete overview

CONTENT

2 Concrete overview 9

2.1 Introduction 9

2.2 Cement 11

2.2.1 Introduction 11

2.2.2 Cement manufacturing process 11

2.2.3 Types of cements 14

2.2.4 Supplementary Cementitious Materials (SCM) 14

2.3 Fillers 16

2.4 Aggregates 17

2.4.1 Introduction 17

2.4.2 Aggregates classification 18

2.4.3 Aggregate consumption 24

2.4.4 Aggregate properties 26

2.4.5 Aggregate gradation 27

2.5 Admixtures 29

2.6 Water 30

2.7 Mix-design methods 31

2.7.1 Standard mix design methods 33

2.7.2 Particle packing optimization methods 38

2.7.3 Paste demand 50
2.8 Concrete manufacturing process 57
2.8.1 Mixing process 57
2.8.2 Transport to work site 59
2.8.3 Placing and compacting 59
2.9 Summary and conclusions 60
2.10 References 61

2 Concrete overview

In chapter 2, an overview of the knowledge concerning standard components used for the manufacture of concrete and in concrete mix design, both with conventional and with Particle Packing Models (PPM), will be presented. The review of the literature will focus on the limitations and the suitability of various concrete mix design methods, especially PPM, for the design of eco-friendly concrete mixes with aggregates of different morphologies such as Electric Arc Furnace (EAF) slag aggregate. Finally, the concluding remarks will discuss the limits and the future lines of research into the improvement of mix designs for concretes that contain these alternative aggregates.

2.1 Introduction

Concrete, one of the oldest artificial composite materials, has been in use for over 2000 years. Many ancient stone and concrete structures are still standing, due to their durability that resists the effects of weathering and the passage of time, (Li 2011; Gromicko & Shepard 2016). Concrete is mainly composed of a granular skeleton, which consists of a suitable mixture of fine and coarse mineral aggregates, and cement paste, consisting of either a natural or synthetic cement binder and water, which coats the aggregate surface and fills any voids, thereby bonding together all the components (see Fig. 2.1). Chemical admixtures are also frequently added to the mixture, to supply additional benefits in both the fresh and the hardened state (Mehta & Monteiro 2014c). A review of each cement material and its function and influence on the properties of concrete may be found under each of the following sections: Cement-2.2; Fillers-2.3; Aggregates-2.4; Admixtures-2.5; Water-2.6.

Concrete has for decades been used in large quantities (33 billion tons/year) and is, after water, consumed more than any other material in the world (Mehta & Monteiro 2014c). In Western society, it can be found in an endless number of construction applications, from structural applications to pavements, curbs, and drains. The main reasons for its widespread use are its cost effectiveness, general availability, ease of casting and pouring, and its technical properties, especially its inherent durability (Mehta & Monteiro 2014c). However, the use of concrete also has high environmental impacts, mainly associated with the manufacture of Portland cement. Cement accounts for more than 74% of concrete-related CO_2 emissions and its production alone is responsible for 5-7% of all global CO_2 of anthropogenic origin (Flower et al. 2007; Van Den Heede & De Belie 2012).

Fig. 2.1. Conventional concrete proportions by volume [1].

Concrete manufacturing starts with the concrete-mix design process. The concrete components are first selected and proportioned, to meet any one specific type of concrete design that may be needed. There are different types of concrete for each use, from conventional Portland Cement concrete mixtures to special concretes designed for different types of materials and with adaptable mix-proportions, to develop the required properties (Mehta & Monteiro 2014c). In concrete manufacturing, the selection and the proportioning of each concrete material are therefore of special relevance.

Ideally, concrete should be designed to achieve the three technical requirements of workability, strength, and durability under given environmental conditions, at the lowest economic and environmental costs. Thus, consideration is not only given to technical aspects, but also to economic and environmental ones. Both (economic and environmental) requirements are highly affected by the amount of Portland cement that is used in concrete and its material availability in the zone, due to high transport costs and the environmental impact of transport compared to the costs of the material that is transported.

Although several mix-design methods for concrete are available, most of them are limited by the type of materials (generally they are only useful for conventional concrete components) and by the technical requirements for specific types of concrete. In addition, few methods include environmental and economic considerations and experimental testing is usually required to refine the theoretical mix design. This gap in concrete technology is due to the many properties of concrete components and the many variables that are at play, including the different methods of mixing, placing, and curing concrete, which all influence both its fresh and its hardened properties. Hence,

[1] Portland Cement Association (PCA) https://www.cement.org/cement-concrete-applications/how-concrete-is-made

most concrete mix designers consider the mix-design process as a science that is also bordering on an art (Mehta & Monteiro 2014c).

2.2 Cement

2.2.1 Introduction

Cement is a basic construction-sector material. Its main function is to bind all the concrete components together. In 2018, global cement production reached over 4.1 billion metric tons half of which was produced in China alone (2.4 billion metric tons in 2018). From the range of available cements in the market, hydraulic cement, specifically Portland cement, is by far the most widely used in construction applications. This type of cement hardens in reaction to water to the point of forming a water-resistant product (Mehta & Monteiro 2014b).

Cement has been used for thousands of years. The Macedonians of ancient Greece, the Egyptians, and the Romans all used hydraulic binders in many construction works. However, it was only quite recently, in 1824, that Joseph Aspdin patented the cement that is known today as Portland cement (Neville & Brooks 2010).

Although, cement only represents anywhere between 7 and 15% of total concrete volume, it has a major influence on both the environmental and the economic impact of concrete. Over 74% of concrete CO_2 emissions come from cement production (Flower et al. 2007; Van Den Heede & De Belie 2012).

Cement manufacturing is an energy-intensive process. Over 40% of total production costs are due to both fuel and electricity consumption (Oggioni et al. 2011). On average, 3.5-6.0 GJ (depending on plant efficiency) per ton of cement will be required for the calcination process and a modern cement works will normally consume 110–120 kWh of electricity per ton of cement (Rahman et al. 2013).

2.2.2 Cement manufacturing process

The Ordinary Portland Cement (OPC) manufacturing process starts with the *extraction of raw materials (see* Fig. 2.2*)*. OPC is mainly constituted by calcium silicates; therefore, raw materials must provide calcium and silicate in appropriate forms and proportions. The raw materials (lime, silica, alumina and iron oxide) generally used to provide the required components are typically, calcareous material, such as limestones or chalk and silica and alumina found as clay or shale. Sometimes, minerals such as bauxite and iron ore are also added to the raw mix to provide alumina and iron (Neville & Brooks 2010). An example of the raw materials proportion is shown in Table 2.1. Approximately 1.5-

1.6 tons of raw materials are required to produce 1 ton of cement. Losses are due to the calcination reaction.

Table 2.1. General raw material mix composition in cement making. Adapted from (Heilderberg, 2008).

Raw material	Components that contain	Component proportion
Limestone	Calcium carbonate ($CaCO_3$)	90-93%
Clay	Silica (SiO_2)	2-3%
Bauxite	Alumina (Al_2O_3)	2-3%
Iron ore	Iron oxide (Fe_2O_3)	1-2%

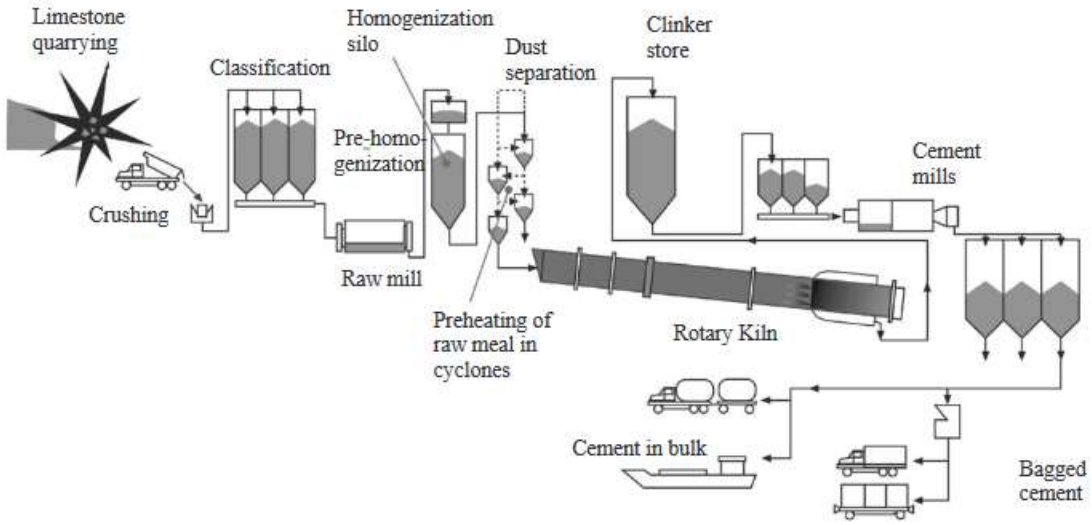

Fig. 2.2. Cement manufacturing process (Kääntee et al. 2004).

In a second step, *raw materials are crushed, ground*, *and blended*, to facilitate the formation of the desired compounds in the clinker during the heat-treatment process. Raw material grinding and mixing can be performed in either water or under dry conditions. However, energy consumption is lower in the dry cement process, because there is no need to evaporate the slurry before the clinkerization process (Mehta & Monteiro 2014b).

Once the raw materials have been prepared, the mixture is fed into a rotary kiln to obtain the clinker. Dry-processing consists of the follow steps (Neville & Brooks 2010):

1. The raw materials are pre-heated. Mixed components pass through a pre-heating chamber with several vertical cyclones before entering the kiln. The pre-heating chamber normally uses the hot gases emitted by the kiln.
2. There is an optional pre-calcination phase, to ensure complete calcination of the mix.

3. The pre-heating mix is fed into the rotatory kiln and the clinkerization process begins. In the kiln, the temperature progressively increases, until it reaches 1450ºC. The kiln therefore induces various chemical changes.

A sequence of chemical reactions will occur during the calcination process (Li 2011).

a. Clay decomposition

$$Clay \xrightarrow{600\,^{\circ}C} SiO_2 + Al_2O_3 + Fe_2O_3 + H_2O \quad (2.1)$$

b. Limestone decomposition

$$CaCO_2 \xrightarrow{1000\,^{\circ}C} CaO + CO_2 \quad (2.2)$$

c. Compounds form between 1000 ˚C and 1450˚C. The initial formation of C_2S occurs at a temperature of approximately 1200˚C. C_3S is formed at around 1400 ˚C.

$$\begin{matrix} Limestone \\ Clay \\ Iron\ ore, bauxite \end{matrix} \xrightarrow[High\ Temperature]{1450^{\circ}C} \begin{cases} 3CaO \cdot SiO_2 \\ 2CaO \cdot SiO_2 \\ 3CaO \cdot Al_2O_3 \\ 4CaO \cdot Al_2O_3 \cdot Fe_2O_3 \end{cases} \quad (2.3)$$

The calcination process for a cement clinker is as follows (Imbabi et al. 2013):

$$\underset{Calcium\ carbonate}{3CaCO_3} + \underset{silica}{SiO_2} \rightarrow \underset{Calcium\ silicate\ (clinker)}{Ca_3SiO_5} + \underset{Carbon\ dioxide}{CO_2} \quad (2.4)$$

4. Finally, the clinker product obtained from the rotary kiln drops into the coolers.

The final operational phase in the production of OPC consists of pulverizing the clinker to a range of particle sizes between 10 and 15 µm. Finer grinding of the clinker will lead to faster reactions, due to the increased surface area of cement powder in contact with water. Balls mills are normally used for this function. In addition, approximately 5% of gypsum is mixed with the clinker to control the early setting of the cement and its hardening behavior (Mehta & Monteiro 2014b).

There are four cement production technologies: dry, wet, semi-dry, and semi-wet processes. The most efficient production process in terms of energy production is the dry process, commonly found in Western Europe (Benhelal et al. 2012).

2.2.3 Types of cements

In UNE-EN 197-1, cements are generally classified by the type and the amount of mineral additions. Basically, two general groups can be distinguished:

- Cement without any addition. CEM I.
- Cement with mineral additions such as silica fume, limestone, slag, fly ash (CEM II; CEM III; CEM IV; CEM V; CEM VI).

European standard UNE-EN 197-recognizes blast furnace slag, silica fume, (natural and natural calcined) pozzolans, fly ash (siliceous and calcareous), burnt shale, and limestone as admissible cementitious components, together with clinker, and it specifies 27 different categories of cements based on the percentile contents of those components (Dhir OBE et al. 2017).

From the industrial perspective, the second category is obtained by dilution of the first with the different mineral additions, as specified by the standard. An overview of those typical Supplementary Cementitious Materials (SCM) and their use in substitution of cement is included in section 2.2.4.

In addition to OPC, other alternative binders designed to reduce CO_2 emissions are available. The most interesting alternative clinkers to Portland cement clinker for the reduction of CO_2 emissions appears to be cement clinker that is high in belite (Popescu et al. 2003) and sulfoaluminate cement clinker (Alaoui et al. 2007). Other promising alternatives are calcium aluminate cements, Alkali-Activated Cements (AAC) (Palomo et al. 1999) and supersulfated cements.

2.2.4 Supplementary Cementitious Materials (SCM)

Nowadays, SCM are widely used in concrete, both to reduce the environmental impact and to improve concrete performance in both the fresh and the hardened state. SCM are generally by-products from other industries or natural materials. Most SCM are pozzolanic (rich in SiO_2) or latent-hydraulic industrial by-products; materials that contribute to the properties of concrete through either hydraulic or pozzolanic activity (Imbabi et al. 2012).

The rates of SCM replacement and the quality requirement of SCM are restricted by the standards. SCM can be blended directly with cements or separately added to a concrete mixer (Lothenbach et al. 2011). Generally, in Europe, SCM are directly added to cement, a practice reinforced by the European norm (UNE-EN 197-1 2011) (see Table 2.2). However, in the USA the second option is preferred.

Table 2.2. Classification of cement types according to EN 197-1:2011. (Imbabi et al. 2012)

CEM I Portland cement	Portland cement and up to 5% of minor additional constituents (OPC).
CEM II Portland composite cement	Portland cement with up to 35% of other Supplementary Cementitious Material (SCM) such as ground limestone, fly ash and Ground Granulated Blast Furnace Slag (GGBFS).
CEM III blast furnace cement	Portland cement with a higher percentage of blast furnace slag, usually around 60% to 75%.
CEM IV pozzolanic cement	Portland cement with up to 55% of selected pozzolanic constituent.
CEM V composite cement	Portland cement blended with GGBFS or fly ash and pozzolanic material.

The use of SCM in partial substitution of OPC will significantly reduce the overall environmental impact, because the manufacturing process of SCM involves no clinkering process (preheater, calciner, kiln and coolers account for ±90% of total energy consumption in the manufacture of cement (Afkhami et al. 2015)). In addition, the replacement of a certain mass of clinker by an equivalent mass of SCM will valorize by-products and waste from other industries (Lothenbach et al. 2011). The use and interest of SMCs is increasing and different combinations between SCM and new by-product materials are under study (Table 2.3). However, further research is needed for the development of standards.

The most well-investigated SCM are briefly described below:

Table 2.3. SCM, sources, reactivity and usual dosages

Type	**Waste stream**	**Reactivity**	**Usual dosage** (Li 2011)
Fly-ash	Fine residues generated in coal (and biomass) (co-)combustion of electricity plants.	Pozzolanic reactivity from silicate glass containing Al_2O_3, Fe_2O_3 and alkalis .	10-40%
Granulated blast-furnace slag	Obtained by quenching molten iron slag (a by-product of iron and steel-making) from a blast furnace in water or steam.	Cementitious material from silicate glass containing mainly CaO, MgO, Al_2O_3 and SiO_2.	20-75%
Silica fume	By-product of the induction arc furnaces in the silicon metal and ferrosilicon alloy industries.	Pozzolanic reactivity from amorphous SiO_2.	5-15%
Metakaoline	Calcination of kaolinite clay.	Reactivity from Al_2O_3 and dehydroxylated SiO_2.	5-10%

- *Fly ash*

  Fly ash is a residue from the burning of coal to generate electricity. Its non-combustible particulates have been removed (generally by electrostatic

precipitation) from the flue gases. Fly ash contains silicate glass Al_2O_3, Fe_2O_3 and alkalis with pozzolanic properties, which will vary depending on the source of the burnt coal.

- *Ground granulated blast furnace slag (GGBFS)* (Chindaprasirt & Cao 2015). A by-product of the iron and steel industry, GGBFS is the result of rapidly cooled molten slag under a jet of water, leaving it with a sand-like appearance. It is ground to obtain a similar particle size to normal Portland cement. GGBFS are used to enhance workability, increase setting times, and strengthen resistance to sulphates and alkali-silica reaction improving its durability.
- *Silica fume*

  A by-product of the production of silicon and silicon alloys in electric arc furnaces, silica fume is also known as microsilica. Its particle sizes are 100 times smaller than cement particle. The use of silica fume in concrete reduces the permeability of concrete and increases its durability. It is only used in certain special concretes, on account of its expense and unavailability in most locations (Damineli et al. 2013). Although the replacement of cement by silica fume will reduce CO_2 emissions, its recovery process is not as easy as GGBS and fly ash (Imbabi et al. 2012).
- *Metakaolin*

  A product of the thermal transformation of kaolin clays, metakaolin has a pozzolanic reactivity and quickly reacts, due to its high surface area. The typical replacement levels are about 5-10%.

The rate of replacement of SCM by OPC is mainly limited by cement/by-product compatibility. Different combinations of by-products and mechanical-chemical activation processes are under continuous development to improve compatibility (Sobolev et al. 2018).

2.3 Fillers

Fillers are normally used in replacement of Portland cement, changing the rheological properties of the concrete. The replacement rate is roughly 15-35%, varying with the standards of certain countries, and the grain size distribution is similar to Portland cement (Aïtcin 2015).

Fillers interact with cement in several ways. Although fillers will generally have no binding properties, they can indirectly affect the chemical structure of cement paste and concrete, as their large specific surface area means the paste will benefit from positive nucleation, densification, and homogenization (Lagerblad & Forssberg 2004).

The most common fillers are made of limestone and silica; however, by-products from other industries can be also used as fillers. In addition to their influence on both the

fresh and the hardened properties of concrete, the use of fillers will reduce costs and environmental impacts, as these components undergo no calcination in a kiln (Lagerblad & Forssberg 2004; Aïtcin 2015).

2.4 Aggregates

2.4.1 Introduction

Aggregates occupy between 60 to 80% of total concrete volume, so their properties will largely determine the final properties of the concrete (Mehta & Monteiro 2014c). They provide strength, dimensional stability and durability to hardened concrete.

Generally, aggregates are the cheapest concrete ingredient. In this way, an optimized dosage will help to reduce the total cost of the concrete mix. Another relevant aspect is the environmental impact. Aggregates have a low environmental impact, especially in comparison with the environmental emissions of cement. Decreasing cement/aggregate ratios with an optimized aggregate skeleton will reduce environmental impacts and still meet performance requirements.

Nowadays, concrete can be designed using several types of aggregates from different sources and morphologies. The design of grading and particle packing are some of the critical aspects to be studied, in order to obtain a successful concrete mixture (Alexander & Mindess 2005).

The use of waste materials can reduce demand for natural resources and decrease environmental contamination associated with waste disposal and mining. Furthermore, the use of aggregates from waste streams can reduce the cost of concrete production. For these reasons, recycled aggregate and electric arc furnace slag are currently incorporated into some concrete mixtures.

Construction & Demolition Waste (C&DW) has been identified as a priority waste stream in the European Union, as it accounts for approximately 20-35% of all waste generated (European Commission 2018). Thus, Europe has established targets to recycle and to reuse all C&DW that is generated by 2020 (Waste Framework Directive (2008/98/EC) 2008). Recycling and re-use of C&DW has high potential, especially given the high resource value of some of its components to the construction sector, particularly as aggregates.

In the Basque Country, natural crushed aggregates are the most widely used, especially aggregates from limestone, which is the predominant rock type. C&DW accounts for 25% of total waste generated in this region with 60% recycled over the past year[2]. Another important source of waste is the metal industry. Steel slag represents the

[2] https://www.residuosprofesional.com/euskadi-recicla-60-residuos-de-construccion/

second most significant waste stream in the Basque Country in terms of its production (16%) (Gobierno Vasco 2018). It is generally disposed of in landfill sites, even though current technological advances have demonstrated its great potential - particularly Electric Arc Furnace Slag (EAFS) or 'black slag' - for its recovery and valorization as aggregate in civil and building works.

2.4.2 Aggregates classification

The European standard EN 12620-2002+A1:2008, which specifies the aggregate properties used in concrete, defines three categories according to the aggregate source, Natural aggregates, Manufactured aggregates and Recycled aggregates.

In terms of their physical characteristics, aggregates are classified by particle size and by density. According to European standards (EN 12620-2002+A1:2008), aggregates are considered coarse, when the biggest particles are larger than 4 mm and the smallest particles are equal or larger than 2 mm, and fine when the largest particle is smaller or equal to 4 mm. Regarding classification by density, aggregates with densities over 2000 kg/m^3 (determined after drying the aggregate) are considered to be of normal weight, while aggregates with a lower density or a bulk density no larger than 1200 kg/m^3 are classified as lightweight aggregates (EN 13055-1:2002).

Petrology is a further aspect to take into account for the classification of the aggregate, which refers to its mineralogical composition and their relative proportions (Alexander & Mindess 2005). Petrological and mineralogical characterizations of aggregates are very useful for assessing the performance of an aggregate in concrete (see Table 2.4).

Table 2.4. Rock mineral constituents by class of rock.

Igneous rocks	Sedimentary rocks	Metamorphic rocks
Granite	Conglomerate	Marble
Syenite	Sandstone	Metaquartzite
Diorite	Quartzite	Slate
Gabbro	Graywacke	Phyllite
Peridotite	Subgraywacke	Schist
Pegmatite	Arkose	Amphibolite
Volcanic glass	Claystone, siltstone,	Hornfels Gneiss
Felsite	argillite, and shale	Serpentinite
Basalt	Limestone	
	Dolomite	
	Marl	
	Chalk	
	Chert	

a. Natural aggregate

Natural aggregates, as the name suggests, are produced by mechanical processes from natural rocks with no further additives. In some countries or regions, these materials are the only available source of quality aggregates for concrete.

Sources: Natural aggregates can be extracted from *pits, riverbanks and beds, seabeds, gravels, beach and dunes, and any other natural deposit*. The physical and chemical properties such as density, strength, stiffness, hardness, permeability pore structure, and mineral composition are influenced by the parent rock, categorized by igneous rock (formed by the cooling of molten magma or lava), sedimentary rock (formed from the physico/mechanical and chemical breakdown of other pre-existing rocks); and metamorphic rock (originally either igneous or sedimentary rocks, which have subsequently metamorphosed due to extreme heat and pressure) (Table 2.4) (Alexander & Mindess 2005).

Origin and processing: The processing of aggregates will depend on their source and is mainly related to the construction properties that may be required. Thus, the properties and the quality of gravel and sand obtained from *pits* will vary enormously, depending on their origin, weathering and transportation, and subsequent processing; aggregate from *rivers* will be influenced by the different flow rates of the watercourse, which cause sedimentation and stratification; *sand from beaches and dunes* will be blended or mixed with other aggregates, to provide acceptable fines, because they are usually poorly graded (more than one particle size), due to the turbulence of waves and wind; and aggregates from *rock quarries* will depend on the qualities of the parent rock, the degree of weathering, the extraction methods, and the crushing process (Alexander & Mindess 2005).

The main processes used to obtain suitable aggregate sizes will depend on the extraction source, some of which are summarized below:

1. *Firstly*, aggregates from pits, rivers and dunes are exploited in bulk generally using heavy earth-moving equipment and excavators, even, occasionally, high-pressure water jetting. In contrast, there are several methods to extract aggregates from quarries: blasting, mechanical ripping, rock-breaking techniques, etc. (Alexander & Mindess 2005).

Then, three processing techniques are available, to obtain adequate grading and suitable aggregate properties:

2. *Crushing process.* This process reduces the large boulders to sizes that are appropriate for concrete. The steps that this process follows will depend on

the source and the required size of the aggregate. For example, partial crushing, is generally sufficient to reduce large or oversize particles from pits, while further steps are needed to obtain suitable aggregate sizes from quarrying. The typical steps are as follow (Alexander & Mindess 2005):

i. *Primary crushing.* Large sizes of rocks are reduced to more manageable size generally using jaw or gyratory crushers. Crushing processes are performed at the quarry or at the cement processing plant.

ii. *Secondary crushing.* In this phase, cone crushers and impact breakers crush the concrete to the necessary size for use in concrete.

iii. *Tertiary crushing.* The third step is occasionally used for major reduction of aggregate size and to improve the particle shape. The equipment in use is similar to the secondary crushing process.

3. *Screening and sorting.* These processes are applied to obtain a proper size gradation for producing good concrete. Alternatively, fine aggregates can be sorted by a water-settling (Alexander & Mindess 2005).
4. *Washing and scrubbing.* The main objective of washing gravel and sand is to remove unwanted material, mainly the excess clay or silt. A water jet or hose applied during screening or a washer barrel (Alexander & Mindess 2005).

b. Manufactured aggregates

Manufactured aggregates are sourced from industrial processes and are generally considered by-products rather than waste. Industrial by-products that may be used as aggregates include coal ash, various slags from the siderurgical industry, industrial sludges and other wastes such as pulp from paper mills, mine tailings, food and agriculture, and leather (Brito & Saikia 2013).

Slag from the metallurgical industry is currently one of the most suitable manufactured aggregates, due to the mechanical resistance of slag grains that is higher than many natural aggregates and the expressed acceptance of its use as granular material in the European standards.

Slags

Sources and manufacturing process: Ferrous slags are produced during the production of iron using blast furnaces and for the separation of impurities from molten steel in steel-making furnaces (steel slag) (Brito & Saikia 2013). Their chemical composition and morphology depend on the metal that is produced and the solidification process in use (Grubeša et al. 2016). Thus, iron slags from the blast furnace are divided into Air-cooled Blast furnace Slag (ABS) and Granulated Blast Furnace Slag (GBFS) and steel slags can be categorized into Basic Oxygen Furnace (BOF) slag, Electric Arc Furnace Slag (EAFS), and Ladle Furnace slag (LFS), depending on the steel manufacturing process (Jiang et al. 2018). Additionally, EAF and LF slags can be obtained by the EAF process too, by using

steel scraps as major raw material components instead of the iron ore used in the blast furnace line production.

ABS is produced by leaving molten slag to cool in the open air, while GBFS is produced by rapidly cooling molten slag with a jet of water. The former has the appearance of crushed stone while the latter has a sandy appearance. Coarse BF slag aggregate for concrete mixing is produced by crushing air-cooled slag and then screening it (see Fig. 2.3); fine aggregate is produced by lightly crushing granulated slag to control the grain size and then screening the fines (Miyamoto et al. 2015).

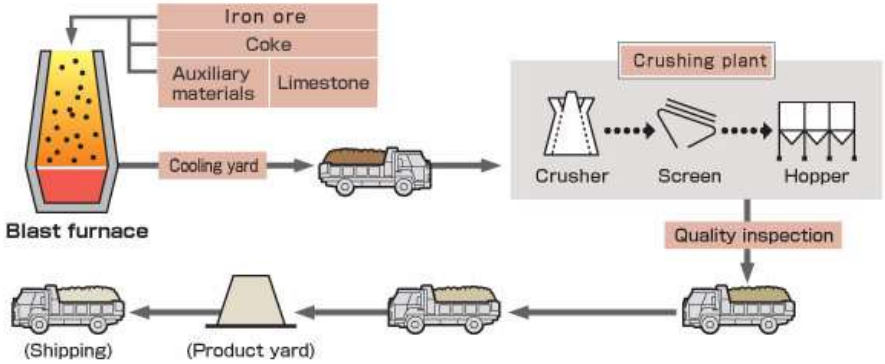

Fig. 2.3. Manufacturing process for blast furnace slag coarse aggregate. [3]

The processing of ABS aggregates from EAFS mainly consists of crushing and/or screening (see Fig. 2.5). Those processes grade the aggregates and give them other related properties, in accordance with standards and specifications agreed with the client. Sometimes magnetic separation will also be needed. For more detailed information, the steel slag processes to obtain the final by-products have been summarized in a very recent review (Jiang et al. 2018) on the characteristics of steel slag and their use in cement and concrete.

All slag types will never be suitable for use as concrete aggregate, due to their different compositions that will depend on the production process and the cooling system. The most appropriate are EAFS and ABS.

The use of EAF slag as a concrete aggregate has been studied by several authors (Manso et al. 2006; San-José et al. 2014; Chunlin et al. 2011; Pellegrino et al. 2013; Arribas et al. 2014; Sosa et al. 2020; Santamaria et al. 2018). These studies have shown how this type of slag can be successfully incorporated in concrete, providing good workability and greater mechanical strength, due to stronger bonding between the EAFS and the cement paste. In addition, it has been demonstrated that EAFS has a slightly positive effect on samples subjected to freezing-thawing, wetting-drying, sulphate and fire resistance tests, showing no volumetric expansion.

[3] http://www.slg.jp/e/slag/product/kotuzai.html

The different properties between the EAF aggregates and the natural aggregates have to be considered to reach a successful concrete mix design. One of the critical properties is the shape and the specific surface of the EAF aggregates. For a similar volume of concrete, EAF aggregate concretes will need larger amounts of water and cement paste than conventional concrete, to bond the cavernous and irregular surfaces of the slag particles (see Fig. 2.3 and see Fig. 2.4) *(Thomas et al. 2019)*.

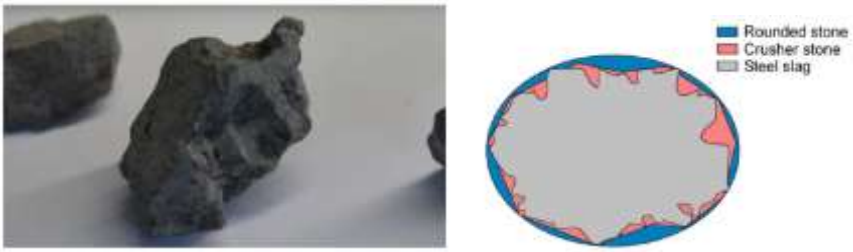

Fig. 2.4. Left) Detail of the irregular surface of EAFS particles. Right) representation of the different aggregate shapes for the same aggregate size (Thomas et al. 2019).

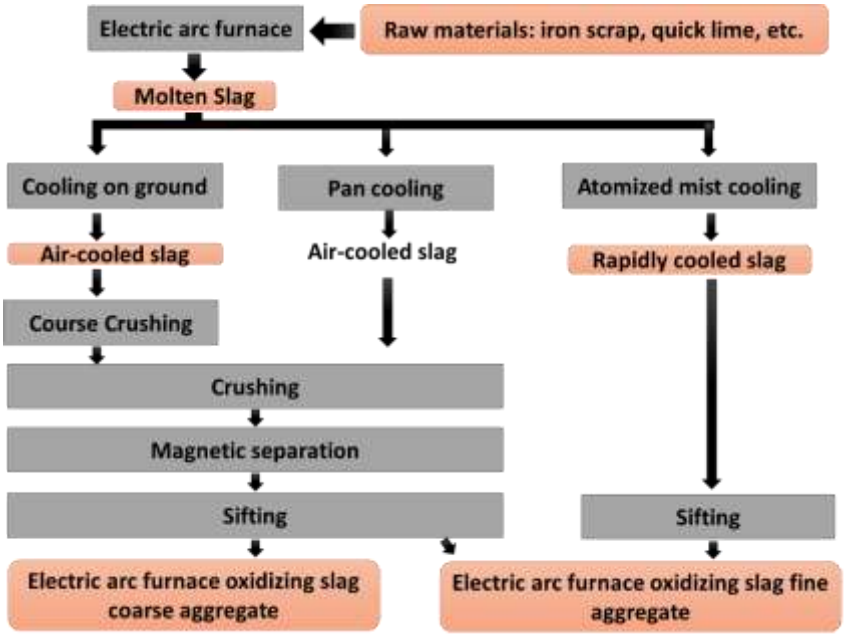

Fig. 2.5. Manufacturing process for Electric Arc Furnace slag aggregates. [4]

Slag production: Every year, some 45 million tons of ferrous slag (iron and steel slag) are generated in Europe[5] while slag generation in the Basque Country, in 2016, amounted to 517,099 tons, of which 81% was black slag (EAFS) and the remainder (19%) white slag (LFS) and other miscellaneous forms (Gobierno Vasco 2018).

c. Recycled aggregate

Recycled aggregates are sourced from processed inorganic material previously used for construction purposes (UNE-EN 12620:2003+A1 2009). Aggregates obtained just from

[4] http://www.slg.jp/e/slag/product/kotuzai.html
[5] EUROSLAG- http://www.euroslag.com/

concrete waste are called Recycled Concrete Aggregate (RCA), while if the waste sources contain other inorganic materials, they are classified either as general Recycled Aggregate (RA) or as Mixed Recycled Aggregate (MRA) (Mas et al. 2012).

Sources: Both demolition activities and natural disasters are sources of construction waste (Özalp et al. 2016). Most C&DW is produced during the demolition phase, however, waste generation occurs throughout the construction process, from the construction phase up until the demolition phase, including the rehabilitation, the reform, and the repair processes. Thus, recycled aggregate could come from C&DW from concrete structures, airport runways, bridge supports, concrete roadbeds, and rejected prefabricated concrete products, etc. (Tam et al. 2018; Sainz-Aja et al. 2020).

Components: The composition of the C&DW is influenced by the source of the stream. C&DW is a mixture of different components such as concrete, wood, bricks, glass, metal and asphalt. However, most of the components can be considered as inert materials and the stony nature has a variation between 75-95% in most cases.

Processing: C&DW needs to be separated, collected, and processed. Only the stony fraction is useful for concrete applications. Thus, once the stony fraction has been separated, wood and metal components are all recycled and plastic waste is energetically revalorized in other sectors.

The production plants for recycled aggregates can be divided into permanent plants and mobile plants, the production capacity of permanent plants being substantially higher.

The following treatment steps are needed, to obtain suitable aggregates for use in concrete:

1. The first step consists of the selective demolition in-situ, to prevent hazardous materials from contaminating the waste stream. The aim of selective demolition is to improve the conditions for classification and recovery at source, extending the life cycle of construction materials, favoring reuse and generating less waste, the final destination of which will be landfill sites. For all these reasons, selective demolition is essential for efficient recycling of the C&DW. Its application, nevertheless, has certain difficulties, especially because the buildings will not have been designed with selective demolition and demolition criteria in mind, which implies higher demolition costs that will only partially be compensated by the reduction of treatment costs and the higher value of the materials that are recovered.
2. After the demolition process, the resulting material can be treated at either permanent or mobile plants. Although the process will vary depending on the needs and the final destination, the follow processing steps are generally followed at permanent C&DW management plants.

- *Primary triage:* A manual or mechanical selection of the reception material is performed. The larger-size impurities are therefore removed before the crushing process commences.
- *C&DW treatment*: In this step the stony fraction is separated from the rest of the fraction.
    - Fines fraction screening. The small size materials are separated and collected for shipment to their destination. This process is performed through screening technologies.
    - Light waste separation by air. The process consists of a blower that removes the lightest fractions (dust, small plastic particle, paper, etc.). Blowers and/or cyclones are used to supply air with sufficient force to raise particles upwards, in such a way that gravity will separate the materials by their specific weight.
    - Manual or automatic triage of undesirable materials (plaster, heavy plastics, wood, etc.). The waste (plastics, wood, aluminum...) is identified and manually removed, leaving only the stone materials. For the separation of plasters and plaster, certain plants have densiometric baths.
    - Magnetic separator (electromagnets) to eliminate the metallic elements of the stony fraction.
- *Crushing and screening step.* Primary and secondary crushing is followed by screening with different sieve sizes, using conveyors to classify the material by particle size and composition.

During the C&DW treatment process a variety of sub-products are generated. Some are recycled such as plastic, pasteboard, wood, metal, etc.

Other technologies, especially flotation separation and near infrared sorting, are currently in use to increase the quality of the final recycled product.

2.4.3 Aggregate consumption

Aggregates are the second most consumed raw material in the world after water. In Europe 2.7 billion tons per year [EU28+EFTA, 2016] are consumed (5 tons per capita per year) (European Aggregates Association 2018). Their production and consumption vary widely, depending on the development of a country or region, its economic activity, the nature of construction work, and so on. Thus, Spain consumed 112 million tons in 2017, of which 5.5 tons were consumed, in 2017, in the Basque Country (ANEFA 2018) (see Fig. 2.5). The consumption of aggregates in nearby countries such as Portugal and the analysis of the properties of concrete manufactured with these aggregates these references can be consulted (Pacheco et al. 2019; Pacheco et al. 2020).

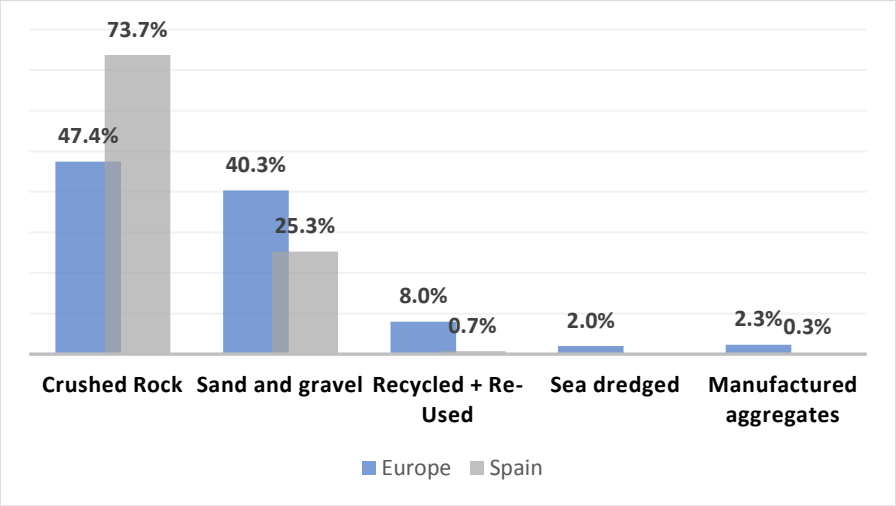

Fig. 2.6. Aggregates sources in Europe and Spain (2016). (European Aggregates Association 2018; ANEFA 2018).

If we focus on the Basque Country, aggregate consumption has increased by 12% year-on-year, although that value is lower than the European reference. The production of recycled aggregate in 2016 was 830 thousand tons, of which only half was consumed. Recycled aggregate consumption is therefore around 7.5% of the total aggregate consumption, a value close to the European average (see Fig. 2.6) (ANEFA 2018; Gobierno Vasco 2018). In 2016, there were 35 quarries and 3 pits from which natural aggregates were extracted (ANEFA 2018), mainly producing crushed limestone aggregate. In Spain, limestone is the most common rock type (46.2 %) used as aggregate. Table 2.5 shows the proportion of natural aggregates used in Spain in 2017.

Transporting large tonnages of aggregate over long distances is very costly, so materials that are locally produced in the region are generally consumed. In consequence, most of the concrete produced in the Basque Country contains limestone aggregate. Generally speaking, limestone aggregate from Bizkaia has some problems related to the fines content (fines are defined by EHE-08 as those aggregates that pass through the 0.06mm sieve). In this area, the percentage of fines is considered optimum between 8-10% (Ramirez & Barcena 1981). However, sand with a fines content of 15% or even 18% are common. Various solutions have been proposed to reduce the aggregate fines content: washing systems, cyclone equipment, and sieving processes. All of them are related with the high energy consumption for sand drying and other environmental problems. The use of a special mill that produces fewer fine contents is the most suitable process (Ramirez & Barcena 1981). The nature of limestone fines has positive effects on concrete workability, due to their reactivity. These fines require less water to achieve acceptable workability in comparison, for example, with siliceous aggregates, among others.

Beach sand, extensively used in old buildings, is no longer considered a valid option, given the high levels of armature corrosion that it can cause, due to its high salinity and

mollusks dispersed in the sand that result in chloride attacks, progressively weakening concrete strength. The benefits are the lack of assorted fine sizes and an optimal grain size that combines with the limestone sand, providing the concrete with better workability (Ramirez & Barcena 1981).

Table 2.5. Distribution of the rock type used as aggregates in Construction, Spain, 2017. Source: (ANEFA 2018).

Limestone	46.2 %
Sand and Gravel	29 %
Granite	7.5 %
Dolomite	4.4 %
Siliceous sand	1.6 %
Marble	1.1 %

2.4.4 Aggregate properties

The properties of aggregates and filler aggregates from natural, manufactured, and recycled sources and the mixtures of those aggregates for use in concrete are defined in European standard EN 12620:2002+A1:2008 (under review: prEN 12620).

Several key physical properties of concrete aggregate are defined below (Ghasemi 2017):

Density: defined as the mass per unit volume. Several measures of density can be considered for aggregate characterization. Relative density (specific gravity) is one of the most widely used in concrete design. It is calculated from the oven-dry mass and the Saturated Surface Dry (SSD) volume of the aggregate. Bulk density depends on the packing of the particles, which in turn depends on particle shape, surface texture, grading and compaction energy.

Absorption and moisture: absorption is directly related to porosity. It is measured as the ratio of changes to the mass of dried aggregate and SSD aggregate. The moisture level is the moisture available within each particle. Moisture levels influence the total water content of a concrete mix and the most useful moisture state is SSD (saturated surface density).

Porosity: a measure of the internal volume of pores.

Void content: the void content of a group of particles is defined by the voids between particle edges that fail to fit together closely. Particle size, shape, grading and packing properties all influence the measure.

Grading: a measure of aggregate size distribution.

Surface texture: usually a qualitative classification such as either rough or smooth, surface texture depends on pore structure, texture of the parent rock, production methods, amount of wear on the particles and grain size

Flakiness ratio: the thickness-breadth ratio that can be estimated using a thickness gauge. The elongation ratio is normally obtained from image analysis. Sphericity is normally defined as the ratio of the surface area of a sphere and the actual surface area of a particle. Convexity is a measure of overall roundness.

Particle shape: there is no well-established method to measure its value. The shape parameter can include angularity, flakiness, and sphericity, among others.

Fineness Modulus (FM): a measure of the average particle size that characterizes aggregate grading. The FM parameter represents the cumulative percentages of material retained on each standard sieve after dividing the sum by 100. Grading with the same fineness modulus will require a similar water content, to produce a concrete with the same workability.

2.4.5 Aggregate gradation

There is no ideal gradation to achieve the perfect concrete mix. The choice of using either continuous or a gap-graded mixes depends on the technical advantages of each mix method and the local availability of material, which is closely linked to their costs. Another factor is local social acceptance of the practice. For example, continuously graded mixes are more common in UK and Europe, while a gap-graded mix is more common in South Africa, due to the predominance of both coarse and fine crushed aggregates (Alexander & Mindess 2005).

In a gap-graded aggregate distribution, some intermediate sizes are omitted, resulting in a mix of coarse and fine aggregates (see Fig. 2.7). Those aggregate combinations are used to obtain uniform textures for exposed-aggregate concrete (e.g. porous pavements) and can also increase strength and reduce creep and shrinkage. Continuously graded aggregates follow a homogeneous distribution from coarse to fine sizes with no gaps between the sizes, unlike gap-graded aggregates. The Fuller (Fuller & Thompson 1907) curve is the perfect example of continuous aggregate size distribution. The purpose of this curve is to achieve a maximum packing density (Zhang et al. 2011).

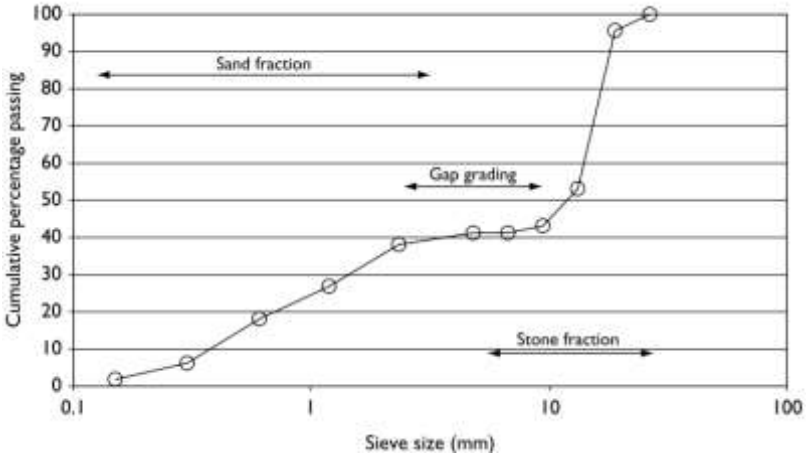

Fig. 2.7. Gap-grading curve (Alexander & Mindess 2005).

Continuous distribution may be preferable to avoid segregation in self-compacting concrete. Whereas gap-graded aggregate distribution is more applicable for concrete which after compaction is immediate demolded (precast concrete), or when the temperature effects from the hydration reaction in the mass concrete need to be reduced as a higher degree of compaction is obtained for gap-graded aggregate and therefore less cement paste is needed to fill the voids (Richardson 2014). The main benefits of using gap-graded or continuously graded aggregate are summarized in Table 2.6.

The optimal aggregate combination should show no lack of size gaps and spaces should be filled with smaller aggregate particles without compromising concrete workability whenever interlocking aggregates cause problematic interference. Nevertheless, these gradings have the advantage of reducing the amount of cement required in a mix, and result in workable mixes when particle shape and texture are acceptable (Alexander & Mindess 2005).

Table 2.6. Technical advantages of gap-graded and continuously graded mixes (Alexander & Mindess 2005).

Gap-graded aggregates	Continuously graded aggregates
Less chance of particle interference.	Less segregation of higher slump mixes.
Greater sensitivity of slump spread to changes relating to water content, which aids more accurate control of mixing water.	Less sensitivity to slight changes relating to water content, which is advantageous for uniform workability.
Greater responsiveness to vibration of stiff mixes.	Improved pumpability, especially at higher pressures.
	Improved flexural strength, due to the increased surface area of graded stone.

2.5 Admixtures

The study of admixtures in concrete mix design falls outside the scope of this thesis. However, admixtures are widely used in concrete today, to resolve issues with cement and concrete quality for technical, economic, and even environmental purposes, therefore, in this section a brief summary is included in Table 2.7 (Portland Cement Association (PCA) 2016).

Table 2.7. Most widely used types of admixtures. Functions and materials.

Type of admixture	Function	Example of materials used
Air-Entraining admixtures	These admixtures introduce and stabilize microscopic air bubbles in concrete. They are used to improve concrete workability, the ease of placing and the durability of concrete exposed to frost, sulphate, and alkali reactive environments (Mehta & Monteiro 2014a).	Surfactants: salts of wood resins, proteinaceous materials and petroleum acids (Mehta & Monteiro 2014a).
Water-reducing (Plasticizer)	The main function is to reduce the water required to reach the required workability in concrete mix. Therefore, these admixtures are used to reduce water-cement ratio and thus, increase the concrete strength, durability, reduce the cement content or increase the slump (Li 2011).	Surfactants: salts and modificators and derivatives of lignosulfonic acid, hydrocylated carboxylic acids and polysaccharides (Mehta & Monteiro 2014a).
Superplasticizers	Superplasticizers and plasticizer are aimed at the same objective. However, the capacity to reduce the mixing water of superplasticizers is three to four times more effectively than the water-reducing admixtures (rates of reduction between 15-40%) (Mehta & Monteiro 2014a).	Sulfonates salts of melamin or neaphthalene formaldehyde condensates. Polycarbocylic ether-based (PCE) (Mehta & Monteiro 2014a).
Accelerating	Accelerating admixtures reduce the hardening time (setting) of concrete and increase the development of early strength. (Portland Cement Association (PCA) 2016).	Calcium Chloride (Mehta & Monteiro 2014a).

Admixtures are defined by the European standard (EN 934-2 2009) as products added to the concrete mix, at dosages no greater than 5% by mass, in relation to the cement content, to modify the concrete properties, in both the fresh and the hardened state. Proper additions of admixtures in concrete mix design will improve several concrete

properties such as durability, strength, chemical resistance, adjustments to the water/ cement ratio, workability, and setting times (Ramachandran 1996; Albayrak et al. 2015).

Admixtures can be mineral or chemical products which vary widely in composition, from surfactants and soluble salts to polymers and insoluble salts (Mehta & Monteiro 2014a). They are available either as liquids or as water-soluble solids or powders and are typically added before or during the mixing process. Admixtures are usually classified according to their function; however, it is worth remembering that many admixtures perform more than one function. The range of admixtures on the market can enhance concrete properties for a wide range of construction applications (Niaounakis 2015).

2.6 Water

Water, the most widely consumed resource in the world, is responsible for cement hydration reactions and concrete workability. It is therefore considered one of the most critical factors for the manufacture of concrete. The total water amount in a concrete mix and the Water-to-Cement ratio (W/C) must be carefully selected, to reach the desired workability without comprising the strength and durability requirements for hardened concrete. Free water in a concrete mix will mainly serve three functions (Li 2011):

- To react with the cement to maximize the degree of hydration. (Generally, the amount of water for acceptable workability will always be greater than the amount needed for complete hydration of the cement).
- To provide workability to the fresh mixture by acting as a lubricant.
- To supply the space needed in the paste for the development of hydration products.

In the manufacturing process of concrete, water is not only needed during the concrete mixing process, but also during the curing and washing processes.

Water quality is important, because any impurities will not only affect the fresh concrete properties, such as setting times and workability, but also strength and durability (Neville & Brooks 2010). In practice, mains water is normally used, to ensure that the water contains no organic substances, chlorides or alkalis. However, there may be some exceptions applicable to water with certain minerals or sugar dissolved in it (Li 2011).

Water impurities can appear as suspended solids such as silt, clay, organic matter and colloids, dissolved solids, and dissolved inorganic material. Depending on the type of impurity and its concentration, water can be used without comprising the concrete properties. As an example, water from the sea can be used to make concrete, if specific precautions are considered (Li 2011).

The water used during aggregate washing should be clean enough, so as not to produce harmful films or coatings on the aggregate surfaces.

A low W/C ratio is advised especially in more demanding applications.

The concrete industry continues to address standards that allow greater use of no potable water both in concrete and in its production processes, to help to reduce pressure on limited supplies of drinkable (potable) water.

There are four ways to use and to recycle water: i) to reuse water on-site for repeated cycles of the same task; ii) to treat and to reuse water on-site for multiple purposes; iii) to use greywater after solids have been eliminated; and, iv) to collect water from natural sources such as rainwater, lakes, rivers, and ponds for use in construction (Bourj, 2004).

Furthermore, mixtures with less water should be developed with new technologies to create mortar and concrete containing a minimal amount of water. As an example, the incorporation of high volumes of fly ash in concrete will reduce water demand.

2.7 Mix-design methods

The purpose of concrete mix-design methods is to select the different concrete components (cement, SCM, water, aggregates and admixtures) and to find their suitable proportions, in order to achieve the concrete requirements of workability, strength, and durability at the lowest cost. Hence, the priority is at times to find suitable materials that are locally available, rather than simply suitable (K et al. 2014).

Some authors define the process of mixing concretes as an art, in spite of the variety of methods and numerical processes that exist for concrete mix design, technical approaches may not always function as desired, precisely because of the great variety of materials and their characteristics (Ghasemi 2017; K et al. 2014).

In concrete mix optimization, deep knowledge of each component and its function, both in the fresh and in the hard state is fundamental, to ensure high-quality concrete.

In literature, there are evidences of numerical studies to predict the properties of green concretes designed with advanced cementitious material and recycled aggregates (Barros et al. 2017). For example, (Pepe et al. 2016) designed a novel mix design methodology for recycled aggregate mix concrete.

The workability of fresh concrete and the compression strength of hardened concrete at a specified age, are generally the two most essential requirements. Durability is another important factor, however, it is generally assumed to be satisfactory under normal conditions of exposure after the concrete has reached the necessary strength (K et al. 2014).

Workability is influenced by water requirements, which in turn is influenced by aggregate characteristics (shape, grading, and fines content). In the hardened state, concrete strength and permeability is highly influenced by the W/C ratio, and cement characteristics and performance (Ghasemi 2017).

Currently, environmental concerns are assuming increasing importance in the construction sector. Thus, the optimization of the concrete mix according to concrete environmental impacts should be considered, in order to minimize the environmental impact in an effective way.

Over recent years, interest has been growing in computational concrete mix optimization. It is mainly due to the current trend of using different types of natural, by-products or even waste materials as concrete components that potentially increase the range of possibilities for concrete mix design that increase its complexity. In addition, performance, and environmental and economic requirements are increasingly stringent. (DeRousseau et al. 2018) published a recent review on the computational design optimization of concrete mixes. They analyzed the typical problem of concrete mix design optimization and the available methods to address such a variable relationship. Those methods included linear combinations, statistics, machine learning, and physics. Their classification of concrete mix design methods was as follows (DeRousseau et al. 2018):

- *Prescriptive design* consisting of following a concrete design methodology step by step in order to obtain an acceptable mix. Standard mix design methods are the main example. Previous experience is incorporated in those methods, among the advantages of which are a high degree of certainty according to standard requirements with no need to make design decisions.
- *Experimental optimization* is normally based on a prior objective, for example, the maximization of compressive strength by varying the W/C ratio, aggregate proportions, and curing temperature. Some drawbacks of that methodology are that it requires many experiments whenever many variables are involved and any generalization of the results will normally be limited. It is mainly due to the specific characteristic and chemical composition of the concrete components that are used.
- *Optimization*, a method that consists of three-steps: problem formulation, objective modeling, and solving the concrete mix optimization problem. In the problem formulation step, all decisions, objectives, and constraints are defined. Mathematical expressions are applied to the modeling of the mix-design objectives, in order to relate the decisions (i.e. type and amounts of cement, aggregate, SCM, and admixture) with the objectives. Among other methodologies, some include linear relationships, LCA, statistical methods,

machine learning and physics-based models. Finally, mathematical optimization techniques are used, to solve the problem and to find the optimal concrete mix.

They highlighted that concrete optimization is achieved with the last-mentioned method in which decision criteria are to some extent personalized.

In this section, the available resources to optimize concrete mix design in a rational way are reviewed. The analysis is divided in two general groups:

- The standard mix design methods which involve the global design of concrete.
- The proportion of the concrete components from the perspective of maximum particle packing density. It involves the particle packing methods and the water and cement demand or paste theories. In addition, the prediction models of concrete strength are also reviewed.

2.7.1 Standard mix design methods

In the literature review, several mix-design methods from different countries were found. Most methods, were developed when SCM and admixtures were not extensively used in concrete. Therefore, their application is very limited to concrete produced with natural aggregates, OPC, and water.

In addition, all methods recommend adjustments to the final concrete dosage from trial batches, due to the high number of relevant variables and the influence of the source and the properties of the material in a concrete mix.

In 1983, the international Technical Committee RILEM TC 70-OMD compared the predictions of various design models for normal concrete from the compression strength and slump requirements. Surprisingly, the variability of the concrete mix proportion results was substantial, and even usable mix proportions were found. These finding may be explained, because the calibration of the models was based on the local materials (de Larrard 1999).

Some of the available methods are described and analyzed below.

2.7.1.1 US method (ACI 211)

The American Concrete Institute method (ACI 2002) is probably the most widely used method across the world for the design of normal concrete mixes.

The ACI 211.1-91 method provides an initial approximation to concrete components for normal, heavyweight, and mass concrete. The proportions must be adjusted to meet the requirements of each concrete mix and verified by preparing trial batches.

This method is based mainly on the works of Abrams and Power (de Larrard 1999).

Developed in 1919, Abrams' law relates concrete strength and the W/C ratio through the follow empirical equation:

$$f_c = \frac{K_1}{K_2^{\frac{w}{C}}} \qquad 2.5$$

where, f_c is the compressive strength of concrete, K_1 and K_2 are constants depending on the age, material, and curing conditions, W is the mass of free water, and C is the mass of cement per unit volume. The K_1 and K_2 values are calculated by linear regression on the log strength versus W/C ratio (Sear et al. 1996).

Power's law defines another relationship between the W/C ratio and strength (Abd 2014).

$$f_c = K_1 \cdot \left(\frac{W}{C}\right)^{-K_2} \qquad 2.6$$

where, f_c is the compressive strength, K_1 and K_2 are experimental parameters for a given age, and W/C is the water cement ratio.

The ACI method is applicable to cast-in-place construction applications. The concrete components involved are cement with and without other cementitious materials and chemical admixtures.

The following input data are needed (ACI 2002):

- Grading analyses of fine and coarse aggregate.
- Bulk specific gravities and aggregate adsorption rates.
- Relationships between strength and water-binder ratio, for available binder/aggregate combinations.
- Specific gravities of cement and other cementitious materials.
- Optimum combination of coarse aggregate to meet the maximum density.

This method assumes three premises: First, the workability depends on the water content and the maximum size of aggregate; second, the strength is only dependent on the water-cement ratio; and third, the bulk volume of coarse aggregate per unit volume of concrete depends on the maximum size of the coarse aggregate and the grading of the fine aggregate, expressed as the fineness modulus.

The method commences with the definition of the required concrete consistency (slump) according to the concrete application. Then, the amount of water is selected, which depends on the maximum size of coarse aggregate. The cement content is calculated from the W/C ratio, established as a function of the strength and the water content. The volume of coarse aggregate is then determined using the bulk volume and multiplying the value by a tabulated coefficient which depends on the maximum size of aggregate and the fineness modulus of the sand. Finally, the fine aggregate content is

given by subtracting the volume (or weight) of other components from the total volume (or weight) of concrete.

Limitations:

The water content is estimated by Caquot's[6] law and Lyse's[7] rules. However, the particle shape effect is not considered.

Concrete strength is dependent on the W/C ratio. However, if there are changes to the maximum aggregate size, granulometry, surface texture, shape, aggregate strength and hardness, and if there are different types of cement of different origin, and changes to air content and the use of additives, then different strengths can be generated with the same W/C ratio.

In the ACI method, the packing density of the aggregate is hardly considered (de Larrard 1999). The amount of sand is calculated by the difference between the total concrete volume and the rest of the constituents, which it means that it can only decrease, and the coarse/fine aggregate ratio will increase. Another drawback is that only two aggregate fractions can be used.

2.7.1.2 British Standard (BS) method (BRE 1997)

The Design of Normal Concrete Mixes was published by the Building Research Establishment Ltd. in 1997.

The method starts with the choice of the W/C ratio, on the basis of the concrete compression strength required for ages ranging from 3 to 91 days. The type of cement (Ordinary Portland cement, Rapid-Hardening Portland cement and Sulphate Resisting Portland cement) and the type of aggregate (crushed or uncrushed) are also considered in this selection process. Then, the water content is estimated. As with the ACI method, it depends on the maximum size of coarse aggregate, and the slump. In addition, the shape of the aggregate particles is also a factor in the BRE method. The cement content is calculated from the W/C ratio. The volume of aggregate is then determined, by subtracting the cement and water content from the fresh density of the concrete mix. The density is calculated from the specific gravity of the aggregate. The fine aggregate proportion depends on the aggregate maximum size, the slump, the W/C ratio and the amount of fine aggregate passing through a 0.6 mm sieve (BRE 1997).

The method differentiates between crushed and uncrushed aggregate, as the difference in behavior is quite significant. The grading of coarse aggregate is assumed to meet British standards, so it is ignored. The grading of fine aggregate is considered in the method as a factor that will affect the degree of concrete workability.

[6] Caquot's law claims that the porosity of a granular mix in controlled by its grading span.

[7] Lyse's rule assumes that the concrete workability is controlled by its water content.

Limitation:

Although the influence of the concrete constituents and ages over 28 days are considered when calculating compressive strength, neither will all cements, even in the same category, show the same strength development, nor will crushed aggregate make the same contribution to compressive strength.

F. de Larrard mentions in his book (de Larrard 1999), that the weakness of the British method is the absence of packing measurements on aggregate fractions.

2.7.1.3 Portland Argentine Cement Institute (ICPA)

The ICPA model was developed by the *Instituto del Cemento Portland Argentino* (Argentinian Portland Cement Institute).

The method starts by selecting the type of cement according to the strength (CP30, CP40 or CP50) and the slump. Then, the amount of air entrainment is chosen, depending on the maximum aggregate size. The aggregate proportion is determined by an optimized curve (for example, the Fuller curve) or an appropriate grain size defined by the standards. Having established the aggregate proportions, the fineness modulus is calculated. Afterwards, the water content is calculated, taking into account the slump and the finesses modulus. The W/C ratio is chosen according to the concrete compression strength required at 28 days. Some considerations are assumed when the aggregate is crushed instead of uncrushed. The cement content is calculated from the W/C ratio. Finally, the volume of aggregate is then determined by subtracting the cement, water content, and air content from the total volume of the mix (ICPA 2015). A web application for the method is available online[8].

Limitations:

As in the ACI method the W/C ratio is considered exclusively dependent on the expected strength.

One key point of the method is the consideration of aggregate packing density using optimization curves. Thus, the water content in this method will depend on the workability and total aggregate grading (fineness modulus) instead of considering only the maximum aggregate size, thereby providing a more accurate approximation.

The user has the possibility to select the optimization curves that will produce proportional differences according to the amount of material, and therefore in the final concrete properties.

[8] http://www.icpa.org.ar/publico/proghormigon/index.html

2.7.1.4 Indian method (IS 10262:2009)

The Indian standard provides a guideline for proportioning concrete mixes to meet the requirements for compressive strength, workability, and durability.

In this method, the first step is the selection of the compressive concrete strength. Then, the W/C ratio is selected from the established rules on the minimum content of cement, maximum water-cement ratio and minimum grade of concrete for different exposures. Selection of the water amount depends on the maximum size of coarse aggregate, the slump and the aggregate shape. The cement content is calculated from the W/C ratio. The volume proportion of coarse aggregate is then determined according to the maximum aggregate size and the different zones of fine aggregate. A combination of different coarse aggregate can be considered. Finally, the fine aggregate content is established by subtracting the volume (or weight) of other components from the total volume (or weight) of the concrete (IS 10262 2009).

In conclusion, there is no universal method for concrete mix design, because of differences attributable to regional climate, exposure and local materials. In general, the current concrete mix-design standards and methods are limited to the following aspects:

- Aggregate optimization methods.
- The optimization of SCM.
- Modern superplasticizers and air-entraining admixtures.
- Environmental and economic assessment.

In addition, the relations of cause and effect between the properties of the components and the characteristics of the concrete are too complex for them to be all considered within one single model.

2.7.1.5 EHE Method

According to the Spanish structural concrete instruction EHE-08 (EHE 2008), concrete will be dosed in accordance with the methods deemed appropriate, subject to the following limitations:

- The minimum quantity of cement per cubic meter of concrete shall be as laid down in EHE-08, 37.3.2 (EHE 2008) section.

- The maximum quantity of cement per cubic meter of concrete shall be 400 kg. In exceptional cases, subject to experimental justification and express authorization from the Works Management, this limit may be exceeded.

- A W/C ratio greater than the maximum established in the 37.3.2 section of the EHE-08 (EHE 2008) shall not be used.

This dosage shall take into account not only the mechanical resistance and consistency to be obtained, but also the type of environment to which the concrete will be subjected, due to the possible risk of deterioration of the concrete or the reinforcements due to attack by external agents.

2.7.2 Particle packing optimization methods

Since aggregate occupies 60-80% of total concrete volume, its function is fundamental in both fresh and hardened concrete. Furthermore, optimizing the aggregate proportions for a lower void content, to achieve maximum packing density can increase concrete strength and durability.

Particle packing density methods can be used in concrete mix design with the aim of minimizing the voids between particles, in order to reduce the amount of paste. Thus, the reduced amounts of cement in the concrete mix contribute to environmentally friendly and low-cost concrete.

Packing density has been defined by several authors as the ratio of solid volumes to the bulk volume of solid particles (Toufar et al., 1976; Quiroga et al., 2004)

There are several methods to achieve an optimized aggregate proportion, from the most traditional, adjusting the grading size to an ideal grading curve, to complex models. Traditional methods such as Fuller's (Fuller & Thompson 1907), Bolomey (Bolomey 1935) and Funk and Dinger (Funk et al. 1980) have been used for many years for concrete dosages made of natural aggregates. Other models have also taken into account aggregate geometry and the particle interaction effect (wall and loosening effect) of binary and multicomponent mixes, such as the Compressible Packing Model (Alexander & Mindess 2005) development by F. Larrard, which has been used to predict the packing density of natural and recycled concrete aggregates.

Particle packing density can be categorized as follows:

- Optimization curves (continuous methods)
- Particle Packing Model (discrete methods)
- Computational models

Other authors classified the particle packing model as either a continuous model or a discrete model (Pradhan et al. 2017). Alternative options also exist.

2.7.2.1 Optimization curves

Optimization curves are continuous particle size distributions based on geometrical considerations. The aim of theses curves is to lead to the highest packing density, by optimal particle-size combination. The ease of use and the limited amount of input parameters (mainly particle size distribution) make these methods very practical.

Feret (Feret 1892) was one of the first researchers to recognize the influence of aggregate choice on concrete strength. Subsequently, several research projects were conducted to find the ideal grading curve, among which Fuller (Fuller & Thompson 1907), Bolomey (Bolomey 1935), Andreasen and Andersen (Andreasen & Andersen 1930), and Funk and Dinger (Funk et al. 1980). At the same time, in 1929, Furnas (Furnas 1929), presented the first analytical packing model to predict the void ratio of a dry mixture.

The best-known curve that is still in use today was developed by Fuller (Fuller & Thompson 1907).

The major disadvantage of these models is that they make no distinction between differences relating to particle shape, surface texture, interaction between particle and other factors, that can affect compaction and packing.

The Fuller curve, also known as the Gessner parabola is defined by the following equation:

$$P(d) = \left(\frac{d}{d_{max}}\right)^{q} \qquad 2.7$$

where, P is the fraction that can pass the sieve with an opening d, dmax is the maximum particle size, and q is 0.5 of the Fuller curve. Although, Fuller uses q=0.5, in asphalt concrete mix design a value of 0.45 is preferred.

The Fuller curve is suitable for continuous grading of aggregate ranging from 250 µm to the maximum size. It is not therefore useful for concrete made with gap-graded aggregate, self-compacting concrete (SCC), and high-strength concrete where fines size are commonly used (Ghasemi 2017).

In 1930, Andreasen and Andersen (Andreasen & Andersen 1930) sought to improve this curve, including an experimental factor, “q”, which depends on the particle characteristics. They suggested using values for the q-parameter that ranged between 0.33-0.50 depending on the particle characteristics. Thus, the ideal curve for an angular coarse particle will be better suited to a lower “q” value, because finer aggregate would be needed to fill the voids (Fennis & Walraven 2012).

The A&A (Andreasen and Andersen) equation, which assumed the smallest particle as infinitesimally small, was modified in 1980 by Funk and Dinger (Funk et al. 1980), who considered the smallest grain in the curve equation:

$$P(d) = \left(\frac{d - d_{min}}{d_{max} - d_{min}}\right)^{q} \qquad 2.8$$

They proposed, for optimum packing, a q value of 0.37. However, that value can change depending on the type of aggregates (roundness or crushed), the mother rock origin or even the required workability. Thus, to select a suitable q-factor range, the workability

requirements of the concrete mixture must be considered. The smaller q values will provide better workability, because of the higher volumes of fine particles. In contrast, higher q-factor values should be used to achieve a concrete mix with a zero-slump. For example, a q value of 0.2-0.30 is suggested for high-performance concrete.

As presented in Fig. 2.8 some packing curves are shown for a maximum particle size of 32mm and a minimum particle size of 63 μm (Fennis 2009a).

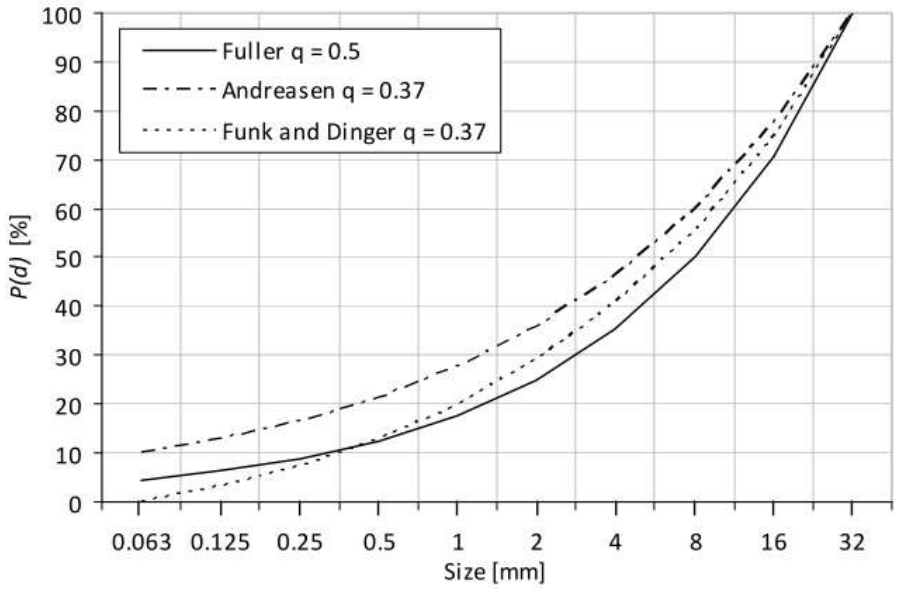

Fig. 2.8. Fuller, Andreasen and Funk and Dinger packing curves for a maximum particle size of 32mm and a minimum particle size of 63 μm (Fennis 2009a).

In 1990, Zheng et al. (Zheng et al. 1990) attempted to account for the shape factor by determining q as the average of all q-values for each class with varying particle shapes. Other authors optimized their concrete mixtures, by adjusting the q factor, as with the Funk and Dinger model, based on experimental results and the required workability.

In conclusion, there is no consensus on the q value that will yield the optimal packing density.

2.7.2.2 Particle packing models using discrete methods

The aim of packing models is to provide the aggregate proportions that will yield dense packing. However, as previously mentioned, the maximum packing density can result in less workable mixtures. Therefore, the optimum packing density will depend on the concrete application and will not be equal to maximum packing.

Analytical particle packing models consist of mathematical equations that are used to predict the geometrical interaction between different particle sizes.

Currently, there are numerous discrete particle packing models available to calculate packing density. Some examples are as follows: Furnas model, Aïm model, Modified

Toufar model, Dewar model, Linear Packing Model, Solid Suspension Model (SSM), Compressible Packing Model (CPM), and 3-Parameter Packing Model (3-P). These methods (see respective references at bibliography section) assume that each size class contributes to the mixture of particles of various size classes to achieve the maximum packing density.

The first packing density model was developed by Furnas (Furnas 1929). Most of the discrete models are based on the equations that form this model, which are basically related to particle geometry (Alexander & Mindess 2005). The fundamental assumption is that each class of particle will pack to a maximum density within the available volume.

The Furnas model and the Aïm and Le Goff model are only valid for two mono-sized groups of particles and assume no interaction between particles and spherical particles. Both models assume that the smaller-sized particles will fill up the voids between the larger size particles without disturbing the packing of the larger ones. Pradhan (Pradhan et al. 2017) indicated that both models are unsuitable for concrete mixes, because they assume spherical particles and any interaction effects are not computed by the models.

Several authors have sought to improve the models, by considering particle interaction and multicomponent mixtures. In 1930, Westman and Hugill (Westman & Hugill 1930), developed an algorithm to consider multiple particle groups. In 1969, the packing model developed by Powers took account of the loosening effect. After that, Aïm and Goff (Aïm & Goff 1967) and Toufar considered the wall effect. In addition, Toufar extended the binary model to form a ternary mixture, which was simulated as a binary model with the binary mixture of coarse and medium size aggregate.

The advanced packing density models (de Larrard 1999) included both the wall effects, and the loosening effects, as well as interactions. De Larrard postulated different approaches for concrete design: the Linear Packing density Model (LPM), the Solid Suspension Model (SSM), and the Compressive Packing Model (CPM) (de Larrard 1999).

Some authors attempted to improve the CPM. In 2009, Fennis (Fennis 2009a) presented the Compaction-Interaction Packing Model (CIPM), which processes particle interactions of <125 μm, computing the Vander Waal forces and electrostatic charges. In 2013, the 3-parameter packing model included the wedding effect (Kwan et al. 2013) and the 4-parameter Compressible Packing Model, developed in 2017 (Roquier 2017) presented a new theory on the wall effect and the loosening effect. This last-mentioned method requires additional inputs, among which, the characterization of shape, angularity and the surface texture to the packing density prediction, although it was not developed for concrete mixtures.

Particle diameter is an input parameter in all discrete particle packing density model and therefore plays an important role. Various authors have assessed different methods for the determination of particle diameters, although there is no agreement. For example,

Goltermann et al. (Goltermann et al. 1997) calculated the characteristic diameter according to the Rosin-Rammler distribution (Vesilind 1980), considering a cumulative probability of 0.37. In contrast F. Larrard (de Larrard 1999) considered the average diameter as the geometric mean of maximum and minimum particle size, while other researchers simply accounted for the mean diameter, corresponding to 50% of the particles retained after sieving. Using the Rosin-Rammler distribution, the assumption of monosize and spherical particles can be overcome. The second approximation can be sufficiently accurate when a narrow particle size grading is considered.

A review of the literature referring to packing density models that are applied to concrete design is discussed below:

Moutassem (Moutassem 2016) assessed nine Packing Density Models for dry mixtures made with natural crushed coarse aggregate (CA) (max. size 19mm) and fine aggregate (FA) (fineness modulus of 2.69). The experiments were performed with three compaction methods, loose, rodding and vibration. Furthermore, packing density measurement of every size was done, to obtain the required input data and to apply the CPM method. The results showed that only three methods (Compressible Packing Model (CPM); Modified Toufar Model (MTM) and Theory of Particle Mixtures (TPM)) generated accurate predictions of the Packing Density (PD) of concrete aggregate. Particularly, the CPM method using the characteristic diameter had the best results, compared to the experimental results, even better results that the CPM, considering the aggregate grading that required more computational work. Furthermore, as a consequence of his study, F. Moutassem proposed the inclusion of one of the PD methods in the ACI 211 methodology, as a means of considering the diversity of aggregate properties for selection of the proportion of aggregate to include in the mix.

Ghasemi researched the particle packing accuracy of three packing models (Toufar, CPM and 4C) over aggregates from three different sources. Only loose packing methods were used for the test included in his Bachelor's degree thesis (Ghasemi 2017). Although within CPM requirements, a wide range of fractions (0-2mm, 0-4mm, 4-8mm and 8-16mm) were used to prepare the binary mixes. Both continuous grading and gap-graded mixes were tested.

In a Master's degree thesis, Moini (Moini 2015) studied the packing density of 40 natural aggregate blends from Wisconsin, combining both computational and packing models (Toufar and Aïm). The experimental packing density was performed with two packing methods, one for loose and the other for compacted packing. The tests were performed for binary and ternary aggregate mixes. As well as comparing the experimental and modeled aggregate packing density, he studied the effect of the aggregate proportion on concrete compressive strength, keeping the paste content and aggregate volume and only modifying the aggregate proportion. The results showed that the maximum

aggregate compaction was not equatable with maximum compressive strength, probably due to poor optimization of cement paste resulting in unfilled aggregate voids.

Fennis (Fennis 2009a) developed an Ecological concrete mix-design method by particle packing optimization in his thesis. He used the CPM method and developed a new method named Compaction-Interaction Packing Model (CPIM), in which the inter-particular forces of aggregates <125 µm were considered. The loose packing method was used to measure the packing density of narrow aggregate fractions with a diameter higher than 125 µm and, the mixing energy test packing method (wet method), was applied to particles smaller than 125 µm. Although the maximum packing density of the particles mix was not directly related to the compressive strength, the mortar test results reflected the distance between the cement particles and the concrete compressive strength that was good. This factor depends on the maximum packing density, the amount of water, and the volumetric fraction of the cement particles.

Amario et al. (Amario et al. 2017) analyzed the possibility of applying the concrete mixture proportion system developed by Larrard for proportioning concrete mixtures made with recycled concrete aggregates. To do so, they measured the packing density according to CPM methodology (Compression 10KPa + vibration) for mono-size fractions from natural sand, granite coarse aggregate, and recycled concrete aggregate, and they used the BétonlabPro software to obtain the aggregate proportion with no experimental verification of aggregate packing density. Their conclusion was that the system applying CPM methodology, with which the proportions of each component in the concrete mix were assigned, could be applied to the mixture proportion of Recycled Aggregate Concrete (RAC).

Sunayana et al. (Sunayana & Barai V. 2017) applied particle packing methods to the proportion of RAC incorporating fly ash as partial replacement of cement. The experimental packing density was determined by combining two different coarse aggregate sizes. Once the maximum packing density of both fractions had been found, this proportion was mixed with the fine aggregate following the same steps. The experimental packing density was compared to the theoretical model (Modified Andreasen curve and the CPIM), obtaining a good fit when the Modified Andreasen curve was considered with a q coefficient value of 0.35. Compared to the concrete dosage using the PPM method and the conventional method (according to Indian Standard code method), a reduction of up to 28% of cement was observed.

Current studies (Amario et al. 2017; Pepe 2014) have analyzed the feasibility of a semi-empirical CPM model (de Larrard 1999) to predict the compression strength of recycled aggregate concrete resulting in high correlations between CPM predictions and experimental results.

Packing density was applied by Sunayana et al. (Sunayana & Barai 2017) for proportioning recycled aggregate with fly ash. They compared the conventional methods, specifically modified Andreasen with the CIPM. The results showed comparable results with the conventional mix design method, in terms of hardened concrete at the same water-binder ratio. They concluded that the PPM mix design method was useful to design concrete incorporating 100% of recycled aggregate and up to 30% of Fly ash.

These models are usually based on assumptions which can conflict with experimental aggregate packing results. The main assumptions are (Moini 2015):

- The aggregate size is a perfect disk or a perfect sphere.
- The aggregates are mono-size.
- Fine and coarse aggregates differ in their characteristic diameter.

Generally, the input aggregate parameters of these theoretical models are particle size distribution and packing density.

A summary of whole collected methods is included in Table 2.8 and Table 2.9.

Table 2.8. Review of papers comparing theoretical packing density models and experimental packing density

Refence	Mix type	Aggregate	Compaction method	Model tested	Test level	Diameter
(Moutassem 2016)	Binary	CA (Crushed) FA	Dry (Loose, Rodding and Vibration)	FM, AGM, MTM, LPM, MLPM, MPM, LMPM, TPM, CPM	Aggregates	Characteristic diameter
(Ghasemi 2017)	Binary	CA and FA (Natural, crushed and cubic crushed)	Dry (Loose)	Toufar (MTM), CPM and 4C	Aggregates	Unspecified
(Moini 2015)	Binary (MTM) and Ternary (AGM)	CA, MA and FA (Limestone and glacial)	Dry (Loose and Compacted-Vebe Consistometer)	Toufar (MTM), Aim model (AGM)	Aggregate and concrete	Characteristic diameter
(Fennis 2009a)	Binary and ternary	MA and FA (rounded river sand and gravel)	Dry (Loose) Wet (Mixing energy test)	CPM	Aggregates, cement paste and mortars	Characteristic diameter

Refence	Mix type	Aggregate	Compaction method	Model tested	Test level	Diameter
(Amario et al. 2017)	Binary and Ternary	Natural FA, Granite CA and recycled concrete CA	Dry (Compression 10KPa and vibration)	CPM	Aggregates and concrete	According to the CPM method
(Sunayana & Barai V. 2017)	Binary and Ternary		Loose	Modified Andersen curve and CIPM	Aggregate and concrete	Unspecified

Table 2.9. Packing model chronology. Adapted from (Moutassem 2016)

Model	Definition and source	Type of particle interaction	Year
FM	Furnas Model (Furnas 1929)	Spherical, no interaction, 2 particle sizes	1929
AGM	Aim and Goff Model (Aïm & Goff 1967)	Spherical, wall effect, 2 particles sizes	1967
MTM	Modified Toufar Model (Toufar et al. 1976)	Multicomponent mixtures	1976
LPM	Linear Packing Model (Stovall et al. 1986)	Polydisperse granular mixtures, Wall effect, Loosening effect	1991
MLPM	Modified Linear Packing Model (Yu et al. 1996)	Wall effect, Loosening effect	1996
MPM	Mixture Packing Model (Yu & Standish 1991)	Wall effect, Loosening effect	1991
LMPM	Linear-Mixture Packing Model (Yu & Standish 1991)	Wall effect, Loosening effect	1991
TPM	Theory of Particle Mixtures (Dewar 1999)	-	1999
CPM	Compressible Packing Model (de Larrard 1999)	Wall effect, Loosening, Compaction index (K)	1999
CIPM	Compaction-Interaction Packing Model (Fennis 2009a)	Wall effect, Loosening effect	2009
3-P	3-parameter Packing model (Kwan et al. 2013)	Wall effect, loosening effect, wedging effect	2013
4-parameter CPM	4-parameter Compressible Packing model (Roquier 2017)	Loosening effect, wall effect, compaction index, critical cavity-size ratio	2017

2.7.2.2.1 Compressible Packing Model (CPM)

CPM model is an extension of the LPM. The innovation of the CPM was the distinction between actual packing density, Φ, and virtual packing density, β. Furthermore, the CMP model can optimize any number of individual aggregate fractions of a mono-size distribution (narrow range of particle size distribution).

The virtual packing density is defined as the maximum packing density of a mixture when each particle retains its original shape and the particles are placed one by one. Thus, the virtual packing density of a mix of mono-size spheres is equal to 0.74, while the physical packing density that can be measured in a random mix is closer to 0.60/0.64, depending on compaction (de Larrard 1999). The actual packing density depends on the placing process of the mix. Therefore, the CPM model relates the actual packing density and the virtual packing density through a compaction index, K, which is a scalar parameter that reflects the energy of the compaction process.

The K values for the different packing process are shown in Table 2.10.

Table 2.10. K values for the different packing processes (de Larrard 1999).

Packing process	Pouring	Sticking with a rod	Vibration	Vibration + compression 10kPa	Proctor test	Virtual
K Value	4.1	4.5	4.75	9	12	∞

The CPM model assumes two interactions between binary mixtures: the wall effect and the loosening effect. Two coefficients, a_{ij} and b_{ij}, were included in the CPM, to take into account the interactions (see equation 2.10 and 2.11). These factors are constants for a given size-ratio.

The wall effect is produced when the small particles are so close to a large particle or the container wall that they cannot reach their maximum packing density. And the loosening effect is generated when the smaller particles are too large to be located within the interstices of the large particles and the packing of large particles is disturbed (see Fig. 2.9).

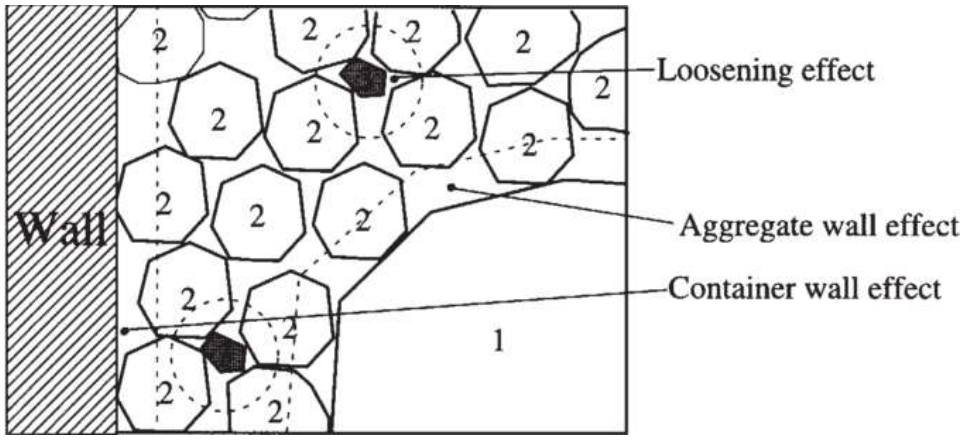

Fig. 2.9. Aggregate wall and loosening effect and container wall effect (de Larrard 1999).

The general equation of the model for a mixture containing n-size classes with a dominant category is presented below

$$\gamma_i = \frac{\beta_i}{1 - \sum_{j=1}^{i-1}\left[1 - \beta_i + b_{ij}\beta_i(1 - \frac{1}{\beta_j})\right] r_j - \sum_{j=i+1}^{n}\left[1 - a_{ij}\beta_i/\beta_j\right] r_j} \quad 2.9$$

The coefficients a_{ij} and b_{ij} represent the loosening effect and the wall effect, respectively.

$$a_{ij} = \sqrt{1 - \left(1 - \frac{d_j}{d_i}\right)^{1.02}} \quad 2.10$$

$$b_{ij} = 1 - \left(1 - \frac{d_i}{d_j}\right)^{1.50} \quad 2.11$$

The packing density is indirectly determined from equation 2.12.

$$K = \sum_{i=1}^{n} K_i = \sum_{i=1}^{n} \frac{\frac{r_i}{\beta_i}}{\frac{1}{\Phi} - \frac{1}{\gamma_i}} \quad 2.12$$

In a mono-size mix, the equation is simplified as follows:

$$\beta = \left(1 + \frac{1}{K}\right) \cdot \Phi \quad 2.13$$

2.7.2.3 Computational models

In the analytic packing density methods, the shape effects and the packing method are as yet not well established and experimental methods are very time-consuming. Computer simulation is therefore seen as a future solution (He 2010).

The computational packing density models can be classified into two general groups (He 2010):

- Random sequential addition (RSA): an algorithm is used that randomly places particles within a mold. In the RSA model, the particles are only placed and any flocculation, agglomeration, and clustering problems are overlooked. It is not valid for real concrete packing density, because the particle interaction is missed.
- Concurrent algorithm-based simulation (CAS) and discrete element method (DEM): both methods solve the limitations of the RSA system. Although the DEM algorithm is normally used to model particle interaction, other algorithms are also used to resolve the interaction problems.

The Table 2.11 includes some of the particle packing systems.

Table 2.11. Computational Particle packing systems (He 2010).

References of models	Shape of particles	Classification	Application
(Wittmann et al. 1984)	Circles, polygons, arbitrary, 2D shapes	RSA	Concrete
(Cooper 1988)	Spheres	RSA	Physics
(Evans & Ferrar 1989)	Overlapping spheres	RSA	Fibers
(van Breugel 1997)	Spheres	RSA	Cement
(Coelho et al. 1997)	Spheres, ellipsoids	RSA	Physics
(Sherwood 1997)	Spheroids	RSA	Physics
(Lin & Ng 1997): ELLIPSE 3D	Ellipsoids	CAS/DEM	Soil
(Thomas & Bray 1999)	Disk clusters	CAS/DEM	Physics
(Stroeven & Stroeven 1999)	Spheres	CAS/DEM	Concrete
(Kochevets et al. 2001)	Spheres	CAS/DEM	Aerospace
(Jia & Williams 2001): DigPac	Pixel or voxel based shapes	CAS/DEM	Materials
(Fu & Dekelbab 2003)	Spheres	CAS/DEM	Concrete
(Williams & Philipse 2003)	Spheres, spherocylinders	CAS	Physics

As an example, the SPACE (Stroeven & Stroeven 1999) system consists of a dynamic simulation capable of predicting the maximum packing of aggregate at a meso-level and the particle density distribution of cement and mineral admixtures at a micro level (ITZ). Particle shape is not included in the method.
Although computational packing is a promising alternative to concrete design through packing density methods, further research on the way particle shapes can interlock is considered necessary. In addition, the number of variables affecting packing and the number of particles that should be considered by the models, requires lengthy computation times.

2.7.2.4 Fine particle packing and wet methods

Some authors have concluded that aggregate combinations with higher packing density alone may not give the maximum density when water and cement are added to make concrete (Fennis 2012). It will depend on the voids to be filled by the paste.

Hence, Li et al. recommended the use of wet packing density methods, to obtain a higher packing density of fines, SCM, and coarse aggregate (Li & Kwan 2014) and Li et. al 2018).

Although dry packing density of particles is standardized by loose packing, there is no recommended universal wet packing density method. Wet packing methodologies were analyzed by Fennis (Fennis 2009b), in order to determine the maximum packing density of cement pastes or micro powders material. The methods under analysis were as follows:

Table 2.12. Wet packing methodologies.

Method	Author	Brief description
Water demand-France	(de Larrard 1999)	Packing density is calculated through the minimum water demand of 350g of powder to form a thick paste.

Method	Author	Brief description
Water demand-Germany	(Puntke 2002)	A method based on searching for the saturation point by carefully adding water to 50 g of powder. The saturation point is reached when the powder surface levels off and starts to shine.
Water demand by determining mixing energy	(Marquardt 2002)	This method predicts water demand by the differences in internal pendular bond strength. It measures the power used during the process of mixing powder with water.
Proctor test	(UNE-EN 13286-2 2004)	A method used for unbound and hydraulically bonded mixtures in road construction. Its main limitation for cement packing measurement is the need to dry the powder to determine the water content.
Centrifugal consolidation	(Miller et al. 1996)	In this method, a known paste composition is introduced in a centrifugal tube and the excess water remaining on the surface is measured, in order to calculate the water needed to fill the powder voids.
Water demand-Japan	(Okamura & Ozawa 1995)	Minimum water demand from a ratio established by mixing and testing pastes with a higher water/powder ratio than the water demand.
Rheology measurements	(Mansoutre et al. 1999)	The packing density is indirectly determined by measuring the viscosity and fitting the results to the Krieger-Dougherty equation

The aim of these methods is to determine the minimum amount of water necessary to fill the voids between particles in the packing process. In some methods, such as water demand-France and water demand-Germany, the minimum water demand of the paste is calculated, by slowly adding water until all the voids are filled and a thick homogenous paste is achieved. In contrast, the water demand-mixing energy method assumes that the internal pendular bond strength can be determined by measuring the mixing energy. Thus, a constant water volume is supplied over a powder volume in a mortar mixer, while the voltage, electricity and the phase shift between the voltage and the electricity consumption of the mixes are registered. In this method the water demand of the mix is reached when the maximum power is measured. Among other methods, water demand-Japan is used to determine the minimum water from the water/powder ratio by mixing and testing paste with a water/powder ratio that is higher than the water demand.

The water demand method developed by Larrard and Puntke depends on the perception of the technician. In a proctor test, drying is necessary to determine the water content, therefore this method is not suitable for determining the packing density of cement.

However, none of the above methods are capable of verifying that the maximum packing density has been achieved and that no excess amount of water still surrounds the particles. Fennis concluded (Fennis 2009a) that the method with the highest

reproducibility for the determination of the maximum packing density is the water demand method by measuring the mixing energy.

Further detailed information can be found in (Fennis 2009a).

2.7.3 Paste demand

Considering the hypothesis that particle packing density will have an important effect on concrete performance, once the maximum packing of the solid particle of concrete is known (and consequently the voids to be filled by water or cement paste), the next step will be to determine the excess amount of paste and water that will be needed to supply flowability and workability to the concrete mix.

Many authors claim that compressive strength is mainly determined by the W/C ratio, and in section 2.7.3.1 the most relevant predictions models are discussed, in order to determine the cement content. Moreover, recent studies on water, paste or mortar layer theories (see section 2.7.3.2) have focused on finding the effect that the thickness of those layers will have on the rheological properties of pastes, mortars and concrete and the use of those parameters to determine the inputs for concrete and mortar mix design (Li & Kwan 2013; Li & Kwan 2011; Zhang & Panesar 2017; Kwan & Li 2012; Ghasemi et al. 2019a)

2.7.3.1 Prediction models of concrete compressive strength

Many models to predict the compressive strength of concrete have been developed throughout history. However, the current solutions to predict the compressive strength of concrete are limited, as so many variables can influence concrete strength. In addition, most models are focused on paste quality, underestimating the influence of aggregates.

The compressive strength of a concrete mix can be increased in a variety of ways. Some of most common practices are as follows:

- Increasing the amount of cement.
- Adding SCMs in an effective proportion.
- Decreasing the amount of water.
- Adding proper amounts of admixtures.
- Improving particle size distribution, increasing particle density.

As Brito et al. observed (Brito & Kurda 2018) in their research on aggregate properties that influence the compressive strength of concrete, compressive strength mainly depends on paste quality, although aggregate properties are also important.

Porosity relates to both, paste and concrete and is a relevant parameter in concrete compressive strength. The hydrated product of cement paste and porosity depends on

the chemical and physical properties of cement compounds. In a concrete mix, porosity is related to the maximum size of aggregate, the particle size distribution, the mixing procedure, placement, and compaction.

Concrete strength can also be indirectly affected by aggregates. Both shape and surface texture will affect the ITZ zone where the cement paste bonds with the aggregate.

Many authors have reported that the ITZ zone is a failure zone for most concretes with aggregate strengths that are higher than their cement paste strength. The failure occurs because the W/C ratio is higher in this zone, due to capillary absorption between the cement paste and the aggregates, which is affected by water absorption and the density of the concrete components (Brito & Kurda 2018).

The equations of some of the most relevant models are included in Table 2.13.

Feret (1982) was the first to develop a model capable of predicting the compressive strength of concrete. He considered the cement-to-paste ratio and the amount of air in the mix.

Abram's law (equation 2.5) was limited to normal structural concrete with maximum aggregate sizes of 38 mm and a W/C ratio greater than 0.4. Duff Abrams in 1919 assumed that the effect on concrete strength of the aggregate properties was negligible.

The applicability of all these models are limited, because calibration factors, which depend on both the properties and the nature of the concrete components, must be defined.

In another study (Moutassem & Chidiac 2016), several concrete strength prediction models were assessed. The authors concluded that although most model predictions are acceptable, the Average Paste Thickness (ATP) model provided the most accurate compressive strength results at 28 days. The W/C ratio was the most influential parameter for concrete compressive strength, which explained why most models were capable of predicting compressive strength. It should be also mentioned that only concrete manufactured with common OPC and crushed coarse aggregate were analyzed.

In that model, concrete is considered as a mixture of aggregate and cement paste. Thus, the paste needed in the concrete mix is the amount of paste needed to fill the voids between aggregates and an additional amount of cement paste needed to lubricate the concrete mixture.

(Chidiac et al. 2013) combined four models for the prediction of the compressive strength of concrete: the cement hydration model, average paste thickness (APT), the bond strength model, and the cement paste strength model. Thus, cement type and hydration degree, aggregate type and proportion (packing density), paste to aggregate bond strength, and air content were all considered. The authors claimed that the model

could predict compressive strength in an accurate way and that it could be used to design concrete mixtures, in order to achieve the strength requirements.

The APT model takes account of the chemical properties of the cement, bonding strength between paste and aggregate, cement properties and strength, degree of hydration, the amount of water filling the capillary pores, aggregate properties and proportions, porosity, age, and air entrainment. The APT model therefore incorporates the cement hydration model.

In Table 2.13 some of the compressive strength models are included. More detailed information on each one can be found in (Moutassem & Chidiac 2016).

Table 2.13. Equations to predict the compressive strength of concrete mixes

Feret (1892)	$f_c = K_1 \left(\frac{V_c}{V_c + V_w + V_a}\right)^{K_2}$	2.14
Abrams (1919)	$f_c = \frac{K_1}{K_2^{\frac{w}{c}}}$	2.15
Powers (1960)	$f_c = K_1 \cdot \left(\frac{w}{c}\right)^{-K_2}$	2.16
Powers (1960)	$f_c = K_1 \cdot (X)^{K_2} = K_1 \cdot \left(\frac{0.66\alpha}{\frac{w + V_a}{c} + 0.32\alpha}\right)^{K_2}$	2.17
Popovics (1985)	$f_c = K_1 \cdot \left(\frac{c}{w}\right) + K_2 \cdot 10^{c.V_a}$	2.18
Popovics (2008)	$f_c = \frac{K_1}{K_2^{(\frac{w}{c} + Ea)}} \cdot 10^{c.V_a}$	2.19
de Larrard (1999)	MPT=$d_{max}\left(\sqrt[3]{\frac{\phi_{max}}{\phi}} - 1\right)$	2.20
de Larrard (1999)	$f_c = KR_{c28}(0.2\,[C_3S] - 1.65)\left[K_1 log\left(\frac{t}{28}\right) + \left(\frac{V_c}{V_c + V_w + V_a}\right)^{K_2}\right] \cdot MPT^{K_3}$	2.21
Chindiac (2013)	$f_c(t) = \begin{cases} 0 & \alpha(t) \le \alpha_{cr} \\ KR_{c28} \cdot \left(\frac{APT}{D}\right)^{K_1} \cdot K_2^{\frac{w+V_a}{K_3}}(\alpha(t) - \alpha_{cr}) & \alpha(t) > \alpha_{cr} \end{cases}$	2.22

2.7.3.2 Water/paste/mortar thickness layer theories

Over recent years, water/paste and mortar thickness layer theories have been related in several published papers, to describe ways of controlling the flow behavior of mortars and concrete. Flowability not only depends on the water content or the water cement ratio of a mixture, but it also depends on particle packing and the fineness of the particles, as mixtures with the same workability can have different water content or W/C ratios. So flowability will depend on the characteristics of the components (Ghasemi et al. 2019a). All the dependent factors of the concrete and mortar workability (water

content, packing density and specific surface area) are included in the water film thickness factor (Li et al. 2018).

Ghasemi et al. studied the possibility of establishing concrete and mortar flowability by measuring the thickness of the water films that cover granular components. They considered concrete as two separate phases, all the granular constituents (solids) and the water.

The thickness of the layer of water, paste or mortar (WFT, PFT, MFT) around a particle, which will depend of the Specific Surface Area (SSA) of the particles (see section 2.7.3.2.1), was calculated with the standard method from the maximum packing density of the particles (see Fig. 2.10).

$$\delta = \left(\frac{W_{excess}}{A_m}\right) \qquad 2.23$$

where, δ is the average Water Film Thickness (WFT) of all the particles, A_m is the average SSA, and W_{excess} is the excess of water once all the matrix voids have been filled by water. The W_{excess} value can be calculated from the packing density and the water-to-solid volume ratio.

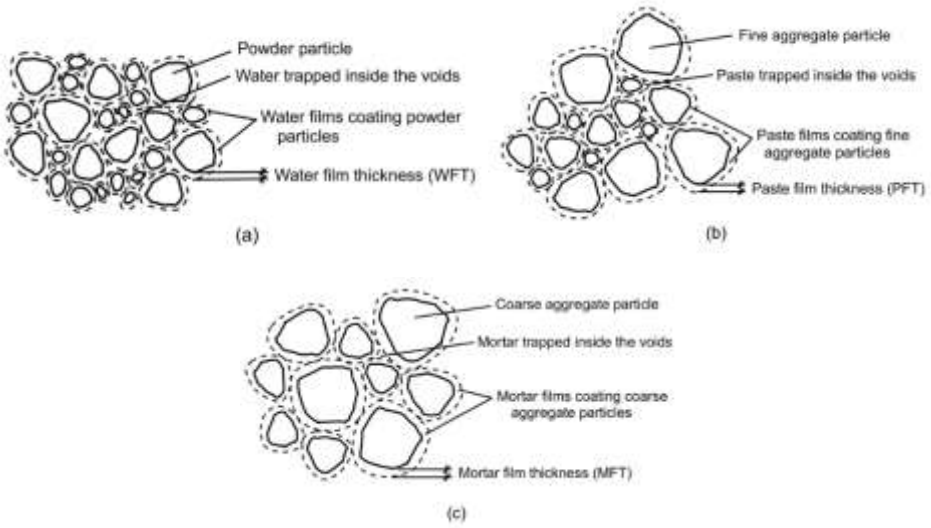

Fig. 2.10. (a) Water film thickness (WFT); (b) Paste film thickness (PFT); (c) Mortar film thickness (MFT) (Ng et al. 2016).

They calculated the water needed to fill the voids between the particles in terms of particle packing density (calculated by loose experiments following ASTM standards and using the modified Toufar model). This water content provides no slump to the concrete mix. They likewise calculated the water excess which is divided into two-steps: one is the excess of water required to reach the start point to fluid (onset point) and the other one is the excess required to achieve the desired slump. The excess water was calculated on the basis of the specific surface area and experimental testing (Ghasemi et al. 2019a), as shown in Fig. 2.11.

Table 2.14. Considerations taken by Ghasemi to perform the methodology (Ghasemi et al. 2019a).

Packing density	Toufar model works well.
	Fine particle packing density can be measured through dry packing. (The forces interacting between fine particles are neglected).
SSA	The specific surface area of the particles can be successfully calculated based on the particle size distribution curve and assuming identical dodecahedra and cubical shapes for natural and crushed aggregates respectively.
Water film thickness	The water film thickness is equal for particles of different sizes.
Distribution of particles	All particles are perfectly blended with no segregation or agglomeration effects.

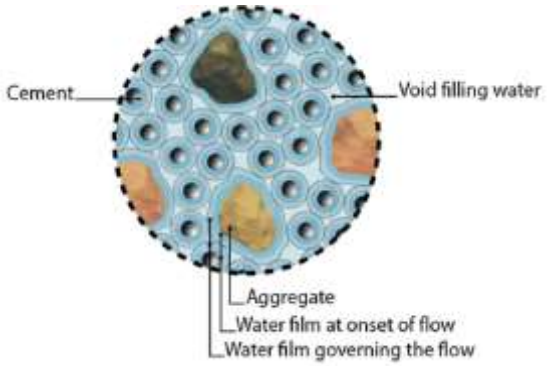

Fig. 2.11. Schematic representation of the water functions in a concrete mix. Source (Ghasemi et al. 2019b)

(Zhang & Panesar 2017) developed a new method with no need for experimental tests to determine the particle packing density, due to the disadvantages of calculating the packing density to obtain the WFT. It is based on the packing of spherical particles and it assumes that the voids between particles will all be filled when the particle surfaces have all entered into contact with water.

Li et al. (Li et al., 2013) analyzed the effect of WFT and PFT in concrete dosages. They tested the slump-flow, strength, and packing density of different concrete mixes, modifying the W/C ratios, paste volume and fine to total aggregate ratios. They concluded that both factors, WFT and PFT, can influence the concrete mix design. In addition, they developed two graphics for concrete mix design showing strength and concrete flows, from which the need for both WFT and PFT could be estimated (Li & Kwan 2013).

They assumed that aggregates smaller than 75 µm were included in the paste as it became inseparable after the concrete mix. The packing density was measured with the wet method (Kwan et al. 2012). The method of measuring the SSA was not specified.

Both WFT and PFT were calculated: the WFT, by dividing the excess of water by the specific surface of all the solid particles in the WFT; and, the PFT was calculated by dividing the excess of paste (including the aggregate fraction smaller than 75 µm) and specific surface of the aggregate higher than 75 µm (Li & Kwan 2013).

Ng et al. (Ng et al. 2016) proposed a three-tier method based on thickness theories - WFT, PFT and MFT- in high-performance concrete mix design. The measurement of WFT, PFT and MFT was performed by wet packing methods in the same way as the previously mentioned methodology (Kwan et al. 2012). From the results that were obtained, the authors gave some recommendations for WFT, PFT and MFT values, and HPC mix-design (Ng et al. 2016):

- WFT: 0.14 µm to 0.40 µm
- PFT: 20 µm to 60µm
- MFT: In accordance with the flow rate. Approximately 0.9 mm will yield self-consolidating properties.

Table 2.15 and Table 2.16 show the results obtained by (Kwan & Mckinley 2014), as an example of the relationship between workability, strength, and packing density, WFT, and PFT on mortars.

Table 2.15. Mix proportions, packing density, WFT and PFT results of mortar samples (Kwan & Mckinley 2014).

Mix no.	Materials content in the mortar (kg/m^3)					Packing density	WFT (µm)	PFT (µm)
	OPC	LF	FA	Water	SP			
M-50-0	609	0	1307	294	11	0.720	0.111	32.7
M-50-4	609	106	1202	293	12	0.717	0.087	42.7
M-50-8	609	211	1098	292	13	0.710	0.054	54.6
M-50-12	609	317	993	291	14	0.705	0.032	69.0

Table 2.16. Flowability and strength results of mortar samples (Kwan & Mckinley 2014).

Mix no.	Flow spread (mm)	Flow rate (ml/s)	7-day cube strength (MPa)	28-day cube strength (MPa)
M-50-0	60	98	50.5	58.7
M-50-4	75	73	51.2	59.5
M-50-8	65	38	52.9	61.3
M-50-12	50	40	56.5	62.7

2.7.3.2.1 Specific Surface Area (SSA)

Concrete paste demand is heavily influenced by aggregate Specific Surface Area (SSA). The parameter provides information on the amount of paste needed to cover the aggregate surface. Therefore, the SSA value should be considered when determining the

amount of paste needed to fill the available voids left by the aggregate skeleton. The relation between the paste demand and the aggregate SSA was introduced for the first time, in 1918, by Edwards (Edwards 1918). However, it should be considered that the relation between the water demand, or cement paste demand and particle SSA will not have the same relevance when particles are smaller than 150µm (Alexander & Mindess 2005). The addition of particles smaller than 150 µm in acceptable proportions provided the concrete with a lubrication effect, greatly improving workability and reducing the amount of water that was required. This effect, dependent on particle sphericity and the nature of the aggregate, was also higher as the sphericity of the particles became more obvious (Alexander & Mindess 2005).

The SSA is considered as the ratio of total surface area to the volume of particles and their value depends on the granular grading and the particle shape, roughness and texture. Determining the SSA value is no trivial exercise. Although there are standardized test methods such as the BET technique and the Blaine test, as well as computational methods to measure the SSA, they are generally complex and will normally not provide accurate values for aggregate particles. According to some authors (Ghasemi et al. 2019b), certain limitations of these tests are as follows:

- *Blaine test:* specifically developed to determine cement fineness. Therefore, it may not be useful to measure powder of angular shape or with different densities and packing.
- *BET:* The BET technique determines the SSA by absorption of a gas into the surface area of the particle. The main limitation is that inner pores of the particles are also determined.

Another extended way of establish the SSA value of aggregates, is to use mathematical estimation. The simplest way is to calculate the value, consisting of calculating all spherical particles and calculating the SSA from the aggregate gradation. However, the shape of aggregate, especially when crushed, is far from spherical, and the less spherical the particle, then the greater the specific surface area. One study showed errors of up to 30% when crushed aggregates were supposed to be spherical (Cepuritis et al. 2017). Ghasemi (Ghasemi et al. 2018) studied the possibility of approximating aggregate shape to Platonic solids, in order to find a better approximation, to account for aggregate angularity. They proved a good approximation with SSA measured by X-ray microtomography when a dodecahedron shape is considered for natural aggregate and a cubical shape for crushed aggregate. There are further methods applied in other fields where the SSA of aggregates is an influential parameter. For example the method provided by the department of transportation of New York (Geotechnical Engineering Bureau 2015), which used correction factors, in order to estimate aggregate shape, and the empirical method (Panda et al. 2016), to estimate the SSA of aggregate in hot mix asphalt.

2.8 Concrete manufacturing process

Once the concrete mix has been designed, the concrete manufacturing process will involve the following stages:

- Mixing process.
- Transport to work site.
- Placing and compacting.
- Curing.

In this section the technologies, equipment and processes involved in concrete manufacture will be briefly reviewed.

2.8.1 Mixing process

The essential aim of the mixing process is to blend all the concrete components into a uniform mass. There are several pieces of equipment available to perform this operation (See Fig. 2.12). The most usual are the batch mixers such as tilting drum mixers, non-tilting drum mixers, pan-type mixers, and dual drum mixers, as well as continuous mixers (Neville & Brooks 2010).

Fig. 2.12. Concrete mixers [9]

The quantity of concrete and the cost of the work usually determines the type of mixer to be used. Mixing parameters such as the order of pouring materials, mixing time, mixing speed, mixing energy, temperature etc. all influence concrete quality. Dils et al. published a review and some experimental test results, analyzing the influence of those parameters (Dils et al. 2012).

[9] https://gharpedia.com/types-of-concrete-mixer/

The order in which the components should be blended has not previously been defined. It is usually established by trial and error (Ferraris 2001) or by applying general guidelines according to the type of mixer and the properties of the mix.

Mixer efficiency is measured by the homogeneity of the final concrete mix. The concrete composition and the variation of some concrete properties (workability, fresh density, air content, and compressive strength) are typically measured to control homogeneity (Ferraris 2001), as shown in Fig. 2.13.

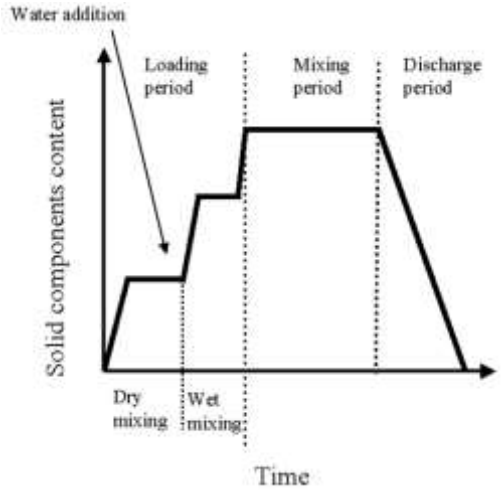

Fig. 2.13. General stages of the mixing process (Ferraris 2001).

At an industrial scale it is important to minimize the mixing time to produce a uniform concrete mix. The time depends on both the properties of mixer (type, size and speed) and the quality of blending components. Generally to make a conventional concrete the time is between 1.5 min and 2 min (Neville & Brooks 2010).

Ready-mixed concrete is prepared in a mixing plant rather than by on-site manufacturing. It is sometimes preferred, because of the number of advantages that it offers, one of the most remarkable of which is high-quality control (Neville & Brooks 2010). In relation to the environmental impact, efficient control and better handling in this type of plants helps to reduce cement wastage.

The distance from the ready-mixed concrete plant to the work-site should be considered as the mixing can all be done at the plant and can then be transported in a concrete mixer truck to the work site, or it can just be partially mixed, or be batched in the concrete plant, leaving the mixing process to be finished in an agitator truck traveling to the site (Neville & Brooks 2010).

2.8.2 Transport to work site

Many methods are available to transport concrete to the worksite. Wheelbarrows, buckets, skips, and belt conveyors are generally used over short distances, while for long distances concrete mixer trucks are especially available (Neville & Brooks 2010).

2.8.3 Placing and compacting

The aim of these operations is to place concrete as close as possible to its final position, avoiding segregation and facilitating its total compaction. Placing and compacting are sometimes carried out simultaneously (Neville & Brooks 2010).

Special methods of placing concrete such as slip-forming, tremie techniques, shotcreting, preplaced aggregate concrete and roller compacted concrete are available to place concrete in specific locations or with special performance requirements (Neville & Brooks 2010).

Compaction is generally performed with vibration techniques. These methods consist of forcing particles to maximum packing and minimize air entrapment, to produce a far stronger and more durable concrete. The three most widely used methods to vibrate the concrete mix are internal vibrators (70-200Hz and 4g accelerations), external vibrators (50-150Hz), and vibration tables (25-120Hz and 4g to 7g accelerations). External vibrators and vibration tables are usually used for precast concrete compaction. Neither the optimum frequency nor the optimum amplitude can be predicted for a given concrete mix. However, some authors recommend increased frequencies and decreased amplitudes, to induce movement and to obtain partial compaction. Finally, higher frequencies are used to enhance inter-particulate movements and their adjustment (Neville & Brooks 2010).

One special case is pumpable concrete that is generally pumped through pipelines in areas of difficult access. In addition, a large volume of concrete can be placed within a short time. Two methods are the most widely used, ground line pumps or boom pumps. The concrete properties at the fresh stage have to be carefully designed for suitable working of the pump system (Neville & Brooks 2010).

Self-compacting concrete is a type of concrete designed to facilitate placing and compacting operations. It is compacted and placed by its own weight reducing time, energy, and the cost of either placing or pouring and compacting operations (Neville & Brooks 2010).

Shotcrete is designed to be pneumatically projected onto a surface. There are two methods: the dry mix process and the wet mix process. The consistency of concrete mix should be relatively dry to support itself in any proportion and wet enough to achieve compaction without rebound (Neville & Brooks 2010).

2.9 Summary and conclusions

From the review of the literature, the following remarks may be reflected upon:

- Concrete mix design is an increasingly complex matter, due to the variety of materials that can be used, their diverse influence and the interdependence of their properties within the concrete. It is well-known that more eco-friendly concrete can be made by optimizing the concrete components and the material selection. However, even though the standardized methods for concrete mix design comply with current regulations, their application is somewhat limited to conventional materials and their characteristics and they lean towards safety margins that tend to overestimate the cement content.
- The optimization of aggregate contents through ideal optimization curves is a very extended practice, although their optimization will not inevitably imply that the highest packing density is reached, as aggregate shape is as yet not a factor that may be determined. The analytic Particle Packing Model (PPM) methods appear to offer suitable and accurate packing density predictions, particularly, the CPM model and recent models that include additional interaction parameters, such as the 3-parameter packing model (3-P). However, there is a scarcity of research into the applicability and the validation of these methods to aggregates of different morphologies. For example, the results of their use with EAF aggregates have yet to be reported.
- These models, due to their discrete nature, are designed to determine the interaction parameters of elementary granular size (very narrow granular size distribution fractions), which requires prior screening of the commercial aggregate fractions and numerous and tedious characterization tests and calculations. This fact reduces the applicability of analytic PPM at an industrial scale, since it can be time-consuming and difficult. It is therefore necessary to assess the suitability and accuracy of this method, considering the common aggregate fractions that are available on the market and that may be used in concrete. In addition, the interaction parameter developed previously for elementary particles size should be researched.
- Although there are standards for measuring the relative density of aggregates, there is no consensus over the most advantageous method to measure packing density. In addition, some authors question the extent of dry packing, as it does not include the effects of water and additives on granular materials. Apart from the fact that they are very sensitive to the compaction method and the results may be affected by the intermolecular forces of fine particles that cause agglomeration. Therefore, the suitability of the packing density models, which depend on the compaction method to measure the packing density, requires further analysis.

- Some authors have claimed that the optimum packing density is not equal to the maximum packing density, because the latter depends on the concrete application. The highest packing density generally requires a high content of fine particles to fill the voids, increasing their specific surface area, and therefore increasing the water requirement to achieve the required workability, which can be detrimental to the hardened properties. Thus, attention should be focused on the selection of the maximum or optimal packing density.
- Layered theories of water, paste, and mortar in combination with packing density analysis have been closely examined in relation to mortar and concrete mix design, over recent years. However, several assumptions are necessary (calculation of the SSA, calculation of the water, paste or mortar in excess in the mix) to calculate these values, which will require further analysis.

2.10 References

Abd, M. (2014) 'Compressive strength prediction of Portland cement concrete with age using a new model', *HBRC Journal*. Housing and Building National Research Center, 10(2), pp. 145–155. doi: 10.1016/j.hbrcj.2013.09.005.

ACI (2002) 'Standard Practice for Selecting Proportions for Normal , Heavyweight , and Mass Concrete (ACI 211.1-91)', *ACI Manual of Concrete Practice, Part 1*, (Reapproved), pp. 1–38.

Afkhami, B., Akbarian, B., A, N. B., Kakaee, A. H. and Shabani, B. (2015) 'Energy consumption assessment in a cement production plant', *Sustainable Energy Technologies and Assessments*, 10, pp. 84–89. doi: 10.1016/j.seta.2015.03.003.

Aïm, R. and Goff, P. (1967) 'Effet de paroi dans les empilements désordonnés de sphères et application à la porosité de mélanges binaires', *Powder Technology*, 1(5), pp. 281–290.

Aïtcin, P. C. (2015) *Supplementary cementitious materials and blended cements*, *Science and Technology of Concrete Admixtures*. Elsevier Ltd. doi: 10.1016/B978-0-08-100693-1.00004-7.

Alaoui, A., Feraille, A., Steckmeyer, A. and Le Roy, R. (2007) 'New Cements for Sustainable Development', in *Proceedings of the 12th International Congress on the Chemistry of Cement*. Montreal (Canada), p. 8.

Albayrak, G., Canbaz, M. and Albayrak, U. (2015) 'Statistical analysis of chemical admixtures usage for concrete: A survey of Eskisehir city, Turkey', in *International Conference on Sustainable Design, Engineering and Construction*. Turkey, pp. 1236–1241. doi: 10.1016/j.proeng.2015.08.475.

Alexander, M. and Mindess, S. (2005) *Aggregate in Concrete*. Taylor & Francis.

Amario, M., Rangel, C. S., Pepe, M. and Toledo Filho, R. D. (2017) 'Optimization of normal and high strength recycled aggregate concrete mixtures by using packing model', *Cement and Concrete Composites*. Elsevier Ltd, 84, pp. 83–92. doi:

10.1016/j.cemconcomp.2017.08.016.

Andreasen, A. and Andersen, J. (1930) 'Über die Beziehung zwischen Kornabstufung und Zwischenraum in Produkten aus losen Körnern (mit einigen Experimenten).', *Colloid & Polymer Science*, 50(3), pp. 217–228.

ANEFA (2018) *Informe de situación económica sectorial 2018*.

Arribas, I., Vegas, I., San-José, J. T. and Manso, J. M. (2014) 'Durability studies on steelmaking slag concretes', *Materials and Design*, 63, pp. 168–176. doi: 10.1016/j.matdes.2014.06.002.

Benhelal, E., Rafiei, A. and Shamsaei, E. (2012) 'Green Cement Production: Potentials and Achievements', *International Journal of Chemical Engineering and Applications*, 3(6), pp. 407–409. doi: 10.7763/IJCEA.2012.V3.229.

Bolomey, J. (1935) 'Granulation et prevision de la résistance probable des bétons', *Travaux*, 19(30), pp. 228–232.

BRE (1997) 'Design of normal concrete mixes'.

van Breugel, K. (1997) *Simulation of hydration and formation of structure in hardening of cement-based materials*. Delft University Press.

Brito, J. De and Kurda, R. (2018) 'Can We Truly Predict the Compressive Strength of Concrete without Knowing the Properties of Aggregates?', *Applied sciences (MDPI)*, (8), pp. 1–21. doi: 10.3390/app8071095.

Brito, J. and Saikia, N. (2013) 'Industrial Waste Aggregates', in *Recycled Aggregate in Concrete*, pp. 23–80. doi: 10.1007/978-1-4471-4540-0.

Cepuritis, R., Garboczi, E. J., Ferraris, C. F., Jacobsen, S. and Sørensen, B. E. (2017) 'Measurement of particle size distribution and specific surface area for crushed concrete aggregate fines', *Advanced Powder Technology*. Society of Powder Technology Japan, 28(3), pp. 706–720. doi: 10.1016/j.apt.2016.11.018.

Chidiac, S. E., Moutassem, F. and Mahmoodzadeh, F. (2013) 'Compressive strength model for concrete', *Magazine of Concrete Research*, 65(9), pp. 557–572. doi: 10.1680/macr.12.00167.

Chindaprasirt, P. and Cao, T. (2015) '8 - The properties and durability of high-pozzolanic industrial by-products content concrete masonry blocks', in Pacheco-Torgal, F., Lourenço, P. B., Labrincha, J. A., Kumar, S., and Chindaprasirt, P. (eds) *Eco-Efficient Masonry Bricks and Blocks*. Oxford: Woodhead Publishing, pp. 191–214. doi: https://doi.org/10.1016/B978-1-78242-305-8.00008-5.

Chunlin, L., Kunpeng, Z. and Depeng, C. (2011) 'Possibility of Concrete Prepared with Steel Slag as Fine and Coarse Aggregates : A Preliminary Study', in *2011 International Conference on Advances in Engineering (ICAE 2011) Possibility*, pp. 412–416. doi: 10.1016/j.proeng.2011.11.2667.

Coelho, D., Thovert, J. F. and Adler, P. M. (1997) 'Geometrical and transport properties of random packings of spheres and spherical particles', *Physics*, (55), pp. 1959–1978.

Cooper, D. W. (1988) 'Random-sequential-packing simulations in three dimensions for

spheres', *Phys. Rev. A*. American Physical Society, 38(1), pp. 522–524. doi: 10.1103/PhysRevA.38.522.

Damineli, B. L., Pileggi, R. G. and John, V. M. (2013) '2 - Lower binder intensity eco-efficient concretes', in Pacheco-Torgal, F., Jalali, S., Labrincha, J., and John, V. M. (eds) *Eco-Efficient Concrete*. Woodhead Publishing (Woodhead Publishing Series in Civil and Structural Engineering), pp. 26–44. doi: https://doi.org/10.1533/9780857098993.1.26.

DeRousseau, M. A., Kasprzyk, J. R. and Srubar, W. . (2018) 'Cement and Concrete Research Computational design optimization of concrete mixtures : A review', *Cement and Concrete Research*. Elsevier, 109, pp. 42–53. doi: 10.1016/j.cemconres.2018.04.007.

Dewar, J. (1999) 'Computer Modelling of Concrete Mixtures', *E & FN Spon Press, London*.

Dhir OBE, R. K., Ghataora, G. S. and Lynn, C. J. (2017) '5. Concrete. Related Applications', in *Sutainable Construction Materials*. doi: 10.1016/B978-0-08-100987-1.00005-6.

Dils, J., De Schutter, G. and Boel, V. (2012) 'Influence of mixing procedure and mixer type on fresh and hardened properties of concrete: a review', *Materials and Structures*. doi: 10.1617/s11527-012-9864-8.

Edwards, L. N. (1918) 'Proportioning the materials of mortars and concretes by surface area of aggregates', in *Proceedings ASTM, 18, Part II,* pp. 235–302.

EHE (2008) 'Instrucción de Hormigón Estructural (EHE-08)'. Available at: https://www.fomento.gob.es/organos-colegiados/mas-organos-colegiados/comision-permanente-del-hormigon/cph/instrucciones/ehe-08-version-en-castellano.

EN 934-2 (2009) 'Aditivos para hormigones, morteros y pastas. Parte 2: Aditivos para hormigones. Definición, requisitos, conformidad, marcado y etiquetado'.

European Aggregates Association (2018) *European Aggregates Association. Annual Review 2017-2018*. doi: 10.1016/S0893-9659(02)80020-9.

European Commission (2018) *European Commission Construction and Demolition Waste (CDW)*. Available at: http://ec.europa.eu/environment/waste/construction_demolition.htm.

Evans, K. E. and Ferrar, M. (1989) 'The packing of thick fibres', *Physics*, (22), p. 354. doi: 10.1088/0022-3727/22/2/020.

Fennis, S. A. A. M. (2009) *Design of Ecological Concrete by Particle Packing Optimization*.

Fennis, S. A. A. M. (2009) 'Measuring water demand or packing density of micro powders – Comparision of methods', in. Available at: http://repository.tudelft.nl/search/ir/?q=fennis&w=Publication s&faculty=&department=&type=&year=.

Fennis, S. A. A. M. and Walraven, J. C. (2012) 'Using particle packing technology for sustainable concrete mixture design', *Heron*, 57(2), pp. 73–101.

Feret, R. (1892) 'Sur la compacité des mortiers hydrauliques', *Annales des Ponts et Chaussess*, 4, pp. 5–16.

Ferraris, C. F. (2001) 'Concrete Mixing Methods and Concrete Mixers: State of the Art', 106(2), pp. 391–399.

Flower, D. J. M., Sanjayan, J. G. and Hellweg, S. (2007) 'Green House Gas Emissions Green House Gas Emissions due to Concrete Manufacture*', *Int. J. LCA*, 12(125), pp. 12–282. doi: 10.1065/lca2007.05.327.

Fu, G. and Dekelbab, W. (2003) '3-D random packing of polydisperse particles and concrete aggregate grading', *Powder Technology*, 133(1), pp. 147–155. doi: https://doi.org/10.1016/S0032-5910(03)00082-2.

Fuller, W. B. and Thompson, S. E. (1907) 'The laws of proportioning concrete', *ASCE J.Transport*, 59, pp. 67–143.

Funk, J. E., Dinger, D. R. and Funk, J. E. J. (1980) 'Caol Grinding and Particle Size Distribution Studies for Coal-Water Slurries at High Solids Content', *Final Report, Empire State Electric Energy Research Corporation (ESEERCO)*. New York.

Furnas, C. . (1929) 'Flow of gasses through beds of broken solids', *Bureau of Mines Bulletin*, 307.

Geotechnical Engineering Bureau (2015) 'Test procedure for specific surface analysis GTP-5', *Department of transportation of New York*, (August).

Ghasemi, Y. (2017) *Aggregates in Concrete Mix Design*. Luleå University of Technology.

Ghasemi, Y., Emborg, M. and Cwirzen, A. (2019a) 'Effect of water film thickness on the flow in conventional mortars and concrete', *Materials and Structures*. Springer Netherlands, 52(3), pp. 1–15. doi: 10.1617/s11527-019-1362-9.

Ghasemi, Y., Emborg, M. and Cwirzen, A. (2019b) 'Exploring the relation between the flow of mortar and specific surface area of its constituents', *Construction and Building Materials*. Elsevier Ltd, 211, pp. 492–501. doi: 10.1016/j.conbuildmat.2019.03.260.

Ghasemi, Y., Rajczakowska, M. and Cwirzen, A. (2018) 'Shape-dependent calculation of specific surface area of aggregates versus X-ray microtomography', *Magazine of Concrete Research*. doi: 10.1680/jmacr.18.00121.

Gobierno Vasco (2018) *Inventario residuos no peligrosos de País Vasco 2016*.

Goltermann, P., Johansen, V. and Palbol, L. (1997) 'Packing of Aggregates: An Alternative Tool to Determine the Optimal Aggregate Mix', *Materials Journal*, 94(5). doi: 10.14359/328.

Gromicko, N. and Shepard, K. (2016) *The History of Concrete*, *International Association of Certified Home Inspectors, Inc*. Available at: https://www.nachi.org/history-of-concrete.htm (Accessed: 9 June 2019).

Grubeša, I. N., Barišić, I., Fucic, A. and Bansode, S. S. (2016) '1 - Introduction', in Grubeša, I. N., Barišić, I., Fucic, A., and Bansode, S. S. (eds) *Characteristics and Uses of Steel Slag in Building Construction*. Woodhead Publishing, pp. 1–14. doi: https://doi.org/10.1016/B978-0-08-100368-8.00001-4.

He, H. (2010) *Computational Modelling of Particle Packing in Concrete*. TU Delft.

Van Den Heede, P. and De Belie, N. (2012) 'Environmental impact and life cycle assessment (LCA) of traditional and "green" concretes: Literature review and theoretical calculations', *Cement and Concrete Composites*. Elsevier Ltd, 34(4), pp. 431–442. doi:

10.1016/j.cemconcomp.2012.01.004.

Heilderberg (2008) 'Cement manufacturing process'. Available at: http://www.mycemco.com/sites/default/files/Cement manufacturing process_1.pdf.

ICPA (2015) 'Diseño racional de mezclas de hormigón – método ICPA', *Instituto del cemento Pórtland argentino*, pp. 1–26. Available at: www.icpa.org.ar/publico/files/DOSIFICACION DE HORMIGONES.pdf.

Imbabi, M. S., Carrigan, C. and Mckenna, S. (2013) 'Trends and developments in green cement and concrete technology', *International Journal of Sustainable Built Environment*. The Gulf Organisation for Research and Development, 1(2), pp. 194–216. doi: 10.1016/j.ijsbe.2013.05.001.

Imbabi, M. S., Carrigan, C. and McKenna, S. (2012) 'Trends and developments in green cement and concrete technology', *International Journal of Sustainable Built Environment*. The Gulf Organisation for Research and Development, 1(2), pp. 194–216. doi: 10.1016/j.ijsbe.2013.05.001.

IS 10262 (2009) 'Concrete Mix proportioning-Guidelines. Bureau of Indian Standards'.

Jia, X. and Williams, R. A. (2001) 'A packing algorithm for particles of arbitrary shapes', *Powder Technology*, 120(3), pp. 175–186. doi: https://doi.org/10.1016/S0032-5910(01)00268-6.

Jiang, Y., Ling, T., Shi, C. and Pan, S. (2018) 'Characteristics of steel slags and their use in cement and concrete — A review', *Resources, Conservation & Recycling*. Elsevier, 136(December 2017), pp. 187–197. doi: 10.1016/j.resconrec.2018.04.023.

Joaquim, B., Liberato, F. and Martinelli, E. (2017) *Recent Advances on Green Concrete for Structural Purposes*. Springer. Available at: https://www.springer.com/gp/book/9783319567952.

Kääntee, U., Zevenhove, R., Backman, R. and Hupa, M. (2004) 'Cement manufacturing using alternative fuels and the advantages of process modelling', *Fuel Processing Technology*, 85, pp. 293–301. doi: 10.1016/S0378-3820(03)00203-0.

Kochevets, S., Buckmaster, J., Hegab, A. and Jackson, T. (2001) 'Random Packs and Their Use in Modeling Heterogeneous Solid Propellant Combustion', *Journal of Propulsion and Power*, 17, pp. 883–891. doi: 10.2514/2.5820.

Kwan, A. K. H., Chan, K. W. and Wong, V. (2013) 'A 3-parameter particle packing model incorporating the wedging effect', *Powder Technology*. Elsevier B.V., 237, pp. 172–179. doi: 10.1016/j.powtec.2013.01.043.

Kwan, A. K. H. and Li, L. G. (2012) 'Combined effects of water film thickness and paste film thickness on rheology of mortar', *Materials and Structures*, 45(9), pp. 1359–1374. doi: 10.1617/s11527-012-9837-y.

Kwan, A. K. H., Li, L. G. and Fung, W. W. S. (2012) 'Wet packing of blended fine and coarse aggregate', *Materials and Structures*, 45, pp. 817–828. doi: 10.1617/s11527-011-9800-3.

Kwan, A. K. H. and Mckinley, M. (2014) 'Packing density and filling effect of limestone

fines', *Advances in Concrete Construction*, 2(3), pp. 209–227.

Lagerblad, B. and Forssberg, E. (2004) 'The function of fillers in concrete', *Materials and Structures*, 37, pp. 74–81.

de Larrard, F. (1999) *Concrete Mixture Proportioning*. E & FN SPON.

Li, L. G., Chu, S. H., Zeng, K. L., Zhu, J. and Kwan, A. K. H. (2018) 'Roles of water film thickness and fibre factor in workability of polypropylene fibre reinforced mortar', *Cement and Concrete Composites*, 93(April), pp. 196–204. doi: 10.1016/j.cemconcomp.2018.07.014.

Li, L. G. and Kwan, A. K. H. (2011) 'Mortar design based on water film thickness', *Construction and Building Materials*, 25, pp. 2381–2390. doi: 10.1016/j.conbuildmat.2010.11.038.

Li, L. G. and Kwan, A. K. H. (2013) 'Concrete mix design based on water film thickness and paste film thickness', *Cement and Concrete Composites*. Elsevier Ltd, 39, pp. 33–42. doi: 10.1016/j.cemconcomp.2013.03.021.

Li, L. G. and Kwan, A. K. H. (2014) 'Packing density of concrete mix under dry and wet conditions', *Powder Technology*, 253, pp. 514–521. doi: 10.1016/j.powtec.2013.12.020.

Li, Z. (2011) *Advanced concrete Technology*. New Jersey: John Wiley & Sons, Inc.

Lin, X. and Ng, T. (1997) 'A three-dimensional discrete element model using arrays of ellipsoids', *Géotechnique*, 4(2), pp. 319–329.

Lothenbach, B., Scrivener, K. and Hooton, R. D. (2011) 'Supplementary cementitious materials', *Cement and Concrete Research*. Elsevier Ltd, 41(12), pp. 1244–1256. doi: 10.1016/j.cemconres.2010.12.001.

Manso, J. M., Polanco, J. A., Losan, M. and Gonza, J. J. (2006) 'Durability of concrete made with EAF slag as aggregate', *Cement and Concrete Composites*, 28, pp. 528–534. doi: 10.1016/j.cemconcomp.2006.02.008.

Mansoutre, S., Colombet, P. and Damme, H. Van (1999) 'Water retention and granular rheological behavior of fresh C3S paste as a function of concentration11This paper was originally submitted to Advanced Cement Based Materials. It was received at the Editorial Office of Cement and Concrete Research on 27 Augu', *Cement and Concrete Research*, 29(9), pp. 1441–1453. doi: https://doi.org/10.1016/S0008-8846(99)00129-5.

Marquardt, I. (2002) 'Ein Misschungskonzept für selbstverdichtenden Beton auf der Basis der Volumenkenngrössen und Wasseransprüche der Ausgangsstoff', *Fak. für Ingenieurswissenschaften, Fachbereich Bauingenieurswesen*, p. 190.

Mas, B., Cladera, A., Olmo, T. and Pitarch, F. (2012) 'Influence of the amount of mixed recycled aggregates on the properties of concrete for non-structural use', *Construction and Building Materials*. Elsevier Ltd, 27(1), pp. 612–622. doi: 10.1016/j.conbuildmat.2011.06.073.

Mehta, P. K. and Monteiro, P. (2014a) 'Admixtures', in *Concrete: Microstructure, Properties, and Materials*. McGraw-Hill Education.

Mehta, P. K. and Monteiro, P. (2014b) 'Introduction', in *Concretre: Microstructure,*

Propeties and Materials. Fourth Edi. McGraw-Hill Education. doi: https://doi.org/10.1142/9781848161269_0001.

Mehta, P. K. and Monteiro, P. J. M. (2014a) 'Hydraulic Cements', in *Concrete: Microstructure, Properties, and Materials*. Fourth Edi. McGraw-Hill Education, pp. 1–17.

Mehta, P. K. and Monteiro, P. J. M. (2014b) 'Proportioning Concrete Mixtures', in *Concrete: Microstructure, Properties, and Materials*. McGraw-Hill Education.

Miller, K. T., Melant, R. M. and Zukoski, C. F. (1996) 'Comparison of the Compressive Yield Response of Aggregated Suspensions: Pressure Filtration, Centrifugation, and Osmotic Consolidation', *Journal of the American Ceramic Society*, 79(10), pp. 2545–2556. doi: 10.1111/j.1151-2916.1996.tb09014.x.

Miyamoto, T., Akahane, K., Torii, K. and Hayashiguchi, S. (2015) *Production and Use of Blast Furnace Slag Aggregate for Concrete*.

Moini, M. (2015) *The Optimization of Concrete Mixtures for Use in Highway Applications*. The University of Wisconsin-Milwaukee. doi: 10.13140/RG.2.1.1429.0966.

Moutassem, F. (2016) 'Assessment of Packing Density Models and Optimizing Concrete Mixtures', *International Journal of Civil, Mechanical and Energy Science (IJCMES)*, 2(4), pp. 2455–5304. Available at: www.ijcmes.com.

Moutassem, F. and Chidiac, S. E. (2016) 'Assessment of concrete compressive strength prediction models', *KSCE Journal of Civil Engineering*, 20(1), pp. 343–358. doi: 10.1007/s12205-015-0722-4.

Neville, A. M. and Brooks, J. J. (2010) *Concrete Technology*. Pearson Education Limited.

Ng, P., Kwan, A. K. H. and Li, L. G. (2016) 'Packing and film thickness theories for the mix design of high-performance concrete', *Zhejiang University-SCIENCE A (Applied Physics & Engineering) ISSN*, 17(10), pp. 759–781.

Niaounakis, M. (2015) '10 Building and Construction Applications', in *Biopolymers: Applications and Trends*. doi: 10.1016/B978-0-323-35399-1.00010-7.

Oggioni, G., Riccardi, R. and Toninelli, R. (2011) 'Eco-efficiency of the world cement industry : A data envelopment analysis', *Energy Policy*. Elsevier, 39(5), pp. 2842–2854. doi: 10.1016/j.enpol.2011.02.057.

Okamura, H. and Ozawa, K. (1995) 'Mix design for self-compacting concrete', *Concrete library of the JSCE*, (25), pp. 107–120.

Özalp, F., Dils, H., Kara, M., Kaya, Ö. and Aylin, S. (2016) 'Effects of recycled aggregates from construction and demolition wastes on mechanical and permeability properties of paving stone, kerb and concrete pipes', *Construction and Building Materials*, 110, pp. 17–23. doi: 10.1016/j.conbuildmat.2016.01.030.

Pacheco, J. N., de Brito, J., Chastre, C. and Evangelista, L. (2019) 'Statistical analysis of Portuguese ready-mixed concrete production', *Construction and Building Materials*, 209, pp. 283–294. doi: 10.1016/j.conbuildmat.2019.03.089.

Pacheco, J. N., de Brito, J., Chastre, C. and Evangelista, L. (2020) 'Uncertainty of shear resistance models: Influence of recycled concrete aggregate on beams with and without

shear reinforcement', *Engineering Structures*. Elsevier, 204(October), p. 109905. doi: 10.1016/j.engstruct.2019.109905.

Palomo, A., Grutzeck, M. W. and Blanco, M. T. (1999) 'Alkali-activated fly ashes A cement for the future', *Cement and Concrete Research*, 29, pp. 1323–1329.

Panda, R. P., Sekhar, S. and Sahoo, P. K. (2016) 'An empirical method for estimating surface area of aggregates in hot mix asphalt', *Journal of Traffic and Transportation Engineering*. Elsevier Ltd, 3(2), pp. 127–136. doi: 10.1016/j.jtte.2015.10.007.

Pellegrino, C., Cavagnis, P., Faleschini, F. and Brunelli, K. (2013) 'Cement & Concrete Composites Properties of concretes with Black / Oxidizing Electric Arc Furnace slag aggregate', *Cement and Concrete Composites*, 37, pp. 232–240. doi: 10.1016/j.cemconcomp.2012.09.001.

Pepe, M. (2014) *A conceptual model to design recycled aggregate concrete for structural applications*. Springer. doi: 10.1007/978-3-319-26473-8.

Pepe, M., Dias, R., Filho, T., Koenders, E. and Martinelli, E. (2016) 'A novel mix design methodology for Recycled Aggregate Concrete'. doi: 10.1016/j.conbuildmat.2016.06.061.

Popescu, C. D., Muntean, M. and Sharp, J. H. (2003) 'Industrial trial production of low energy belite cement', 25, pp. 689–693. doi: 10.1016/S0958-9465(02)00097-5.

Portland Cement Association (PCA) (2016) *Design and Control of Concrete Mixtures*.

Pradhan, S., Kumar, S. and Barai, S. V (2017) 'Recycled aggregate concrete: Particle Packing Method (PPM) of mix design approach', *Construction and Building Materials*. Elsevier Ltd, 152, pp. 269–284. doi: 10.1016/j.conbuildmat.2017.06.171.

Puntke, W. (2002) 'Wasseranspruch von feinen Kornhauf-werken', *beton 52*, (5), pp. 242–248.

Rahman, A., Rasul, M. G., Khan, M. M. K. and Sharma, S. (2013) 'Impact of alternative fuels on the cement manufacturing plant performance : an overview', in *5th BSME International Conference on Thermal Engineering*. Elsevier B.V., pp. 393–400. doi: 10.1016/j.proeng.2013.03.138.

Ramachandran, V. S. (1996) '3 - Admixture Interactions in Concrete', in Ramachandran, V. S. (ed.) *Concrete Admixtures Handbook (Second Edition)*. Second Edi. Park Ridge, NJ: William Andrew Publishing, pp. 95–136. doi: https://doi.org/10.1016/B978-081551373-5.50007-6.

Ramirez, J. L. and Barcena, J. M. (1981) *Problematica Resistente en el Hormigón Armado: Origen, Deteccion, Análisis y Remedios*. Bilbao.

Richardson, J. (2014) *Supervision of Concrete Construction 1*. CRC Press.

Roquier, G. (2017) 'The 4-parameter Compressible Packing Model (CPM) including a critical cavity size ratio', 2009, pp. 10–13.

Sainz-Aja, J., Carrascal, I., Polanco, J. A. and Thomas, C. (2020) 'Fatigue failure micromechanisms in recycled aggregate mortar by µCT analysis', *Journal of Building Engineering*. Elsevier Ltd, 28(October 2019), p. 101027. doi:

10.1016/j.jobe.2019.101027.

San-José, J. T., Vegas, I., Arribas, I. and Marcos, I. (2014) 'The performance of steel-making slag concretes in the hardened state', *Materials and Design*, 60, pp. 612–619. doi: 10.1016/j.matdes.2014.04.030.

Santamaria, A., Faleschini, F., Giacomello, G., Brunelli, K., San José, J. T., Pellegrino, C. and Pasetto, M. (2018) 'Dimensional stability of electric arc furnace slag in civil engineering applications', *Journal of Cleaner Production*, 205, pp. 599–609. doi: 10.1016/j.jclepro.2018.09.122.

Sear, L. K. A., Dews, J., Kite, B., Harris, F. C. and Troy, J. F. (1996) 'Abrams law, air and high water-to-cement ratios', *Construction and Building Materials*, 10(3), pp. 221–226. doi: 10.1016/0950-0618(95)00079-8.

Sherwood, J. D. (1997) 'Packing of spheroids in three-dimensional space by random sequential addition', *Journal of Physics A: Mathematical and General*, 30(24).

Sobolev, K., Kozhukhova, M., Sideris, K., Menéndez, E. and Santhanam, M. (2018) 'Alternative Supplementary Cementitious Materials BT - Properties of Fresh and Hardened Concrete Containing Supplementary Cementitious Materials: State-of-the-Art Report of the RILEM Technical Committee 238-SCM, Working Group 4', in De Belie, N., Soutsos, M., and Gruyaert, E. (eds). Cham: Springer International Publishing, pp. 233–282. doi: 10.1007/978-3-319-70606-1_7.

Sosa, I., Thomas, C., Polanco, J. A., Setién, J. and Tamayo, P. (2020) 'High Performance Self-Compacting Concrete with Electric Arc Furnace Slag Aggregate and Cupola Slag Powder', *Applied Sciences*, 10(3), p. 773. doi: 10.3390/app10030773.

Stovall, T., Larrard, F. and Buil, M. (1986) 'Linear Packing Density Model of Grain Mixtures', *Powder Technology*, 48, pp. 1–12.

Stroeven, M. and Stroeven, P. (1999) 'SPACE system for simulation of aggregated matter application to cement hydration', *Cement and Concrete Research*, 29(8), pp. 1299–1304. doi: https://doi.org/10.1016/S0008-8846(99)00077-0.

Sunayana, S. and Barai, S. V (2017) 'Recycled aggregate concrete incorporating fly ash : Comparative study on particle packing and conventional method', *Construction and Building Materials*. Elsevier Ltd, 156, pp. 376–386. doi: 10.1016/j.conbuildmat.2017.08.132.

Sunayana, S. and Barai V., S. (2017) 'Recycled aggregate concrete incorporating fly ash: Comparative study on particle packing and conventional method', *Construction and Building Materials*. Elsevier Ltd, 156, pp. 376–386. doi: 10.1016/j.conbuildmat.2017.08.132.

Tam, V. W. Y., Soomro, M., Catarina, A. and Evangelista, J. (2018) 'A review of recycled aggregate in concrete applications (2000 – 2017)', *Construction and Building Materials*. Elsevier Ltd, 172, pp. 272–292. doi: 10.1016/j.conbuildmat.2018.03.240.

Thomas, C., Rosales, J., Polanco, J. A. and Agrela, F. (2019) *7. Steel slags*, *New Trends in Eco-efficient and Recycled Concrete*. Elsevier Ltd. doi: 10.1016/B978-0-08-102480-5.00007-5.

Thomas, P. A. and Bray, J. D. (1999) 'Capturing Nonspherical Shape of Granular Media with Disk Clusters', *Journal of Geotechnical and Geoenvironmental Engineering*, 125(3).

Toufar, W., Born, M. and Klose, E. (1976) 'Contribution of Optimization of Components of different Density in Polydispersed Particles Systems', *Freiberger Booklet A*, 558, pp. 29–44.

UNE-EN 12620:2003+A1 (2009) 'Áridos para hormigón'.

UNE-EN 13286-2 (2004) 'Unbound and hydraulically bound mixtures - Part 2: Test methods for the determination of the laboratory reference density and water content - Proctor compaction'.

UNE-EN 197-1 (2011) 'Cemento. Composición, especificaciones y criterios de conformidad de los cementos comunes', *AENOR*, pp. 9–11.

Vesilind, P. A. (1980) 'The Rosin-Rammler particle size distribution', *Resource Recovery and Conservation*, 5(3), pp. 275–277. doi: https://doi.org/10.1016/0304-3967(80)90007-4.

Waste Framework Directive (2008/98/EC) (2008) 'Directive 2008/98/EC of the European Parliament and of the Council', pp. 3–30.

Westman, A. E. R. and Hugill, H. R. (1930) 'The packing of particles', *Journal of the American Ceramic Society*, 13(10), pp. 767–779.

Williams, S. R. and Philipse, A. P. (2003) 'Random packings of spheres and spherocylinders simulated by mechanical contraction', *Phys Rev E*, (67), pp. 1–9.

Wittmann, F. H., Roelfstra, P. E. and Sadouki, H. (1984) 'Simulation and Analysis of Composite Structures', *Mater. Sci. Eng.*, (68), pp. 239–48.

Yu, A. and Standish, N. (1991) 'Estimation of the Porosity of Particle Mixtures by a Linear-Mixture Packing Model', *Industrial & Engineering Chemical Research*, 30, pp. 1372–1385.

Yu, A., Zou, R. and Standish, N. (1996) 'Modifying the Linear Packing Model for Predicting the Porosity of Nonspherical Particle Mixtures', *Industrial & Engineering Chemical Research*, 35, pp. 3730–3741.

Zhang, R. and Panesar, D. K. (2017) 'New approach to calculate water film thickness and the correlation to the rheology of mortar and concrete containing reactive MgO', *Construction and Building Materials*. Elsevier Ltd, 150, pp. 892–902. doi: 10.1016/j.conbuildmat.2017.05.218.

Zhang, T., Yu, Q., Wei, J. and Zhang, P. (2011) 'Cement & Concrete Composites A new gap-graded particle size distribution and resulting consequences on properties of blended cement', *Cement and Concrete Composites*. Elsevier Ltd, 33(5), pp. 543–550. doi: 10.1016/j.cemconcomp.2011.02.013.

Zheng, J., Johnson, P. and Reed, J. (1990) 'Improved Equation of the Continuous Particle Size Distribution for Dense Packing', *Journal of the America Ceramic Society*, 73(5), pp. 1392–1398.

3

Concrete environmental and economic assessment

CONTENT

3 Concrete environmental and economic assessment 73

3.1 Introduction 73

3.2 Environmental impacts 76

3.3 Economic impacts 79

3.4 Assessment methods 80

3.4.1 Life Cycle Assessment (LCA) approach 80

3.4.2 Environmental Product Declarations (EPD) 88

3.4.3 Product Environmental Footprint (PEF) 89

3.4.4 LCI of concrete industries 89

3.4.5 Review of environmental assessment methods and tools 91

3.4.6 Environmental and economic indicators 94

3.4.7 LCA of concrete made with alternative aggregates 95

3.5 Multiple-Criteria Decision Methods (MCDM) 95

3.5.1 Analytic Hierarchy Process (AHP) 97

3.5.2 Technique for Order of Preference by Similarity to Ideal Solution (TOPSIS) 98

3.5.3 The Preference Ranking Organization Method for Enrichment of Evaluations (PROMEHTEE) 98

3.5.4 Elimination and Choice Expressing Reality (ELECTRE) 99

3.5.5 Integrated Value Model for Sustainable Assessment (MIVES) 99
3.6 Integration of LCA and MCDM methods 99
3.7 Summary and conclusions 102
3.8 References 103

3 Concrete environmental and economic assessment

In chapter 3, the background on strategies for reducing the environmental and economic impact of concrete and current methodologies for assessing environmental impact will be presented. The review will focus on the limitations of current methods and new developments for the integration of environmental, economic and functional aspects that may facilitate decision-making when working on a concrete mix design.

3.1 Introduction

Concrete is, after water, the most widely used material in the world. Although concrete has low CO_2 emissions (200 kg CO_2 eq./t of concrete) compared to other construction materials (see Fig. 3.1) (recycled steel 1100 kg CO_2 eq./t of steel), its massive consumption, causes a substantial environmental impact (Favier et al. 2018). The impacts are not only because of the CO_2 emissions, but also because of the huge consumption of raw materials and the waste that is generated during its life cycle (Rodríguez-Robles, et al. 2019). As a reference, the European construction sector accounts for more than 50% of the consumption of the natural resources (Rodríguez-Robles, et al. 2019), around 35%[10] of all greenhouse emission and 11% of all European concrete waste (European Commission (DG ENV) 2011).

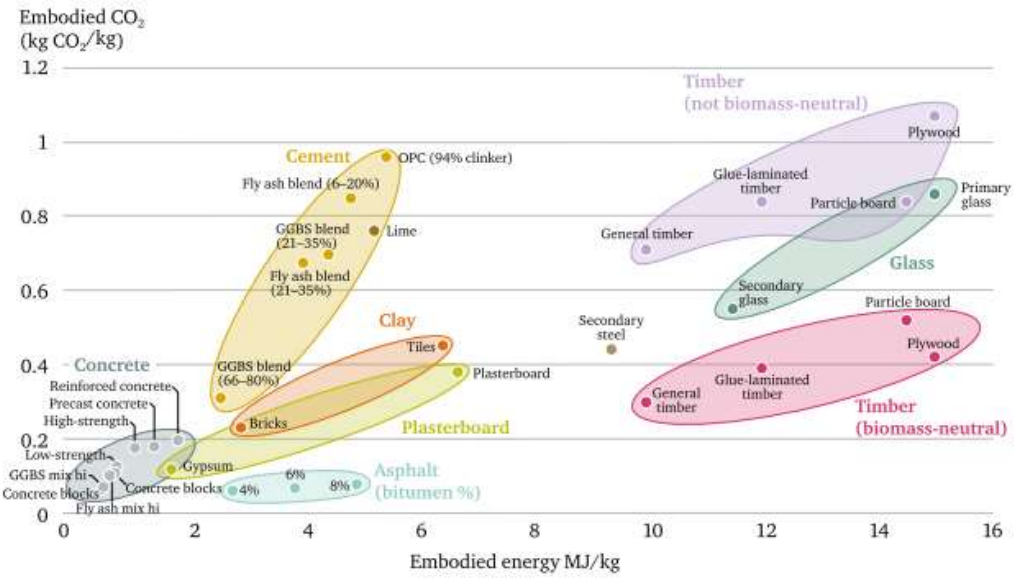

Fig. 3.1. Embodied emissions and energy for materials used for construction in the UK (Lehne & Preston 2018).

[10] https://ec.europa.eu/growth/sectors/construction_en

Sustainability is defined by the World Business Council for Sustainable Development (WBCSD) as: "Forms of progress that meet the needs of the present without compromising the ability of future generations to meet their needs". From the perspective of sustainability, concrete manufacturing must respond to the triple bottom line of sustainability, seeking a balance between economic aspects (reducing costs throughout its life cycle), environmental factors (minimizing the environmental impact of concrete), and social (improving quality of life) concerns. According to the premises of sustainable development (Westkamper et al. 2008), concrete products and services should be developed, so that safety and ecological sustainability last throughout their life cycle. Concrete must be durable, reparable, readily recycled and even compostable and biodegradable and it should use the minimal amount of energy and materials associated with high environmental impacts.

Different strategies have been proposed, studied and analyzed over past decades, to grapple with the environmental impacts of concrete, specifically CO_2 emissions, (Damtoft et al. 2008; John 2003; Meyer 2009). Most of those impacts have been classified according to the value chain of cementitious construction in Table 3.1.

Table 3.1. CO_2 reduction strategies in the value chain of cementitious construction. Data extracted from (Favier et al. 2018).

Level of impact on the value chain	Strategy	Solutions
Clinker	Improving energy efficiency.	Improving thermal efficiency. Use of alternative fuels.
	Development and use of new binders.	Enhancing the use of alternative binders.
Cement	Reduction of clinker ratio.	Using SCM and filler.
Concrete	Reduction of cement.	Optimization of concrete mix design by increasing the packing and the use of admixtures.
Products and structures	Reduction of the concrete amount use. Improving performance properties.	Adapting concrete mix design and the element shape to the final application.

In addition to the alternatives that are proposed, Carbon Capture Storage (CCS) is another possible solution, which has acquired special relevance in the construction industry, to increase the rate of reduction of greenhouse gas (GHG) in the cement industry (Müller 2008).

Aggregates represent approximately 80% by mass of concrete, which means that concrete is a potential receptor of large quantities of granular waste materials (Rodríguez-Robles, et al 2019 and 2019b). The rate of replacement is generally limited

by the quality of the waste material and its chemical and mechanical properties. In the literature, several studies have reported the successful substitution of natural aggregates by C&DW and EAFS. At present, the use of waste streams is regulated by national standards. However, higher ratios of replacement than those specified in the standards have been successfully introduced in concrete. A review of the use of recycled aggregate in concrete shows the production and the use of those materials on a global scale (Tam et al. 2018). This strategy reduces the consumption of natural resources avoiding both the depletion of natural resources and negative environmental impacts on the land, as well as the reduction of waste streams. The production loop of concrete aggregates that are replaced by recycled concrete aggregate is closed, as the waste is transformed into resources within the circular cement-based economy (Rodríguez-Robles, et al. 2019).

With all the components available for concrete mix design (SCM, Admixtures, recycled aggregates), it can be difficult to select the most sustainable option for a specific application. Thus, there is a diverse audience of decision makers and manufacturers with an interest both in understanding and in lowering the environmental impact of concrete. From among the available methods to assess the environmental impact of concrete, Life Cycle Assessment (LCA) is perhaps the most widely used (Pradhan et al. 2019; Schuurmans et al. 2005; Turk et al. 2015; Hossain et al. 2016a; Hossain et al. 2017; Simion et al. 2013; Chen et al. 2010; Smith & Durham 2016; Hossain et al. 2016b; Salas et al. 2016; García-Gusano et al. 2014; Penteado et al. 2015; Gursel et al. 2014; Ruan & Unluer 2016). LCA is a widely accepted international standardized method that can be used for quantitative measurement of the environmental impact of a product or system. However, its use presents some limitations.

Although, there are several guidelines (EC-JRC 2010) for the application of LCA within a general framework ISO 14040-46, the flexibility of the different LCA methodologies complicates their comparison (Dossche et al. 2017). An attempt to deal with this problem was the development of the Environmental Product Declaration (EPD). In that context, EN 15804 was developed that specifies the regulations for the application of an EPD to construction products. However, variations due to the use of different datasets or Life Cycle Impact Assessment (LCIA) studies have resulted in different product assessment procedures. A more recent methodology developed by the European Commission, the Product Environmental Footprint (PEF)(EC-JRC 2012) is intended to provide a “common way of measuring environmental performance”. It specifies different rules for different product categories, to ensure that significant environmental impacts are not overlooked. Another drawback of LCA is that economic and social aspects are not taken into account. Finally, the tool shows the environmental impact, but it takes no decision on which product is better, in addition the normalization factors and there are no established weighting values for concrete assessment.

Another important point is the data collection and the lack of data. A critical study on concrete Life Cycle Inventory (LCI) (Gursel et al. 2014) shows three important limitations

- A lack of holistic assessment, because most LCA focus only on GHG emissions and energy consumption.
- A lack of geographic and technological representativity, as data comes mainly from national or continent averages.
- A lack of attention to some concrete production processes such as water consumption and admixture production.

The use of Multi-criteria Decision Making (MCDM) methodologies alone and combined with LCA analysis has spread over recent years, due to the need to integrate environmental, economic, and functional aspects in concrete design. These two techniques can be combined to achieve practical and transparent objectives for the decision makers.

One example is a recent paper that developed a tool based on MCDC and integrated LCA analysis for concrete optimization, according to the application requirements (Kurda et al. 2019) .

Generally, an environmental impact study is performed after the concrete production process. Therefore, many combinations of concrete components are neglected. An optimized concrete mix-design tool for the selection of concrete components from a database on the basis of economic, environmental, and functional requirements should help construction experts take better decisions.

3.2 Environmental impacts

Environmental indicators have been the subject of intense study over many decades. A set of sustainable indicators were developed by the Commission on Sustainable Development (CSD) including economic, social and environmental. The most relevant environmental indicators are carbon dioxide emissions, urban air pollutant levels, proportion of total water resources, greenhouse gas emissions, land degradation and fertilizer use efficiency (Pellegrino & Faleschini 2016).

The environmental impact of concrete has been classified by their concrete components:

CEMENT

From among the main concrete components (cement, aggregates, water and admixtures), cement bears most responsibility for concrete emissions. It accounts for approximately 74-81% of total CO_2 emissions (Flower et al. 2007). Cement production alone is responsible for 5-7% of current anthropogenic CO_2 emissions in the world.

CO_2 emissions attributable to cement production currently range between 0.65 and 0.92 t CO_2/t cement, depending on production process efficiency and technology and the amount and type of energy that is consumed. It should also be considered that CO_2 concrete emissions are generally accounted for by ton of cement, regardless of the clinker amount which is mainly responsible for CO_2 emissions.

The sources of CO_2 emissions during cement production are mainly from the decarbonation of limestone and thermal and electricity energy consumption. Thus, CO_2 cement emissions can be divided as follows (Müller 2008):

- 50% of CO_2 emission are released during the calcination process of limestone.
- 40% are associated with thermal energy.
- 5% are associated with electricity consumption (this value varies from 1% to 10% depending of the local electricity mix).
- 5% are associated with fuel and electricity for mining quarries and transportation.

In Fig. 3.2 cement CO_2 emission and the mitigation solutions are included.

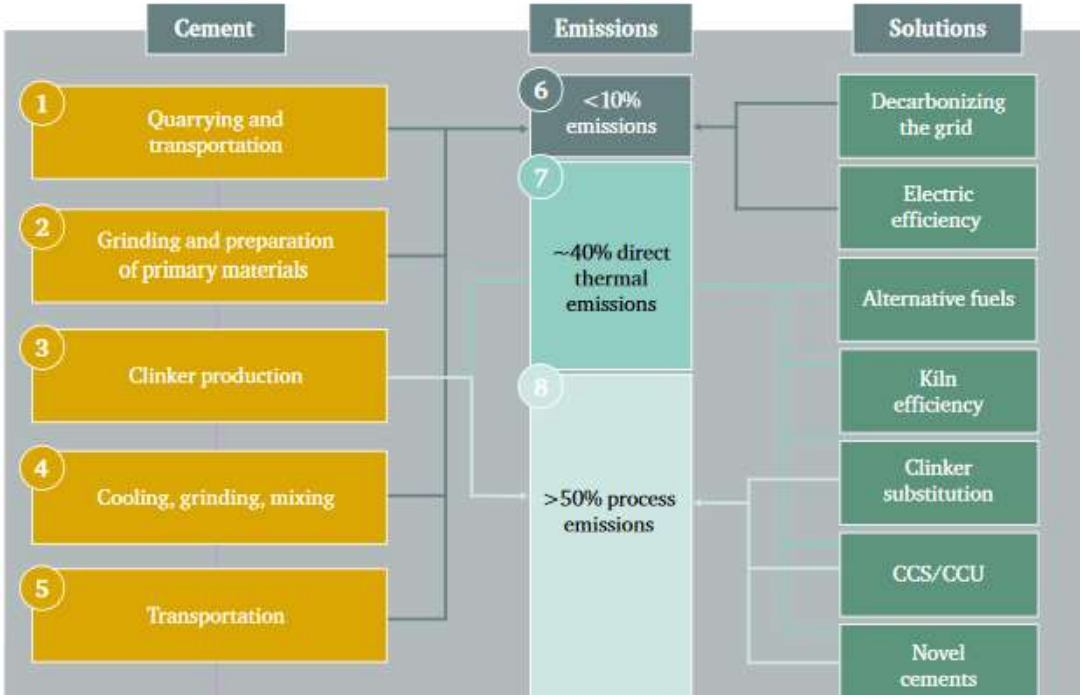

Fig. 3.2. Emission of CO_2 and mitigation solutions throughout the cement supply chain (Lehne & Preston 2018).

The thermal energy consumption of a European cement plant is approximately 3300 MJ/t clinker (Favier et al. 2018). Energy efficiency improvements can lessen consumption lowering the CO_2 emissions. Although, the use of biomass fuels increased by 10% between 2000 and 2010, the rate of fuel replacement is limited by the low calorific value of most organic waste and the impact of clinker chemistry, for example

increasing chloride emissions when plastics are used, and the availability of waste and its legislation (Favier et al. 2018).

During concrete manufacturing, the use of both electricity and fossil fuels are the main contributors to the environmental impact of concrete (Gursel 2014). Therefore, the electricity-mix of a region is a relevant factor in the concrete environmental impact.

LCA studies of concrete structures tend to focus on GHG emissions. However, other impacts at different scales (Global, regional and local) should also be considered.

At a global level, climate change has been the focus. Hence, CO_2 emissions related to concrete production are widely studied and average values are provided by many authors, some of which are gathered in (Rodríguez-Robles et al. 2019).

At a regional scale the emissions which contribute to acid rain (SO_2 and NOx) are considered. SO_2 is mainly a consequence of fuel combustion and the raw materials heated in kilns. NOx molecules are released into the air from fuel and energy consumption linked to cement production. An overview of those emissions may be found in (Rodríguez-Robles et al. 2019).

At a local scale, the emission of dust has a major impact. The amount of cement kiln dust accounts for approximately 15-20% by mass of all clinker that is produced. However, the reported values can vary immensely. The carbonation of this waste can reduce health risks associated with cement dust. Other emissions to consider at a local scale are metal emissions and polychlorinated dibenzo-p-dioxins and dibenzofurans (PCDD/Fs), because they can be transmitted to humans through air, groundwater, soil and vegetation. In addition, the chromium content of cement should be also considered (Rodríguez-Robles et al. 2019).

SCM

SCM from other industries are considered as by-products. Their environmental impact should therefore also be allocated and the way that is done can have a great impact on the assessment of SCM.

For example, if allocation by mass is applied to CO_2 emissions of silica fume and fly ash, it will result in higher emission values than cement. The economic allocation is therefore not directly linked to the cement industry per se. However, it would also present an immense disadvantage, as the cost varies depending on availability and location.

AGGREGATES

Aggregates only account for 17%–25% of the embodied energy of concrete (O'brien et al. 2009). Aggregate emissions can include emissions from explosives used for raw material extraction and from electricity and fuel consumption to perform the crushing, grinding, screening and transport operations.

Aggregates are sometimes considered limitless, in terms of the most common resources depletion indicators. At a global scale, this aspect could perhaps be neglected, although there are clear indicators of depletion at a local level (Rodríguez-Robles et al. 2019).

In addition, mineral extraction has terrestrial, fluvial, and coastal impacts and can change the landscape.

ADMIXTURES

Admixture emissions contribute to the potential acidification of land and water, eutrophication, and photochemical oxidation, fossil fuel depletion, and of course the warming potential (Rodríguez-Robles et al. 2019). Admixture impacts have been provided by the European Federation of Concrete Admixture Association in the form of EPDs. Although the environmental impact of admixtures is generally higher than cement, only small amounts are used in concrete so their impacts are therefore low.

WATER

Water is consumed at all stages of concrete production. During cement production, approximately 4 litres/tonne are required, in addition to water for cooling and controlling the emission systems. During aggregate production, water is also needed, accounting for approximately 1000L per ton. During concrete manufacturing, water is needed not only as a concrete component, but also for curing and cleansing processes. Water consumption also has an impact on the potential depletion of resources (Rodríguez-Robles et al. 2019).

The most common impact categories that are assessed in the concrete industry and their related emission levels are summarized in Table 3.6.

3.3 Economic impacts

From a sustainability perspective, economic and environmental impacts are essential and, in general, closely related. A lot of environmental degradation occurs when people are struggling to obtain the resources that are essential for life (food, water, shelter, etc.), and it is inevitable that the basic economic struggle may take precedence over environmental sustainability (Struble & Godfrey 2001). Conversely, environmental deterioration exacerbates economic inequity, for example diseases associated with lack of clean water are a significant cause of poverty.

In Europe, the economic impact of the construction industry accounts for roughly 9% of GDP in the EU and is directly associated with roughly 18 million jobs[11].

Analyzing the production cost of a conventional ready-mix concrete (see Table 3.2), cement is the most influential material, and the material costs alone account for over

[11] https://ec.europa.eu/growth/sectors/construction_en

70% of total production costs (Proin 2010). Therefore, the reduction of OPC in concrete mixes represents the most potential option to reduce costs, followed by the reduction of fine and coarse aggregate costs. One promising solution could be to maximize packing of the granular skeleton and to use low-cost aggregate such as waste and by-products (for example, RCA and EAF aggregates), in order to reduce cement consumption.

Table 3.2. Breakdown of production costs of conventional C25/30 ready-mixed concrete.

Materials (including transport to concrete plant)	Costs
Cement	40.46%
Fine aggregates	15.14%
Coarse aggregates	15.14%
Additions and admixtures	1.32%
Water	0.28%
Total for materials	72.34%
Concrete transport	15.42%
Direct costs (personnel and others)	7.88%
Indirect costs (management and selling)	4.36%

3.4 Assessment methods

Several attempts have been made to quantify the environmental impact of cement-based materials, concrete products and building infrastructures. Some of the most relevant are analyzed below.

3.4.1 Life Cycle Assessment (LCA) approach

Life Cycle Assessment (LCA) is a standardized methodology for evaluating the environmental impacts associated with a certain system/product throughout its life cycle. An LCA is used in a rigorous and scientific way to calculate the consumption of energy and resources, the release of emissions into the air, the earth, and water, and waste generation. The LCA structure is defined and described in ISO standards (ISO 14040 - ISO 14044:2006), providing a comprehensive methodology for the implementation of an LCA. The four phases (see Fig. 3.3) (goal and scope definition, Life Cycle Inventory (LCI), Life Cycle Impact Assessment (LCIA) and interpretation) involved in an LCA are described below.

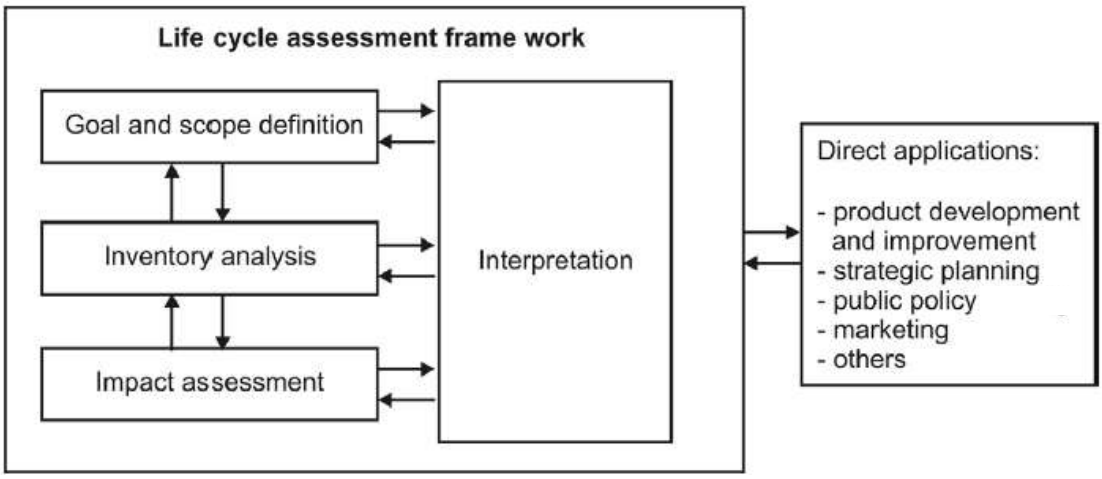

Fig. 3.3. Stages of an LCA according EN ISO 14040.

1. Goal and scope definition: In this step, the reason and the objectives for performing the LCA are determined and defined.

The ISO 14040:2006 (in its p. 11) defines the goal of an LCA as:

- The intended application (for what?);
- The reasons for carrying out the study (why?);
- The intended audience (for whom?);
- Whether the results of the study are intended to be used in comparative reports for public release (e.g. stating publicly that product A is better than product B).

The scope refers to the definitions of the functional unit, the system boundaries, the allocation procedures, the assumptions, the data requirements and the limitations, among others.

The selection of the *Functional Unit* (FU) requires special attention as it will depend on the function of the product or system. For example, the environmental impact of construction material can be measured only by volume or by mass, or it can also include functional properties (such as compressive strength) and durability properties in the concept of product functionality. Therefore, if the objective is to compare two products with the same functionality, the functional unit could simply be the product mass or volume. However, any comparison of two products with different properties or functions should include functionality in the functional unit, in order to analyze the environmental impact from an objective perspective (Marinković 2013).

In the LCA of concrete, there are three approaches to select the *system boundaries (*see Fig. 3.4*)* (Cao 2017; Marinković 2013).

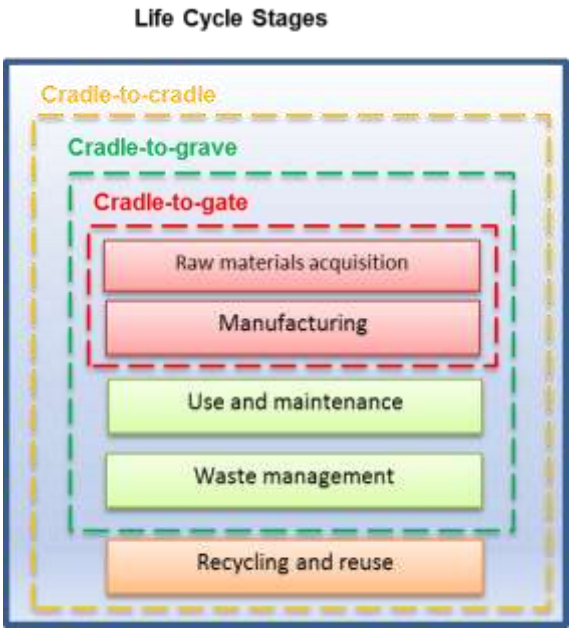

Fig. 3.4. System boundaries of each life cycle stage.

However, the first two are the most commonly applied:

a. *Cradle-to-gate.* Concrete is assessed as a material for a specific application. The system boundaries only involve the production stage. Environmental Product Declarations (EPD) (see chapter 3.4.2) are performed through this type of analysis.
b. *Cradle-to-grave*. A product made with concrete is fully assessed throughout the whole life cycle. The system boundaries run from the resource extraction stage to both the use and the demolition stage. It is used to analyze the environmental impact of a building, bridge, road, etc.
c. *Cradle-to-cradle.* This approach goes one step further. It involves not only the whole life cycle of a product, but also the recycling or valorization process of the product.

At that stage, the environmental impact to be assessed must be also selected.

2. Life cycle Inventory analysis (LCI): the second phase of the LCA. Here the necessary inputs and outputs to perform the LCA by the objectives are collected. Although, databases are available to facilitate data collection, it is the most time-consuming stage in an LCA. After collection, the data for the different processes have to be calculated in relation to the functional unit and aggregated per life cycle stage. The functional unit is a quantity to which all inputs and outputs have to refer.

The data quality can also be established at this stage. The goal during data collection is to amass reliable, complete, up-to-date and geographically and technologically representative data. However, this will often not be feasible to achieve and any inconsistencies will have to be identified.

Allocation

The LCI of concrete requires allocations when alternative materials are used, from other industrial sources such as fly ash and GBFS. In many LCA, these materials are considered as waste and only the environmental impacts of processing are considered. However, according to the European Union directives (European Union 2008), SCM from other industries are considered as by-products rather than waste. The ISO standards recommend the use of allocation for the treatment of multifunctional processes, if and only if it is inevitable. Allocation (see equation 3.4) can be performed by physical causality, such as mass or energetic value or by other causalities, such as economic value (Habert 2013). The choice of the allocation type is very influential in the results of an LCA and is therefore one of the most controversial issues in LCA (Chen et al. 2010). The difficulty of impact allocation is to determine the environmental impact attributable to each manufacturing process.

$$\bar{I}_{SCM} = C \cdot \bar{I}_{primary\_process} + \bar{I}_{treatment} \quad 3.1$$

where, $\bar{I}$ is the environmental impact of SCM and C is the allocation factor to attribute the environmental impact corresponding to the primary process. In the above equation, the allocation process is applied over the environmental impact rather than the LCI (Habert 2013).

Some authors have studied the effect of applying allocation to the by-products used in concrete (see Table 3.3).

Table 3.3. Relevant studies on the influence of SCM in cement production and its allocation.

Source	Materials	Allocation type	Description
(Habert 2013)	Fly ash GBFS	Economic	A method for economic allocation that avoids price fluctuation. The allocation coefficient yields similar benefits for all companies and stakeholders. The main drawback of the method is that it has to be calculated for each impact category.
(Chen et al. 2010)	Fly ash GBFS	No-allocation Economic Mass	A comparison of three allocation process to assess FA and GBFS. The results showed that economic allocation is more feasible in the concrete industry.
(Seto et al. 2017)	Fly ash	No-allocation Economic Mass Disposal Avoidance	A study of the application of different allocation methods for fly ash and their consequences. The conclusion was that economic and mass allocation will result in higher environmental impacts than no-allocation or disposal avoidance methods.

In the concrete industry, the main advantage of mass allocation is that the value remains constant. However, mass allocation of SCM is unfeasible when the replacement of OPC is studied, as the impact of SCM is generally higher than the impact of cement (Chen et al. 2010). The allocation factor can be calculated with the following equation 3.2:

$$C_m = \frac{m_{SCM}}{m_{product} + m_{SCM}} \qquad 3.2$$

In contrast, economic allocation has the capacity to decrease the environmental impact associated with SCM, however it presents unstable values, due to market price fluctuations (Chen et al. 2010).

$$C_e = \frac{(€.m)_{SCM}}{(€.m)_{product} + (€.m)_{SCM}} \qquad 3.3$$

Other allocation methods considered in literature include the so-called 'avoided burdens' when calculating the environmental burden of a by-product. However, they fail to address allocation problems (Habert 2013).

LCI data collection:

In the book "Life Cycle Assessment. Environmental Management" (Muralikrishna & Manickam 2017), two types of data were distinguished: foreground and background data. Foreground data include the data needed to model the system while background data are data linked to generic systems that are less relevant to the LCA objective. These data can be found in databases, the literature, and EPD specifications. For a highly reliable LCA, the ISO standards recommend data extraction, in the order shown below:

1. Industrial sources;
2. EPDs;
3. Public databases;
4. Environmental Reports (ERs).

First-hand data results in a more reliable LCI, however it is not always provided by the companies, because of confidentiality issues. Another source from which to obtain high quality and suitable data is the Environmental Product Declaration (EPD).

3. Life cycle impact assessment (LCIA): The aim of this phase is to evaluate the environmental impact based on the LCI flows. It involves the steps listed in Table 3.4.

The first three steps are mandatory while the remaining are optional. Generally the impacts considered in a Life Cycle Impact Assessment include climate change, ozone depletion, eutrophication, acidification, human toxicity (cancer and non-cancer related) respiratory inorganics, ionizing radiation, ecotoxicity, photochemical ozone formation, land use, and resource depletion. In the LCIA phase, the flows (resouces and emissions) from the LCI are linked to each of these categories. Finally during the characterization step, input and output parameters are converted into indicators using impact

assessment models (EC-JRC 2010). Normalization, grouping, and weighting – may be conducted depending on the goal and scope of the LCA study.

Table 3.4. Summary of the LCIA elements

Steps	ISO requirements	Description
Selection and identification of impact categories.	Mandatory	Definition of the relevant environmental impact.
Classification	Mandatory	Assignation of LCI flows to impact categories.
Characterization	Mandatory	Characterization of the LCI using one of many possible LCIA methodologies. The LCI flows are multiplied by the characterization factors to transform values into common equivalence units that are then summed up, to provide an overall impact category total.
Normalization	Optional	The impacts are associated with a common reference to facilitate comparison across impact categories.
Weighting	Optional	A weighting factor is assigned to each impact category according to its relative importance.
Grouping	Optional	Grouping consists of sorting and possibly ranking the impact categories.

Characterization factors are clasified into two groups:

- Midpoint level model
- Endpoint level model

The midpoint approach, also known as problem-oriented analysis, is the most conventional approach. Its category indicator is located in between the LCI results and the category end points. They quantify the emissions that contribute to a problem without considering the actual environmental damage. One example is climate change expressed in kg of CO_2 eq. In contrast, endpoint approaches have a more explicit focus on the actual effect. They attempt to model the actual environmental damage (EC-JRC 2010). Fig. 3.5 shows the relation between LCI, and midpoint and endpoint LCIA.

ISO 14044:2006 requires a deliberate assessment of all relevant impact categories for an LCA study; it is therefore not allowed to leave out impact categories that make a significant impact. The selection of the appropriate impact categories is therefore an important step. There are many LCIA methods and models available, developed by various research teams all over the world.

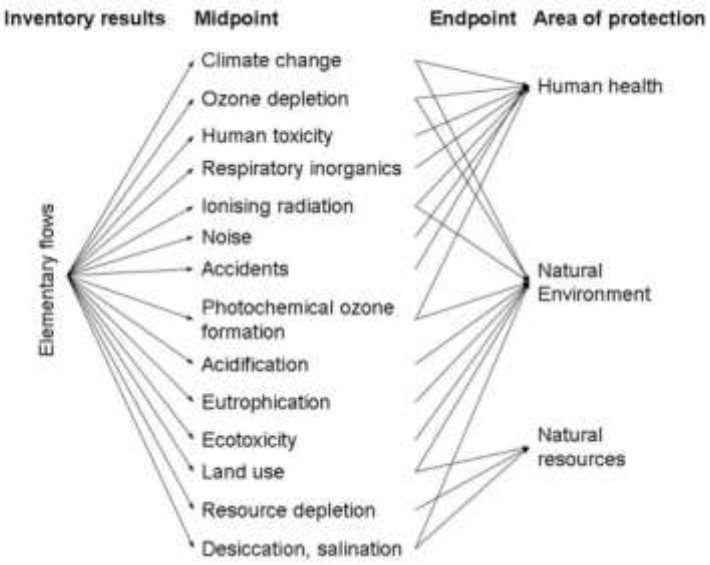

Fig. 3.5. Framework of impact categories for characterization modelling at midpoint and endpoint levels (EC-JRC 2010).

Standards EN 15804:2012+A1:2013 and EN 15978:2011 outline the use of the following seven impact categories for environmental product declarations (EPD) of building products and for the environmental assessment of buildings, respectively (see Table 3.4).

Table 3.5. Mandatory LCIA indicators according to EN 15804:2012+A1:2013 and EN 15978:2011

LCIA indicators		**Abbreviations**	**Units**
1	Global warming potential (climate change)	GWP	kg CO_2 eq.
2	Ozone depletion potential	ODP	kg CFC-11 eq.
3	Acidification potential	AP	kg SO_2 eq.
4	Eutrophication potential	EP	kg $(PO_4)^{3-}$ eq.
5	Photochemical ozone creation potential	POCP	kg ethene eq.
6	Abiotic depletion potential - elements	ADP-elements	kg Sb eq.
7	Abiotic depletion potential – phosil fuel	ADP-fossil fuel	MJ
Life Cycle Inventory Data			
8	Total renewable primary energy consumption	Pe-Re	MJ
9	Total non-renewable primary energy consumption	Pe-NRe	MJ

Several scientific studies, however, indicate the need for a broader environmental perspective. For instance, the Product Environmental Footprint (PEF) Guide contains fourteen default impact categories. The selection of impact categories used within the PEF framework is based on the ILCD recommendations from the Joint Research Centre of the European Commission (EC-JCR 2011) The team of the EC-JRC evaluated different LCIA methods for relevant impact categories. The scientific criteria used by the EC-JRC are:

1. Completeness of the scope;
2. Environmental relevance;
3. Scientific robustness and certainty;
4. Documentation, transparency and reproducibility;
5. Applicability;
6. Stakeholder acceptancy.

The list of impact categories at midpoint that are recommended by the EC-JRC can be consulted in the PEF guide (EC-JRC 2012)

4. Interpretation: the final phase of an LCA analysis. The main purpose of this stage is to discuss the results of the LCI and LCIA and to provide conclusions, recommendations and decision-making (Lehtinen et al. 2011). At this stage, sensitivity and uncertainty analyses will sometimes precede the conclusions (Muralikrishna & Manickam 2017).

As a brief summary of present section see Fig. 3.6 and Table 3.6.

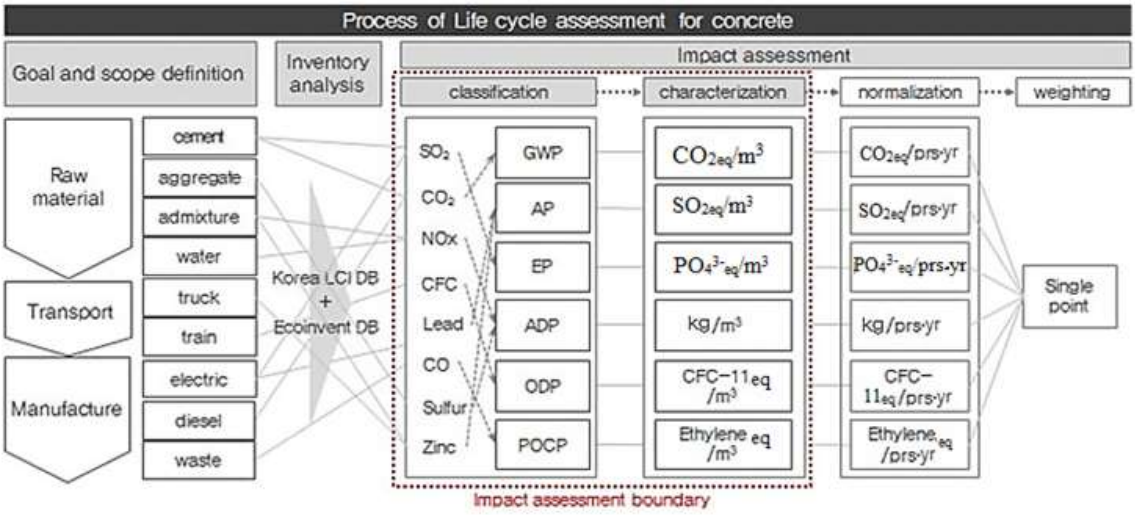

Fig. 3.6. Global process of Life Cycle Assessment for concrete (Kim & Tae 2016)

Table 3.6. Commonly used Life Cycle Impact categories and associated endpoints.(US EPA 2006)

Impact category	Scale	Emissions	Endpoint effects
Global Warming	Global	Carbon Dioxide (CO_2); Nitrogen Dioxide (NO_2); Methane (CH_4); Chlorofluorocarbons (CFCs); Hydrochlorofluorocarbons (HCFCs); Methyl Bromide (CH_2Br)	Polar melt, soil moisture loss, longer seasons, forest loss/change, and change in wind and ocean patterns
Stratospheric Ozone Depletion	Global	Chlorofluorocarbons (CFCs); Hydrochlorofluorocarbons (HCFCs); Halons, Methyl Bromide (CH_3Br)	Increased ultraviolet radiation

Impact category	Scale	Emissions	Endpoint effects
Acidification	Regional Local	Sulphur Oxides (SOx); Nitrogen Oxides (NOx); Hydrochloric Acid (HCL); Hydrofluoric Acid (HF); Ammonia (NH_4)	Building corrosion, water body acidification, vegetation effects, and soil effects
Eutrophication	Local	Phosphate (PO4), Nitrogen Oxide (NO) Nitrogen Dioxide (NO2) Nitrates Ammonia (NH4)	Nutrients enter water bodies, such as lakes, estuaries and slow-moving streams, causing excessive plant growth and oxygen depletion
Photochemical Smog	Local	Non-methane hydrocarbon (NMHC)	"Smog", decreased visibility, eye irritation, respiratory tract and lung irritation, and vegetation damage.
Terrestrial Toxicity	Local	Toxic chemicals with a reported lethal concentration to rodents	Decreased production and biodiversity and decreased wildlife for hunting or viewing
Aquatic Toxicity	Local	Toxic chemicals with reported lethal concentrations for fish	Decreased aquatic plant and insect production and biodiversity and decreased commercial or recreational fishing
Human health	Global Regional Local	Total releases to air, water and soil	Increases morbidity and mortality
Resource Depletion	Global Regional Local	Quantity of minerals used Quantity of fossil fuels used	Decreased resources for future generations
Land Use	Global Regional Local	Quantity disposed of in landfill sites or other earthworks	Loss of terrestrial habitat for wildlife and decreased landfill space
Water Use	Regional Local	Water used or consumed	Loss of available water from groundwater and surface water sources

3.4.2 Environmental Product Declarations (EPD)

An EPD (Environmental Product Declaration) is a verified and registered document that communicates transparent and comparable information on the life-cycle environmental impact of a product. Construction EPDs are based on ISO 14025 (ISO-14025 2010) and EN 15804 (UNE-EN 15804 2013). The latter provides a structure to ensure that Environmental Product Declarations (EPD) of construction products, construction services, and construction processes are obtained, verified and presented in a harmonized manner. Guidelines presented in Product Category Rules (PCR) documents are also available.

EPD quantifies the environmental information for a product relying on LCA according to environmental indicators for different impact categories, in addition to including other environmental information. The information covers the global warming potential,

acidification, eutrophication, destruction of the ozone layer, smog formation and consumption of energy and resources (Gursel 2014).

Although several program operators are currently available (BRE Global, EPD Norge, International EPD, etc.), the standards and PCR ensure that the EPD information can be comparable regardless of the program operator (Cao 2017).

Over the past 4 years, the number of EPD and program operators has increased internationally. This fact has resulted in different schemes with different requirements for issuing an EPD (PCRs), lessening the comparability of the environmental results.

3.4.3 Product Environmental Footprint (PEF)

After the request by the experts to develop a general guideline for measuring the environmental impact of a product that guarantees reproducible, comparable and verifiable results, the European Union began to develop the Product Environmental Footprint (PEF). The aim of the PEF is to harmonize the environmental impacts of products. The first guide was published in 2013.

In the construction industry, the EN 15804 standard for environmental impact assessments is broadly accepted. The PEF guidelines have yet to specify construction products. However, the benefits of adhering to PEF rules when assessing construction products has been analyzed[12].

Experts claim that the convergence between EPD and PEF is difficult. However, a common scientific methodology for construction products and system assessments would indeed be beneficial[13].

The main differences between both approaches are:

- The end of life approach.
- The list of impact assessment categories.
- The aim of EPD is to provide consumers with full environmental information while the PEF approach also promotes benchmarking.

In addition, uncertainty and credibility problems associated with both EPD and PEF assessment, due to the use of heterogeneous databases, also need to be addressed.

3.4.4 LCI of concrete industries

Many general database sets are available on the market. However, the data on construction materials especially, of concrete components and cement types, is limited. The most widely known at an international level are the Ecoinvent database (Wernet et

[12] https://www.pre-sustainability.com/customer-cases/applying-pef-rules-construction-products
[13] https://www.construction-products.eu/publications/publications/epd-current-debate-and-challenges

al. 2016) and the Gabi database (Thinkstep 2018). At a European level the ELCD (ELCD - EPLCA 2015) database stores data on a large number of European products and processes and is free of charge. A brief review of some of the databases on the market, which include construction materials, is shown in Table 3.7.

Table 3.7. Construction materials Database

Database	Brief description	Availability	Web
Ecoinvent	It is one of the most famous LCA database. It accounts with approximately 6 LCI related to cementitious material, aggregates and concrete are available.	Licensee is needed	https://www.ecoinvent.org/home.html
GaBi	Together with the Ecoinvent database, it is leader of the LCI database. Its database of concrete ingredients and products is by far the most extended, including even alternative cement such as CSA cement.	Licensee is needed	http://www.gabi-software.com/international/index/
ÖKOBAUDAT	Dutch database. It includes only construction materials.	Licensee is needed	https://www.oekobaudat.de/
ELCD	ELCD is the European reference Life Cycle Database. It was established by the EC JRC. The LCI for construction materials is limited 24. Only 12 cementitious materials, aggregates or granular particles and types of concrete are registered.	Free	https://eplca.jrc.ec.europa.eu/ELCD3/
NEEDS	Needs is an international database. It includes the LCI of clinker production in the future (2025 and 2050).	Free	http://www.needs-project.org/needswebdb/
AusLCI	Australian database. It includes a set of concrete data.	Linked to Ecoinvent or Gabi license	http://www.auslci.com.au/index.php/Contributors
NREL-USLCI	It is the U.S. life cycle database.	Free	https://www.nrel.gov/lci/about.html
OpenDAP	It is part of a DATA European project. It a very extensive data base of construction products with harmonize data of the CO_2 emissions.	Free	https://www.opendap.es/

For more detailed information, an extensive review on databases of building materials and their limitations can be consulted in (Martínez-Rocamora et al. 2016).

Concrete LCI mainly involves the following inputs and outputs (Gursel 2014):

- Inputs: The concrete components that include raw materials (Limestone, aggregates, clay, pozzolan), cement, admixtures, by-products and water, in addition to energy consumption such as fuel and electricity.
- Outputs: Air, water and land emissions.

Cement LCI studies:

Several LCI of cements produced in Europe were compared in (Josa et al. 2004). The results showed low accuracy and representativity of the cement LCI. In addition, the variations of the system boundaries complicated any comparison of the data.

Concrete LCI studies:

Petek Gursel et al. (2014) analyzed the quality of various concrete LCIs. They highlighted three limitations: lack of holistic assessments of environmental impacts, the non-consideration of geographic and technological variables and insufficient attention to LCA parts considered insignificant at 1 unit of concrete, although they can assume relevance at a macroscale analysis, for example, with regard to water consumption.

3.4.5 Review of environmental assessment methods and tools

There are various tools for assessing the environmental impact of different products and systems for a particular field of industry, most of which are based on LCA. Sometimes, databases are included in the tool and they are specifically designed for the use of a specific software (Lehtinen, et al., 2011).

A list of existing LCA-related tool is included in Table 3.8.

Table 3.8. List of some LCA and LCC tools for the construction industry. Adapted from (Lehtinen, et al., 2011)

Tool name	Supplier	Language	Main database	LCIA method	System boundaries	Special area if any	Free?	Web page
ATHENA	Athena Sustainable Material Institute (USA)	EN	Athena Institute	TRACI	Products, building assemblies, whole structure, building portfolios and roadways	Construction Industry	Yes	http://www.athenasmi.org/our-software-data/overview/
BEES 4.0	National Institute of Standards and Technology (NIST) (USA)	EN	Bees database from SimaPro	TRACI (Environmental) + economic	Building products	Construction industry	yes	http://www.nist.gov/el/economics/BEESSoftware.cfm
CCaLC Tool	The University of Manchester	EN	CCaLC database including EcoInvent database	(excel tool)	Cradle to gate Cradle to Cradle	Generic	yes	http://www.ccalc.org.uk/index.php
Eco-Bat 2.1	Haute Ecole d'Ingénierie et de Gestion du Canton de Vaud	FR, IT, EN	Eco-Bat database (data extracted from Eco-invent)		Building materials and building.	Construction industry	No	http://www.eco-bat.ch/index.php?option=com_content&view=frontpage&Itemid=1&lang=en
Environmental Impact	Athena Sustainable Materials Institute	EN	Own database Athena Institute	TRACI	Products, building assemblies, whole structure, building	Construction Industry	Yes	http://www.athenasmi.org/our-software-data/overview/

Tool name	Supplier	Language	Main database	LCIA method	System boundaries	Special area if any	Free?	Web page
Estimator V3.0.2					portfolios and roadways			
GaBi 4	PE International GmbH University of Stuttgart, LBP-GaBi	EN	Gabi database	Many LCIA methods		Generic	No	http://www.gabi-software.com/index.php?id=85&L=0&redirect=1
Green Concrete LCA Web Tool	University of Berkeley	EN		TRACI	Concrete and its constituents Cradle to grave	Construction Industry	Yes	https://greenconcrete.berkeley.edu/
LEGEP 1.4	LEGEP Software GmbH	EN, GER	LEGEP Database		Whole life cycle of a building LCA + LCC	Construction industry	No	http://www.legep.de/index.php?AktivId=1125
OpenLCA	GreenDeltaTC GmbH	EN	Market or open Database can be imported			Generic	yes	http://www.openlca.org
SimaPro 7	PRé Consultants B.V.	E.g. ES, FR, IT, GER, EN	SimaPro database				No	http://www.pre.nl/
Umberto	Ifu Hamburg Member of iPoint Group	EN	Ecoinvent and Gabi		LCA+LCC	Generic	No	https://www.ifu.com/en/umberto/lca-software/

GREEN CONCRETE LCA TOOL

Green Concrete LCA is an environmental assessment tool of ready-mixed concrete that was developed at Berkeley university (Gursel 2014). The tool serves to quantify and to compare the environmental impacts of different concretes and to assist with the decision-making processes of construction managers, contractors, civil engineers, architects and proprietors for the selection of materials. The scope of the tool includes the whole production process of concrete (raw material extraction, cement production, SCM processing, production of chemical admixtures, electricity of the process that is considered and transportation of the materials). The tool is based on LCA methodology and the environmental impacts are assessed with TRACI LCIA methodology.

The characteristic feature of the tool is that it is dynamic and flexible because it integrates regional, technological and mix-design alternatives. Therefore, the electricity mix and the sources of energy consumption can be adapted to regional values. In addition, the technology of the processes, to obtain each concrete ingredient can be also selected (Gursel 2014). Its other advantages are that it is a user-friendly tool with a free online version[14].

[14] https://greenconcrete.berkeley.edu/environimpacts.html

This tool presents the following limitations (Gursel 2014):

- The tool only assesses the environmental impact of concrete without considering the economic aspects.
- The components of concrete mix design to be analyzed are limited by the tool. Although some SCM such as Fly ash, GBFS, and limestone have been included, no consideration is given to other types of aggregates. (Aggregate impacts are considered as the average energy values for fine and coarse aggregates, overlooking the influence of energy consumption during the processing of different aggregate types.)
- Allocation was not considered in the environmental impact of SCM by-products.
- The admixture LCI data and the water consumption were also limited, as it was taken from one source, presenting uncertainty.
- The tool is limited to the cradle-to- gate analysis of concrete.
- The impact assessment is based on TRACI methodology without the possibility of choosing another characterization factor to calculate the final impacts. TRACI methodology is commonly used in the US, because the characterization factors are associated with the environmental necessities of the country. Methodologies such as CML and PEF are at present more widely used in Europe.

CLAS

The Concrete Life Cycle Assessment System (CLAS) was developed in Korea by Kim, et al. (T. Kim et al. 2013). The tool goes one step further, by integrating and optimizing the system, based on evolution algorithms and neuronal networks, which identify the specific concrete mix design, minimizing the CO_2 emission and the total concrete production cost. CLAS was developed in visual basic and integrates environmental, economic and functional aspects. Environmental assessment is based on LCA methodology and applies a cradle-to-gate analysis of concrete. The tool has a database of 800 concrete mixes from which an optimal mix design is generated.

The limitations of this tool are as follows:

- The LCI is based on a Korean database, which means that the results are to some extent limited to that region.
- CLAS only considers CO_2 concrete emissions as environmental impacts. This information is very limited when assessing the environmental impact of a concrete. A larger number of impacts should be considered for decision making.
- The components of concrete mix design that can be analyzed are limited by the tool. Although some SCM such as Fly ash and GBFS have been included, the tool cannot process other aggregate types. Aggregate impacts were considered as the average of energy values for fine and coarse aggregates. This factor neglects

the influence of energy consumption during the processing of different types of aggregates.

- Only plain concrete and concrete with a fly ash or/and blast furnace slag additions can be optimized, due to the limitation of the initial database of concrete mixes.

3.4.6 Environmental and economic indicators

The best way of measuring the efficiency of cement has been discussed in the literature for a long time. In a pioneering paper, Popovics (Popovics 1990) presented an indicator, f_{eco}, based on a measure of the efficiency of concrete. It is defined as the compressive strength by unit of cement mass. In a more general approach, total binder, instead of the cement amount was considered to measure the economic and the environmental efficiency of cement per unit of concrete performance (compressive strength, bending strength, modulus of elasticity, carbonation resistance, etc.) (Damineli et al. 2013; Aïtcin 2000).

Damineli et al. introduced the concept of binder intensity (bi_{cs}) to measure concrete efficiency. This indicator was designed to be simple, familiar and easy to use. They selected the binder content (removing the amount of limestone filler from calcination) needed to provide 1 MPa at a given age as the concrete efficiency indicator, because the trend with most potential to reduce the environmental impact of concrete is related to the replacement of OPC by other binders. CO_2 intensity (ci_{cs}) was also proposed as another indicator to measure the concrete footprint. It is defined as the amount of CO_2 released by 1 m^3 of concrete per performance unit; in this case 1MPa of compressive strength (Damineli et al. 2010).

$$bi_{\mathrm{cs}} = \left(\frac{kg\ binder}{MPa \cdot m^3}\right) \tag{3.4}$$

$$ci_{\mathrm{cs}} = \left(\frac{kg\ CO_2}{MPa \cdot m^3}\right) \tag{3.5}$$

Applying this system to several concrete mixes, they showed the risk of taking only the volumetric or mass unit of concrete as an indicator. In addition, both indicators can be easily modified to measure concrete efficiency, taking account of other concrete performance indices (such as service life, durability etc.), environmental impacts, and economic impact.

3.4.7 LCA of concrete made with alternative aggregates

Although the environmental impact of concrete has been analyzed since 1983, interest in alternative aggregates has increased over recent years (Colangelo et al. 2018).

Dr. Gursel (2014) included an exhaustive state-of-the-art review of LCAs used in the construction sectors in her thesis. She analyzed LCA studies at three levels, cement manufacturing, concrete manufacturing, and commercial buildings (Gursel 2014).

Some limitations observed from the analysis of Concrete LCA studies are as follows (Gursel 2014):

- Lack of individual LCA and LCI for concrete components that differ from cement (aggregates, admixtures, and water consumption).
- In most concrete LCAs, the environmental impact of admixtures is considered negligible.
- Different allocation systems were applied for by-products. There is lack of agreement.
- Lack of regional and technological considerations. There is an extended use of average factors at national level for mass and energy flow.
- Lack of data on solid and liquid wastes generated from concrete production.
- Lack of data on water consumption and withdrawal impacts.
- Lack of data is generally assumed or estimates are given insufficient attention.

In recent years, some authors have studied the environmental impact of using EAFS as a substitute for natural aggregates (Faleschini et al. 2014; Anastasiou et al. 2017; Evangelista et al. 2018). However, these are very limited, compared to the studies that can be found in the literature on recycled concrete aggregates (Braga et al. 2017; Faleschini et al. 2016; Rosado et al. 2017; Rodríguez-Robles et al. 2019; Yazdanbakhsh & Lagouin 2019; Marinković et al. 2013; Hossain et al. 2016a; Pradhan et al. 2019; Zhang et al. 2019).

3.5 Multiple-Criteria Decision Methods (MCDM)

MCDM has been developed to assist decision-making when faced with several alternatives and criteria that can often be conflictive. It should be taken into account that no optimal solution exists when multiple criteria have to be considered. Thus, the decision is taken based on stakeholder preferences (Pavan et al. 2009), as presents in Fig. 3.7.

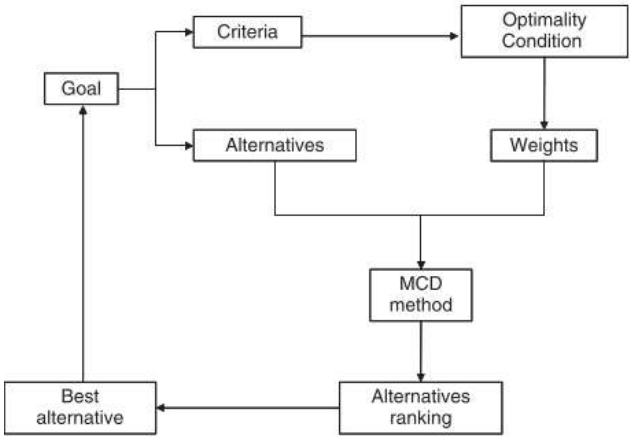

Fig. 3.7. General structure of the Multicriteria Decision-Making (MCDM) process (Pavan et al. 2009).

The MCDM provides a choice, ranking, classification and sorting of the alternatives that are proposed and the criteria that are often established by a panel of experts.

MCDM applies hierarchical rankings in the development of methods that are used to quantify and to prioritize the available options. The methodology basically consists of three stages (Triantaphyllou 2000):

- Generate the set of alternatives related to the problem and select the criteria.
- Define the numerical factor associated with the relative importance of the criteria and the impacts of the alternatives to those criteria.
- Process the numerical values to determine a ranking for each alternative.

There are many MCDM methods (see Table 3.9) that all have their own advantages and disadvantages, so no consensus exists over which is the best application.

Table 3.9. Summary of MCDM methods. (Velasquez & Hester 2013)

MCDM methods	Advantages	Disadvantages	Fields of application
Multi-Attribute Utility Theory (MAUT)	Uncertainty is accounting	Many inputs are needed Very precise preferences	Economic and water, energy and agricultural management
Analytic Hierarchy Process (AHP)	Ease of use Scalability	It bases on pairwise comparison: interdependence between criteria and alternatives	Resource management, corporate policy and strategy, public policy, political strategy and planning
Fuzzy Set Theory	Imprecise inputs are allowed	Difficult to develop (many simulations are sometimes required)	Engineering, economic, environmental, social, medical and management
Case-based Reasoning (CBR)	Little effort to collect data (use of database) Can Improve over time	Sensitive to inconsistency in data. It requires many cases	Business, vehicle insurance, medicine, engineering design
Data Envelopment Analysis (DEA)	Multiple inputs and outputs can be considered Efficiency can be analysed and quantified	Data must be precise	Economic, medical, utilities, road safety, agriculture, retail and business problem
Simple Multi-Attribute Rating Technique (SMART)	Simple	Procedure may not be convenient considering the framework	Environmental, construction, transportation and logistics, military, manufacturing and assembly problems

MCDM methods	Advantages	Disadvantages	Fields of application
Goal Programming	Capable of handling large-scale problems; can produce infinite alternatives	It's ability to weight coefficients; typically needs to be used in combination with other MCDM methods to weight coefficients	Production planning, scheduling, health care, portfolio selection, distribution systems, energy planning, water reservoir management, scheduling, wildlife management
ELECTRE	Takes uncertainty and vagueness into account	Its process and outcome can be difficult to explain in layman's terms; outranking causes the strengths and weaknesses of the alternatives to not be directly identified.	Energy, economics, environmental, water management, and transportation problems
PROMETHEE	Easy to use; does not require assumption that criteria are proportionate	Does not provide a clear method by which to assign weights.	Environmental, hydrology, water management, business and finance, chemistry, logistics and transportation, manufacturing and assembly, energy, agriculture
Simple Additive Weighting (SAW)	Ability to compensate among criteria; intuitive to decision makers; calculation is simple does not require complex computer programs	Estimates revealed do not always reflect the real situation; result obtained may not be logical	Water management, business, and financial management
Technique for Order of Preference by Similarity to Ideal solution (TOPSIS)	Has a simple process; easy to use and program; the number of steps remains the same regardless of the number of attributes	Its use of Euclidean Distance does not consider the correlation of attributes; difficult to weight and keep consistency of judgment	Supply chain management and logistics, engineering, manufacturing systems, business and marketing, environmental, human resources, and water resources management

Some of the most relevant ones used in construction sector (Navarro et al. 2018) are briefly described below.

3.5.1 Analytic Hierarchy Process (AHP)

AHP is "a theory of measurement through pairwise comparisons and relies on the judgments of experts to derive priority scales" (Saaty 1990). It was developed by Saaty and today it is one of the most popular MCDM methods to assess the sustainability of civil-engineering problems (Navarro et al. 2018).

The method comprises three steps. Firstly, the general problem is divided into smaller problems that are hierarchically classified. Several levels are modelled according to the need of the problem. Thus, for example, sustainability is led by three main levels economic, environmental and social criteria and these are decomposed into sub-criteria according to the scope of the problem. The decision-makers then assess the criteria of each level through a pairwise comparison. Finally, AHP transforms the preferences of decision-makers into weighted factors for each criterion. This method is also used in

combination with other MCDM methods such as weighting techniques (Navarro et al. 2018).

The main advantage of this method is its ease of use and its scalability. The hierarchical structure makes it possible to adjust the size. However, interdependence problems between criteria and alternatives can also exist due to the pairwise comparison. Another drawback is its susceptibility to rank reversal when alternatives are added at the end (Velasquez & Hester 2013). Fig. 3.8 presents a concrete example *(Henry & Kato 2011)*.

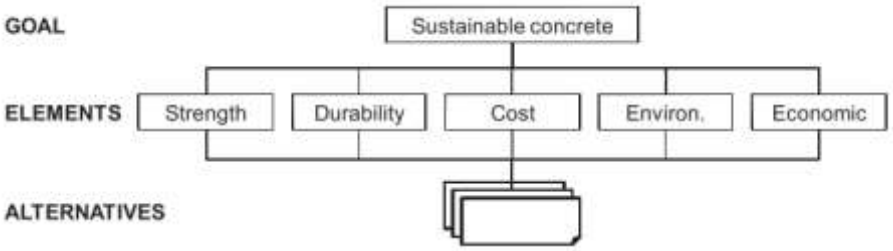

Fig. 3.8. Example of AHP hierarchy to assess concrete materials (Henry & Kato 2011).

3.5.2 Technique for Order of Preference by Similarity to Ideal Solution (TOPSIS)

TOPSIS finds the best or the most preferable option by searching for the shortest geometric distance to the best solution. This method can consider quantitative and qualitative criteria simultaneously. In TOPSIS, compensation between bad and good results of a criterion is possible. Its simplicity means that the method is easy to use. However, it should be considered that that the correlation of attributes is not based on Euclidean distance (Navarro et al. 2018; Velasquez & Hester 2013).

3.5.3 The Preference Ranking Organization Method for Enrichment of Evaluations (PROMEHTEE)

PROMETHEE was developed by Brans (Brans & Vincke 1985). It is an outranking methodology based on the pairwise comparison of alternatives considering the established criteria. This method uses preference functions which will depend on the nature of the criteria and the scope of the problem to be solved. The best option is decided through the evaluation of the deviation between alternatives according to the criteria (Navarro et al. 2018).

Although the PROMETHEE family currently includes six outranking methods, the original version, PROMETHEE I (Partial ranking of alternatives), and PROMETHEE II (Complete ranking of alternatives) are the most widely used (Velasquez & Hester 2013).

The main limitation of the method is that although the assignment of weight values is needed, the method will not specify any. Thus, sometimes the AHP method is used for the weighting function in combination with PROMETHEE (Pavan et al. 2009).

3.5.4 Elimination and Choice Expressing Reality (ELECTRE)

Similar to PROMETHEE method, ELECTRE is also an outranking MCDM methodology that is based on pairwise comparations of alternatives considering individual criteria. ELECTRE is composed of seven different models (I, II, III, IV, a, IS and TRI) and a hybrid method for fuzzy MCDM (FELECTRE). Unlike other MCDM, ELECTRE III is not compensatory (a bad score cannot be compensated by good scores on other criteria) and it includes the fuzzy nature of the decision maker. Its main disadvantage is the complexity of its application (Tscheikner-Gratl et al. 2017).

3.5.5 Integrated Value Model for Sustainable Assessment (MIVES)

MIVES is a Multi-Criteria Decision Making (MCDM) tool which combines value functions, that transform indicators with different units into single values between 0 and 1, and AHP methodology, to assign the weights of each requirement, criterion, and indicator. It includes the following steps:

1- Define the requirements, criteria, and indicators of the requirements tree.
2- Assign the weights to each requirement, criteria, and indicator.
3- Define the value functions.

The method was applied to make assessments and decisions in different fields such as, for example, the assessment of university professors (Viñolas et al. 2009), taking technical-economic decisions related to the construction of a new metro line in Barcelona (Ormazabal et al. 2008), assessing the environmental impact of industrial buildings (San-José & Cuadrado 2010), the sustainability of concrete structures within the Spanish structural concrete code (Aguado et al. 2012), the sustainability of building technologies used to construct school buildings (Pons & Aguado 2012), and the sustainability of concrete structures (De la Fuente & Fernández-Ordóñez 2018).

3.6 Integration of LCA and MCDM methods

LCA generates the environmental impacts of products and systems according to a set of previously selected environmental indicators, however it does not solve the need for deciding on the basis of several criteria. Economic and social aspects are not integrated in the results of an LCA. In addition, the mandatory steps of this methodology only provide information on isolated environmental impacts without proposing decisions.

The normalization and weighting step of the LCA methodology is designed to provide a global environmental indicator involving different impact categories, with no possibility of integrating economic, functional, and social aspects. As a solution, many authors have attempted to use the MCDM methodologies and even integrate LCA with this methodology, to assess the sustainability of both the concrete and the construction process. The most recent examples are briefly summarized below:

- (Kim et al. 2013) developed a decision-making procedure combining LCC and LCA tool and Analytical Hierarchy Process (AHP) for civil-engineering structures (see Fig. 3.9). They compared two methods to optimize the structures, the conversion of CO_2 emissions to monetary value and AHP methodology. They concluded that both methods can be successfully used.

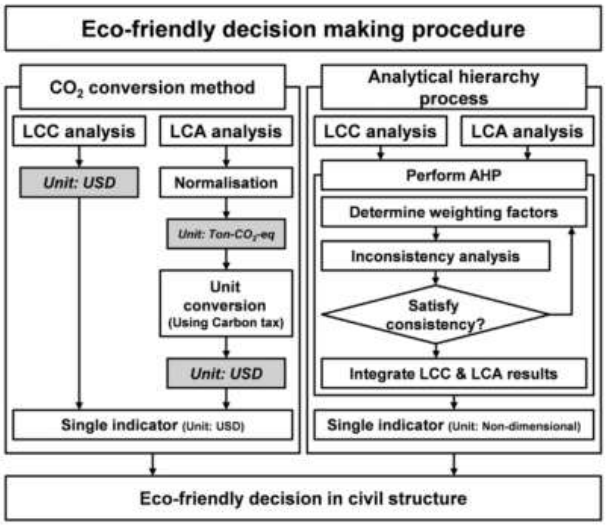

Fig. 3.9. Eco-friendly decision-making procedure developed (Kim et al. 2013).

- Amrina & Vilsi (2015) proposed a set of key performance indicators for cement sustainable assessment at economic, environmental, and social level. They used the AHP methodology to prioritize the indicator. This method is only able to assess cement sustainability on a qualitative scale.
- De la Fuente & Fernández-Ordóñez (2018) used the MIVES model to assess concrete product and system sustainability including the three pillars of economic, environmental and social sustainability. They presented three real case studies to demonstrate its applicability (wind precast concrete towers; steel fiber reinforced precast concrete tunnel linings, and reinforced concrete pile-supported slabs)
- CONCRETop is a recent multi-criteria decision method for concrete optimization (Kurda & Brito 2019). It was developed to optimize concrete mixes (conventional and non-conventional) on the basis of three perspectives: performance, environmental impact, and cost efficiency. The requested characteristic

demanded by the consumer will depend on the target application of concrete. Therefore, the optimization of concrete will depend on the application.

The tool comprises the following steps (Kurda & Brito 2019):

- The first step is the selection of the concrete application and the specification of the required properties. Whenever the requirements are unknown, the tool will propose 5 scenarios (Green, Strength, Service live, Cost and Business as usual) to cover most of the concrete application.
- In the second step, the most relevant categories at environmental, economic and technical performance level are selected (see Fig. 3.10).
- The third step consists of a ranking of the previously selected categories. The ranking is divided into 5 groups, from best to worse.
- In step four, the categories are standardized to rank mixes from high to low impact.
- The five steps consist of establishing the weighing factor for each category according to the application scenario.
- In step six, the threshold values of each category selected in two steps are established
- Finally, the tool shows a ranking of the concrete mix, showing the optimum concrete mix for each application.

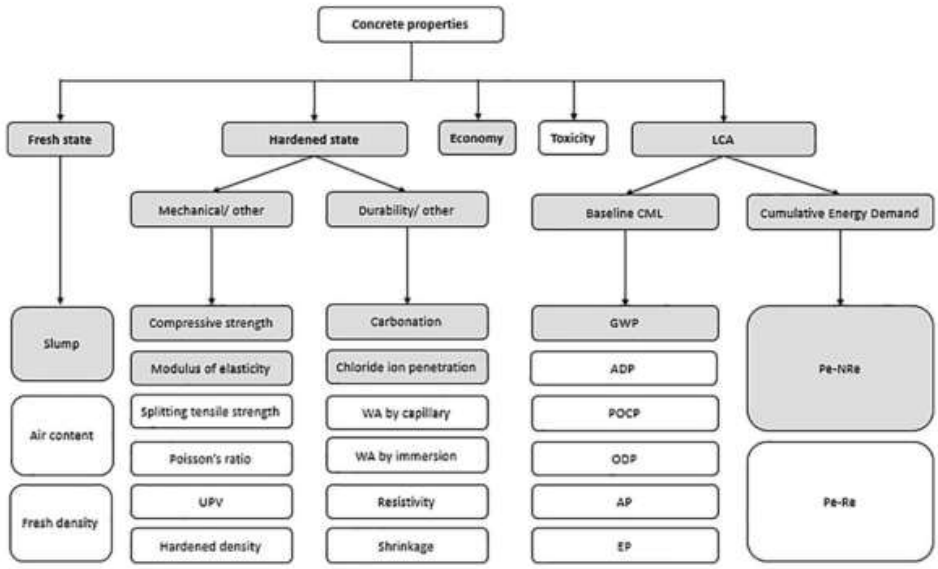

Fig. 3.10. Main categories that can be used for the optimization. The grey color presents the categories used in the CONCRETop optimization method (Kurda et al. 2019).

- In order to validate the tool, CONCRETop was applied to non-conventional concrete made with different proportions of fly ash and recycled aggregates (Kurda et al. 2019).

3.7 Summary and conclusions

From the review of the literature, the following observations and conclusions are worthy of consideration:

- LCA methodology is used to evaluate the environmental impact of concrete and is widely accepted in the literature. In addition, LCA is also used to perform the EPD in accordance with EN.15804.
- Direct comparison of the environmental impact results of different concretes is not always valid. The LCA is quite flexible, although the selection of the system boundaries, functional unit, LCIA method and background data set must first of all be agreed for realistic benchmarking. In addition, as the normalization and weighted steps are optional in the LCA methodology and their factors are not commonly established, decision-making based on the environmental impact results is complex, as several individual impacts have to be weighed up. To solve most of these difficulties, PEF intends to establish common guidelines with norms for assessing the environmental credentials of a product. Thus, the use of the LCIA, normalization, and weighting factors, together with the dataset provided by PEF will, in the near future, be frequently employed.
- Another barrier to the use of the LCA methodology is the lack of geographical, technological and temporal data for carrying out LCA, especially for the individual components of concrete, and the lack of consensus over the method of allocating the flows. For example, in the case of aggregate production, due to the lack of a specific database, averaged values are in widespread use at both national and continental level, regardless of either the source or the technology used to obtain the different granularities, which will affect the final assessment. Moreover, in the case of alternative aggregates, the difference between regions is even greater, as the technology used to treat the aggregate and the transport conditions may vary significantly.
- In concrete, 1 m^3 of concrete is usually selected as the functional unit for performing LCAs, which limits the environmental-impact comparisons with other concretes that may have identical functional properties. Concretes with different properties and their functionalities must therefore be included in the functional unit, in order to analyse their environmental impact from an objective perspective.
- In line with the design of concrete mixtures according to economic and environmental criteria, performing an economic and environmental impact assessment prior to the design of concrete mixtures can help with the selection of concrete components with lower environmental and economic impacts.

3.8 References

Aguado, A., Caño, A. Del, De La Cruz, M. P., Gómez, D. and Josa, A. (2012) 'Sustainability assessment of concrete structures within the Spanish structural concrete code', *Journal of Construction Engineering and Management*, 138(2), pp. 268–276. doi: 10.1061/(ASCE)CO.1943-7862.0000419.

Aïtcin, P.-C. (2000) 'Cements of yesterday and today Concrete of tomorrow', *Cement and Concrete Research*, 30, pp. 1349–1359.

Amario, M., Rangel, C. S., Pepe, M. and Toledo Filho, R. D. (2017) 'Optimization of normal and high strength recycled aggregate concrete mixtures by using packing model', *Cement and Concrete Composites*. Elsevier Ltd, 84, pp. 83–92. doi: 10.1016/j.cemconcomp.2017.08.016.

Amrina, E. and Vilsi, A. L. (2015) 'Key Performance Indicators for Sustainable Manufacturing Evaluation in Cement Industry', in *12th Global Conference on Sustainable Manufacturing*. Elsevier B.V., pp. 19–23. doi: 10.1016/j.procir.2014.07.173.

Anastasiou, E. K., Liapis, A. and Papachristoforou, M. (2017) 'Life Cycle Assessment of Concrete Products for Special Applications Containing EAF Slag', *Procedia Environmental Sciences*. The Author(s), 38, pp. 469–476. doi: 10.1016/j.proenv.2017.03.138.

Arribas, I., Santamaría, A., Ruiz, E., Ortega-López, V. and Manso, J. M. (2015) 'Electric arc furnace slag and its use in hydraulic concrete', *Construction and Building Materials*. Elsevier Ltd, 90, pp. 68–79. doi: 10.1016/j.conbuildmat.2015.05.003.

Braga, A. M., Silvestre, J. D. and de Brito, J. (2017) 'Compared environmental and economic impact from cradle to gate of concrete with natural and recycled coarse aggregates', *Journal of Cleaner Production*, 162(2017), pp. 529–543. doi: 10.1016/j.jclepro.2017.06.057.

Brans, J. P. and Vincke, P. A. (1985) 'A Preference Ranking Organization Method (the PROMETHEE Method for Multiple Criteria Decision Making)', *Manage. Sci.*, (31), pp. 647–656.

Cao, C. (2017) '21 - Sustainability and life assessment of high strength natural fibre composites in construction', in *Advanced High Strength Natural Fibre Composites in Construction*. Elsevier Ltd, pp. 529–544. doi: 10.1016/B978-0-08-100411-1.00021-2.

Cao, Z., Shen, L., Zhao, J., Liu, L., Zhong, S., Sun, Y. and Yang, Y. (2016) 'Toward a better practice for estimating the CO2 emission factors of cement production: An experience from China', *Journal of Cleaner Production*. Elsevier Ltd, 139, pp. 527–539. doi: 10.1016/j.jclepro.2016.08.070.

Chen, C., Habert, G., Bouzidi, Y., Jullien, A. and Ventura, A. (2010) 'Resources , Conservation and Recycling LCA allocation procedure used as an incitative method for waste recycling : An application to mineral additions in concrete', *'Resources, Conservation & Recycling'*. Elsevier B.V., 54(12), pp. 1231–1240. doi: 10.1016/j.resconrec.2010.04.001.

Colangelo, F., Forcina, A., Farina, I. and Petrillo, A. (2018) 'Life Cycle Assessment (LCA) of

different kinds of concrete containing waste for sustainable construction', *Buildings*, 8(5). doi: 10.3390/buildings8050070.

Damineli, B. L., Kemeid, F. M., Aguiar, P. S. and John, V. M. (2010) 'Measuring the eco-efficiency of cement use', *Cement and Concrete Composites*, 32, pp. 555–562. doi: 10.1016/j.cemconcomp.2010.07.009.

Damineli, B. L., Pileggi, R. G. and John, V. M. (2013) 'Lower binder intensity eco-efficient concretes', in *Eco-Efficient Concrete*, pp. 26–44. doi: 10.1533/9780857098993.1.26.

Damtoft, J. S., Lukasik, J., Herfort, D., Sorrentino, D. and Gartner, E. M. (2008) 'Sustainable development and climate change initiatives', *Cement and Concrete Research*, 38, pp. 115–127. doi: 10.1016/j.cemconres.2007.09.008.

Dossche, C., Boel, V. and De Corte, W. (2017) 'Use of Life Cycle Assessments in the Construction Sector: Critical Review', in *Procedia Engineering. Sustainable Civil Engineering Structures and Construction Materials, SCESCM*, pp. 302–311. doi: 10.1016/j.proeng.2017.01.338.

EC-JCR (2011) 'ILCD handbook. Recommendations for Life Cycle Impact Assessment in the European context', *ILCD handbook. Europeran comission-Joint Research Centre*. doi: 10.278/33030.

EC-JRC (2010) *'ILCD Framework and Requirements for Life Cycle Impact Assessment Models and Indicators'*, *Europeran comission-Joint Research Centre*. doi: 10.2788/38719.

EC-JRC (2012) 'Product Environmental Footprint (PEF) Guide', *Eropean Commision Joint Research Centre*, p. 154. doi: Ares(2012)873782 - 17/07/2012.

ELCD - EPLCA (2015) *European reference Life Cycle Database*, *ELCD 3.2*. Available at: https://eplca.jrc.ec.europa.eu/ELCD3/.

European Commission (DG ENV) (2011) *Management of Construction and Demolition Waste in EU27*, *Final Report elaborated by BIO Intelligence Service*. doi: 10.1016/S0140-6736(01)80522-5.

European Union (2008) 'Directive 2008/98/EC of the European parliament and of the council on waste and repealing certain directives.', p. L312: 3–30.

Evangelista, B. L., Rosado, L. P. and Penteado, C. S. G. (2018) 'Life cycle assessment of concrete paving blocks using electric arc furnace slag as natural coarse aggregate substitute', *Journal of Cleaner Production*. Elsevier Ltd, 178(February), pp. 176–185. doi: 10.1016/j.jclepro.2018.01.007.

Faleschini, F., De Marzi, P. and Pellegrino, C. (2014) 'Recycled concrete containing EAF slag: Environmental assessment through LCA', *European Journal of Environmental and Civil Engineering*, 18(9), pp. 1009–1024. doi: 10.1080/19648189.2014.922505.

Faleschini, F., Zanini, M. A., Pellegrino, C. and Pasinato, S. (2016) 'Sustainable management and supply of natural and recycled aggregates in a medium-size integrated plant', *Waste Management*. Elsevier Ltd, 49(2016), pp. 146–155. doi: 10.1016/j.wasman.2016.01.013.

Favier, A., de Wolf, C., Scrivener, K. and Habert, G. (2018) *A sustainable future for the*

european cement and concrete industry. Technology assessment for full decarbonisation of the industry by 2050. Switzerland.

Flower, D. J. M., Sanjayan, J. G. and Hellweg, S. (2007) 'Green House Gas Emissions Green House Gas Emissions due to Concrete Manufacture*', *Int. J. LCA*, 12(125), pp. 12–282. doi: 10.1065/lca2007.05.327.

García-Gusano, D., Herrera, I., Garraín, D., Lechón, Y. and Cabal, H. (2014) 'Life cycle assessment of the Spanish cement industry: implementation of environmental-friendly solutions', *Clean Technologies and Environmental Policy*, pp. 59–73. doi: 10.1007/s10098-014-0757-0.

Gursel, A. P. (2014) *Life-Cycle Assessment of Concrete: Decision-Support Tool and Case Study Application*. Berkeley. doi: 10.1017/CBO9781107415324.004.

Gursel, P., Masanet, E., Horvath, A. and Stadel, A. (2014) 'Life-cycle inventory analysis of concrete production: A critical review', *Cement and Concrete Composites*. Elsevier Ltd, 51, pp. 38–48. doi: 10.1016/j.cemconcomp.2014.03.005.

Habert, G. (2013) 'A method for allocation according to the economic behaviour in the EU-ETS for by-products used in cement industry', *International Journal of Life Cycle Assessment*, 18(1), pp. 113–126. doi: 10.1007/s11367-012-0464-1.

Henry, M. and Kato, Y. (2011) 'An assessment framework based on social perspectives and Analytic Hierarchy Process: A case study on sustainability in the Japanese concrete industry', *Journal of Engineering and Technology Management*. Elsevier B.V., 28(4), pp. 300–316. doi: 10.1016/j.jengtecman.2011.06.006.

Hossain, M. U., Poon, C. S., Lo, I. M. C. and Cheng, J. C. P. (2016a) 'Comparative environmental evaluation of aggregate production from recycled waste materials and virgin sources by LCA', *Resources, Conservation and Recycling*. Elsevier B.V., 109, pp. 67–77. doi: 10.1016/j.resconrec.2016.02.009.

Hossain, M. U., Poon, C. S., Lo, I. M. C. and Cheng, J. C. P. (2016b) 'Evaluation of environmental friendliness of concrete paving eco-blocks using LCA approach', *International Journal of Life Cycle Assessment*, 21(1), pp. 70–84. doi: 10.1007/s11367-015-0988-2.

Hossain, M. U., Poon, C. S., Lo, I. M. C. and Cheng, J. C. P. (2017) 'Comparative LCA on using waste materials in the cement industry: A Hong Kong case study', *Resources, Conservation & Recycling*, 120, pp. 199–208. doi: 10.1016/j.resconrec.2016.12.012.

ISO-14025 (2010) 'Environmental labels and declarations - Type III environmental declarations - Principles and procedures (ISO-14025:2010)'.

ISO 14040:2006 (no date) 'Environmental management - Life cycle assessment - Principles and framework'.

John, V. M. (2003) 'On the sustainability of concrete', *UNEP Indrustry and Environmentl*, pp. 62–63.

Josa, A., Aguado, A., Heino, A., Byars, E. and Cardim, A. (2004) 'Comparative analysis of available life cycle inventories of cement in the EU', *Cement and Concrete Research*, 34(8), pp. 1313–1320. doi: 10.1016/j.cemconres.2003.12.020.

Kim, S., Choi, M., Mha, H. and Joung, J. (2013) 'Environmental impact assessment and eco-friendly decision-making in civil structures', *Journal of Environmental Management*. Elsevier Ltd, 126, pp. 105–112. doi: 10.1016/j.jenvman.2013.03.045.

Kim, T. H. and Tae, S. H. (2016) 'Proposal of environmental impact assessment method for concrete in South Korea: An application in LCA (life cycle assessment)', *International Journal of Environmental Research and Public Health*, 13(11). doi: 10.3390/ijerph13111074.

Kim, T., Tae, S. and Roh, S. (2013) 'Assessment of the CO2 emission and cost reduction performance of a low-carbon-emission concrete mix design using an optimal mix design system', *Renewable and Sustainable Energy Reviews*. Elsevier, 25, pp. 729–741. doi: 10.1016/j.rser.2013.05.013.

Kurda, R. and Brito, J. De (2019) 'CONCRETop method : Optimization of concrete with various incorporation ratios of fl y ash and recycled aggregates in terms of quality performance and life-cycle cost and environmental impacts', *Journal of Cleaner Production*, 226, pp. 642–657. doi: 10.1016/j.jclepro.2019.04.070.

Kurda, R., Brito, J. De and Silvestre, J. D. (2019) 'CONCRETop - A multi-criteria decision method for concrete optimization', *Environmental Impact Assessment Review*. Elsevier, 74, pp. 73–85. doi: 10.1016/j.eiar.2018.10.006.

De la Fuente, A. and Fernández-Ordóñez, D. (2018) 'A multi-criteria decision-making based approach to assess the sustainability of concrete structures', in *IOP Conf. Ser.:Mater. Sci. Eng*, p. 442. doi: 10.1088/1757-899X/442/1/012008.

Lehne, J. and Preston, F. (2018) *Making Concrete Change Innovation in Low-carbon Cement and Concrete*. Chatham House.

Lehtinen, H., Saarentaus, A., Rouhiainen, J., Pits, M. and Azapagic, A. (2011) 'A review of LCA methods and tools and their suitability for SMEs', *Eco- innovation BIOCHEM*, p. 24.

Marinković, S. B. (2013) 'Life cycle assessment (LCA) aspects of concrete', in *Eco-Efficient Concrete*. Woodhead Publishing. doi: 10.1533/9780857098993.1.45.

Marinković, S. B., Ignjatović, I. and Radonjanin, V. (2013) '23 - Life-cycle assessment (LCA) of concrete with recycled aggregates (RAs)', in Pacheco-Torgal, F., Tam, V. W. Y., Labrincha, J. A., Ding, Y., and de Brito, J. (eds) *Handbook of Recycled Concrete and Demolition Waste*. Woodhead Publishing (Woodhead Publishing Series in Civil and Structural Engineering), pp. 569–604. doi: https://doi.org/10.1533/9780857096906.4.569.

Martínez-Rocamora, A., Solís-Guzmán, J. and Marrero, M. (2016) 'LCA databases focused on construction materials: A review', *Renewable and Sustainable Energy Reviews*, 58, pp. 565–573. doi: 10.1016/j.rser.2015.12.243.

Meyer, C. (2009) 'The greening of the concrete industry', *Cement and Concrete Composites*. Elsevier Ltd, 31(8), pp. 601–605. doi: 10.1016/j.cemconcomp.2008.12.010.

Moreno-Juez, J., Vegas, I. J., Gebremariam, A. T., García-Cortés, V. and Maio, F. Di (2020) 'Treatment of End-of-Life Concrete in an innovative Heating-air Classification System for Circular Cement-based Products .', *Journal of Cleaner Production*. Elsevier Ltd, p.

121515. doi: 10.1016/j.jclepro.2020.121515.

Müller, N. H. . (2008) *A blueprint for a climate friendly cement industry*.

Muralikrishna, I. V and Manickam, V. (2017) 'Chapter 5: Life Cycle Assessment', in *Life Cycle Assessment. Environmental Management*, pp. 57–75. doi: 10.1016/b978-0-12-811989-1.00005-1.

Navarro, I., Martí Albiñana, J. V. and Yepes Piqueras, V. (2018) 'Multi-Criteria Decision Making Techniques in Civil Engineering Education for Sustainability', in *ICERI2018 Conference*. Seville, Spain, pp. 9798–9807. doi: 10.21125/iceri.2018.0813.

O'brien, K. R., Ménaché, J., O 'moore, L. M., O 'brien, K. R., Ménaché, J. and O 'moore, : L M (2009) 'Impact of fly ash content and fly ash transportation distance on embodied greenhouse gas emissions and water consumption in concrete', *Int J Life Cycle Assess*, 14, pp. 621–629. doi: 10.1007/s11367-009-0105-5.

Ormazabal, G., Viñolas, B. and Aguado, A. (2008) 'Enhancing value in crucial decisions: Line 9 of the Barcelona subway', *Journal of Management in Engineering*, 24(4), pp. 265–272. doi: 10.1061/(ASCE)0742-597X(2008)24:4(265).

Pavan, M., Commission, E., Todeschini, R., Notation, B., Example, I., Methods, M. D. M., Ranking, S. A., Technique, H. D. and Programming, G. (2009) '1.19 Multicriteria Decision-Making Methods'.

Pellegrino, C. and Faleschini, F. (2016) *Sustainability Improvements in the Concrete Industry: Use of Recycled Materials for Structural Concrete Production*. Springer. doi: 10.1007/978-3-319-28540-5.

Penteado, C. S. ., Rosado, L. . and Lopes, A. . (2015) 'Life cycle assessment of construction and demolition waste from small generators', in *Fifteenth International Waste Management and Landfill Symposium*. Sardania, pp. 196–205. doi: 10.1016/j.wasman.2015.07.011.

Pons, O. and Aguado, A. (2012) 'Integrated value model for sustainable assessment applied to technologies used to build schools in Catalonia, Spain', *Building and Environment*. Elsevier Ltd, 53, pp. 49–58. doi: 10.1016/j.buildenv.2012.01.007.

Popovics, S. (1990) 'Analysis of the concrete strength versus water-cement ratio relationship', *ACI Mater J.*

Pradhan, S., Tiwari, B. R., Kumar, S. and Barai, S. V (2019a) 'Comparative LCA of recycled and natural aggregate concrete using Particle Packing Method and conventional method of design mix', *Journal of Cleaner Production*. Elsevier Ltd, 228, pp. 679–691. doi: 10.1016/j.jclepro.2019.04.328.

Pradhan, S., Tiwari, B. R., Kumar, S. and Barai, S. V (2019b) 'Comparative LCA of recycled and natural aggregate concrete using Particle Packing Method and conventional method of design mix', *Journal of Cleaner Production*. Elsevier Ltd, 228, pp. 679–691. doi: 10.1016/j.jclepro.2019.04.328.

Proin (2010) *Resumen de las nuevas aplicaciones y funcionalidades*. Available at: http://www.proin.es/pdf/novedades_proin.pdf.

Rodríguez-Robles, D., van den Heede, P. V and de Belie, N. (2019) '9-Life cycle assessment applied to recycled aggregate concrete', in de Brito, J. and Agrela, F. (eds) *New Trends in Eco-efficient and Recycled Concrete*. Woodhead Publishing (Woodhead Publishing Series in Civil and Structural Engineering), pp. 207–256. doi: 10.1016/B978-0-08-102480-5.00009-9.

Rosado, L. P., Vitale, P., Penteado, C. S. G. and Arena, U. (2017) 'Life cycle assessment of natural and mixed recycled aggregate production in Brazil', *Journal of Cleaner Production*. Elsevier Ltd, 151, pp. 634–642. doi: 10.1016/j.jclepro.2017.03.068.

Ruan, S. and Unluer, C. (2016) 'Comparative life cycle assessment of reactive MgO and Portland cement production', *Journal of Cleaner Production*, 137, pp. 258–273. doi: 10.1016/j.jclepro.2016.07.071.

Saaty, T. . (1990) *The Analytic Hierarchy Process: Planning, Priority Setting, Resource Allocation*. McGraw-Hill.

Salas, D. A., Ramirez, A. D., Rodriguez, C. R., Petroche, D. M., Boero, A. J. and Duque-Rivera, J. (2016) 'Environmental impacts, life cycle assessment and potential improvement measures for cement production: A literature review', *Journal of Cleaner Production*, 113, pp. 114–122. doi: 10.1016/j.jclepro.2015.11.078.

San-José, J. T. and Cuadrado, J. (2010) 'Industrial building design stage based on a system approach to their environmental sustainability', *Construction and Building Materials*. Elsevier Ltd, 24(4), pp. 438–447. doi: 10.1016/j.conbuildmat.2009.10.019.

Santamaría, A., Ortega-López, V., Skaf, M., Chica, J. A. and Manso, J. M. (2020) 'The study of properties and behavior of self compacting concrete containing Electric Arc Furnace Slag (EAFS) as aggregate', *Ain Shams Engineering Journal*, 11(1), pp. 231–243. doi: 10.1016/j.asej.2019.10.001.

Schuurmans, A., Rouwette, R., Vonk, N., Broers, J., Rijnsburger, H. and Pietersen, H. (2005) 'LCA of Finer Sand in Concrete (5 pp)', *The International Journal of Life Cycle Assessment*, 10(2), pp. 131–135. doi: 10.1065/lca2004.04.154.

Seto, K. E., Churchill, C. J. and Panesar, D. K. (2017) 'In fluence of fly ash allocation approaches on the life cycle assessment of cement-based materials', *Journal of Cleaner Production*. Elsevier Ltd, 157, pp. 65–75. doi: 10.1016/j.jclepro.2017.04.093.

Simion, I. M., Bonoli, A. and Gavrilescu, M. (2013) 'Comparing environmental impacts of natural inert and recycled construction and demolition waste processing using LCA', *Journal of Environmental Engineering and Landscape Management*, 21 (4)(September 2014), pp. 273–287. doi: 10.3846/16486897.2013.852558.

Smith, S. H. and Durham, S. A. (2016) 'A cradle to gate LCA framework for emissions and energy reduction in concrete pavement mixture design', *International Journal of Sustainable Built Environment*. The Gulf Organisation for Research and Development, 5(1), pp. 23–33. doi: 10.1016/j.ijsbe.2016.01.001.

Sosa, I., Thomas, C., Polanco, J. A., Setién, J. and Tamayo, P. (2020) 'High Performance Self-Compacting Concrete with Electric Arc Furnace Slag Aggregate and Cupola Slag Powder', *Applied Sciences*, 10(3), p. 773. doi: 10.3390/app10030773.

Struble, L. and Godfrey, J. (2001) 'How sustainable is concrete?', pp. 201–211.

Tam, V. W. Y., Soomro, M., Catarina, A. and Evangelista, J. (2018) 'A review of recycled aggregate in concrete applications (2000 – 2017)', *Construction and Building Materials*. Elsevier Ltd, 172, pp. 272–292. doi: 10.1016/j.conbuildmat.2018.03.240.

Thinkstep (2018) 'GaBi database'. Available at: http://www.gabi-software.com/international/databases/gabi-databases/.

Thomas, C., Rosales, J., Polanco, J. A. and Agrela, F. (2019) *7. Steel slags*, *New Trends in Eco-efficient and Recycled Concrete*. Elsevier Ltd. doi: 10.1016/B978-0-08-102480-5.00007-5.

Triantaphyllou, E. (2000) *Multi-Criteria Decision Making Methods: A comparative study*. Springer-Science+Businnes Media B.V.

Tscheikner-Gratl, F., Egger, P., Rauch, W. and Kleidorfer, M. (2017) 'Comparison of multi-criteria decision support methods for integrated rehabilitation prioritization', *Water*, 9(2). doi: 10.3390/w9020068.

Turk, J., Cotič, Z., Mladenovič, A. and Šajna, A. (2015) 'Environmental evaluation of green concretes versus conventional concrete by means of LCA.', *Waste management (New York, N.Y.)*, 45(305), pp. 194–205. doi: 10.1016/j.wasman.2015.06.035.

UNE-EN 15804 (2013) 'UNE-EN 15804:2013+A1. Sostenibilidad en la construcción; Declaraciones ambientales de producto; Reglas de categoría de producto básicas para productos de construcción', *AENOR*.

US EPA (2006) 'Life Cycle Assessment: Principles and Practice', *National Risk Management Research Laboratory Office of Research and Development U.S Wnvironmenal Protection Agency*, (May), p. 88. doi: 10.1016/j.marpolbul.2007.03.022.

Velasquez, M. and Hester, P. (2013) 'An Analysis of Multi-Criteria Decision Making Methods', *International Journal of Operational Research*, 10(2), pp. 55–56.

Viñolas, B., Aguado, A., Josa, A., Villegas, N. and Fernández Prada, M. Á. (2009) 'Aplicación del análisis de valor para una evaluación integral y objetiva del profesorado universitario', *Revista de Universidad y Sociedad del Conocimiento*, 6.

Wernet, G., Bauer, C., Steubing, B., Reinhard, J., Moreno-Ruiz, E. and Weidema, B. (2016) 'The ecoinvent database version 3 (part I): overview and methodology', *International Journal of Life Cycle Assessment*, 21(9), pp. 1218–1230. doi: 10.1007/s11367-016-1087-8.

Westkamper, E., Williams, D., Jovane, F., Yoshikawa, H., Alting, L., Boe, C. R., Tseng, M., Seliger, G. and Paci, A. M. (2008) 'CIRP Annals - Manufacturing Technology The incoming global technological and industrial revolution towards competitive sustainable manufacturing', 57, pp. 641–659. doi: 10.1016/j.cirp.2008.09.010.

Yazdanbakhsh, A. and Lagouin, M. (2019) 'The effect of geographic boundaries on the results of a regional life cycle assessment of using recycled aggregate in concrete', *Resources, Conservation and Recycling*. Elsevier, 143(December 2018), pp. 201–209. doi: 10.1016/j.resconrec.2019.01.002.

Zhang, Y., Luo, W., Wang, J., Wang, Y., Xu, Y. and Xiao, J. (2019) 'A review of life cycle assessment of recycled aggregate concrete', *Construction and Building Materials*. Elsevier Ltd, 209, pp. 115–125. doi: 10.1016/j.conbuildmat.2019.03.078.

Zhao, Z., Courard, L., Groslambert, S., Jehin, T., Léonard, A. and Xiao, J. (2020) 'Use of recycled concrete aggregates from precast block for the production of new building blocks: An industrial scale study', *Resources, Conservation and Recycling*. Elsevier, 157(October 2019), p. 104786. doi: 10.1016/j.resconrec.2020.104786.

4

Optimization of concrete granular compacity

CONTENT

4 Optimization of concrete granular compacity 113

4.1 Introduction 113

4.2 Methodology and materials 114

4.2.1 Overall methodological approach 114

4.2.2 Materials 117

4.2.3 Dry packing of aggregates 122

4.2.4 Wet packing of aggregates 126

4.2.5 Wet packing of cement 128

4.2.6 Theoretical models 129

4.2.7 Equipment 136

4.3 Experimental packing density of aggregates with different morphologies 137

4.3.1 Individual aggregate fractions 138

4.3.2 Cement packing density 144

4.3.3 Mixing of aggregate fractions 145

4.4 Comparison of theoretical model and experimental test results 162

4.4.1 Natural limestone aggregates 162

4.4.2 Electric arc furnace (EAF) aggregates 171

4.5 Conclusions 180

4.6 References 182

4 Optimization of concrete granular compacity

In Chapter 4, the results of the experimental investigation on the packing densities of aggregates with different morphologies will be presented. Likewise, the applicability of some of the available models that are used to determine the combination of aggregates with higher packing densities will be discussed.

4.1 Introduction

Optimization of the granular structure of concrete is considered by many experts as the starting point for the design of a concrete mix. It is at this stage that the cement content is reduced, which is expected to enhance both the environmental and the economic impact of the concrete mix design. Once the granular skeleton is fully packed, there will be fewer voids remaining to be filled by the cement paste. However, when the paste fills only the voids, the mixture will have a very compacted structure that will make it difficult to place. Hence, the need for the right quantity of cement paste to achieve the desired workability.

In this chapter, the maximum packing density of two of the most readily available aggregates in the Basque Country will be analysed.

- **Natural Limestone aggregates (NL)**
- **Electric Arc Furnace aggregates (EAF)**

From each type of aggregate, three granular size fractions (0/4 mm, 4/12 mm and 12/22 mm), widely used to make concrete, were selected for experimental testing, to establish the right proportions for the maximum packing density. In addition, rounded aggregates and particles of different size were also used to perform preliminary tests with the aim of comparing the effect of compaction on aggregates with alternative morphologies.

As previously mentioned in reference to the state of the art, many methods are available to predict the maximum packing limit. They range from methods based on ideal grading curves to discrete models that are used to analyse the interactions between different grain sizes, shapes, and surface textures.

Both optimization curves and analytical methods were successfully used for concrete mix design made with natural aggregates. However, the optimal packing of EAF aggregates has scarcely been studied and, generally speaking, different packing methodologies are directly applied with no prior verification of the experimental results.

In this section, the results of the theoretical models tests listed below will be compared with the experiment packing results, to verify their utility for these types of aggregates.

- Fuller curve

- Funk and Dinger curve (also named modified A&A curve)
- Compressible Packing Model (CPM)
- 3-parameter packing model (3-P)

It is well-know that aggregate packing capacity will depend on granular size distribution, granular shape and texture, and the packing method. Size is an easily considered parameter in most methods. However, modelling shape parameters is still a challenge, given the difficulties of accurate mass measurement. In this section, the influence of aggregate morphology will be analysed in relation to the three aggregates that have been selected, because the particular shape of EAF is expected to influence aggregate packing. There is therefore a need to verify the applicability of the available theoretical methodologies when these types of aggregates are used. It should be noted that any calibration of the CPM and the 3-P model for a precise adjustment to the aggregates under study is beyond the scope of this thesis. Current models were therefore directly applied to verify aggregate-packing under realistic scenarios.

The aim of this chapter will therefore be to validate a suitable methodology to select the proportion of each type of aggregate (NL and EAF aggregates) for maximum packing from the basic physical properties of the aggregates (grain size distribution, density, packing density). In addition, the suitability of the methods at industrial scale are also considered, as certain characterizations and experimental tests can be very time-consuming.

4.2 Methodology and materials

4.2.1 Overall methodological approach

The methodology used to optimize the granular skeleton of concrete was applied to two different types of aggregate: limestone aggregates and EAF aggregates. The related concrete mixes consisted of the following:

- Concrete made with NL aggregates, using three size fractions 12/22 mm, 4/12 mm and 0/4 mm
- Concrete made with EAF aggregates, using four size fractions sizes, 12/22 mm, 4/12 mm, 0/5 mm and 0/2 mm. In this mixture the first three fractions of EAF aggregates were combined with the 0/2 mm fraction of NL. This fraction is required to adjust the grading curve of the EAF, as recommended by other researchers (Manso *et al.* 2011).

The proposed methods were used to find the maximum packing density of the aggregates, mixing the most typical fraction size used for concrete manufacturing. The maximum packing density for each method was studied and contrasted, both theoretically and experimentally.

The experimental tests were conducted under both dry and wet methods at different compaction methods (see Table 4.1). Each experimental test is detailed in the following section. As some authors remarked (Li *et al.* 2017; Kwan & Li 2012), wet methods have the advantage of considering the influence of water in the packing process and the possibility of analysing the influence of admixtures on aggregate packing. In addition, the type of compaction applied to wet-packing methods is not as relevant as the one applied to dry-packing processes.

Table 4.1. Compaction tests.

Test type	Dry/wet	Compaction method
D-L	Dry	Loose
D-C	Dry	Compacted using a tamping rod
D-C26	Dry	Compacted at vibration table (26 Hz) and compression (10 kPa)
D-C33	Dry	Compacted at vibration table (33 Hz) and compression (10 kPa)
W	Wet	Compacted using a tamping rod

In general, the methodology followed to determine the maximum Packing Density (PD) of the granular skeleton of concrete was as follows (see Fig. 4.1):

1- Coarse Aggregate (CA) (fraction with the highest aggregate size) was firstly combined with Medium size Aggregate (MA). The amount of MA was incremented in steps of 10% (0:100; 10:90; 20:80; …; 90:10; 100:0), to find the maximum PD.
2- Having defined the maximum PD of CA+MA, the fixed proportion was mixed in the same way with the Fine Aggregate (FA) fraction.
3- Having defined the maximum PD of CA+MA+FA, varied proportions of very fine aggregate (FA2) were added, to set the maximum proportion of the EAF aggregates.
4- Finally, some quantities of cement by mass were added to the optimized aggregate proportion (that provides the maximum packing), to find the cement content that provides the maximum PD of all the particles.

The hierarchy of aggregate mixtures reflected a descending order of particle sizes as the smaller particles filled up the voids between large particles, in order to minimize the voids of the mixture (Pradhan *et al.* 2017). In addition, concrete with a high ratio of coarse aggregate reduced the sand and the cement content for a fixed W/C ratio, obtaining good mechanical properties at reduced costs (Rached *et al.* 2010).

Dry-packing methods across the whole range of solid particles (from the coarse aggregate to the cement particles) were only performed with limestone aggregates, having confirmed that the cement particles were not totally packed with the dry methods and agglomeration added uncertainty to the results due to the high inter-particle forces.

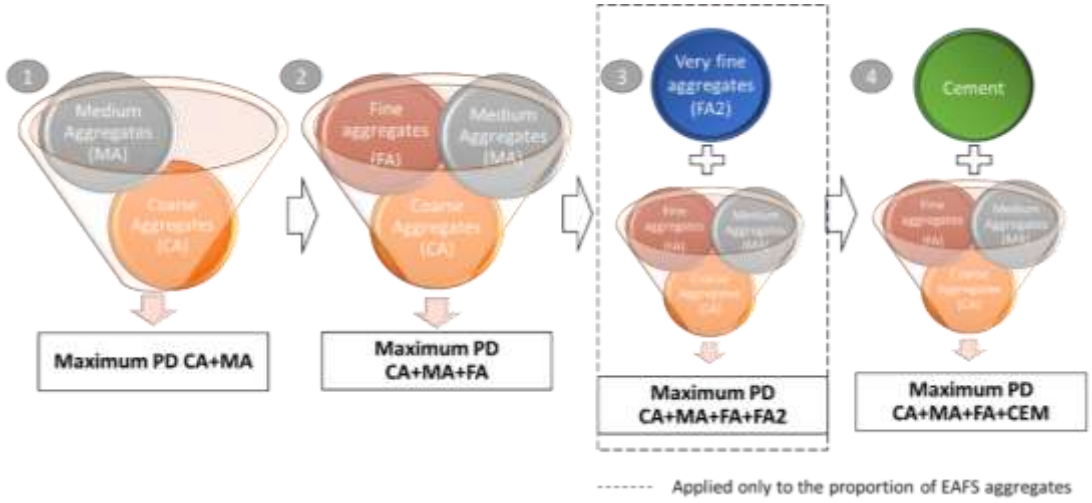

Fig. 4.1. Process followed to obtain the maximum packing value of concrete solid particles.

The optimal aggregate proportions for each type of aggregate under study were also calculated with the theoretical models that appear in Table 4.2.

Table 4.2. Theoretical models.

Model	Type	Required Input	Output
Fuller curve	Optimized curve	Particle-size distribution	Aggregate proportion according to the best fit with the curve
Funk and Dinger curve	Optimized curve	Particle-size distribution	Aggregate proportion according to the best fit with the curve
Compressible Packing Model (CPM)	Discrete model	Characteristic diameter of each granular fraction Particle-size distribution PD of each granular size Compaction index (K)	Prediction of the PD at different aggregate proportions
3 parameters packing model (3-P)	Discrete model	Characteristic diameter of each granular fraction PD of each granular size	Prediction of the PD at different aggregate proportions

The results provided by these models have been compared to the experimental values to prove their effectiveness, usability, and limitations for dosing NL and EAF aggregates.

Packing density and solid concentration represent the same concept and only differ by their method of measurement.

- Packing density (ϕ) has been defined by several authors as the ratio of solid volume to the bulk volume of solid particles (Toufar *et al.*, 1976; Quiroga *et al.*, 2004). Generally, this value is measured under dry conditions, so the voids between particles are only filled with air.
- Solid concentration (θ) is commonly measured under wet conditions and therefore varies with the liquid-to-solid ratio. Solid concentration is also defined as the ratio of the solid volume of the granular material to the bulk volume of

the granular material (Wong & Kwan 2008). In this case the voids can be filled by water and air.

4.2.2 Materials

The essential granular materials used in the experimental work are described below.

4.2.2.1 Aggregates

Two types of aggregates, widely available in the Basque Country, were used to study their compacting capacities to obtain the maximum PD.

- **Natural limestone (NL)** aggregates extracted from quarries. These materials were supplied by a company, AMANTEGUI, and had undergone crushing, screening and sorting processes (see Fig. 4.2).
    - Coarse aggregates: 11/22 mm
    - Medium aggregates: 4/11 mm
    - Fine aggregates: 0/4 mm
    - Very fine aggregates: 0/2 mm
- **Electric arc furnace (EAF)** aggregates. These materials were supplied through a company called HORMOR. The slag was from the ArcelorMittal steel-making company located in Olaberria (see Fig. 4.3) where it is watered and aerated until its volumetric stabilization. HORMOR then adds value to the product by crushing and screening it to obtain the desired granulometry.
    - Coarse aggregates: 11/22 mm
    - Medium aggregates: 4/11 mm
    - Fine aggregates: 0/5 mm

In addition, four different fractions of rounded particles were used to compare the effect of compaction energies on the PD of rounded and crushed aggregates (see Fig. 4.4).

- **Glass marbles (R-GB).** Commercial glass marbles.
    - Size: 16 mm
- **Rounded Siliceous aggregates (R-S).** These materials were supplied in two sizes
    - Medium size aggregate: 2/6 mm
    - Medium size aggregates: 6/12 mm
      from two companies, Sibelco and Esarena, respectively.
- **White tumbled Boulder (R-WTB).** This material was provided by Esarena plc.
    - Coarse aggregate: 11/22 mm

NL (11/22)

NL (4/11)

NL (0/4)

NL (0/2)

Fig. 4.2. Crushed limestone aggregates (NL).

EAF (11/22)

EAF (4/11)

EAF (0/5)

Fig. 4.3. Electric arc furnace (EAF) slag aggregates.

R-WTB (11/22) R-S (6/12) R-S (2/6)

Fig. 4.4. Rounded aggregates.

The aggregates were characterized in accordance with the following standards.

Particle-size distribution

The particle-size distributions of each aggregate fraction were measured according to European standards (UNE-EN 933-1 2012). The results are shown in Fig. 4.5 and Fig. 4.6.

In Fig. 4.5, the similarity is evident between the particle-size distributions of both the coarse and the medium fractions of the NL and the EAF aggregates. On the contrary, the distribution curve of the fine EAF aggregate fraction showed considerable particle-size differences and presented fewer particles ≤4 mm than the NL (0/4) fraction.

In contrast, a narrower particle-size distribution is evident in Fig. 4.6 for the rounded aggregate fractions.

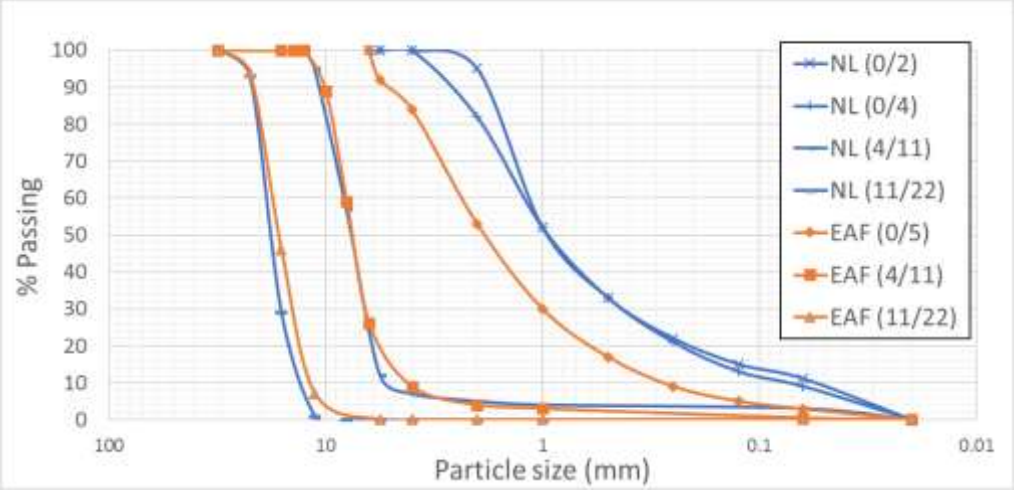

Fig. 4.5. Size distribution of NL and EAF aggregates.

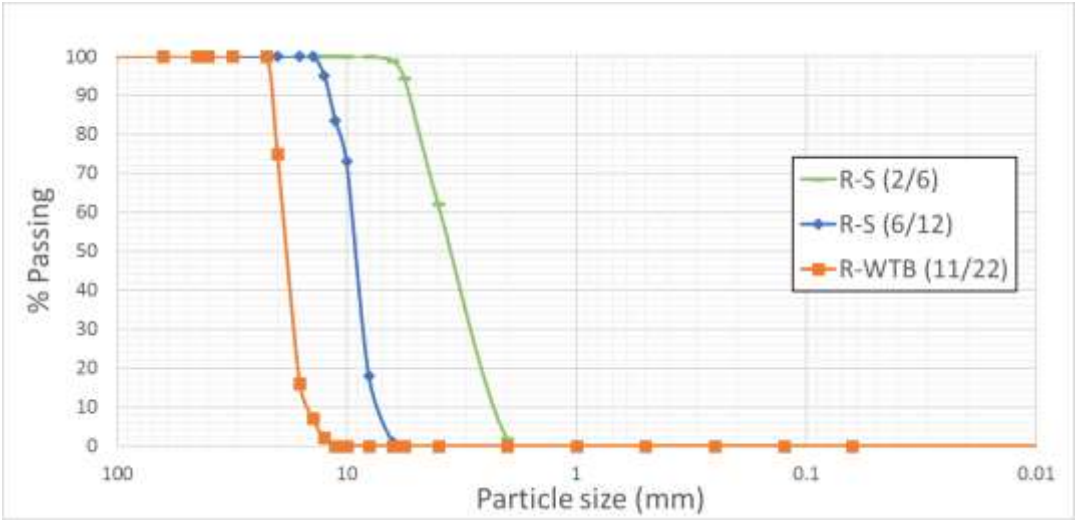

Fig. 4.6. Size distribution of rounded aggregate.

Specific density and absorption

The specific dry density (ρ_D), the saturated surface dry density (ρ_{SSD}) and the absorption of the different aggregates were calculated according to European standards (UNE-EN 1097-6 2014). The results are included in Table 4.3 and Table 4.4.

Bulk density

The bulk density (ρ_{bulk}) of the aggregates was determined as per the relevant European standard (UNE-EN 1097-3 1999).

The standard was strictly applied for aggregate fractions up to a maximum size of 16 mm. In the case of aggregates with a maximum size of 22 mm, a 5 L container was used instead of the volume recommended by the standard (6.9 L) due to operational limitations. The PD was calculated with the loose bulk density method following the same standard.

Fineness modulus (FM)

The FM parameter represents the cumulative percentages of material retained on each standard sieve after dividing the sum by 100. It is a measure of the average particle size that characterizes aggregate grading (Table 4.3 and Table 4.4).

Mean size of aggregate fraction

As mentioned in section 2.7.2, although the particle diameter (or average size) of an aggregate fraction plays an important role in the discrete packing model, there is no agreement on the methodology for its calculation.

In this thesis, the mean size, $\bar{d}$, of each fraction was calculated from the particle-size distribution (see eq. 4.1) (Table 4.3 and Table 4.4).

$$\bar{d} = \frac{\sum_{i=1}^{n} \left(\frac{size_i + size_{i+1}}{2}\right) \cdot y_i}{\sum_{i=1}^{n} y_i} \quad 4.1$$

where, i is the number of the sieve; $size_i$ is the sieve size, i; and, y_i is the percentage of particles retained in sieve i, implying that $\sum_{i=1}^{n} y_i$ should be 100 %.

Table 4.3. Physical properties of natural limestone (NL) and electric arc furnace slag aggregates (EAF).

Acronym	ρ_{SSD} (mg/m³)	ρ_D (mg/m³)	Absorption (%) 24h	ρ_{bulk} (mg/m³)	FM	$\bar{d}$ (mm)
NL (0/2)	2.68	2.66	1.8	1.59	2.83	1.00
NL (0/4)	2.68	2.66	0.9	1.59	2.99	1.20
NL (4/11)	2.64	2.61	1.1	1.35	6.17	7.62
NL (11/22)	2.68	2.67	0.4	1.34	7.71	18.08
EAF (0/5)	3.55	3.50	1.8	2.08	4.02	2.27
EAF (4/11)	3.50	3.42	2.2	1.83	6.22	7.35
EAF (11/22)	3.47	3.42	1.7	1.67	7.53	16.78

Table 4.4. Physical properties of glass balls (R-GB), rounded siliceous aggregates (R-S) and white tumbler boulder (R-WTB).

Acronym	ρ_{SSD} (mg/m³)	ρ_D (mg/m³)	Absorption (%) 24h	ρ_{bulk} (mg/m³)	FM	$\bar{d}$ (mm)
R-GB (16)	2.5	2.5	-	1.26	-	16
R-S (2/6)	2.62	2.63	0.3	1.51	5.36	3.37
R-S (6/12)	2.61	2.65	0.8	1.49	6.82	9.36
R-WTB (11/22)	2.84	2.85	0.3	1.61	7.84	18.17

4.2.2.2 Cement

The type of cement was the same throughout the study.

- **CEM II/A-M (V-L) 42.5R** provided by FYM HeilderbergCement group from the factory located at Arrigorriaga.

  Nominal composition[15]:

Clinker	Fly ash	Limestone	Minor constituents
80%	9%	9%	2%

[15]https://www.fym.es/sites/default/files/assets/document/31/4e/evaluacion_estadistica_de_produccion_-_i.pro_tecno_425r_-_arrigorriaga.pdf

Most of the characteristics of CEM II/A-M (V-L) 42.5 R can be found in the technical data sheet of the supplier[16]. However, the density, fineness and granular size of the cement was tested with European standards.

Specific density

The cement density was measured according to European standards (UNE 80103: 2014). The result is included in Table 4.5.

Specific surface

The cement fineness was measured according to European standards (UNE-EN 196-6 2019). The result is included in Table 4.5.

Table 4.5. Physical properties of CEM II/A-M (V-L) 42,5 R.

Density (mg/m^3)	Specific surface (cm^2/g)
2.9924	4130

Particle-size distribution

The particle-size distribution of the cement was measured with a Mastersizer 3000 laser diffraction particle-size analyzer.

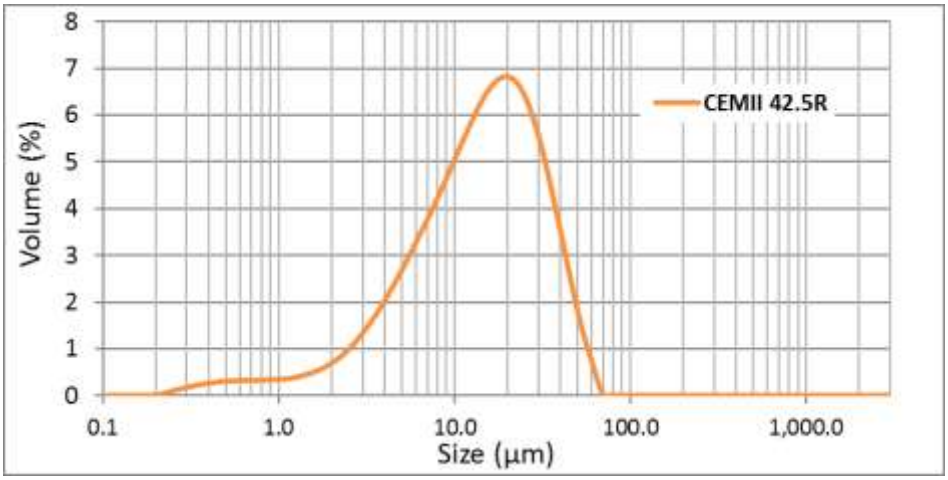

Fig. 4.7. Particle-size distribution of CEMII 42.5R.

4.2.3 Dry packing of aggregates

As is well known, PD measured under dry conditions is very sensitive to the compaction energy that is applied. PD was therefore measured in four different ways (see Table 4.1) by varying the compaction method. Thus, the compaction capacity of each type of aggregate and the precision of the discrete models depending on the applied compaction methodology and the properties of the aggregate can be compared.

[16] https://www.fym.es/es/ipro-tecno-425-r

The four compaction methods are described below:

Loose packing (D-L) and compacted by means of a tamping rod (D-C) can be calculated through the bulk density (UNE-EN 1097-3 1999).

The tests were performed with cylinders of different dimensions, depending on the maximum size of the aggregate.

In addition, the following assumptions were considered when testing the mixing of various aggregate fractions:

- The aggregates are stored at a depot under dry conditions. They had not therefore been previously dried out, as it was considered that the influence of low humidity can be neglected in the density measurement of the packages, as the surface was completely dry.
- Three containers with three different volumes (5 l, 3 l and 1 l) were used depending on the maximum granular size of the aggregate mix. Cylinders with a lower volume than the recommendations in the standard for this maximum size were sometimes used. However, the diameter of the cylinder in use was always at least five times the maximum aggregate size, as recommended by (de Larrard 1999), to avoid the container wall effect.
- Although most of the tests were performed on three sub-samples, a minimum of two sub-samples were prepared for the measurement of the PD of each aggregate.
- In addition, preliminary tests on a single sample validated the reproducibility of the test measurements.

The method consists of filling a steel cylinder of known volume with the aggregates and levelling off any excess with a flat cover plate leaving the measure filled to the brim. The weight of the aggregates is then measured and the PD is calculated with the following equation:

$$PD = \frac{weight\ of\ aggregates\ in\ the\ container}{\rho \cdot cylinder\ volumen} \qquad 4.2$$

Finally, the average of the three sub-samples was calculated to obtain the final PD value.

The main difference between the loose method and the packed method using a tamping rod is the compaction process. In loose packing, the aggregates are simply poured from a maximum height of 10 cm from the edge of the container, whilst the cylinder is filled with the aggregates in three stages with the compaction method and each layer is beaten down with 25 blows from the tamping rod.

Compaction by vibration (26 and 33Hz) and compression (10 kPa) (D-C26 and D-C33). Among the various procedures for measuring the actual PD (experimental PD) with compaction methods, the method suggested by F. de Larrard was selected. This test (de

Larrard 1999) consists of pouring a pre-set amount of aggregate into a cylindrical container (150 mm in diameter and 300 mm in height), the minimum diameter of which must be five times the maximum size of the aggregate. The container is then pressurized (10 kPa) and vibrated (see Fig. 4.8). The aggregate mixture is poured into the cylinder and vibrated at a certain frequency for a limited period of time while it is subjected to a compression force of 10kPa.

The test procedures detailed in (de Larrard 1999) were slightly modified. Vibration was applied at a constant frequency for 3 min (values previously selected from experimental tests using natural limestone aggregates). The tests were performed at two frequencies, 26Hz and 33Hz (de Larrard 1999), as de Larrard recommended a vibration value of approximately 4 g. The two frequencies were selected by calibrating the table vibration with an accelerometer at different frequencies, to achieve a value close to 4 g. Once the vibration time ended, the PD was calculated by dividing the total volume of the mixture by the total volume of the specimen. Each experiment was performed with three rather than two sub-samples, as recommended by de Larrard and the result of the PD was the mean value. This step was modified following the specifications of standard UNE-EN 1097-3:1999, so that the variability of aggregate of the dispersion by size and shape was recorded when measuring the PD.

It should be noted that both test reproducibility and robustness were also checked by measuring the PD of the same sample several times.

The aggregate weight was pre-set at 5.3 or 7 kg, depending on the aggregate density. The higher weight was selected to measure the PD of the EAF aggregates and the lower value was used to measure the PD of the limestone aggregates.

The PD value was calculated by the following equation:

$$PD = \frac{weight\ of\ aggregate\ in\ the\ container}{\rho \cdot volumen\ of\ aggregate\ in\ the\ container} \quad 4.3$$

$$Volumen\ of\ aggregate\ in\ the\ container = \pi \cdot r^2 \cdot h_{aggregate} \quad 4.4$$

where, r is the ratio of the container and $h_{aggregate}$ is the height of the aggregate in the container. The height was measured with a tape measure in two different ways:

- When the piston was placed within the cylinder, the height of the unfilled cylinder, i.e. the distance from the top of the piston to the rim of the cylinder, was measured. The height of the aggregate placed in the cylinder was calculated by subtracting the sum of the height of the piston (124 mm) and the measured value from the total height of the cylinder (300 mm).
- When the piston protrudes from the cylinder, its height within the cylinder can be read from a metric scale on the piston. The height value is calculated by

subtracting the height of the piston within the cylinder from the total height of the cylinder.

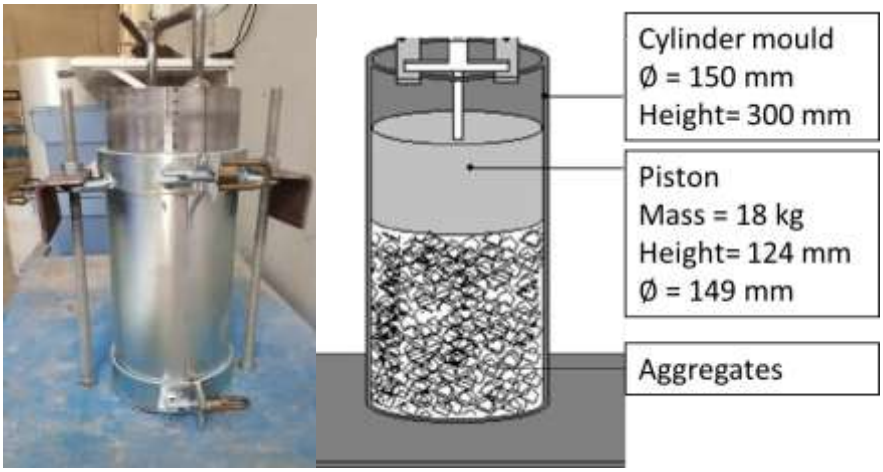

Fig. 4.8. Cylindrical mould, compaction piston and aggregate vibration on the vibration table.

where, r is the ratio of the container, and $h_{aggregate}$ is the height of the aggregate in the container. Aggregate height was measured in two different ways with a tape measure:

- When the piston was placed within the cylinder, the height of the unfilled cylinder was measured, i.e. the distance between the top of the piston and the rim of the cylinder. The height of aggregate was calculated by subtracting the sum of the height of the piston (124 mm) and the measured value from the total height of the cylinder (300 mm).
- When the piston protrudes from the cylinder, its height within the cylinder can be read from the metric scale on the piston. The height value is calculated by subtracting the height of the piston within the cylinder from the total height of the cylinder.

4.2.3.1 Calibration of different parameters for compression and vibration packing method

It is well known that the PD of granular particles will be influenced by the compaction method that is applied, among other factors (aggregates properties). When vibration and compression are applied to simulate the packing of granular particles over time, the vibration characteristics (acceleration, frequency, amplitude, mass, vibration time) and the compression energy affect the PD results.

As mentioned earlier, a compression of 10kPa and an acceleration of ±4g was used by Larrard (de Larrard 1999) to calibrate his CPM model. The characteristic parameters of the model are a packing index, K, related to the aggregate placement (see Table 4.6), and a K value of 9 for vibration and compression at 10kPa.

The vibration table and mould acceleration were tested at different frequencies to obtain a value close to 4g acceleration, so that a K value of 9 could be considered for the test (see Fig. 4.9). In addition, the influence on PD of the time that the table is under vibration during the test was also analysed, to establish a fixed vibration process, which will yield comparable results (For more detail see Annex section). It must be taken into account that, as Larrard (de Larrard 1999) also mentioned, the experimental PD is not a property of the material (it depends on the mix and the process), so there is never a definitive stabilisation of aggregate height within a given period of time.

Table 4.6. Compaction index for different packing processes. Adapted from (de Larrard 1999).

Packing process	K value	Source
Pouring (Loose packing)	4.1	(Cintré,1988)
Tamping with a rod	4.5	(Kantha Rao *et al.*, 1993)
Vibration	4.75	(Joisel, 1952)
Vibration + compression 10kPa	9	(de Larrard *et al.*,1994b)

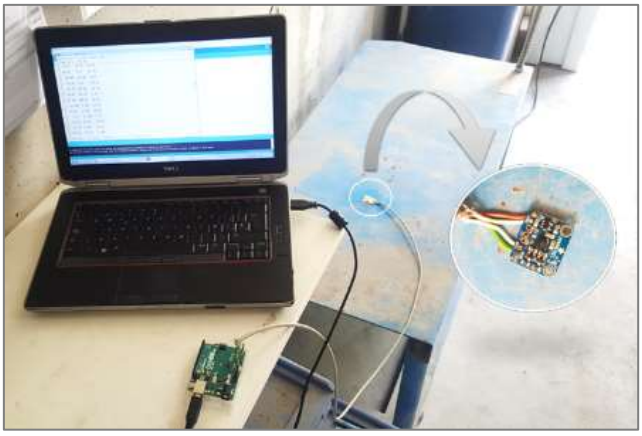

Fig. 4.9. Assembly of the vibration table calibration system

4.2.4 Wet packing of aggregates

The method to measure the wet packing of aggregates and cement was adapted from the method proposed by Wong *et al.* (Wong & Kwan 2008). It was at first applied to measure the PD of cementitious materials and they then applied it to measure concrete PD (Li & Kwan 2014).

The aim of aggregate wet packing is to measure the solid concentration under wet conditions. Thus, the effect of water on the compaction process is considered. Solid aggregate concentrations are a measure of aggregate packing capacity under wet conditions. The method helps to calculate the suitable proportion of aggregate to obtain a packed granular skeleton.

The compaction of aggregates in this method will depend on the W/S ratio by volume. If there is insufficient water to reach the saturation state of the mix, air will be occluded in-between voids and the solid concentration and the W/S will decrease. However, if there is sufficient water or an excess that fills all the voids, then solids will be suspended in water and the solid concentration will decrease as the W/S ratio increases. There will therefore be a point where the solid concentration reaches the maximum value and the voids are minimal (Li & Kwan 2014).

In this thesis, the wet packing of both aggregate and of cement will be separately tested.

The procedure to carry out the wet-packing method for aggregates is described below:

1- Select a W/S ratio. This value can be approximately estimated from the dry-packing results or randomly selected.
2- Pour the solid proportion into the mixer bowl and pre-mix the dry mix for 30 seconds to total homogenization.
3- Weigh the required amount of water according to the desired W/S ratio and aggregate. The effects of aggregate water absorption must be considered in the calculation of the solid concentration value. In a first step, 100% of the water absorption value in EN 1097-6:2014 was considered, after which the value was adjusted, considering the kinetic absorption of the aggregate.
4- Add water to the concrete mixer bowl and mix for 3 minutes.
5- Fill the mix into a cylindrical container of known volume in three layers. Beat down each layer with 25 blows from the tamping rod and smartly tap the container 10 to 15 times or until no large bubbles of air surface on the compacted layer.
6- Level-off the top surface with a flat cover plate, so that the measure is filled to the brim.
7- Weigh the filled container, to determine the weight of the mix.

The solid concentration values are calculated as follow,

$$\theta = \frac{V_s}{V} = \frac{V_s}{\frac{M}{\rho_{bulk}}} = \frac{\rho_{bulk}}{\frac{1}{V_s}(\rho_w V_w + \rho_{a1} V_{a1} + \rho_{a2} V_{a2} + \rho_{a3} V_{a3} + \rho_c V_c)} = \frac{\rho_{bulk}}{(\rho_w u_w + \rho_{a1} r_{a1} + \rho_{a2} r_{a2} + \rho_{a3} r_{a3} + \rho_c r_c)} \quad 4.5$$

V_s is the solid volume, V is the container volume, ρ_w is the density of water, ρ_{a1}, ρ_{a2} and ρ_{a3} are the densities of the different aggregate fractions, and ρ_c is the density of the cement. r_{a1}, r_{a2}, and r_{a3} represent the ratios of the volumetric aggregate fraction and total solid material, and u_w represents the water-to-solid (W/S) ratio by volume.

The void content can be calculated with the following equation:

$$\varepsilon = 1 - \theta = \frac{u}{1+u} \quad 4.6$$

where, ε is the void content and u is the void ratio, defined as the ratio of the volume voids to the solid volume of the particles. The void content is also defined as the sum of the water content (ε_w) and the air content (ε_a).

4.2.5 Wet packing of cement

Although the BS 812:1995 standard specifies methods for the measurement of the bulk density of aggregates and fillers, electrostatic and Van der Waal forces have a huge influence on the packing of fine particles under dry conditions, complicating compaction and producing agglomeration (Yu *et al.* 1997). Pietsch (Wong & Kwan 2008) identified a critical particle size (100 μm), a size beneath which the interplay between gravity and the inter-particle forces gradually changes, somewhat altering the particle packing behaviour. Wong *et al.* (Wong & Kwan 2008) reviewed the available methods and proposed a new one in which the bulk density of various cement paste mixtures is measured at different W/C ratios. The main difference compared to other existing methods is the mixing process. A portion of the cement powder is added to the mixture over water to maintain the mixture in a saturated condition. The time needed for a homogeneous slurry to form is shorter than with conventional mixing methods, because the water-squeezing process that occurs during the coalescence step is avoided. This process is very slow when the water content is low (Wong & Kwan 2008). The method applied to establish the maximum packing of cement is described as follows:

1- Pour water at a W/C volume ratio into a cement mixing bowl.
2- Add half of the cement into the bowl and mix at low speed for 3 min.
3- Divide the remaining cement into three equal portions.
4- Add each part of divided cement into the bowl and after each addition mix at a low speed for 3 min.
5- Once mixed, fill a cylindrical mould of known volume (0.75 l) with cement paste and compact it by tamping the mould on a stable surface.
6- Level-off the surface at the brim with a flat cover plate and weigh the paste into the cylindrical mould to calculate the wet density.
7- Repeat the whole process using different W/C ratios until the highest solid concentration of cement is found.

4.2.6 Theoretical models

4.2.6.1 Ideal distribution curves (Fuller and Funk and Dinger)

Both the Fuller curve (Fuller & Thompson 1907) (see eq. 4.7) and the Funk and Dinger (Funk *et al.* 1980) (see eq.4.8) curve were used to determine an ideal particle-size proportion of each NL aggregate and EAF aggregate for the concrete mixes.

In addition, a second approach was considered, that included the cement fraction to determine the particle-size combination of the total solid content in a concrete mix with the Funk and Dinger model.

These methods determine the optimal proportion of available aggregate fractions to reach the maximum PD (or the optimal PD for a given application, varying the q-factor (see chapter 2 section 2.7.2.1). However, the PD value cannot be directly predicted with them.

The advantages of these methods are their simplicity and practicality. The only input parameters are from the particle-size distribution test UNE EN 933-1:2012: the maximum and minimum particle size and the particle-size distribution.

It should be noted that continuous methods assume that all possible particles sizes are present in the particle distribution system, hence a wide range of particle sizes should be used to find a good fit to the curves.

$$P(d) = \left(\frac{d}{d_{max}}\right)^{q} \quad 4.7$$

$$P(d) = \left(\frac{d - d_{min}}{d_{max} - d_{min}}\right)^{q} \quad 4.8$$

In the present study, a q-value of 0.5 was selected for the Fuller curve, as it is the most widely used value in concrete mix design, even though values between 0.4 and 0.5 are also commonly used. In contrast, several q-values were chosen (q=0.37, 0.33 and 0.31) for the Funk and Dinger curve, in order to determine the effects on the packing processes of the aggregate particles and even the cement.

As reviewed in chapter 2 (section 2.7.2.1), the q-value can be used to measure the effect of the fines content and, by extension, the PD of aggregates of different morphologies, as lower q-values imply higher fine-fractions. Funk and Dinger (Funk *et al.* 1980) proposed a q-value of 0.37 for optimum packing. In contrast, Mangulkar *et al.* (Mangulkar & Jamkar 2013) recommended q-values between 0.25 and 0.3 on the Funk and Dinger curve, in relation to high performance concrete and conventional concretes depending on the grading, the size, and the shape of the aggregate, and q-values lower than 0.23 for self-compacting concrete, and lower than 0.37 for roller compacted concrete.

The optimal fits of the NL aggregate fractions (NL-FA (0/4), NL-MA (4/11) and NL-CA (11/22)) and EAF aggregate fractions (NL-FA (0/2), EAF-FA (0/5), EAF-MA (4/11), EAF-CA (11/22)) with the Fuller and Funk and Dinger curves were automatically calculated with the MS Excel Solver tool. To that end, the Residual Sum of Squares (RSS) (see 4.9) was minimized (Cai 2017). In addition, the EAF aggregate mixture was fitted to the Funk and Dinger curve, factoring in the cement fraction, as recently proposed by Yousuf *et al.*, (Yousuf *et al.* 2019),

$$RSS = \sum (P_{tactual} - P_t)^2 \qquad 4.9$$

where, $P_{tactual}$ is the percentage that passes each sieve (actual particle-size distribution curve) and P_t is the target percentage passing its corresponding sieve.

4.2.6.2 Compressible packing method (CPM)

The CPM requires no sieving and weighting process of the aggregate test fractions. Its accuracy at predicting the particle packing of both aggregates, NL and EAF, was tested by comparison with experimental results

The CPM was selected from among the range of packing density models, because several authors have demonstrated its accuracy at predicting the PD of binary and ternary mixtures of aggregates from different sources (Moutassem 2016; Ghasemi 2017; Fennis 2009).

However, the applicability of the CPM to EAF aggregate and the prediction of its PD has yet to be demonstrated. Moreover, most authors have used the PD of mono-size aggregate fractions (following the definition of de Larrard of a particle size within a sufficiently narrow range of $d_{min}/D_{max}>0.1$) as their model input (Moutassem 2016; Ghasemi 2017; Fennis 2009), which is hardly feasible on an industrial scale in concrete applications, especially with regard to the sand fraction.

In addition, several authors have proposed adaptions to models and new interaction parameters to improve the CPM and its PD prediction with particles of different characteristics (Fennis 2009; Kwan *et al.* 2013; Roquier 2016; Lecomte 2006; Bala *et al.* 2019).

The main innovation of the CPM (de Larrard 1999) was the distinction between actual PD, Φ, and virtual PD, β.

- The actual PD, Φ, is not an intrinsic property of the material, as it depends on the compaction process.
- The virtual PD, β, is defined as the maximum PD of a mixture when each particle retains its original shape and the particles are placed one by one.

Both packing densities, are related in equations 2.12 and 4.17 through a compaction index (K). K is defined as a scalar parameter of compaction process energy (see Table

4.6) and it can be calibrated (de Larrard 1999). Furthermore, the CMP model can predict both the PD of binary mixtures and the PD of multicomponent mixtures.

In the CPM, de Larrard (de Larrard 1999) considered the loosening and the wall interaction effects of granular particles (see Fig. 4.10) by means of two simplified formulas (see eqs. 4.14 and 4.15), which were calibrated for a series of experimental data.

These experimental data were obtained from the PD of binary mixtures of elementary granular size that met the following size ratios (de Larrard 1999; Bala *et al.* 2019):

$$\frac{d_{min}}{D_{max}} > 0.1 \qquad 4.10$$

$$\frac{d_i}{d_j} > 4 \qquad 4.11$$

where, d_{min} and d_{max} are the minimum and the maximum granular size of a granular fraction and d_i and d_j are the characteristic diameters (defined as the geometrical mean of both the maximum and the minimum particle sizes) (see eq. 4.12) of sizes i and j ($d_i \leq d_j$).

$$d_i = \sqrt[2]{D_{max} \cdot d_{min}} \qquad 4.12$$

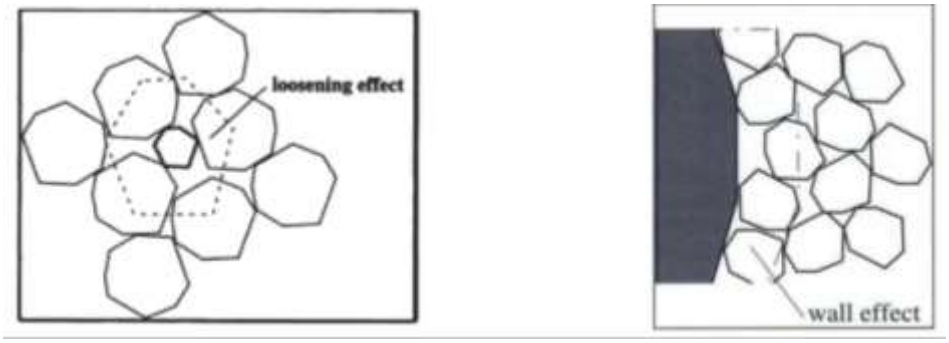

Fig. 4.10. Left: The loosening effect (coarse particles are dominant); Right: The wall effect (fine particles are dominant) (de Larrard 1999).

The general equation of the model for a mixture containing n-size classes with a dominant category is presented below

$$\gamma_i = \frac{\beta_i}{1 - \sum_{j=1}^{i-1}\left[1 - \beta_i + b_{ij}\beta_i\left(1 - \frac{1}{\beta_j}\right)\right] r_j - \sum_{j=i+1}^{n}\left[1 - a_{ij}\beta_i/\beta_j\right] r_j} \qquad 4.13$$

The two coefficients, a_{ij} and b_{ij}, represent the loosening effect and the wall effect, respectively.

$$a_{ij} = \sqrt{1 - \left(1 - \frac{d_j}{d_i}\right)^{1.02}} \quad 4.14$$

$$b_{ij} = 1 - \left(1 - \frac{d_i}{d_j}\right)^{1.50} \quad 4.15$$

The diameters of sizes i and j are d_i and d_j, respectively (where $d_i \leq d_j$).

The PD can be indirectly determined with equation 2.12.

$$K = \sum_{i=1}^{n} K_i = \sum_{i=1}^{n} \frac{\frac{r_i}{\beta_i}}{\frac{1}{\Phi} - \frac{1}{\gamma_i}} \quad 4.16$$

In a mono-size mix, equation 2.12 can be simplified as follows:

$$\beta = \left(1 + \frac{1}{K}\right) \cdot \Phi \quad 4.17$$

The virtual PD of each aggregate fraction was calculated with three different methods:

1- Virtual PD, β, was directly calculated from equation 4.17. The compaction index, K, was established according to the Table 4.6 for each packing methodology used to measure the actual PD Φ. Thus,

Packing method	**Acronym**	**K**
Dry, loose packing	D-L	4.1
Dry, compacted with a tamping rod	D-C	4.5
Dry, compacted under vibration (26Hz) & compression 10kPa	D-C26	9
Dry, compacted under vibration (33Hz) & compression 10kPa	D-C33	9

In this case, each fraction was assumed to be mono-size and the interaction effects between different sized particles were neglected.

2- β was calculated with equations 2.9 and 2.12.
The terms of each equation were determined as follows:
   - As previously mentioned, the experimental PD was performance over the whole fraction, without sieving each faction to obtain the PD of the elementary class of particle size. Therefore, the virtual PD of each particle size, β_i, was assumed to be a constant, β.
   - The volumetric proportion of each elementary class, (r_j), was determined from the particle-size distribution of each aggregate fraction.
   - The sieve sizes were also used to calculate the parameters a_{ij} and b_{ij}. It should be noted that the particle size of each elementary class is graded by sieving, so the passing amount and the sieve sizes will influence the results. In this study, 19 sieve sizes, between 0.056 mm and 31.5 mm,

included all the sieve sizes specified in UNE-EN 13043 (UNE-EN 13043 2003), as well as some others.

- The value of K was taken from ***Table 4.6***, in the same way as for the first method.

Once all the input data had been defined, the system of equations (derived from equations 2.9 and 2.12) was solved with the MS Excel solver function to obtain the virtual PD, β, of the aggregate fraction and γ_i and K_i of each elementary class.

3- β was calculated by applying the same process shown above in method 2. Except that the virtual PD of the aggregate fraction was considered to be the maximum virtual density γ (Lecomte 2006), instead of the value of β.

γ was defined as the minimum virtual PD of class i when the latter was considered the dominant class of the poly-sized mix (see eq. 4.18)

$$\gamma = \min_{1 \le i \le n} \gamma_i \qquad 4.18$$

Having calculated the virtual packing density, β, of each aggregate fraction, the packing densities of several aggregate combinations were predicted for binary, ternary, and quaternary aggregate mixtures.

1- Firstly, the CPM model was applied to binary mixes of coarse and medium aggregate sizes of both NL and EAF aggregates. The input parameters were the virtual PD of each aggregate fraction (calculated as above), the medium aggregate size of each fraction (calculated as described in the second step) and the compaction index, K. The virtual PD was calculated with three different methods and the three different results for each binary mixture were analysed.

2- The mean size of each aggregate fraction was used to calculate the particle interaction (eqs. 4.14 and 4.15) between two aggregate fractions. Each aggregate fraction was considered as a mono-size fraction in this proposal, due to the wide range of particle sizes within each aggregate fraction and as the virtual PD of each particle size was not calculated. According to de Larrard (de Larrard 1999), the mean or the characteristic diameter of a particle-size distribution within a narrow range of (mono-size) particles, can be calculated with the geometric mean of both the minimum and the maximum aggregate sizes ($\sqrt{d_{min} \cdot d_{max}}$). However, in this study, the mean size, $\bar{d}$, of each fraction was calculated with eq. 4.1, as the range of particle sizes was not narrow.

3- The volumetric fraction of each aggregate fraction, r_j, was graded from 0 to 1 at increments of 0.1.

4- Having defined all the input data, the system of equations (derived from equations 2.9 and 2.12) was solved with the MS Excel solver function for each aggregate combination, yielding the PD predicted by the CPM.

5- Finally, the predicted packing densities were compared with the experimental values.

The same methodology was applied to the mixing of coarse, medium, and fine NL aggregates and to the mixing of coarse, medium, and fine-aggregate fractions of EAF and the fine fraction of NL aggregates.

4.2.6.3 3-parameter packing model (3-P)

The 3-P model was applied to verify its applicability for and accuracy at predicting the particle packing of the aggregates under study, NL and EAF. The following equations were used, as defined by Kwan *et al.* (Kwan *et al.* 2015):

$$\frac{1}{\phi_i^*} = \left(\frac{r_i}{\phi_i} + \frac{r_j}{\phi_j}\right) - (1-b)\cdot\left(1-\phi_j\right)\cdot\frac{r_j}{\phi_j}\cdot[1 - c\cdot(2.6^{r_j} - 1)] \quad 4.19$$

$$\frac{1}{\phi_j^*} = \left(\frac{r_i}{\phi_i} + \frac{r_j}{\phi_j}\right) - (1-a)\cdot\frac{r_i}{\phi_i}\cdot[1 - c\cdot(3.8^{r_i} - 1)] \quad 4.20$$

The final PD of the binary mix was calculated with equation 4.21.

$$\phi = \min(\phi_1^*, \phi_2^*) \quad 4.21$$

The diameters of size, i and j, are d_i and d_j, respectively, where $d_i \leq d_j$.

$$s = \frac{d_j}{d_i} \quad 4.22$$

Kwan *et al.* (Kwan *et al.* 2013) considered an additional interaction parameter, the wedging effect, in their PPM. An effect that is caused by the fine particles trapped in narrow gaps between coarse particles (see Fig. 4.11).

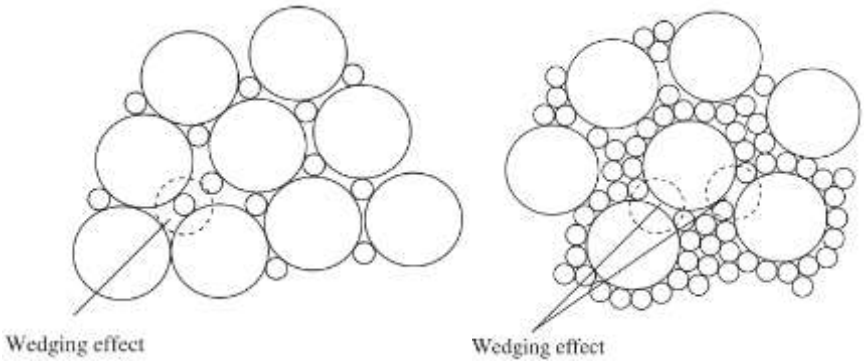

Fig. 4.11. Left side: The wedging effect when coarse particles are dominant; Right: The wedging effect when fine particles are dominant (Kwan et al. 2013).

Parameters a_{ij}, b_{ij}, and c_{ij} represent the particle interaction effects.

a_{ij}: Loosening effect

b_{ij}: Wall effect

c_{ij}: Wedging effect

These parameters are dependent of the size-ratio (s) of the granular particles. Furthermore, Kwan *et al.* (Kwan *et al.* 2013; Kwan *et al.* 2015) predicted the equations of each interaction effect (wall, loosening and wedging) from the a, b, and c values obtained by fitting eqs. 4.19 and 4.20 to the experimental PD results and by regression analysis of the experimental a, b, and c values. So, in addition, the interaction functions of the three parameters of the 3-P model will also vary depending on the type of aggregate that is compacted (spherical or angular) and the compaction energy applied (uncompacted or compacted). In a preliminary study (Kwan *et al.* 2013), spherical particles of different sizes were used to measure the PD of binary mixes for verifying the 3-P model (see eq. 4.23, 4.24 and 4.25). In the subsequent study (Kwan *et al.* 2015), the same authors also validated the model for angular particles, fitting the model to the experimental PD of binary mixes of angular rock aggregate particles (see Table 4.7).

$$a_{ij} = 1 - (1-s)^{3.3} - 2.6 \cdot s \cdot (1-s)^{3.6} \quad 4.23$$

$$b_{ij} = 1 - (1-s)^{1.9} - 2 \cdot s \cdot (1-s)^{6} \quad 4.24$$

$$c_{ij} = 0.322 \cdot \tanh(11.9 \cdot s) \quad 4.25$$

Table 4.7. Particle interaction equations for angular particles using two different methods of compaction, uncompacted, and compacted.

Angular aggregates (uncompacted)	Angular aggregates (compacted)
$a_{ij} = 1 - (1-s)^{5} - 1.9 \cdot s \cdot (1-s)^{3.1}$	$a_{ij} = 1 - (1-s)^{7.1} - 1.9 \cdot s \cdot (1-s)^{3.1}$
$b_{ij} = 1 - (1-s)^{1.9} - 2.1 \cdot s \cdot (1-s)^{10.5} - 0.2 \cdot (1-s)^{7.6}$	$b_{ij} = 1 - (1-s)^{2.2} - 0.7 \cdot s \cdot (1-s)^{9.3} - 0.2 \cdot (1-s)^{10.6}$
$c_{ij} = 0.335 \cdot \tanh(26.9 \cdot s)$	$c_{ij} = 0.335 \cdot \tanh(26.9 \cdot s)$

Although the 3-P model was only tested for angular aggregates, to predict the PD of binary mixtures of a mono-size particle fraction (a narrow range of particle size), its usefulness in concrete mix design was analysed in this thesis by applying the method to aggregates with a wider range of particle sizes, and for ternary and even quaternary mixes.

Both uncompacted and compacted interaction functions for angular aggregates (see Table 4.7) were applied to predict the PD of NL and EAF aggregate and to verify its applicability and accuracy for these types of aggregates.

Firstly, the 3-P model was applied to binary mixes of coarse and medium aggregate sizes of both NL and EAF aggregates. The input parameters were the PD obtained with the dry methods (see section 0) and the mean aggregate size of each fraction that was calculated with eq. 4.17.

The packing densities that the four different compaction energies (D-L, D-C, D-C26 and D-C33) yielded (see section 0) were the inputs used to predict the PD of each mixture. The two methods of applying the model, the interaction function derived from uncompacted packing and the interaction function derived from compacted packing, were therefore tested with the four different PD measurement methods.

The compaction process followed by Kwan *et al.* (Kwan *et al.* 2015) for compacted packing is not exactly the same as the one in this thesis. On the one hand, Kwan *et al.* (Kwan *et al.* 2015) developed the particle interaction equations of compacted angular aggregates by filling the container in three layers and compaction by applying 30 compacted active blows with a tamping rod, while in this thesis 25 blows were applied instead (D-C). Furthermore, two additional methods of compaction were used to calculate the PD: compaction by vibration at 26Hz plus compression at 10kPa (D-C26) and compaction by vibration at 33Hz plus compression at 10kPa (D-C33). The results of both methods were also contrasted with the results of the model.

Having predicted the packing densities with the 3-P model, these values were compared with the experimental packing densities of the mixture of both fractions.

In a second step, the model for multi-component particle mixes, outlined in the thesis of Wong (Wong 2015), was also applied to ternary and quaternary mixtures.

4.2.7 Equipment

The equipment used to perform the above-mentioned tests was as follows:

Dry-packing density test

- **Weighing scale.** COBOS EM-30 KAM
- **Vibrating table**. *Proetisa. Ref:H0111 Vibration power: 50 Hz*
- **Cylindrical mould 150 mm diameter x 300 mm length**
- **Cylindrical moulds of different sizes**
- **Steel piston** *(149 mm diameter and 17.12 kg)*
- **Frequency converter**
- **Bullet-nosed metal rod** (600 mm in length)
- **Oven**

Control of the vibration table

- **Digital Accelerometer:** *MMA8451Q, 3-axis, 14-bit/8-bit*
- **Arduino one SMD edition**

Wet-packing density characterization:

- **Concrete mixer with vertical axis and centre shaft.** (Collomix-Counter Rotating Mixer AOX-S)
- **Cylindrical mould**

- **Weighing scale.** *COBOS BK-40000G*
- **Bullet-nosed metal rod** (600 mm long)
- **Trowel**

Cement packing density

- **Shaking table**
- **Mould for the slump test** (60 mm in height, internal diameter: base 100 mm - top 70 mm)
- **Planetary mixer as specified in Standard EN 196-1**
- **Cylindrical mould** (0.75 l)
- **Prismatic moulds** (10×10×60 mm)

4.3 Experimental packing density of aggregates with different morphologies

In this section, the experimental results are presented for the packing densities of aggregates with different morphologies and for the wet packing of cement. The results are ordered as follows:

- First, the PD of each aggregate fraction directly provided by the suppliers (with no screening or mixing), following its analysis and comparison with the other aggregates.
- Second, the evaluation results of wet packing of the cement.
- Third, the PD values are shown and analysed when the different aggregate fractions are mixed. For each type of aggregate, the combination that presents the maximum packing is obtained. This part is divided into 3 sub-sections by aggregate type: rounded, NL and EAF (4.3.3.1, 4.3.3.2 and 4.3.3.3).

The nomenclature of the mixtures is listed in Fig. 4.12 and Table 4.8.

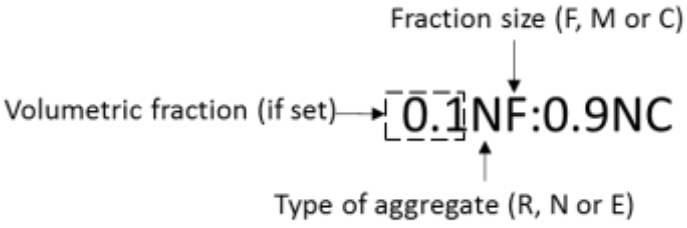

Fig. 4.12. Example of the code for aggregate mixtures. Mixing of 0.1 by volume of fine natural limestone aggregate (NL (0/4)) and 0.9 by volume of coarse natural limestone aggregate (NL (11/22)).

Table 4.8. Code for aggregate mixtures.

Code for mixtures	Corresponding material
NF	NL (0/4)
NF2	NL (0/2)
NM	NL (4/11)

Code for mixtures	Corresponding material
NC	NL (11/22)
EF	EAF (0/5)
EM	EAF (4/11)
EC	EAF (11/22)
RF	R-S (2/6)
RM	R-S (6/12)
RC	R-WTB (11/22)
RC2	R-GB (16)

4.3.1 Individual aggregate fractions

The PD of each fraction size was calculated with four compaction methods, in accordance with the methodology presented in 4.2.3. The PD results for NL and EAF aggregate and for rounded particles are shown in Table 4.9 and Table 4.10.

The granular size and shape of the NL and EAF aggregates can be seen in Fig. 4.14. In addition, Fig. 4.13 shows the appearance of the compacted coarse fraction of NL and the EAF aggregates within the cylindrical mould.

Table 4.9. PD of NL and EAF aggregate under four compaction energies (D-L, D-C, D-C26 and D-C33).

	PD ± SD			
	D-L	**D-C**	**D-C26**	**D-C33**
NL (0/2)	0.597±0.005	0.700±0.006	0.740±0.000	0.740±0.000
NL (0/4)	0.597±0.003	0.709±0.003	0.768±0.004	0.775±0.012
NL (4/11)	0.517±0.002	0.561±0.009	0.614±0.014	0.635±0.009
NL (11/22)	0.502±0.002	0.534±0.006	0.566±0.004	0.594±0.010
EAF (0/5)	0.594±0.001	0.637±0.005	0.716±0.000	0.742±0.002
EAF (4/11)	0.535±0.011	0.596±0.012	0.628±0.012	0.654±0.015
EAF (11/22)	0.482±0.004	0.518±0.001	0.547±0.002	0.582±0.006

Table 4.10. PD of glass balls (R-GB), rounded siliceous aggregates (R-S) and white tumbler boulder (R-WTB) under three compaction energies (D-L, D-C26 and D-C33).

	PD ± SD		
	D-L	**D-C26**	**D-C33**
R-GB (16)	0.504±0.002	0.564±0.000	0.563±0.000
R-S (2/6)	0.575±0.002	0.653±0.002	0.654±0.000
R-S (6/12)	0.561±0.004	0.641±0.000	0.639±0.000
R-WTB (11/22)	0.564±0.003	0.629±0.000	0.629±0.000

Fig. 4.13. Left: NL (11/22) fraction following D-C33 compaction within the cylindrical mould; Right: EAF (11/12) fraction following D-C33 compaction within the cylindrical mould.

Fig. 4.14. Granular size and shape of the EAF and NL aggregates.

PD depends on the aggregate morphology (shape, texture surface and size) and the compaction method that is applied. However, the interaction of so many parameters makes it difficult to determine how the PD of a wide range of fraction sizes might be affected by aggregate shape and surface texture.

As the aggregate PD depends on the granular size, the PD will vary with the mean aggregate size of each fraction and the influence of the compaction process on the PD of aggregates with different morphologies, as shown in Fig. 4.15. The PD of both the NL and the EAF aggregates decreased as their mean particle size increased. However, any such decrease in the case of the rounded particles was not so evident, and the mean size appeared to be less relevant for the PD.

Unlike a range of granular sizes, the mono-size fraction (16 mm) of the rounded aggregates may explain their lower PD. Their behaviour was clearly different as there were no interaction effects between different sized particles.

In the literature, the opposite effect was reported (Kwan *et al.* 2015), in as much as the PD decreased as the mean particle size increased. This fact is attributed to the higher agglomeration effect between finer particles, due to the presence of inter-particular forces. However, the granular size distributions of the fine particles under study here were significantly wider than the fractions from the studies selected from the literature (practically mono-size), therefore finer particles filled the voids left by the larger particles and the agglomeration effect was probably less prevalent, achieving a higher PD.

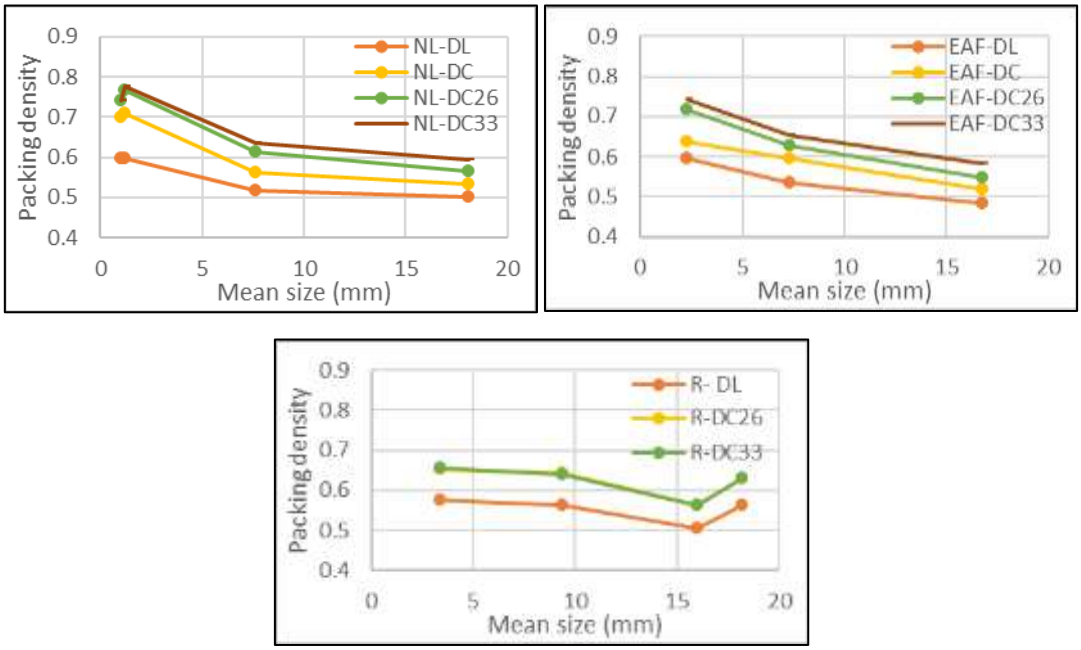

Fig. 4.15. PD and mean particle size under different compaction energies.

However, the crushed aggregates (NL and EAF) were more sensitive to the compaction process, as the irregular and rough surfaces of the aggregates made it more difficult to achieve an arranged structure and extra energy was needed.

No difference was found for the PD of the rounded particles when the frequency of the vibration process was incremented from 26 to 33Hz. This fact can easily be understood by observing Fig. 4.16 where the rounded steel particles were compacted at different intensities. Once the particles had settled at their densest compaction, the PD could not be increased, even under a higher compaction energy.

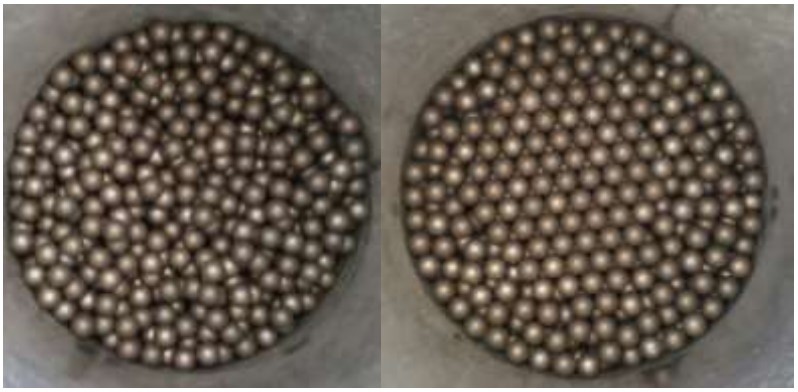

Fig. 4.16. Left: uncompacted steel balls within the cylindrical mould; Right: compacted iron balls after compaction (10kPa) + vibration at 26Hz (D-C26).

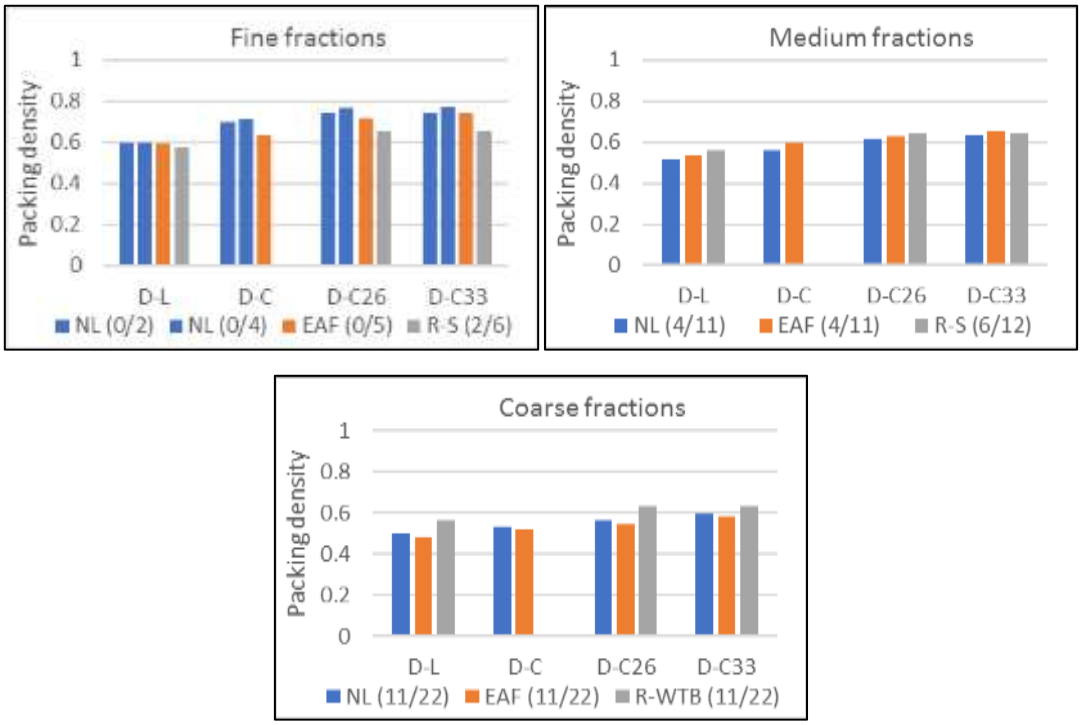

Fig. 4.17. PD of the three aggregates (NL, EAF and R) at different compaction energies divided by aggregate size fraction.

Comparing the PD of each aggregate size of the three (coarse, medium, and fine) aggregate fractions under analysis (see Fig. 4.17), it can be seen that regardless of the compaction method, the aggregate fraction with the highest PD may be defined. However, caution is advisable when determining the PD of the fine fraction, as the D-L compaction process is not always sufficiently energetic to interrupt the interaction forces between the fine particles.

On the other hand, although the grain size distributions and the fineness moduli of NL (4/11) - EAF (4/11) and NL (11/22) - EAF (11/22) were quite similar (see Fig. 4.5 and Table 4.3), PD differences can be observed. The medium fraction of EAF (4/11) has a higher PD

than NL (4/11), while the opposite is true for the coarse fractions (EAF (11/22)-NL (11/22) (see Fig. 4.17). The PD differences will mainly be associated with aggregate surface texture and shape, as mentioned in section 2.4.2. Moreover, it can be seen from Fig. 4.3 and Fig. 4.14 that the EAF presents a cavernous and irregular morphology.

In addition, the EAF aggregate shape and texture depends on the valorisation process. The most commonly used processes are either screening, or crushing and then screening (Thomas *et al.* 2019). The final surface shape affects the compaction capacity and depends on whether the aggregate fraction has been reduced by crushing, which may explain the different compaction behaviours of both EAF aggregate fractions.

However, further research is still needed to confirm the physical factors affecting PD, as both the NL and the EAF fractions show slightly different particle-size distributions.

The influence of aggregate morphology on the PD of the fine fraction is not easily compared, because of the different particle-size distributions of the three fractions. Therefore, both aggregate surface and shape are responsible for the PD value, but also the grain size and its interactions. In Fig. 4.18, the retained fractions of each size of aggregate are listed alongside their different sieve sizes.

In an attempt to find a relationship between the morphonology and the PD of the aggregates, the aggregate angularity factor was used from the British standard (BS-812 1975). However, the British standard was designed to evaluate the aggregate fraction of a single size and takes the PD of a perfectly rounded aggregate (0.670) as a reference. When comparing aggregate fractions with higher packing (generally obtained by mixing particles of different sizes), the angularity number is therefore negative, which renders the method invalid for comparing aggregate fractions with a wide range of particle-size distributions.

The equation for measuring soil compactness was applied, in order to compare the influence of the compaction method on the different aggregate morphologies (natural limestone aggregate, electric arc furnace aggregate and rounded aggregate) and sizes:

$$F = \frac{e_{max} - e_{min}}{e_{min}}$$

In the field, e_{max} represents the index soil voids in their loosest state, and e_{min} represents the index of soil voids in their densest state within the soil. Thus, the well graded soils are easily compactable, and they are associated with a high F-value, while the uniform soils, compactable with greater difficulty, have a small F-value (Yepes 2014).

In this thesis, this concept has been adapted, and both a loose PD and a PD following vibration and compaction at 33Hz and 10kPa were selected to calculate the loosest (e_{max}) and the densest (e_{min}) aggregate voids, respectively. Therefore, a low F-value will indicate that the influence of the compaction energy on that fraction is low and

conversely, aggregate fractions with higher F-values will have a greater influence on the compaction process.

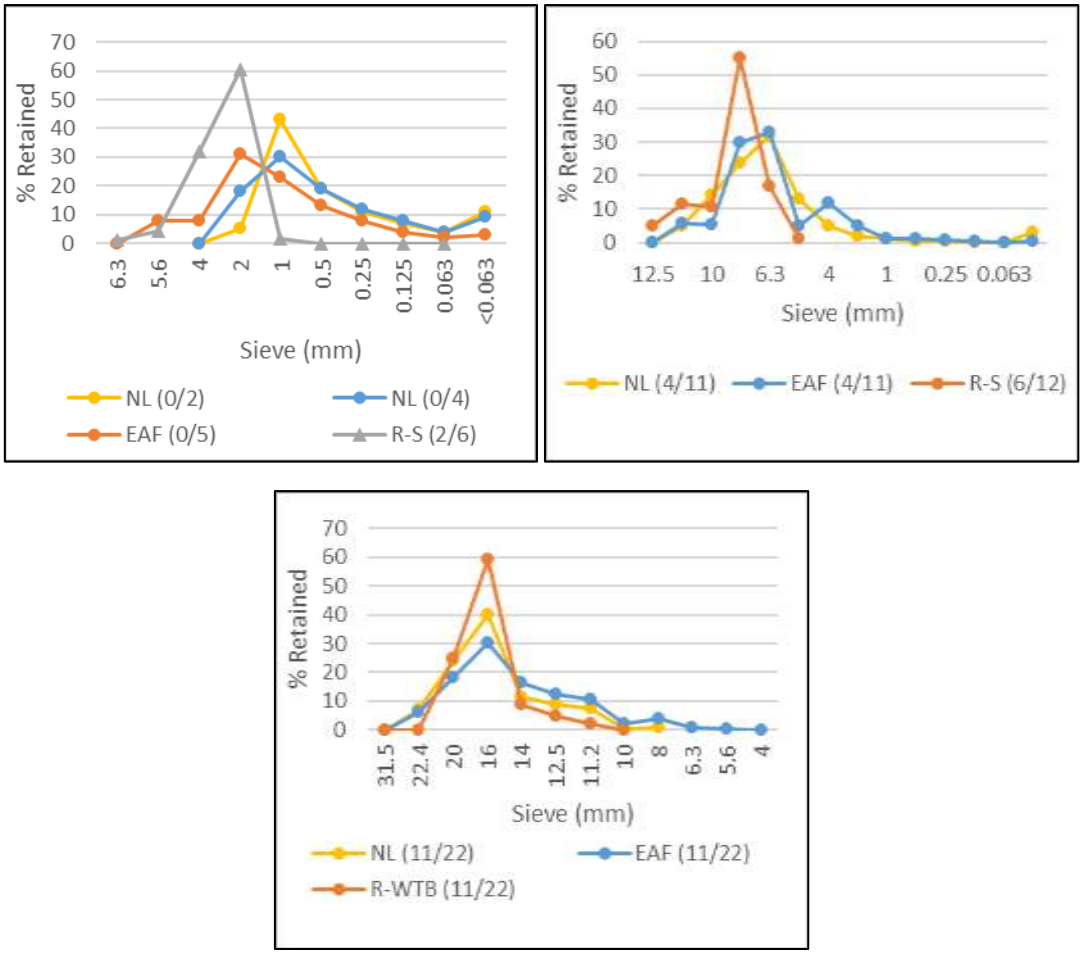

Fig. 4.18. Fraction retention by sieve size.

The compactness, F-value, was directly influenced by the compaction method and indirectly by the morphological characteristics (aggregate surface, shape and size).

As can be seen in Table 4.11, the F-values were similar, when comparing medium (4/11) and coarse fractions (11/22) of NL and EAF aggregates which were of a similar granular size distribution (see Fig. 4.18). Hence, the PD differences were independent of the compaction method applied and may mainly be associated with the shape and surface of the NL and EAF aggregates, as mentioned above.

Table 4.11. Compactness (F) index of the aggregate fractions under study.

	NL (0/2)	NL (0/4)	NL (4/11)	NL (11/22)	EAF (0/5)	EAF (4/11)	EAF (11/22)	R-S (2/6)	R-S (6/12)	R-WTB (12/22)
e_{max}	0.403	0.403	0.483	0.498	0.406	0.465	0.518	0.425	0.439	0.436
e_{min}	0.260	0.225	0.365	0.406	0.258	0.346	0.418	0.346	0.365	0.371
F	0.55	0.79	0.32	0.23	0.57	0.34	0.24	0.23	0.20	0.18

Other general observations derived from the compactness results are:

- The rounded aggregate fractions showed F-values lower than the equivalent fractions of NL and EAF. It could be related more to the rounded shape and smooth surface of these aggregates, which assists compaction, in other words, the aggregates reach their maximum PD under less compacting energy. However, the granular size distribution also influences this parameter and the rounded aggregates under analysis have a narrower particle-size range than the NL and the EAF aggregates, reducing the capacity to increase the PD.
- The coarse fractions of the three types of aggregates present the lowest values of F. It may be related to the size ratio of the aggregate fractions, as the lower the size ratio, the greater the aggregate compaction capacity. These ratios are 11/22=0.5 for coarse aggregate, 4/11=0.36 for medium aggregates, and 0.063/4=0.015 for fine aggregates.
- The fine fractions of NL (0/2 and 0/4) and EAF (0/5) showed the highest values of compactness (F), fractions which therefore showed greater compaction with the compaction method than the coarse and the medium fractions. This fact is probably related not only to the lower size ratio (which promotes high packing), but also to the forces which govern the particles. There will be a higher gravitational pull on the coarse particles than on the fine particles, the inter-particle forces of which will be likely to attract the finer rather than the coarser particles, thereby altering the packing behaviour. The inter-particle forces will continue to attract particles as the aggregate is poured, although those forces will weaken as the compaction energy increases, achieving closer packing.

4.3.2 Cement packing density

As stated by many authors, the wet method is recommended for measuring the PD of cement and the finest 100 μm particles, in order to overcome inter-particle forces without underestimating the packing capacity of the cement.

In this thesis, the PD of the cement was measured based on the wet-packing approach proposed in section 4.2.5. Wet packing depends on the water content of the mix that is optimal at maximum values. The maximum solid concentration was obtained at W/C=0.23. When above the optimum value, the grains will be dispersed in the water decreasing cement compacity and when below that value, the immersion in water of the cement grains will be incomplete, provoking particle agglomeration between the particles, due to their inter-particle forces, making it difficult to reach the maximum PD.

As can be seen in Fig. 4.19, a line of equality can be drawn where Ɛa=0 and u=uw that will represent the air ratio, i.e. the vertical distance between the voids ratio curve and Ɛa=0, as explained by Wong *et al.* (Wong & Kwan 2008). The air ratio for paste with the minimum void ratio (the highest solid concentration) will therefore be higher (about 0.07) than it will be with higher volumes of water, as mixture compaction is easier, due

to the excess water that is available to fill the air voids. In contrast, when the water content is lower than the optimum, the air ratio will be higher as the paste is too dry to reach a good compaction and empty voids are left in the mixture. Accordingly, it should be noted that the paste with the highest PD will not correspond with the maximum concentration of the solid, due to the air and water content of the paste that is also included in the density measure (see Table 4.12).

Table 4.12. Solid concentration of CEM II at different Vw/Vc ratios

Vw/Vc	W/C	Cement paste mass (kg)	ρ_{bulk} (kg/m^3)	Solid concentration θ
1.42	0.47	1.37	1825	0.414
1.20	0.40	1.44	1915	0.457
1.10	0.37	1.47	1948	0.476
1.00	0.33	1.52	2017	0.505
0.90	0.30	1.56	2071	0.532
0.85	0.28	1.55	2066	0.538
0.80	0.27	1.56	2081	0.549
0.75	0.25	1.56	2069	0.553
0.70	0.23	1.54	2047	0.554
0.60	0.20	1.26	1679	0.467

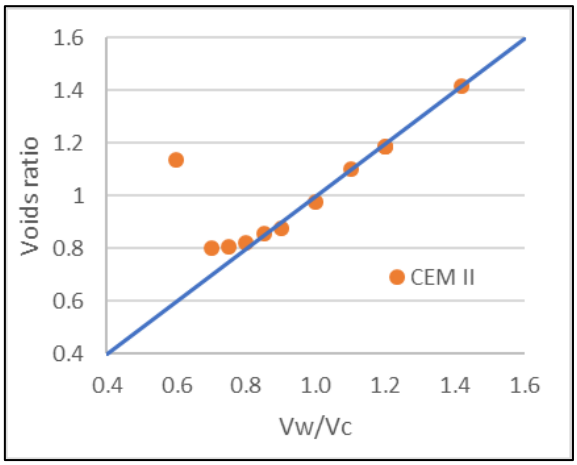

Fig. 4.19. Void ratios of CEM II at different Vw/Vc ratios.

4.3.3 Mixing of aggregate fractions

The main objective of this section is to establish the proportion of aggregates with the highest PD, both for concrete containing NL aggregates and for concrete containing EAF aggregates, combining both the NL and EAF aggregate fractions, respectively.

Although, the use of rounded aggregate for achieving maximum PD is beyond the scope of this thesis, preliminary tests with rounded aggregates were conducted in an attempt

to understand the influence of the aggregate morphology on the PD and the compaction process.

4.3.3.1 Rounded aggregate

The PD of binary mixtures of three aggregate fractions (R-S (2/6), R-S (12/22) and R-WTB (12/22)) were calculated at two compaction energies D-C26 and D-C33 (see Fig. 4.20, Fig. 4.21 and Fig. 4.22).

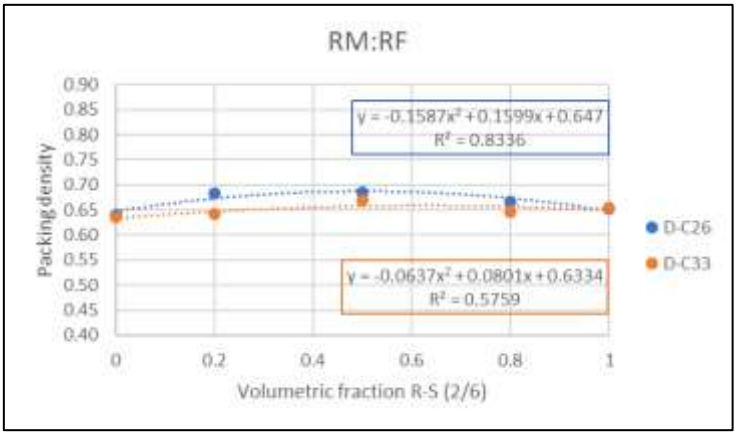

Fig. 4.20. PD of RM:RF mixture under two compaction energies: D-C26 and D-C33. Aggregate size ratio: 0.36.

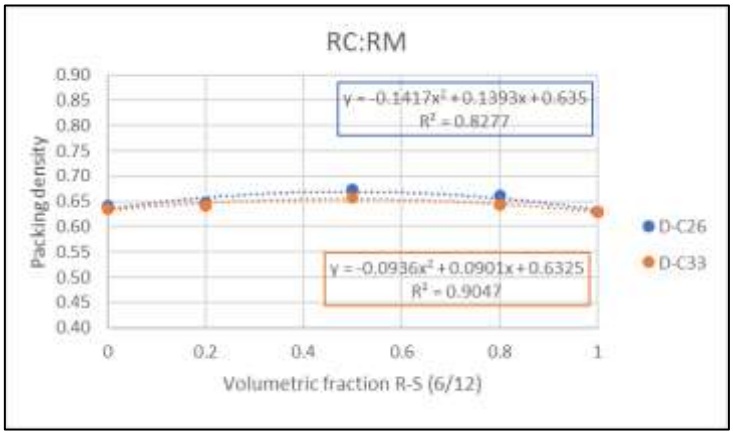

Fig. 4.21. PD of RC:RM mixture under two compaction energies: D-C26 and D-C33. Aggregate size ratio: 0.52.

The PD of the individual rounded aggregate fraction remained constant at the two vibration levels (D-C26 and D-C33). Higher values of PD were achieved with the D-C26 compaction process (see Fig. 4.20, Fig. 4.21 and Fig. 4.22) when different rounded fractions were mixed. These higher PD values can be attributed to the (de Larrard 1999) segregation that may occur after the process of compacting a granular mix by compression and/or vibration when the compaction is not effective, because the fine grains settle on the cylinder floor. For example, the RC:RF mixture (Fig. 4.22) showed the highest difference in the PD measured at two different vibration levels. A finding that is

coincident with other studies, as the larger the difference in particle size, the higher the predisposition of the particles to segregate.

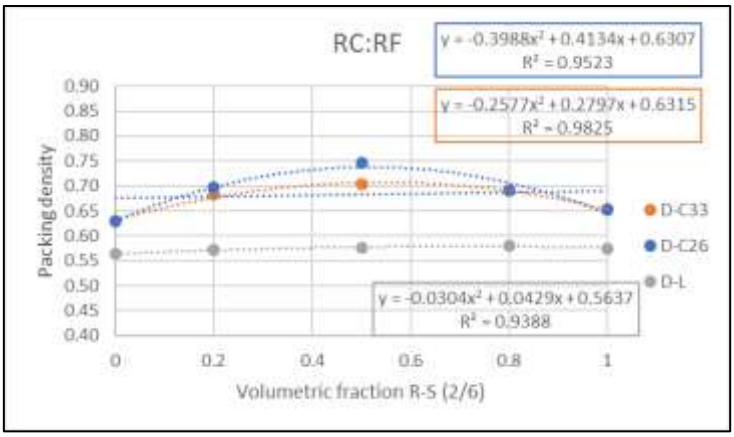

Fig. 4.22. PD of RC:RF mixture under three compaction energies: D-L, D-C26, and D-C33. Aggregate size ratio: 0.19.

Nevertheless, as other authors (Bala *et al.* 2019; de Larrard 1999) affirmed, binary mixtures with lower size ratios present a greater capacity of increasing the PD of the granular mixture, because of lower inter-particle forces and easier filling of the voids formed by the coarse aggregate by aggregates with smaller diameters. This capacity can be noted, following the comparison between Fig. 4.21 and Fig. 4.22 where the aggregate size ratio is 0.52 and 0.19, respectively. In the latter, the mixture of different volumetric fractions of R-S (6/12) and R-WTB (11/22) increased its PD by 7% and, in the former, the PD of the R-S (2/6) and R-WTB (11/22) mixture increased by up to 25%. A finding that is also in line with the results reported by other authors.

Fig. 4.23. Left: Mixing of the fine and coarse fractions (0.5 by volume) of rounded aggregates; Right: Aggregate mixture following the D-C26 compaction process.

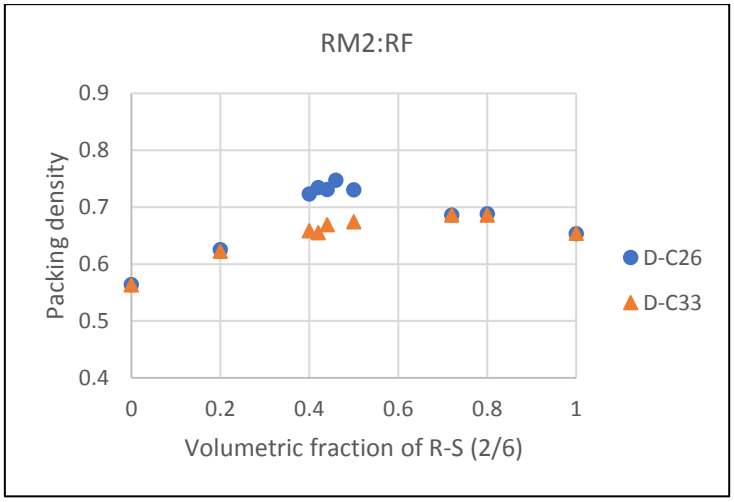

Fig. 4.24. PD of RM2:RF mixture under two compaction energies: D-C26 and D-C33. Aggregate size ratio: 0.21.

Fig. 4.24 shows the packing densities obtained by mixing different volumetric fractions of glass balls (R-GB (16)) and rounded fine aggregate (R-S (2/6)). During the experimental test, segregation was easily observed in mixtures with a volumetric fraction of glass balls between 0.5 and 0.6 when compression and vibration were both applied at 33 Hz (D-C33) (see ***Fig. 4.25***).

Fig. 4.25. The mixture of glass balls and fine rounded aggregate following compaction (0.5 by volume of each material). Left: D-C26 compaction process and Right: D-C33 compaction process.

As may be observed, higher PD can be achieved through gap-graded mixtures (RC:RF and RM2:RF) (mixtures with a low aggregate size ratio), although it also increases the segregation potential.

4.3.3.2 Natural limestone aggregate

The methodology explained in section 4.2 was followed, to obtain the combination of NL (0/4), NL (4/11), and NL (11/22) with the highest PD.

Fig. 4.26 and Table 4.14 show the packing densities of different mixtures of the coarse and medium NL aggregate fractions (NL (4/11) and NL (11/22)). The following may be observed:

- The packing of coarse aggregate increased by up to 11% when mixed with the medium aggregate fraction. As other authors (Bala *et al.* 2019; de Larrard 1999) noted, it is the size ratio (0.42 for this mix) that has the greatest influence on this increase. They defined a size ratio of 0.5 as a possible limit for material with total interaction.
- The PD increase was roughly equal for all mixes when greater compacting energy was applied.
- The combination of aggregates for maximum packing varied depending on the compaction method that was applied. A variance that was attributed to the deviations found when performing the same test on different subsamples, due mainly to the dispersion of the aggregate morphology (see Table 4.14).
- At points near the maximum packing value, the variance of PD values was very small, making it difficult to choose the best option. Three proportions of coarse and medium NL aggregates were therefore mixed with the fine fraction, to verify their influence on the selection of the coarse and medium fraction in the total packing of the mix.
    - 0.4NC:0.6NM (see Fig. 4.27 and Table 4.15). Mixture with highest PD, if the second-degree polynomial curves are considered valid for the packing model.
    - 0.6NC:0.4NM (see Fig. 4.27 and Table 4.16). The optimal mixture proposed for concrete design[17].
    - 0.5NC:0.5NM (see Fig. 4.27 and Table 4.17). Mixture with the highest PD at the highest compaction level (D-C33).

[17] With the objective of selecting the optimum packed aggregate mix for concrete mix design, a threshold value was established, above which we consider that the proportion of aggregate as valid to obtain the maximum PD. This value, set at a maximum variation of 2%, was considered in relation to the maximum packing obtained by each compaction method. The thresholds are shown in Table 4.14. Finally, from the different mixes that exceeded the threshold value, the mix with the highest proportion of coarse aggregate was chosen as the optimum, as coarse aggregate provides strength to the concrete mix.

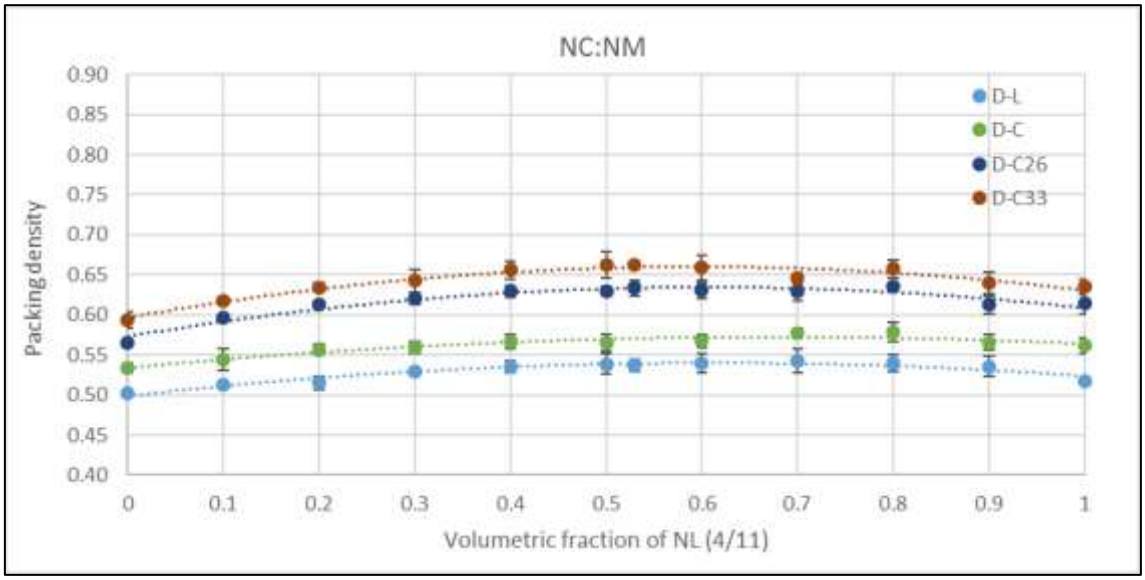

Fig. 4.26. PD of NC:NM mixtures at four different compaction energies (D-L, D-C, D-C26, and D-C33) fitted to a second-degree polynomial curve.

Table 4.13. Maximum PD if the second-degree polynomial curve is considered.

Compaction method	Second-degree polynomial curve	Vertex of the eq. Xv=(-b/2a)	R^2
D-C33	$y = -0.1797x^2 + 0.2136x + 0.5966$	0.59	0.94
D-C26	$y = -0.1674x^2 + 0.2031x + 0.573$	0.61	0.94
D-C	$y = -0.0835x^2 + 0.1134x + 0.5339$	0.68	0.91
D-L	$y = -0.11x^2 + 0.1349x + 0.4987$	0.61	0.93

where, Xv is the vertex of the parabolic equation and is therefore the volumetric fraction of NL (4/11) at which maximum packing is achieved (if the parabolic equation is considered a valid model to fit with the PD values).

Table 4.14. PD of NC:NM mixtures. Mean values ($\bar{x}$ ±σ), coefficient of variation (C.V.), and threshold value.

Vol. fraction (%)		PD (%)											
NL (4/11)	NL (11/22)	D-L			D-C			D-C26			D-C33		
		$\bar{x}$ ±σ		C.V.	$\bar{x}$ ±σ		C.V.	$\bar{x}$ ±σ		C.V.	$\bar{x}$ ±σ		C.V.
0	100	50.2	±0.2	0.4%	53.4	±0.6	1.1%	56.6	±0.4	0.6%	59.4	±1.0	1.7%
10	90	51.2	±0.3	0.6%	54.4	±1.3	2.4%	59.6	±0.1	0.2%	61.7	±0.5	0.8%
20	80	51.6	±0.8	1.6%	55.7	±0.7	1.2%	61.3	±0.5	0.8%	63.5	±0.5	0.7%
30	70	52.9	±0.4	0.8%	55.9	±0.7	1.3%	62.0	±0.7	1.2%	64.2	±1.4	2.2%
40	60	53.5	±0.8	1.4%	56.6	±0.9	1.6%	62.9	±0.7	1.2%	65.6	±1.2	1.8%
50	50	53.9	±1.3	2.4%	56.5	±1.0	1.7%	63.0	±0.5	0.9%	**66.3**	**±1.6**	**2.4%**
53	47	53.7	±0.8	1.5%	-	-	-	**63.4**	**±1.0**	**1.6%**	66.2	±0.2	0.3%
60	40	53.9	±1.2	2.2%	56.8	±0.8	1.5%	63.1	±1.0	1.6%	65.9	±1.6	2.4%
70	30	**54.2**	**±1.5**	**2.7%**	**57.7**	**±0.6**	**1.0%**	63.0	±1.3	2.0%	64.5	±0.7	1.1%
80	20	54.0	±1.1	2.0%	57.7	±1.2	2.1%	**63.4**	**±0.3**	**0.4%**	65.7	±1.1	1.7%
90	10	53.6	±1.3	2.4%	56.6	±0.9	1.6%	61.2	±1.1	1.9%	64.0	±1.4	2.2%
100	0	51.7	±0.1	0.2%	56.1	±0.9	1.7%	61.4	±1.4	2.2%	63.5	±0.9	1.5%
Maximum PD		**54.2**			**57.7**			**63.4**			**66.3**		
Threshold value		**53.1**			**56.5**			**62.1**			**65.0**		

As can be observed from Fig. 4.27, the PD increased significantly when different proportions of fine aggregate were added to both the coarse and the fine-aggregate mixes. The packing of the starting mixture increased by up to 29% when mixed with the fine-aggregate fraction (see Table 4.16, Table 4.15 and Table 4.17). If the increase is compared with the starting fraction (NL (11/22)), the potential increase in PD when mixed with medium (NL (4/11)) and fine aggregate (NL (0/4)) is about 40%.

The PD increases for all mixes when more compaction energy is applied. However, this effect is more evident and the increase in PD is greater when the volumetric fraction of NL (0/4) is dominant (see Fig. 4.27). It may be because the inter-particle forces are overcome when a compaction energy is applied, whereas when the compaction method is simply pouring (D-L), the compaction density is affected by this type of inter-particle forces.

Comparing the three charts in Fig. 4.27, the mixes with higher proportions of coarse aggregate (b and c) clearly need less fine aggregate to reach the maximum (about 50%) while in chart a, the maximum is reached when about 60% of fine aggregate is added.

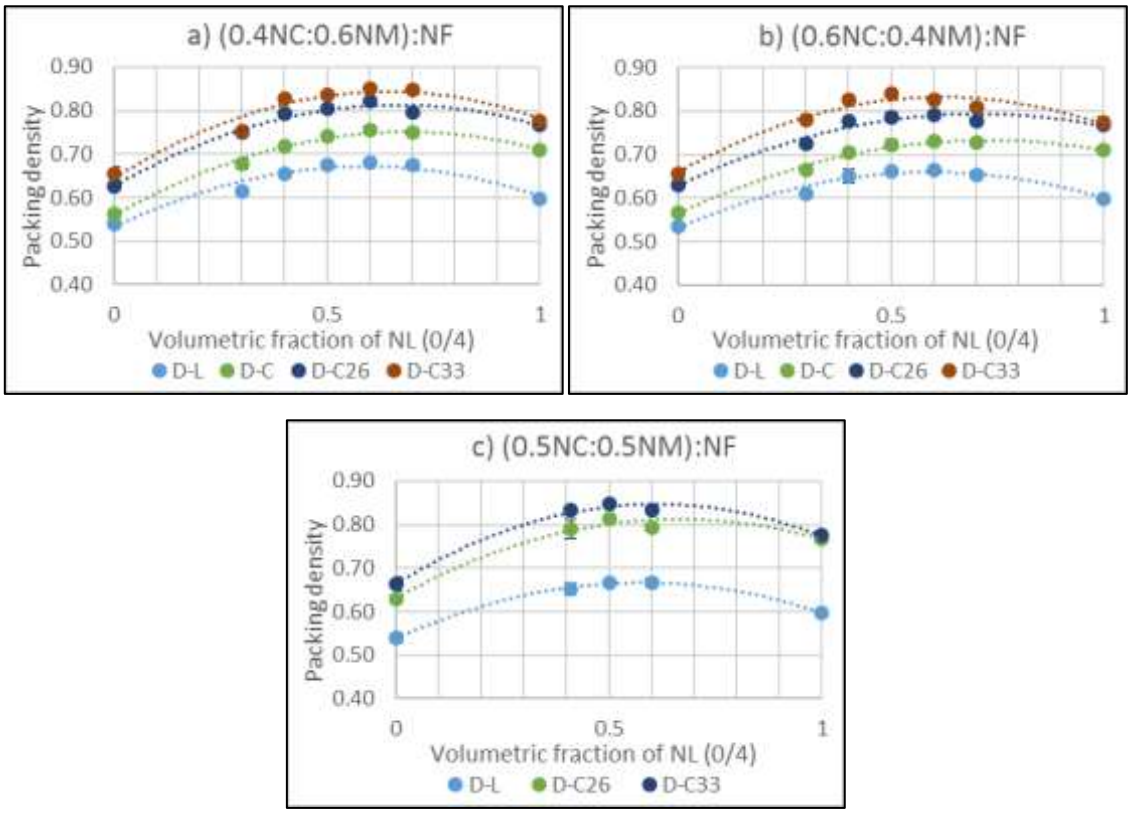

Fig. 4.27. Packing densities fitted to a second-degree polynomial curve of three mixtures of coarse and medium fractions with added fine aggregate, under four different compaction energies (D-L, D-C, D-C26 and D-C33).

Turning to the absolute PD values (see Table 4.16, Table 4.15 and Table 4.17), the maximum packing values were reached for the (0.4NC:0.6NM):NF mixture. However,

the differences between the maximums of the three mixtures were less than 2% and may be explained by sample variability.

Finally, if the threshold value[3] is considered, the optimum PD for the concrete mix design is obtained when 40 to 50% of the fine fraction is added to the coarse and medium mix, in all of the three mixes under analysis. There is therefore little influence on the selection of the medium and coarse ratio that presents the maximum packing, regardless of the method chosen to select the maximum PD.

Another point worth highlighting is that the proportion of aggregates at which the maximum packing is obtained is practically independent of the compaction method applied (at least with the aggregate fractions under analysis), as long as a range of values is contemplated among which the maximum is found and not a single maximum value. However, the fine fractions were noticeably more sensitive to the compaction energy that was applied.

Table 4.15. PD of (0.4NC:0.6NM):NF mixtures. Mean values ($\bar{x}$ ±σ), coefficient of variation (C.V.) and threshold value.

Vol. % fraction			PD (%)											
NL (0/4)	NL (4/11)	NL (11/22)	D-L			D-C			D-C26			D-C33		
			$\bar{x}$ ±σ		C.V.	$\bar{x}$ ±σ		C.V.	$\bar{x}$ ±σ		C.V.	$\bar{x}$ ±σ		C.V.
0	60	40	53.9	±1.2	2.2%	56.8	±0.6	1.0%	63.1	±1.0	1.6%	65.9	±1.6	2.4%
30	42	28	61.5	±0.2	0.4%	67.6	±1.1	1.6%	74.9	±0.6	0.8%	75.1	±0.6	0.8%
40	36	24	65.6	±0.7	1.0%	71.7	±0.7	0.9%	79.2	±0.8	1.0%	82.7	±0.6	0.7%
50	**30**	**20**	67.4	±0.6	0.9%	74.0	±0.8	1.1%	80.4	±0.2	0.3%	83.7	±0.4	0.5%
60	24	16	**68.0**	**±0.3**	0.4%	**75.5**	**±0.8**	1.0%	**82.0**	**±0.2**	0.2%	**85.1**	**±0.2**	**0.3%**
70	18	12	67.4	±0.5	0.7%	74.9	±0.4	0.5%	79.6	±0.0	0.0%	84.6	±0.2	0.2%
100	0	0	59.7	±0.3	0.5%	70.9	±0.3	0.3%	76.8	±0.4	0.6%	77.5	±1.2	1.5%
Maximum PD			**68.0**			**75.5**			**82.0**			**85.1**		
Threshold value			**66.6**			**74.0**			**80.4**			**83.4**		

Table 4.16. PD of (0.6NC:0.4NM):NF mixtures. Mean values ($\bar{x}$ ±σ), coefficient of variation (C.V.), and threshold value.

Vol. fraction (%)			PD (%)											
NL (0/4)	NL (4/11)	NL (11/22)	D-L			D-C			D-C26			D-C33		
			$\bar{x}$ ±σ		C.V.	$\bar{x}$ ±σ		C.V.	$\bar{x}$ ±σ		C.V.	$\bar{x}$ ±σ		C.V.
0	40	60	53.5	±0.8	1.4%	56.6	±0.9	1.6%	62.9	±0.7	1.2%	65.6	±1.2	1.8%
30	28	42	61.1	±0.2	0.3%	66.3	±0.6	0.9%	72.6	±1.0	1.4%	78	±0.8	1.0%
40	**24**	**36**	65.0	±1.6	2.4%	70.4	±0.7	1.0%	77.8	±0.0	0.0%	82.5	±0.4	0.5%
50	**20**	**30**	66.2	±0.3	0.4%	72.3	±1.2	1.7%	78.6	±1.1	1.4%	**83.9**	**±0.6**	**0.7%**
60	16	24	**66.5**	**±0.4**	**0.6%**	**73.0**	**±0.9**	**1.2%**	**79.2**	**±0.6**	**0.7%**	82.5	±0.3	0.4%
70	12	18	65.4	±0.5	0.8%	72.8	±0.4	0.6%	77.8	±0.5	0.6%	80.9	±0.3	0.4%
100	0	0	59.7	±0.3	0.5%	70.9	±0.3	0.3%	76.8	±0.4	0.6%	77.5	±1.2	1.5%
Maximum PD			**66.5**			**73.0**			**79.2**			**83.9**		
Threshold value			**65.2**			**71.5**			**77.6**			**82.2**		

Table 4.17. PD of (0.5NC:0.5NM):NF mixtures. Mean values ($\bar{x}$ ±σ), coefficient of variation (C.V.) and threshold value.

Vol. fraction (%)			PD (%)					
NL (0/4)	NL (4/11)	NL (11/22)	D-L		D-C26		D-C33	
			$\bar{x}$ ±σ	C.V.	$\bar{x}$ ±σ	C.V.	$\bar{x}$ ±σ	C.V.
0	50	50	53.9 ±1.3	2.4%	63.0 ±0.5	0.9%	66.3 ±1.6	2.4%
41	31	28	65.2 ±1.2	1.8%	79.0 ±2.2	2.7%	83.3 ±0.6	0.7%
50	**25**	**25**	**66.7 ±0.5**	**0.7%**	**81.4 ±0.1**	**0.1%**	**84.8 ±0.1**	**0.1%**
60	20	20	66.7 ±0.9	1.3%	79.5 ±0.6	0.7%	83.5 ±0.6	0.8%
100	0	0	59.7 ±0.3	0.5%	76.8 ±0.4	0.6%	77.5 ±1.2	1.5%
Maximum PD			**66.7**		**81.4**		**84.8**	
Threshold value			**65.4**		**79.8**		**83.1**	

In an attempt to obtain the proportions of all the granulated concrete components (including the cement) for dry-packing methods, two mixtures of NL aggregates ((0.4NC:0.6NM):0.6NF and (0.5NC:0.5NM):0.5NF) were mixed with different volumetric fractions of cement (from 0.03 to 0.18).

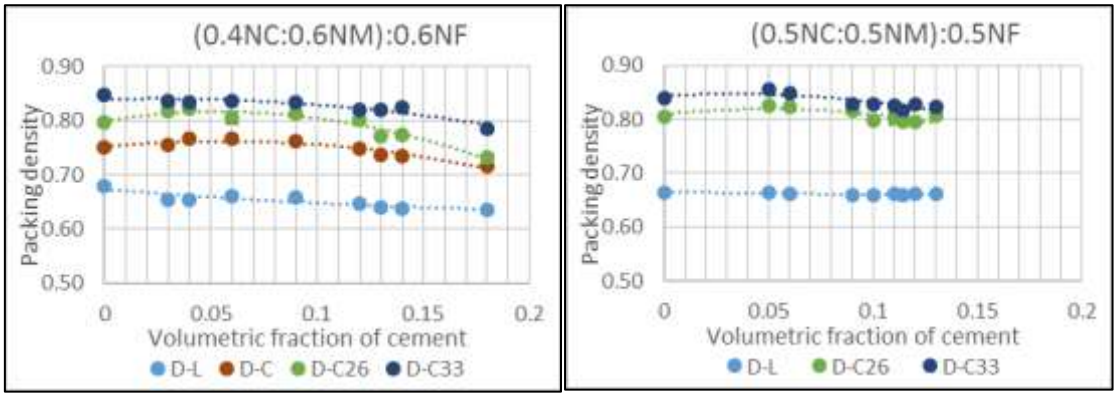

Fig. 4.28. Packing densities of two mixtures ((0.4NC:0.6NM):0.6NF and (0.5NC:0.5NM):0.5NF) with added cement.

There is no increase in the PD when cement is added to the aggregate mixtures, as could be seen in Fig. 4.28. In some cases, it was even lower than the PD of aggregates mixed without cement. Therefore, dry-packing methods are not suitable for measuring the PD of fine particles (lower than 100µm) when these are mixed with larger particles, due to the agglomeration effect caused by the interparticle forces.

Wet-packing methods were also used to analyse the effect of water on aggregate compaction. Firstly, the solid concentrations of the different aggregate mixes were measured, as detailed in 4.2.4.

The proportion of water added to the aggregate was set at 0.15 by volume. Thus, a water-to-solid ratio by volume of 0.18 was considered as the starting point. Aggregate absorbency, especially of the natural limestone aggregates, which are capable of

absorbing ±70% of their total absorption capacity during the mixing process, was considered, to calculate the solid concentration of the mix (which is equivalent to the PD).

Water had no effect on packing, notably in the mixtures of coarse and medium aggregates (see Table 4.18) and the maximum PD was obtained at similar proportions to the dry measurements. However, the specific surface area increased with additions of fine fractions and the water volume therefore needed to be higher. For example, mixtures of (0.4NC:0.6NM):NF (see Table 4.19) needed lower amounts of sand (0.45-0.5 by volume) to obtain the maximum PD in comparison with the dry methods (0.6 by volume). Fig. 4.29 shows the different appearances: the NC:NM mixture voids can be easily observed and in the NC:NM:NF mixture there are no visible voids.

In terms of absolute values, wet-packing methods provided higher PD values when the same compaction method was applied. In addition, the aggregate concrete mixtures were less sensitive to the compaction process (Shekarchi *et al.* 2010; Li & Kwan 2014).

Fig. 4.29. Left: Appearance of the wet mix of NL (11/22) and NL (4/11); Right: Appearance of the wet mix of NL (11/22), NL (4/11) and NL (0/4).

Table 4.18. Solid concentration of NC:NM mixture at 0.18 W/S ratio.

W/S	Volume fraction (%)		ρ_{bulk} (kg/m³)		ρ (kg/m³)	V_s (l)	θ (%)
	NL (4/11)	NL (11/22)					
0.18	0.35	0.65	1603	±8.1	2417	2.70	56.4
0.18	0.4	0.6	1634	±18.4	2415	2.75	57.5
0.18	0.45	0.55	1651	±6.8	2413	2.78	58.1
0.18	0.5	0.5	1660	±9.9	2411	2.80	58.5
0.18	0.55	0.45	1672	±12.7	2409	2.82	59.0
0.18	0.6	0.4	1671	±2.8	2407	2.82	59.0
0.18	**0.65**	**0.35**	**1673**	**±1.7**	**2405**	**2.83**	**59.1**
0.18	0.7	0.3	1603	±8.1	2403	2.81	58.7
Maximum							59.1
Threshold value							57.9

Table 4.19. Solid concentration of (0.4NC:0.6NM):NF mixtures at 0.18 W/S ratio.

W/S	Volume fraction (%)			ρ_{bulk} (kg/m³)		ρ (kg/m³)	V_s (l)	θ (%)
	NL (0/4)	NL (4/11)	NL (11/22)					
0.18	0.4	0.36	0.24	2247	±20.9	2416	3.75	78.4
0.18	**0.45**	**0.33**	**0.22**	**2400**	**±10.4**	**2417**	**4.01**	**83.7**
0.18	**0.5**	**0.3**	**0.2**	**2401**	**±4.4**	**2419**	**4.01**	**83.7**
0.18	0.55	0.27	0.18	2391	±3.0	2420	3.99	83.3
0.18	0.6	0.24	0.16	2387	±1.4	2421	3.98	83.1
0.18	0.7	0.18	0.12	2333	±8.8	2423	3.89	81.2
Maximum								83.7
Threshold value								82.0

In a second approach to the wet-packing methods, the proportion of aggregates were fixed and different volumes of water were added (W/S ratios from 0.1 to 0.3), to obtain the optimal amount of water to reach the maximum aggregate PD (see Fig. 4.30). As happened with wet-cement packing, the concentration of solids increased as the amount of water increased, until a threshold value was reached, beyond which the solid concentrations began to decrease as water was added. Comparing the (0.4NC:0.60NM):NF mixtures, larger volumes of water were required, to obtain the maximum solid concentration when the amount of fine aggregate was greater, due to the higher specific surface. In addition, once the W/S ratio was higher than the threshold value, then the differences between the solid concentrations of both mixtures were reduced.

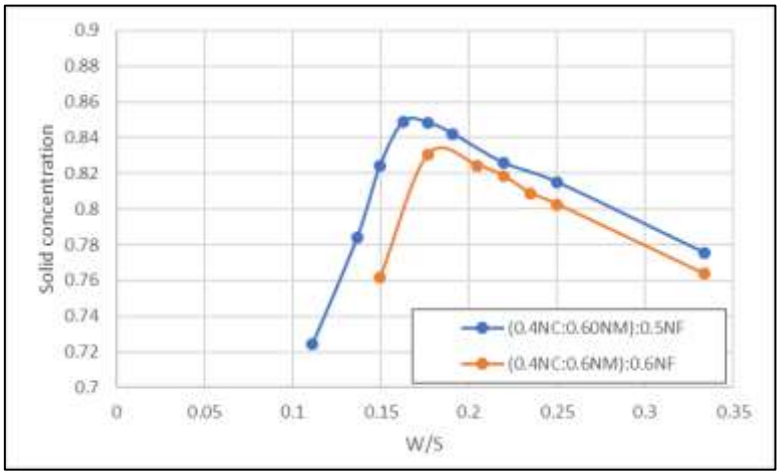

Fig. 4.30. Solid concentration of different mixtures of NL aggregates.

4.3.3.3 Electric arc furnace (EAF) slag aggregates

The methodology explained in section 4.2 was followed, to obtain the combination of NL (0/2), EAF (0/5), EAF (4/11) and EAF (11/22) with the highest PD. Fig. 4.31 shows the appearance of a mixture of EAF aggregates.

Fig. 4.31. Left: Mixture (0.4EC:0.60EM):0.4EF; Right: Appearance of the aggregate mixture following the D-C33 compaction process.

The packing densities of both the coarse and the medium EAF aggregate fraction mixtures (EAF (4/11) and EAF (11/22)) are shown in Fig. 4.32 and in Table 4.20. The following observations may be noted:

- The packing of coarse aggregate increased by up to 17% when mixed with the medium aggregate fraction. As other authors (Bala *et al.* 2019; de Larrard 1999) observed, the size ratio has the greatest influence on this increase. (The size ratio of this mix is 0.43). As the PD of the medium fraction was ±15% higher than the PD of the coarse fraction and the size ratios of the two fractions were high, the maximum PD was achieved when the medium fraction was dominant, as the particles were not small enough to fill the voids formed by the coarse particles.
- The PD increase was roughly equally for all mixes when more compacting energy was applied.
- The combination of aggregates that presented the maximum PD varied in accordance with the compaction method that was applied. This behavior may be attributed to the deviations found when performing the same test on different subsamples, due mainly to the dispersion of the aggregate morphology (see Table 4.20 Table 4.14).
- At points near the maximum packing value, the variation of PD values was very small, making it difficult to pinpoint the best option. So, the influence of the coarse and medium fractions selected for the total packing of the mix was verified, by mixing coarse and medium EAF aggregate with the fine fraction of EAF.
    - 0.2NC:0.8NM (see Fig. 4.34 and Table 4.15). Mixture with the highest PD at the highest compaction level (D-C33).
    - 0.4NC:0.6NM (see Fig. 4.34 and Table 4.16). Proposed optimal mixture for concrete design[3].

Table 4.20. PD of EC:EM mixtures. Mean values ($\bar{x}$ ±σ), coefficient of variation (C.V.) and threshold value.

Vol. fraction (%)		PD (%)											
EAF (4/11)	EAF (11/22)	D-L			D-C			D-C26			D-C33		
		$\bar{x}$ ±σ		C.V.	$\bar{x}$ ±σ		C.V.	$\bar{x}$ ±σ		C.V.	$\bar{x}$ ±σ		C.V.
0	100	48.2	±0.4	0.8%	52.0	±0.1	0.3%	54.7	±0.2	0.4%	58.3	±0.6	1.0%
10	90	49.7	±0.2	0.3%	55.2	±0.6	1.2%	57.1	±0.2	0.4%	60.6	±0.0	0.0%
20	80	50.5	±0.2	0.4%	56.9	±0.2	0.3%	58.4	±0.5	0.9%	62.0	±0.2	0.3%
30	70	53.1	±0.6	1.0%	58.3	±0.7	1.3%	62.1	±0.9	1.4%	65.1	±0.6	0.9%
40	60	51.3	±0.8	1.6%	56.8	±0.5	0.9%	59.7	±0.4	0.7%	63.5	±0.2	0.3%
50	50	52.7	±0.5	0.9%	58.4	±0.6	1.0%	61.4	±1.0	1.6%	65.1	±0.8	1.2%
60	**40**	52.9	±0.7	1.3%	58.5	±0.6	1.0%	62.7	±0.3	0.5%	66.2	±0.5	0.8%
70	30	52.5	±1.0	1.8%	58.2	±1.0	1.7%	62.1	±0.9	1.4%	65.2	±0.5	0.7%
80	20	**54.0**	**±0.4**	0.7%	60.1	±0.3	0.5%	63.2	±0.3	0.5%	**67.0**	**±0.3**	0.5%
90	10	**54.0**	**±0.8**	1.5%	**60.2**	**±0.4**	0.7%	**63.8**	**±0.6**	0.9%	66.3	±0.6	1.0%
100	0	53.5	±1.1	2.0%	59.6	±1.2	2.0%	62.8	±1.2	1.9%	65.4	±1.5	2.3%
Maximum PD		**54.0**			**60.2**			**63.8**			**67.0**		
Threshold value		**52.9**			**59.0**			**62.5**			**65.7**		

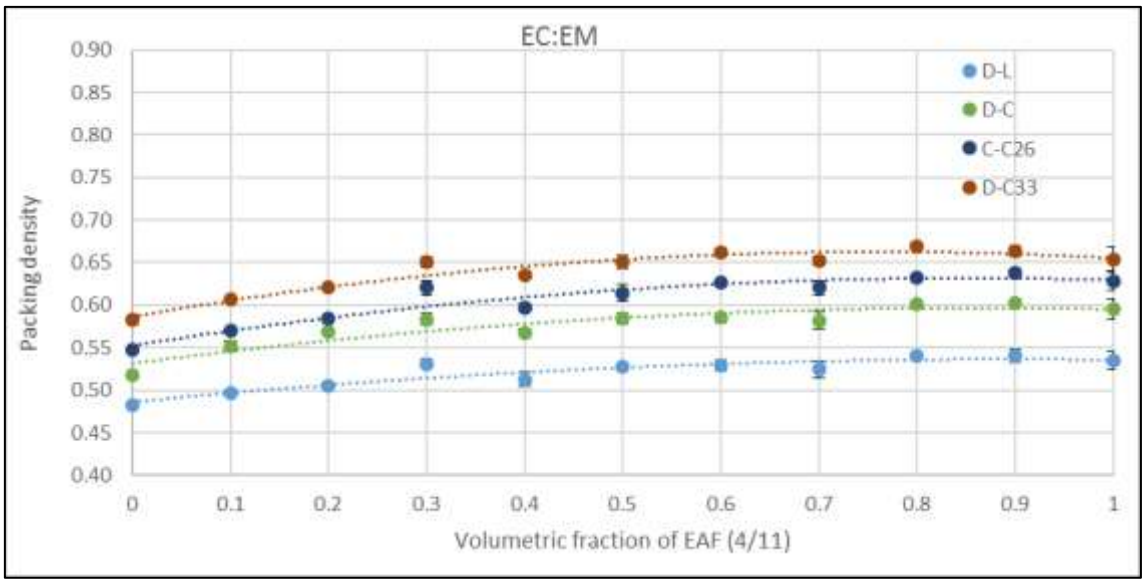

Fig. 4.32. PD of EC:EM mixtures at four different compaction energies (D-L, D-C, D-C26 and D-C33) and fitting to a second-degree polynomial curve.

As can be observed in Fig. 4.33, the PD significantly increased when different proportions of fine aggregate were added to the coarse and medium aggregate mixtures. The packing of the starting mixture following the addition of the fine-aggregate fraction increased by up to 18% (see Table 4.22 and Table 4.23).

The PD of all the mixes increased as greater compacting energy was applied.

Comparing the two charts in Fig. 4.33, it can be seen from Chart b that larger proportions of fine aggregate were needed to reach the maximum when the coarse aggregate proportion was lower (±60%), while in Chart a the maximum was reached after adding ±70% of fine aggregate.

Table 4.21. Maximum PD if the second-degree polynomial curve is considered.

Compaction method	Second-degree polynomial curve	Vertex of eq. Xv=(-b/2a)	R^2
D-C33	$y = -0.1308x^2 + 0.1995x + 0.5867$	0.76	0.92
D-C26	$y = -0.1094x^2 + 0.1865x + 0.5523$	0.85	0.90
D-C	$y = -0.0874x^2 + 0.151x + 0.5316$	0.86	0.85
D-L	$y = -0.0628x^2 + 0.1123x + 0.4862$	0.89	0.86

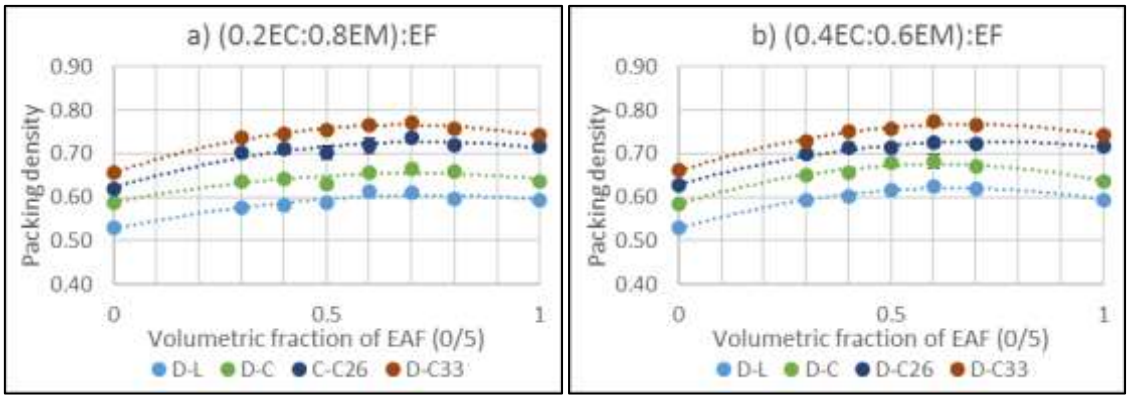

Fig. 4.33. PD fitted to a second-degree polynomial curve of two mixtures of coarse and medium fraction with added fine aggregate at four different compaction energies (D-L, D-C, D-C26 and D-C33).

Finally, if the threshold value[3] is considered, the optimum PD for the concrete mix design was reached after adding 50 to 60% of the fine fraction to the coarse and medium mix for the two mixtures under analysis.

Table 4.22. PD of (0.4EC:0.6EM):EF mixtures. Mean values ($\bar{x}$ ±σ), coefficient of variation (C.V.) and threshold value.

Vol. fraction (%)			PD (%)									
EAF (0/5)	EAF (4/11)	EAF (11/22)	D-L			D-C			D-C26			D-C33		
			$\bar{x}$ ±σ		C.V.	$\bar{x}$ ±σ		C.V.	$\bar{x}$ ±σ		C.V.	$\bar{x}$ ±σ		C.V.
0	60	40	52.9	±0.7	1.3%	58.5	±0.6	1.0%	62.7	±0.3	0.5%	66.2	±0.5	0.8%
30	42	28	59.4	±0.4	0.6%	65.0	±0.8	1.2%	69.8	±0.2	0.3%	73.0	±0.2	0.3%
40	36	24	60.3	±0.5	0.8%	65.7	±0.4	0.6%	71.3	±0.0	0.0%	75.1	±0.0	0.0%
50	**30**	**20**	61.6	±0.7	1.1%	67.9	±0.6	0.8%	71.3	±0.4	0.6%	75.8	±0.3	0.3%
60	24	16	**62.5**	**±0.1**	**0.2%**	**68.2**	**±1.6**	**2.3%**	**72.6**	**±0.0**	**0.0%**	**77.4**	**±0.3**	**0.3%**
70	18	12	61.8	±0.1	0.1%	67.0	±0.7	1.1%	72.4	±0.2	0.3%	76.6	±0.0	0.0%
100	0	0	59.4	±0.1	0.1%	63.7	±0.5	0.8%	71.6	±0.0	0.0%	74.2	±0.2	0.3%
Maximum PD			**62.5**			**68.2**			**72.6**			**77.4**		
Threshold value			**61.3**			**66.8**			**71.1**			**75.8**		

Another aspect worth highlighting is that the aggregate proportions that resulted in the maximum packing value was practically independent of the compaction method that was applied (at least with the aggregate fractions under analysis), as long as a range of values is contemplated among which the maximum is found and not a single maximum

value. However, it should be noted that the sensitivity of the fine fractions to the compaction energy was greater.

Table 4.23. PD of (0.2EC:0.8EM):EF mixtures; mean values ($\bar{x}$ ±σ), coefficient of variation (C.V.), and threshold value.

Vol. fraction (%)			PD (%)							
EAF (0/5)	EAF (4/11)	EAF (11/22)	D-L		D-C		D-C26		D-C33	
			$\bar{x}$ ±σ	C.V.	$\bar{x}$ ±σ	C.V.	$\bar{x}$ ±σ	C.V.	$\bar{x}$ ±σ	C.V.
0	80	20	52.9 ±0.4	0.7%	58.9 ±0.3	0.5%	61.8 ±0.3	0.5%	65.5 ±0.3	0.5%
30	56	14	57.6 ±0.7	1.3%	63.8 ±0.4	0.6%	70.2 ±0.8	1.2%	73.7 ±0.9	1.2%
40	48	12	58.3 ±0.4	0.7%	64.1 ±0.3	0.4%	71.0 ±1.3	1.8%	74.7 ±0.6	0.8%
50	40	10	58.7 ±0.6	1.1%	63.1 ±0.4	0.6%	70.2 ±1.5	2.1%	75.4 ±0.5	0.6%
60	**32**	**8**	**61.2 ±0.8**	1.2%	65.6 ±0.5	0.8%	71.9 ±1.7	2.4%	76.5 ±1.1	1.4%
70	**24**	**6**	61.0 ±0.5	0.9%	**66.4 ±0.4**	**0.6%**	**73.7 ±0.6**	**0.8%**	**77.2 ±0.5**	**0.6%**
80	16	4	59.7 ±1.0	1.7%	65.9 ±0.4	0.6%	72.0 ±0.2	0.3%	75.6 ±0.2	0.3%
100	0	0	59.4 ±0.1	0.1%	63.7 ±0.5	0.8%	71.6 ±0.0	0.0%	74.2 ±0.2	0.3%
Maximum PD			**61.2**		**66.4**		**73.7**		**77.2**	
Threshold value			**60.0**		**65.1**		**72.2**		**75.6**	

As lower PD values were obtained for ternary mixtures of EAF compared with the ternary mixtures of NL, quaternary mixtures with additions of the NL (0/2) fraction were also analysed (see Fig. 4.34, Table 4.24 and Table 4.25). The packing of the starting ternary mixture was increased by up to 10%, by mixing in additions of the natural fine-aggregate fraction that achieved packing densities close to the NL aggregate mixtures.

Comparing the two charts in Fig. 4.34 , it can be seen that similar proportions of fine aggregate were needed to reach the maximum. However, the sum of the fine aggregate (EAF (0/5) + EAF (0/2)) needed to reach the maximum was higher for the mixtures with lower contents of coarse aggregate.

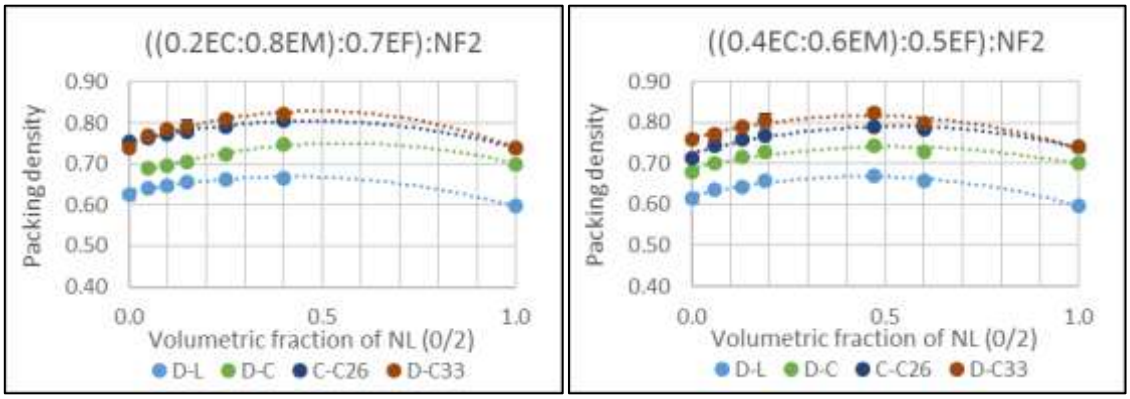

Fig. 4.34. PD of ((0.2EC:0.8EM):0.7EF):NF2 and ((0.4EC:0.6EM):0.5EF):NF2 mixtures on four different energies of compaction (D-L, D-C, D-C26 and D-C33), fitted to a second-degree polynomial curve.

Moreover, if we look at the absolute PD values (see Table 4.24 and Table 4.25), the differences between the maximums were less than 1% and may be associated with the variability of the sample.

Table 4.24. PD of ((0.4EC:0.6EM):0.5EF):NF2. Mean values ($\bar{x}$ ±σ) and coefficient of variation (C.V.).

Vol. fraction (%)				PD (%)											
NL (0/2)	EAF (0/5)	EAF (4/11)	EAF (11/22)	D-L			D-C			D-C26			D-C33		
				$\bar{x}$ ±σ		C.V.	$\bar{x}$ ±σ		C.V.	$\bar{x}$ ±σ		C.V.	$\bar{x}$ ±σ		C.V.
0	50	30	20	61.6	±0.7	1.1%	67.9	±0.6	0.9%	71.3	±0.4	0.6%	75.8	±0.4	0.4%
6	47	28	19	63.6	±1.3	2.0%	70.2	±1.3	1.9%	74.5	±0.5	0.7%	77.2	±0.7	0.9%
13	44	26	17	64.1	±0.5	0.8%	71.5	±0.5	0.7%	75.9	±1.2	1.6%	79.1	±0.5	0.6%
19	41	24	16	65.7	±1.2	1.8%	72.7	±1.1	1.5%	76.9	±0.8	1.0%	80.5	±0.8	1.0%
30	35	21	14	66.1	±0.2	0.30%	73.4	±1	1.40%	77.8	±0.8	1.0%	80.9	±1.3	1.60%
47	27	16	11	**67**	**±1**	1.5%	**74.1**	**±0.5**	0.7%	**79**	**±0.4**	0.5%	**82.1**	**±0.4**	0.5%
60	20	12	8	65.8	±0.4	0.6%	72.7	±0.3	0.4%	78.2	±0.2	0.3%	79.8	±0.3	0.4%
Maximum PD				**67**			**74.1**			**78.7**			**82.1**		
Threshold value				**65.7**			**72.6**			**77.4**			**80.4**		

Table 4.25. PD of ((0.2EC:0.8EM):0.7EF):NF2. Mean values ($\bar{x}$ ±σ) and coefficient of variation (C.V.).

Vol. fraction (%)				PD (%)											
NL (0/2)	EAF (0/5)	EAF (4/11)	EAF (11/22)	D-L			D-C			D-C26			D-C33		
				$\bar{x}$ ±σ		C.V.	$\bar{x}$ ±σ		C.V.	$\bar{x}$ ±σ		C.V.	$\bar{x}$ ±σ		C.V.
0	70	24	6	62.6	±1.5	2.4%	-	-	-	75.4	±0.4	0.5%	73.9	±0.4	0.5%
6	65	22	6	64.1	±1.0	1.5%	68.9	±0.6	0.8%	76.3	±1.2	1.5%	76.8	±0.9	1.1%
13	61	21	5	64.7	±1.3	1.9%	69.6	±0.5	0.7%	77.3	±0.1	0.1%	78.4	±0.5	0.6%
19	57	19	5	65.7	±0.9	1.3%	70.6	±0.5	0.7%	78.0	±0.0	0.0%	79.0	±1.7	2.1%
30	49	17	4	66.3	±0.3	0.4%	72.3	±0.2	0.2%	79.1	±0.8	1.0%	81.0	±1.0	1.3%
47	37	13	3	**66.5**	**±0.1**	0.2%	**74.9**	**±0.2**	0.3%	**80.5**	**±0.2**	0.2%	**82.3**	**±0.0**	0.0%
Maximum PD				**66.5**			**74.9**			**80.5**			**82.3**		
Threshold value				**65.2**			**73.4**			**78.9**			**80.7**		

Wet-packing methods were also performed for the EAF aggregates to compare dry and wet methods. The solid concentrations of different aggregate mixes containing the EAF aggregates were measured, as set out in section 4.2.4, to find the most compacted mix at a W/S ratio. The solid concentration of the mix (equivalent to the PD) was calculated considering aggregate absorption, as EAF aggregates are capable of absorbing ±80% of their maximum absorption capacity during the mixing process.

Both the wet- and the dry-packing results of the coarse and medium aggregate mixtures (see Table 4.26) were similar and the maximum PD with water was at similar proportions to dry measurement. The same happened when the EAFS (0/5) was added to the (0.4EC:0.6EM), although the prediction of the mixture with the maximum PD slightly differed between both the dry and the wet methods.

However, additions of the finer fraction (NL 0/2) to the mixture increased the specific surface area and the influence of the water was therefore greater, as may be seen when comparing Table 4.28 and Table 4.24. When wet packing was applied, the maximum solid concentration had an aggregate proportion of ±0.20 by volume, while for the dry packing, proportions higher than 0.30 were needed to obtain the maximum packing.

Table 4.26. Solid concentration of NC:NM mixture at 0.22 W/S ratio.

W/S	Volume fraction		Fresh density ρ_{bulk} (kg/m³)		Theoretical density (kg/m³)	V_s (l)	θ (%)
	EAF (4/11)	EAF (11/22)					
0.22	0.50	0.50	2103	±7.7	3038	2.72	56.8
0.22	0.55	0.45	2123	±2.1	3039	2.74	57.3
0.22	0.60	0.40	2197	±7.6	3040	2.84	59.2
0.22	**0.70**	**0.30**	**2240**	**±24.3**	**3043**	**2.89**	**60.4**
0.22	0.80	0.20	2146	±15.8	3045	2.77	57.8
Maximum							**60.4**
Threshold value							**59.2**

Table 4.27. Solid concentration of (0.4EC:0.6EM):EF mixtures at 0.21 W/S ratio.

W/S	Volume fraction			Fresh density ρ_{bulk} (kg/m³)		Theoretical density (kg/m³)	V_s (l)	θ (%)
	EAF (0/5)	EAF (4/11)	EAF (11/22)					
0.21	0.40	0.36	0.24	2458	±14	3085	3.17	66.1
0.21	0.45	0.33	0.22	2581	±48	3088	3.32	69.4
0.21	0.50	0.30	0.20	2673	±22.8	3091	3.44	71.8
0.21	**0.55**	**0.27**	**0.18**	**2778**	**±3.55**	**3065**	**3.57**	**74.5**
0.21	0.60	0.24	0.16	2771	±2.09	3093	3.56	74.3
0.21	0.70	0.18	0.12	2458	±15.8	3096	3.50	73.0
Maximum								**74.5**
Threshold value								**73.0**

Table 4.28. Solid concentration of ((0.4EC:0.6EM):0.5EF):NF2 mixtures at 0.18 W/S ratio.

W/S	Volume fraction				Fresh density ρ_{bulk} (kg/m³)		Theoretical density (kg/m³)	V_s (l)	θ (%)
	NL (0/2)	EAF (0/5)	EAF (4/11)	EAF (11/22)					
0.18	0.06	0.46	0.28	0.19	2592	±6.0	3095	3.40	70.9
0.18	0.10	0.44	0.27	0.18	2647	±23.8	3070	3.49	72.9
0.18	0.15	0.42	0.26	0.17	2773	±9.4	3034	3.69	77.1
0.18	0.20	0.40	0.24	0.16	2829	**±3.76**	2998	3.80	79.5
0.18	**0.25**	**0.37**	**0.23**	**0.15**	**2861**	**±12.6**	**2963**	**3.89**	**81.2**
0.18	0.30	0.35	0.21	0.14	2826	±2.71	2927	3.88	81.0
0.18	0.40	0.30	0.18	0.12	2745	±4.8	2856	3.85	80.5
0.18	0.50	0.25	0.15	0.10	2650	±10.3	2784	3.81	79.6
Maximum									**81.2**
Threshold value									**79.5**

As was found for the NL aggregates, the wet-packing methods provided higher PD values when the same compaction method was applied.

4.4 Comparison of theoretical model and experimental test results

In this section, the theoretical models that obtained the most densely packed concrete skeleton will be contrasted with the experimental results. To do so, the results will be divided in two subsections, natural limestone aggregate and EAF aggregates, according to the following structure:

- Ideal distribution curves (Fuller and Funk and Dinger)
    - Aggregates. Fuller (q=0.5) and Funk and Dinger (q=0.37)
    - Aggregates + cement. Funk and Dinger q=0.37; q=0.33 and q=0.31
- Compressible packing model (CPM)
    - Aggregates. The model was applied in three different ways, as explained in section 4.2.6.2.
        a. Virtual PD was calculated by considering each aggregate fraction as mono-size (β_m).
        b. Virtual PD was calculated by considering the size distribution of each aggregate fraction (β).
        c. Virtual PD was also calculated by considering the size distribution of each aggregate fraction, however, the virtual PD was considered as the minimum virtual PD of class i when class i is considered the dominant class of the poly-sized mix (γ).
- 3-Parameter packing model (3-P)
    - Aggregates. The model was applied by.
        a. Considering the uncompacted interaction function for angular aggregates.
        b. Considering the compacted interaction function for angular aggregates.

The methodology explained in section 4.2.6 was followed to obtain all the results.

4.4.1 Natural limestone aggregates

Determination of the optimum aggregate mix design through ideal distribution curves.

The first approach was to determine the proportion and the combination of each fraction of the NL aggregates -(NL(0/4), NL (4/11), and NL(11/22))- with the Fuller and Funk and Dinger method (see Fig. 4.35).

Cement fractions were also considered, as shown in Fig. 4.36.

The results of the optimal proportions were summarised in Table 4.29. Comparing both methods, a slightly higher amount of fine aggregate was needed to achieve the optimal aggregate proportion when the Funk & Dinger curve was employed. It was an expected outcome, as an increased proportion of the fine fraction is likewise recommended when applying the Fuller curve to the crushed aggregates (Martín-Morales *et al.* 2013). Another difference was the coarse and medium aggregate proportion, as a proportion of approximately 0.5NC/0.5CM was predicted with the Fuller method, while a proportion of 0.4NC/0.6NM was preferred for the Funk and Dinger method (q=0.37). If the values are contrasted with the combinations of aggregates that presented the maximum PD experimentally, both methods can be seen to predict the proportion within the ranges where the maximum packing is achieved.

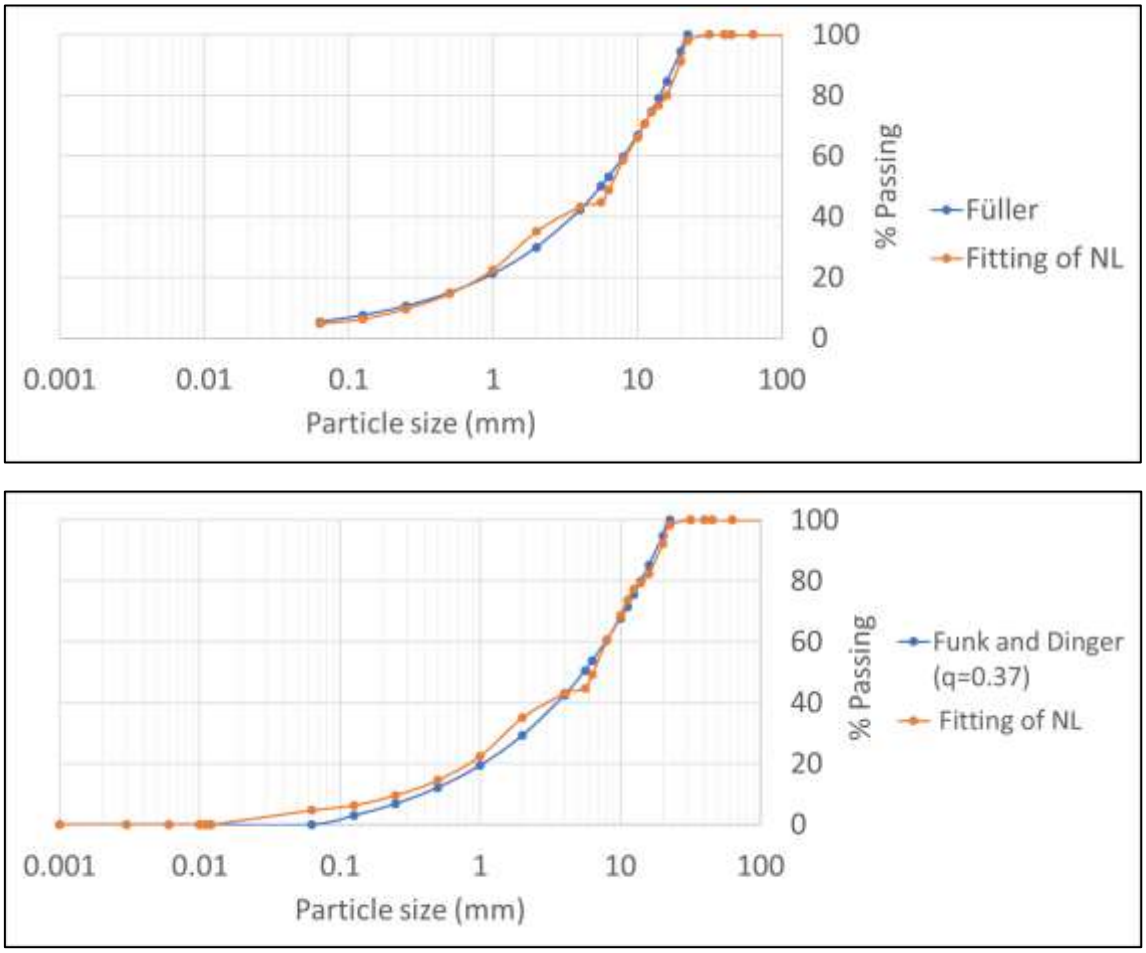

Fig. 4.35. Grading curves of the optimal proportion of NL aggregates.

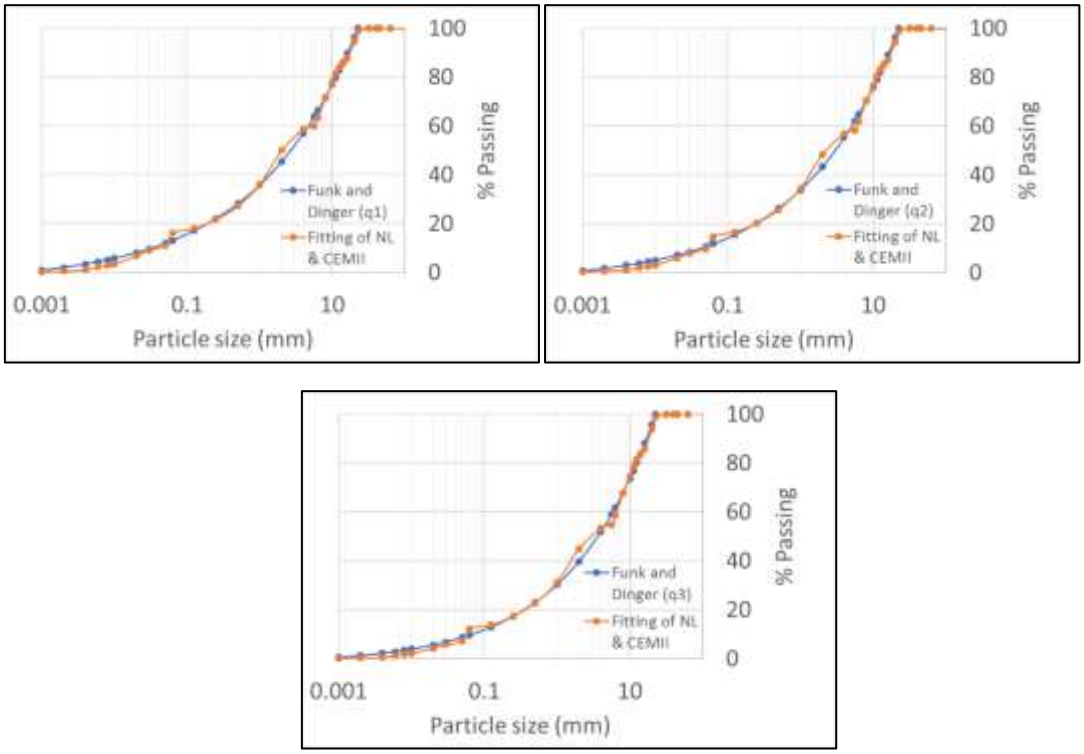

Fig. 4.36. Grading curves of the optimal proportions of NL aggregates & CEMII.

Table 4.29. Optimal granular proportion of NL aggregates by their ideal curves.

Method	Volumetric proportion (%)			
	CEM II	NL (0/4)	NL (4/11)	NL (11/22)
Fuller	-	41%	31%	28%
Funk and Dinger q= 0.37	-	46%	32%	22%
Funk and Dinger q_1= 0.31	11%	46%	26%	17%
Funk and Dinger q_2= 0.33	10%	45%	27%	18%
Funk and Dinger q_3= 0.37	7%	44%	28%	20%

Determination of the optimum aggregate mix design through theoretical models.

Firstly, as detailed in 4.2.6.2 section, the virtual PD of each fraction was determined with the three proposed methods.

By definition, the virtual PD can never be less than the actual PD. However, when the virtual PD was calculated with the virtual packing method, β, the virtual PD was lower for the fine fraction of NL (0/4), regardless of the compaction method applied, and for the medium fraction of NL (4/11) when the highest energy methods were applied (see Table 4.30). Two reasons can help to explain these virtual PD results:

- First, the compaction index under consideration may not be acceptable. In this thesis, compaction indexes previously determined in other works have been assumed to function and it is beyond the scope of the thesis to design and to adjust the models proposed by other authors. There is a possibility that the

compaction index depends not only on the method of compaction, but also on the size of the particles and their morphology.

- Second, applying the CPM model to aggregate fractions with a wide range of granular sizes can also affect the results, especially when small size particles are present.

In view of results and their poor fit with the experimental PD results (see annex), the B: β method of calculating the virtual PD was omitted from subsequent PD aggregate mix predictions.

Table 4.30. Virtual packing densities (PD) of each NL aggregate fraction.

	Packing method D-L				**Packing method D-C**			
	Actual PD	**Virtual PD (K=4.1)**			**Actual PD**	**Virtual PD (K=4.5)**		
	Φ	$A:\beta_m$	$B:\beta$	$C:\gamma$	Φ	$A:\beta_m$	$B:\beta$	$C:\gamma$
NL (0/4)	0.597	0.743	0.558	0.752	0.709	0.867	0.673	0.867
NL (4/11)	0.517	0.643	0.573	0.634	0.561	0.686	0.612	0.674
NL (11/22)	0.502	0.624	0.593	0.621	0.534	0.653	0.620	0.648

	Packing method D-C26				**Packing method D-C33**			
	Actual PD	**Virtual PD (K=9)**			**Actual PD**	**Virtual PD (K=9)**		
	Φ	$A:\beta_m$	$B:\beta$	$C:\gamma$	Φ	$A:\beta_m$	$B:\beta$	$C:\gamma$
NL (0/4)	0.768	0.853	0.643	0.842	0.775	0.861	0.673	0.850
NL (4/11)	0.614	0.682	0.606	0.670	0.635	0.706	0.612	0.692
NL (11/22)	0.566	0.629	0.595	0.623	0.594	0.660	0.620	0.653

In an initial approach, the PD predictions of the two models (the CPM and the 3-parameter packing model (3-P)) were contrasted with the actual packing densities of the binary and ternary mixtures under analysis, to verify the applicability of the models to the NL aggregates (see Fig. 4.37, Fig. 4.38, Fig. 4.39 and Fig. 4.40). The PD values and the deviations with regard to the experimental results are included in the annex section. These values were contrasted with the errors that other authors associated with both models when evaluating their applicability.

- Maximum errors of 2.5% for CPM (Fennis 2009) when narrow size distribution of aggregates are tested.
- Maximum errors ranged from -2.51% to 3.55% and the overall mean percentage error (-0.03%) for binary mixtures of angular aggregates for the 3-parameter packing model. However, by contrasting the results with other studies, Kwan *et al.* estimated an error of 5.9% as small enough to verify the applicability of the 3-P model for angular aggregates (Kwan *et al.* 2015).

It should be noted that both models were designed and calibrated for use with narrow particle-size distribution fractions and the distinctive shape of the EAF aggregate had

not previously been tested. In this study, the parameters that control particle interaction, which are not applied to each mono-size particle fraction, will therefore affect the accuracy of both models.

As can be seen in Fig. 4.37, the different values of both models for predicting the behaviour of the binary mixtures mainly occurs when the coarse fraction is dominant and the packing of the mixtures approaches the maximum PD, which implies both a loosening and a wedging effect.

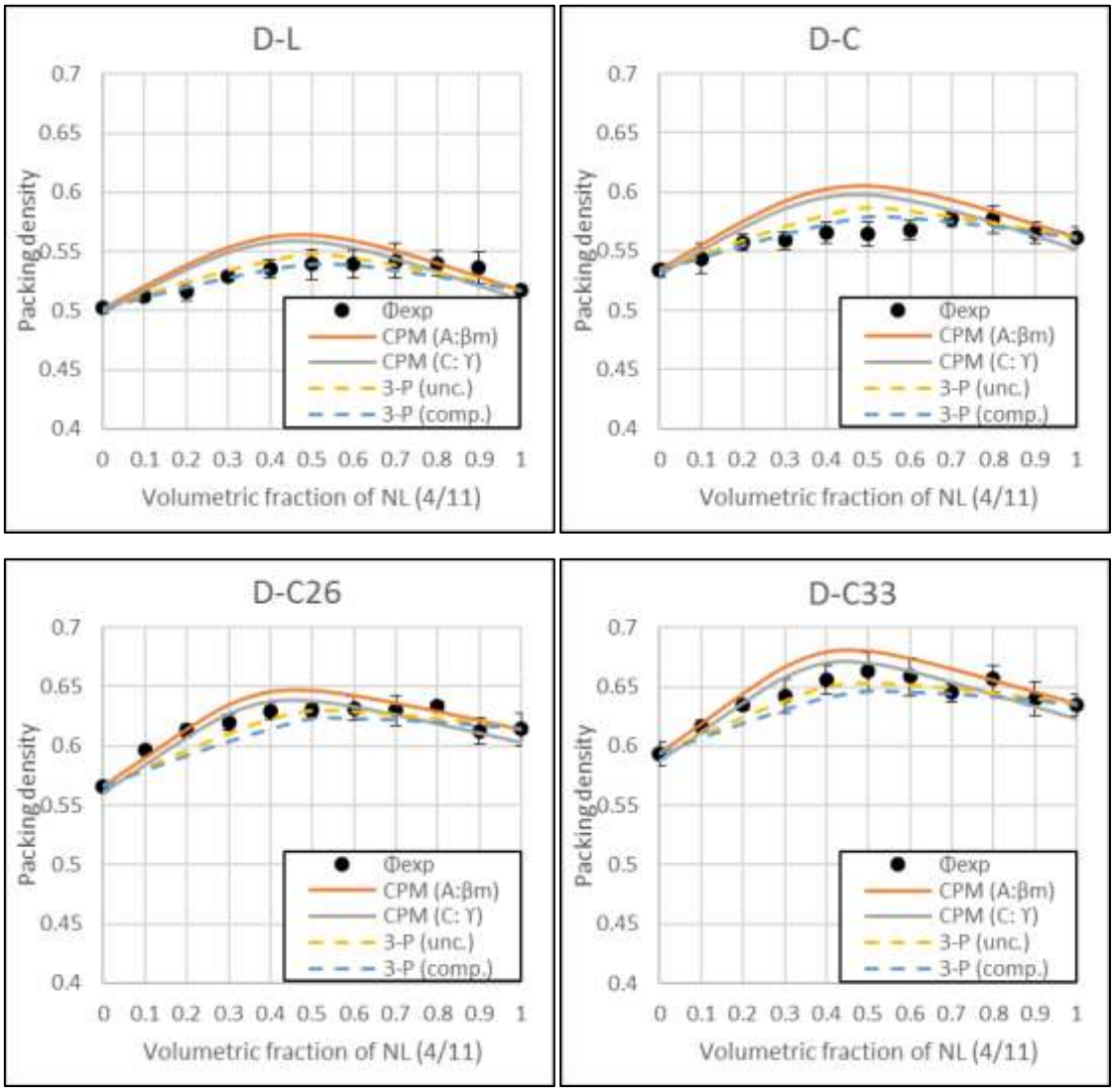

Fig. 4.37. PD of binary mixtures NC:NM.

The model showing the best fit with the experimental packing of the binary mixes was not easily determined, as the deviation of the experimental PD was, in some cases, higher than the fitted results of both models. On the one hand, the CPM tended to overestimate the PD, especially when D-L and D-C compaction methods were applied to determine the virtual PD. Better fits were therefore found when more compaction energy was applied to determine the actual packing (maximum errors close to 2.5% and

mean errors and deviation less than 2%). On the other hand, the PD values predicted with the 3-P model showed mean errors and deviations of below 1.5% for the four compaction methods. Although the interaction parameters of the 3-P model are therefore only calibrated for uncompacted (D-L) and compacted (D-C) methods, accurate prediction was also noted when the PD was calculated with both the D-C26 and the D-C33 compaction methods. In addition, by applying both interaction parameters (uncompacted and compacted) slight differences can be found, which complicates their selection.

The maximum PD was reached at aggregate ratios of 0.5NC:0.5NM and 0.4NC:0.6NM, in line with the experimental results.

As can be seen in Fig. 4.38, Fig. 4.39 and Fig. 4.40, the different predictions from both models for ternary mixtures of NL mainly occurred when the coarse fraction (mixture of coarse and medium aggregate) was dominant.

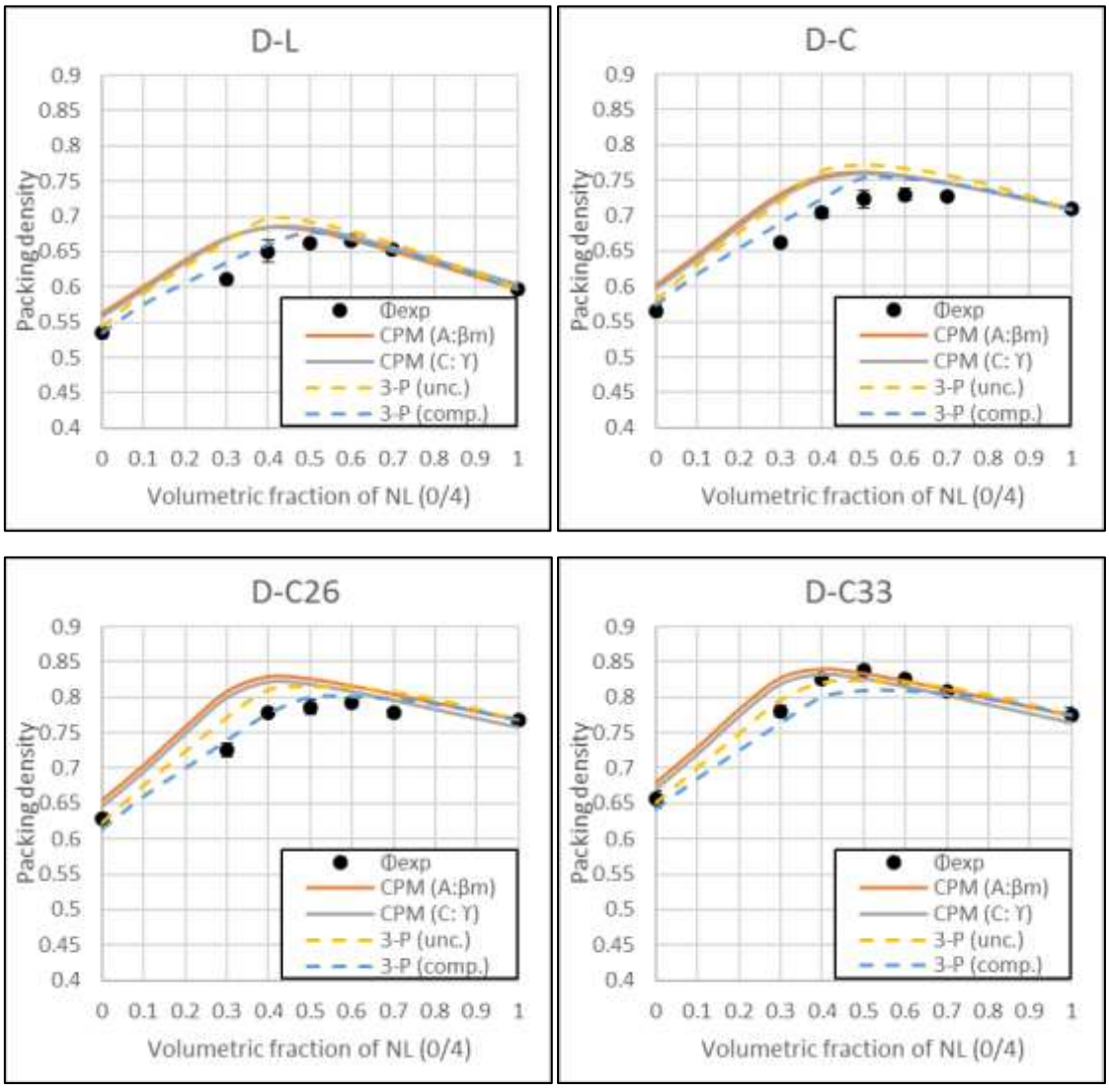

Fig. 4.38. PD of ternary mixtures (0.4NC:0.6NM):NF.

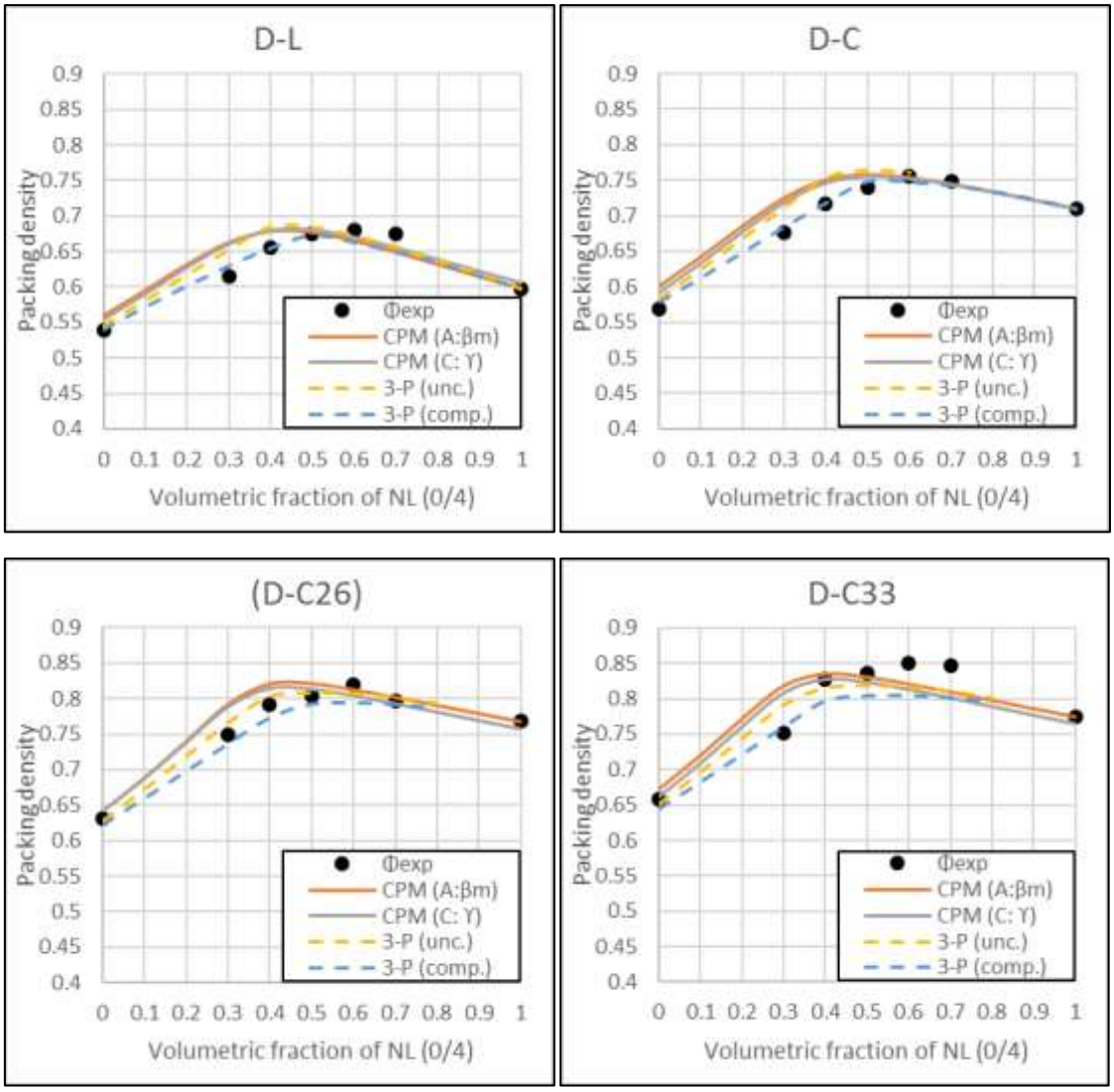

Fig. 4.39. PD of ternary mixtures (0.6NC:0.4NM):NF.

In general, the CPM tended to overestimate the PD of ternary mixtures, especially when the coarse fraction was dominant. However, the PD was underestimated for the mixtures of (0.4NC:0.6NM):NF when D-L and D-C33 were applied. As may be observed, the CPM PD predictions closely fitted the experimental PD when compression and vibration (D-C26; D-C33) were applied, to obtain the individual PD of each fraction.

The 3-P model, using the interaction parameters for compacted mixes, clearly showed a better fit with the actual PD of the three experimentally tested mixtures when coarse aggregate was dominant.

The maximum packing levels (maximum PD) depended on the model and the compaction method that was applied. Both the CPM and the 3-P(unc.) model predictions amounted to a proportion of around 0.4 of fine aggregate to reach the maximum, whilst the 3-P (comp.) model prediction amounted to a proportion of ±0.5 (except when the D-C33 compaction method was applied). Thus,

- An NL proportion of (0/4) ±0.5 was coincident with the experimental results for (0.4NC:0.6NM):NF.
- Both options, 0.4 and 0.5, of NL proportions (0/4) were in agreement with the experimental results for (0.6NC:0.4NM):NF.
- An NL proportion of (0/4) ±0.5 was coincident with the experimental results for (0.5NC:0.5NM):NF.

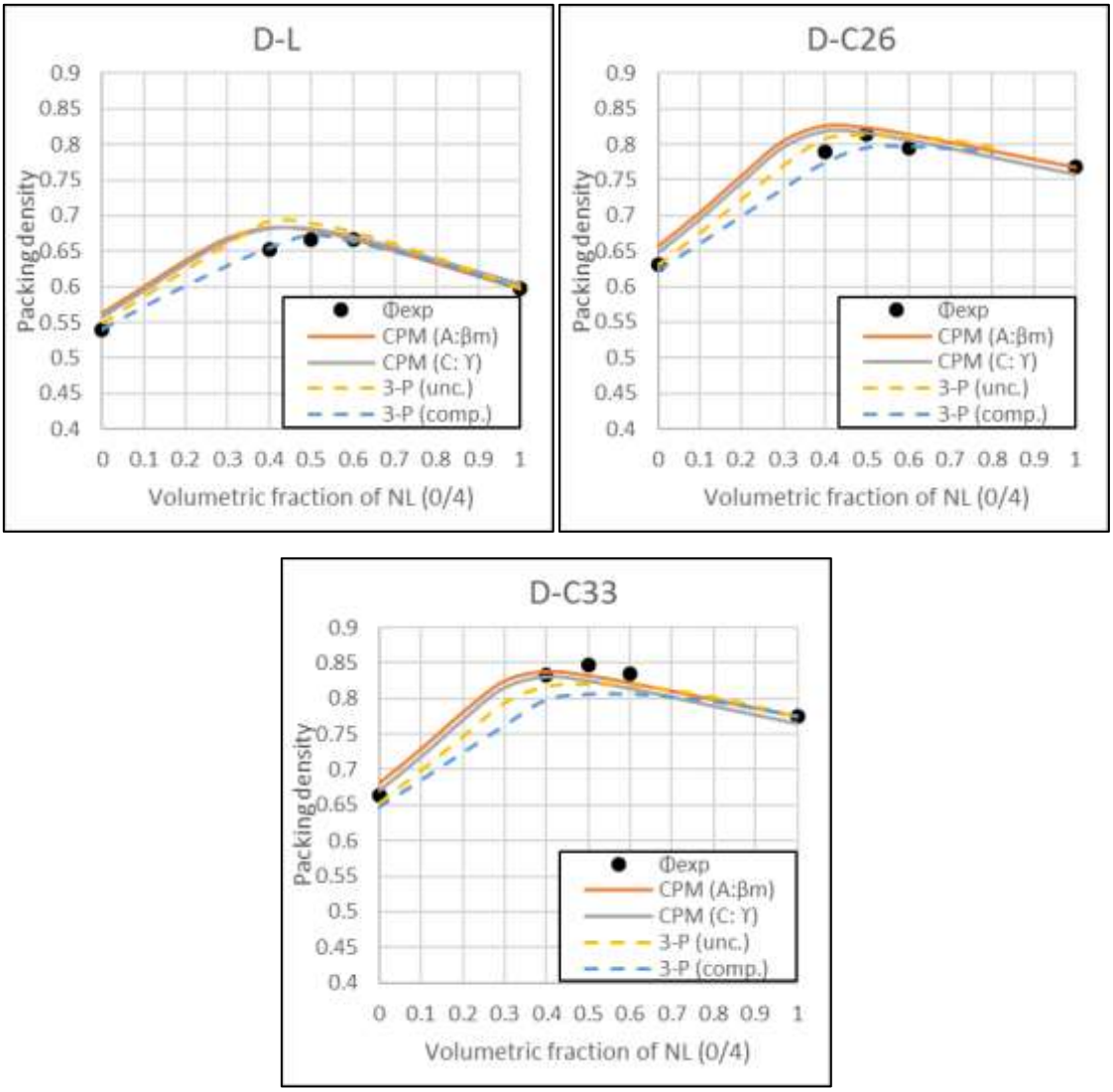

Fig. 4.40. PD of ternary mixtures (0.5NC:0.5NM):NF.

The accuracy of the CPM model for binary mixtures of NL aggregates when the D-L, D-C26 and D-C33 compaction methods were applied, (maximum error lower than 5% and mean error lower than 2%) was good and was even more accurate for D-C26 and D-C33. However, maximum errors higher than 5% were noted for ternary mixtures.

In contrast, the 3-P model showed maximum errors of less than 4% in the worst case and mean errors of -1.5% for the binary mixture with NL. Furthermore, when the interaction parameters for compacted angular aggregates were applied to ternary

mixtures, maximum errors lower than 5.8% (and lower than 5% for most of the mixtures and compaction methods) and mean errors lower than 3.1% were found.

These deviations were compared with the errors noted in other works: 2.5% for CPM when narrow size distributions were tested and errors verging on 5.9% (Kwan *et al.* 2015) when the 3-P model was applied to binary mixtures of angular aggregates with narrow size distributions. It can therefore be said that the 3-P model is suitable for predicting the PD of NL aggregates, regardless of the compaction method applied for a wide size distribution and taking into account the mean diameter of each fraction, as considered in this thesis. However, the interaction parameters and the compaction index should be studied further for the CPM when the model is applied to aggregate fractions with wider distribution sizes.

In a second approach, CPM and the 3-P model were applied to predict the aggregate proportion with the highest PD. This proportion was obtained following the mixing order described in 4.2.1. First, the content of coarse and medium aggregates that presented the densest packing were determined and then different fine-aggregate fractions were added. The results are shown in Table 4.31. Four scenarios were considered according to the methods used to obtain the PD of each aggregate fraction (D-L, D-C, D-C26 and D-C33).

Although an optimal aggregate proportion is only shown in the table, it should be noted that a wide range of aggregate combinations were close to the maximum PD for mixtures of 3 or more granular fractions (even, gap-graded mixes with low particle-size ratios can provide higher-packing values than continuous mixtures). However, the densest compaction is not the only requirement for concrete applications and other aspects such as segregation potential should also be considered.

Although there are different natural aggregate proportions listed in Table 4.31 for the CPM, all the predictions for mixtures ((0.6NC:0.4NM):0.5NF, (0.6NC:0.4NM):0.4NF, (0.5NC:0.5NM):0.4NF and (0.5NC:0.5NM):0.5NF) suggest that they may be considered mixes with the highest PD, regardless of the compaction method in use, as the deviations between the absolute PD value when the four mixes were introduced in the model were lower than 0.005.

Table 4.31. Optimal granular proportion of NL aggregates according to discrete models.

Model	D-L				D-C			
	Volumetric proportion			PD	Volumetric proportion			PD
	NL (0/4)	NL (4/11)	NL (11/22)		NL (0/4)	NL (4/11)	NL (11/22)	
CPM A: β_m	0.4	0.3	0.3	0.683	0.5	0.25	0.25	0.760
CPM C: γ	0.4	0.3	0.3	0.683	0.5	0.25	0.25	0.757
3-P (unc.)	0.4	0.3	0.3	0.692	0.5	0.25	0.25	0.768
3-P (comp.)	0.5	0.25	0.25	0.673	0.5	0.25	0.25	0.751

Model	D-C26				D-C33			
	Volumetric proportion			PD	Volumetric proportion			PD
	NL (0/4)	NL (4/11)	NL (11/22)		NL (0/4)	NL (4/11)	NL (11/22)	
CPM A: β_m	0.4	0.24	0.36	0.826	0.4	0.24	0.36	0.839
CPMC: γ	0.4	0.24	0.36	0.819	0.4	0.24	0.36	0.831
3-P (unc.)	0.5	0.25	0.25	0.812	0.5	0.25	0.25	0.821
3-P (comp.)	0.5	0.25	0.25	0.796	0.5	0.25	0.25	0.806

The optimal proportion predicted by the 3-P model was consistent for all the compaction methods. As with the CPM model, the optimal value was not totally clear, as deviations lower than 0.005 were found for some aggregate proportions close to the maximum predicted PD; for example, with 0.6 or 0.4 of fine aggregate instead of 0.5.

4.4.2 Electric arc furnace (EAF) aggregates

Determination of the optimum aggregate mix design with ideal distribution curves

In the same way as with the NL aggregates, the first approach was to determine the proportion and the combination of each fraction of EAF aggregates (EAF(0/5); EAF (4/11) and EAF (11/22)) with the Fuller and the Funk and Dinger methods (see Fig. 4.41). The curve fitting was also performed with the (0/2) fraction of NL, to supply the lack of fines below 2mm in EAF fractions.

The cement fraction was also considered in Fig. 4.42.

The results of the optimal proportions are summarised in Table 4.32. Comparing both methods for aggregates proportion, the main difference was found in the slightly higher proportion of the fine aggregate when the Funk & Dinger curve was employed. Other differences were the fine EAF and fine NL proportions, which were approximately predicted with the Fuller method for 0.5EF:0.5NF2, while a proportion of 0.65EF:0.35NF2 showed a better fit with the Funk and Dinger (q=0.37) curve. If we contrast those values with the aggregate combinations that presented the maximum experimental PD, we can appreciate the different proportions of coarse and medium aggregate fractions. Thus, while the highest experimental PD values were achieved when the medium fraction was dominant (from 0.4EC:0.6EM), when the fraction was fitted with the ideal curves, a proportion of 0.6EC:0.4EM was predicted. The ideal curves were therefore not in agreement within the experimental results for the EAF aggregates.

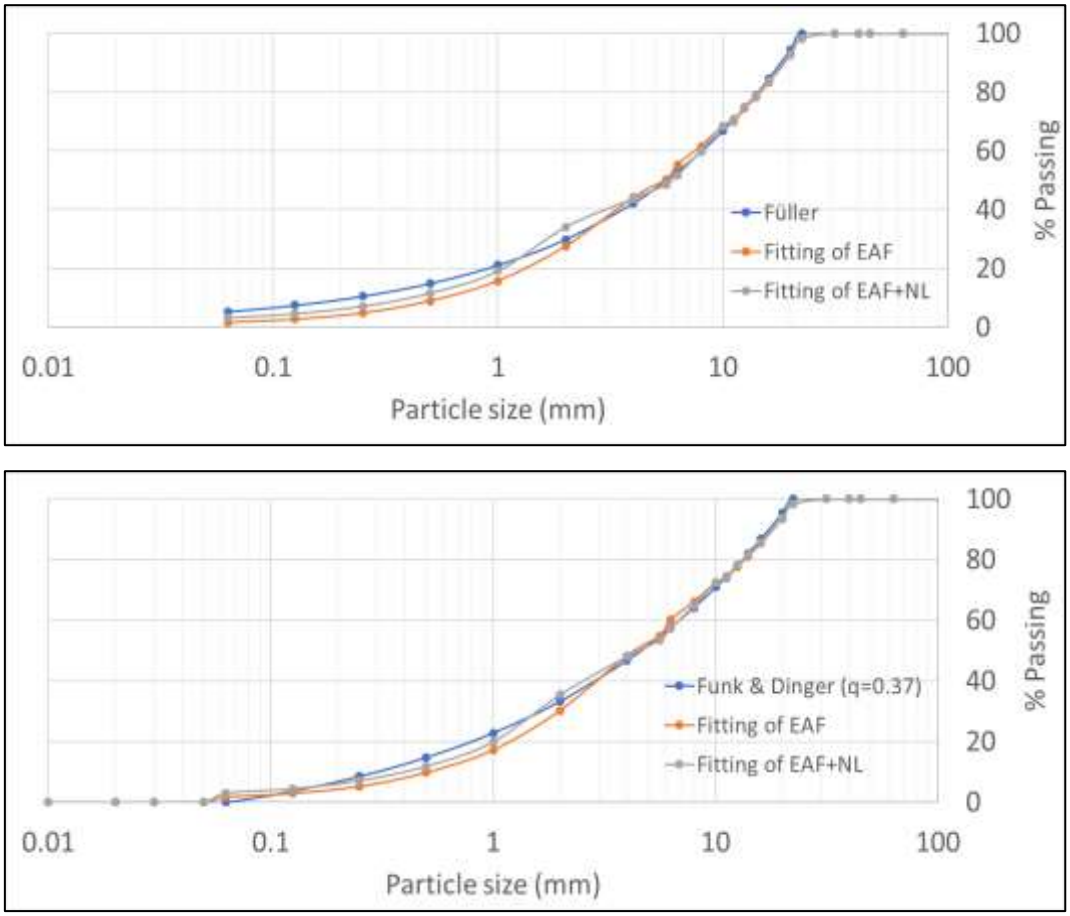

Fig. 4.41. Grading curves of the optimal proportion of EAF aggregates.

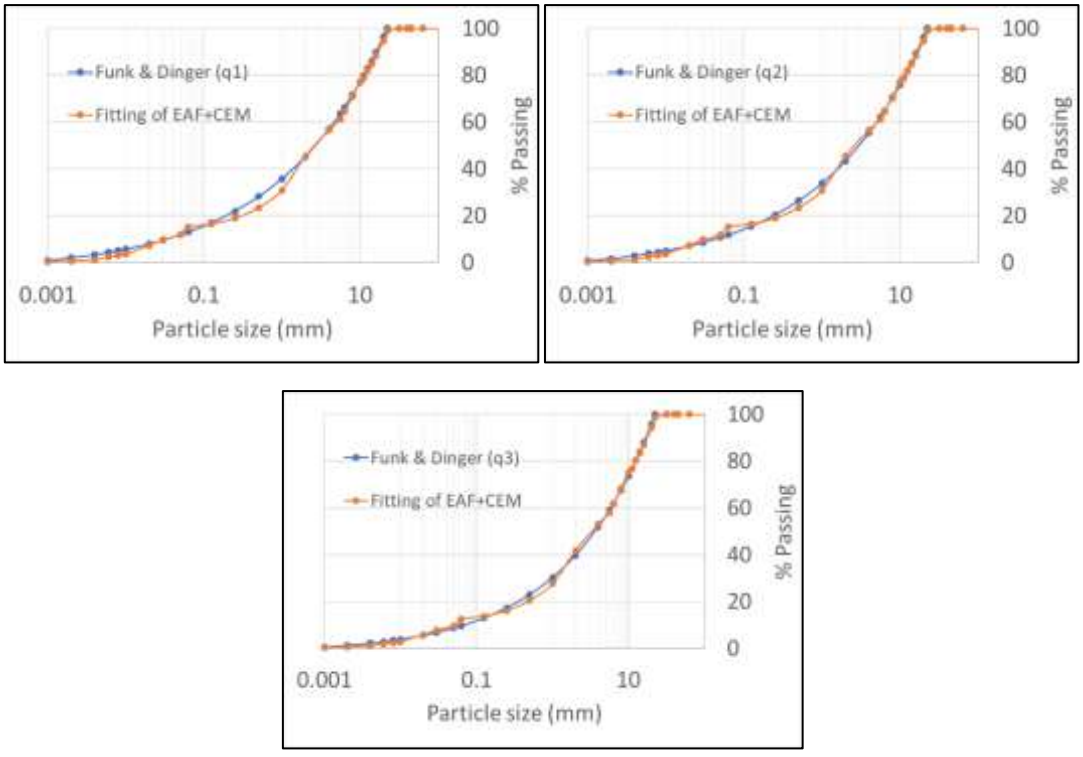

Fig. 4.42. Grading curves of the optimal proportion of EAF aggregates & CEMII.

Table 4.32. Optimal granular proportion of EAF aggregates by their ideal curves.

Method	Volumetric proportion (%)				
	CEM II	NL (0/2)	EAF (0/4)	EAF (4/11)	EAF (11/22)
Fuller	-	-	50%	18%	31%
Fuller	-	22%	24%	24%	30%
Funk and Dinger q= 0.37	-	-	56%	17%	27%
Funk and Dinger q= 0.37	-	17%	35%	22%	26%
Funk and Dinger q_1= 0.31	14%	19%	29%	18%	21%
Funk and Dinger q_2= 0.32	12%	18%	30%	29%	22%
Funk and Dinger q_3= 0.37	10%	15%	31%	20%	24%

Determination of the optimum aggregate mix design with the CPM method

Firstly, as detailed in section 4.2.6.2, the virtual PD of each fraction was determined with the three methods proposed above.

As with the natural aggregate, the virtual packing densities of the fine NL fractions (0/2) and the EAF (0/5) and the medium EAF fraction (4/11) (when the highest energy methods were applied) were lower than the actual PD (see Table 4.33). Therefore, the virtual PD method, β, was not considered for further PD prediction in relation to the different aggregate mixes, in view of its poor fit with the actual PD (see annex).

Table 4.33. Virtual PD of each aggregate fraction (EAF).

	Packing method D-L				Packing method D-C			
	Actual PD	Virtual PD (K=4.1)			Actual PD	Virtual PD (K=4.5)		
	Φ	$A:\beta_m$	$B:\beta$	$C:\gamma$	Φ	$A:\beta_m$	$B:\beta$	$C:\gamma$
NL (0/2)	0.597	0.743	0.561	0.744	0.700	0.856	0.664	0.858
EAF (0/5)	0.594	0.739	0.563	0.738	0.637	0.779	0.597	0.775
EAF (4/11)	0.535	0.665	0.592	0.658	0.596	0.728	0.650	0.72
EAF (11/22)	0.482	0.600	0.559	0.593	0.540	0.660	0.617	0.652

	Packing method D-C26				Packing method D-C33			
	Actual PD	Virtual PD (K=9)			Actual PD	Virtual PD (K=9)		
	Φ	$A:\beta_m$	$B:\beta$	$C:\gamma$	Φ	$A:\beta_m$	$B:\beta$	$C:\gamma$
NL (0/2)	0.740	0.822	0.616	0.806	0.740	0.822	0.616	0.806
EAF (0/5)	0.716	0.796	0.602	0.781	0.742	0.824	0.629	0.809
EAF (4/11)	0.628	0.698	0.617	0.685	0.654	0.727	0.644	0.714
EAF (11/22)	0.547	0.608	0.564	0.599	0.582	0.647	0.602	0.637

In the following figures (Fig. 4.43, Fig. 4.44, Fig. 4.45, Fig. 4.46 and Fig. 4.47), the PD predicted by the two models (CPM and 3-parameter packing model (3-P)) was contrasted with the actual PD of the binary, ternary, and quaternary mixtures under

analysis, to check the applicability of these models to the EAF aggregates. The PD values and the deviations with respect to the experimental results are included in the annex. In the same way as for the NL aggregates, these values were contrasted with the deviations of both models between the theoretical and the actual values found by other authors, to evaluate their advantages.

As can be seen in Fig. 4.43, the experimental PD of the binary mixes showed an uncharacteristic behaviour when compared with both models. Firstly, the PD of the mixes increased when medium aggregate size was added, however when the volumetric fraction exceeded 0.4, then the PD tended to fall, only to rise again when the medium fraction was clearly dominant (higher than 0.7). This trend possibly occurs due to surface roughness and the cavernous morphology of these aggregates that will directly influence the interaction between the particles. It might therefore be thought that the rougher and the more angular the structure, the greater the difficultly for the aggregates to reach maximum packing, as particle interactions will be greater.

The interaction parameters considered in CPM model (when coarse and fine aggregates are dominant) appear to be valid for coarse and medium fractions of EAF mixtures, as there are low deviations between the actual and the predicted PD (see Fig. 4.43). However, the CPM model overestimated the PD whenever one fraction was not clearly dominant.

On the other hand, the 3-P model generated better fits for the intermediate mixes (mean errors and deviation lower than 1.5%), especially when the D-C26 and the D-C33 compaction methods were applied. Whenever a fraction was dominant, the values predicted by the model were also in agreement with the actual PD. However, compaction methods D-C26 and D-C33 yielded a slightly higher maximum error than 5%.

In terms of maximum PD, the proportion of the mix depended on the model and the compaction method in use. A proportion of around 0.4-0.5 (depending on the compaction model) of medium aggregate was needed for the CPM model to reach the maximum, while mixtures with contents above an EAF (4/11) fraction of 60% were needed to approach the maximum PD with the 3-P model. In fact, it can be observed that the medium fraction alone presented higher packing values than when it was mixed. The 3-P model predicted the maximum PD that closely agreed with the aggregate proportions for the maximum PD in the experimental tests (see Table 4.9).

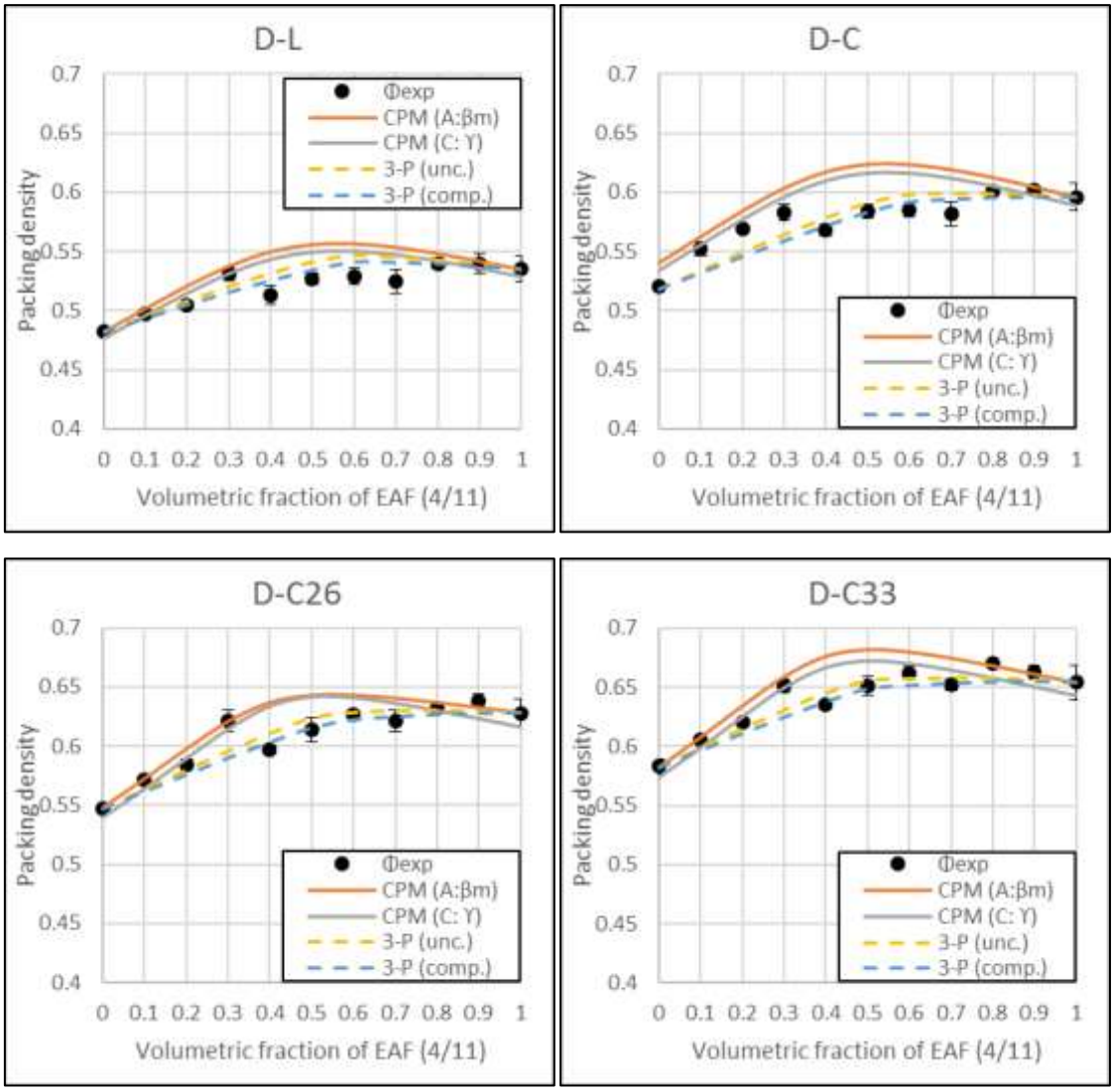

Fig. 4.43. PD of binary mixtures EC:EM.

For ternary mixtures of EAF, as can be seen in both Fig. 4.44 and Fig. 4.45, the values predicted with the CPM model hardly fitted the experimental PD values at all, except for some compaction methods (D-C and D-C33) when the fine fraction was dominant. The higher accuracy in this area, can be explained by the fact that the actual PD of the fine fraction was directly used as an input in the model, however the PD values -both for 0.2EC:0.8EM and for 0.4EC:0.6EM- were predicted from the actual PD of each fraction. Prediction deviations in relation to the actual values of binary mixtures were therefore reflected in the deviations of the following mixtures.

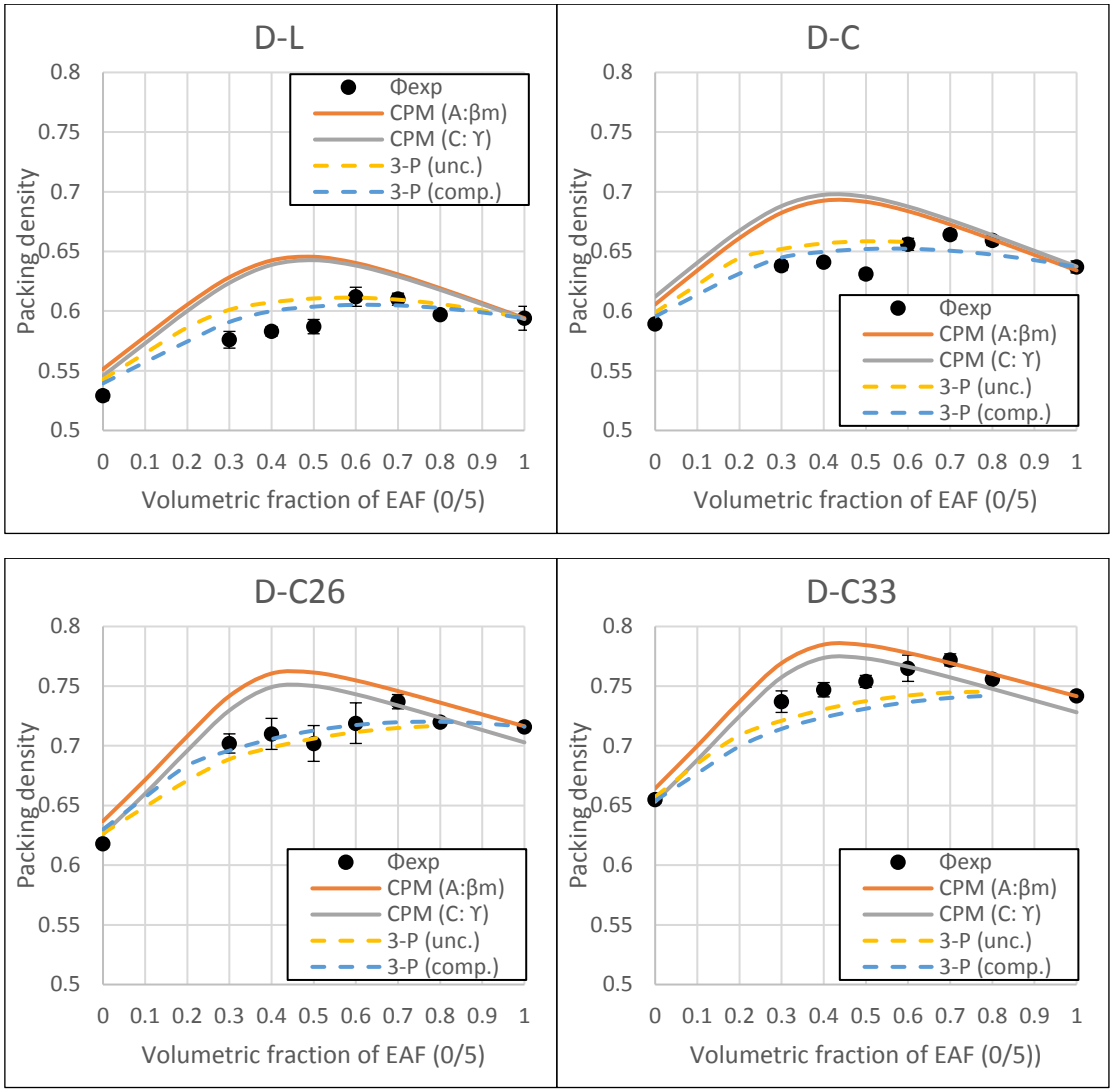

Fig. 4.44. PD of ternary mixtures (0.2EC:0.8EM):EF

In contrast, the 3-P model clearly showed a better fit with the actual PD in the two ternary mixtures of EAF (maximum error lower than 5% and mean error lower than 2%). The largest deviations were found for mixture (0.2EC:0.8EM):EF when the D-C33 packing method was used.

A similar behaviour to the binary mixes was observed in terms of maximum PD. While a proportion of ±0.4-0.5 (depending on the compaction model) of fine aggregate was needed for the CPM model to predict the maximum PD, EAF fractions of over 60% (0/5) were needed to approach the maximum PD. In fact, it can be observed that the maximum values were close to the fine fraction. The maximum experimental PD (Table 4.22 and Table 4.23) was very close to the theoretical maximum PD resulting from the 3-P model that agreed closely with the aggregate proportion.

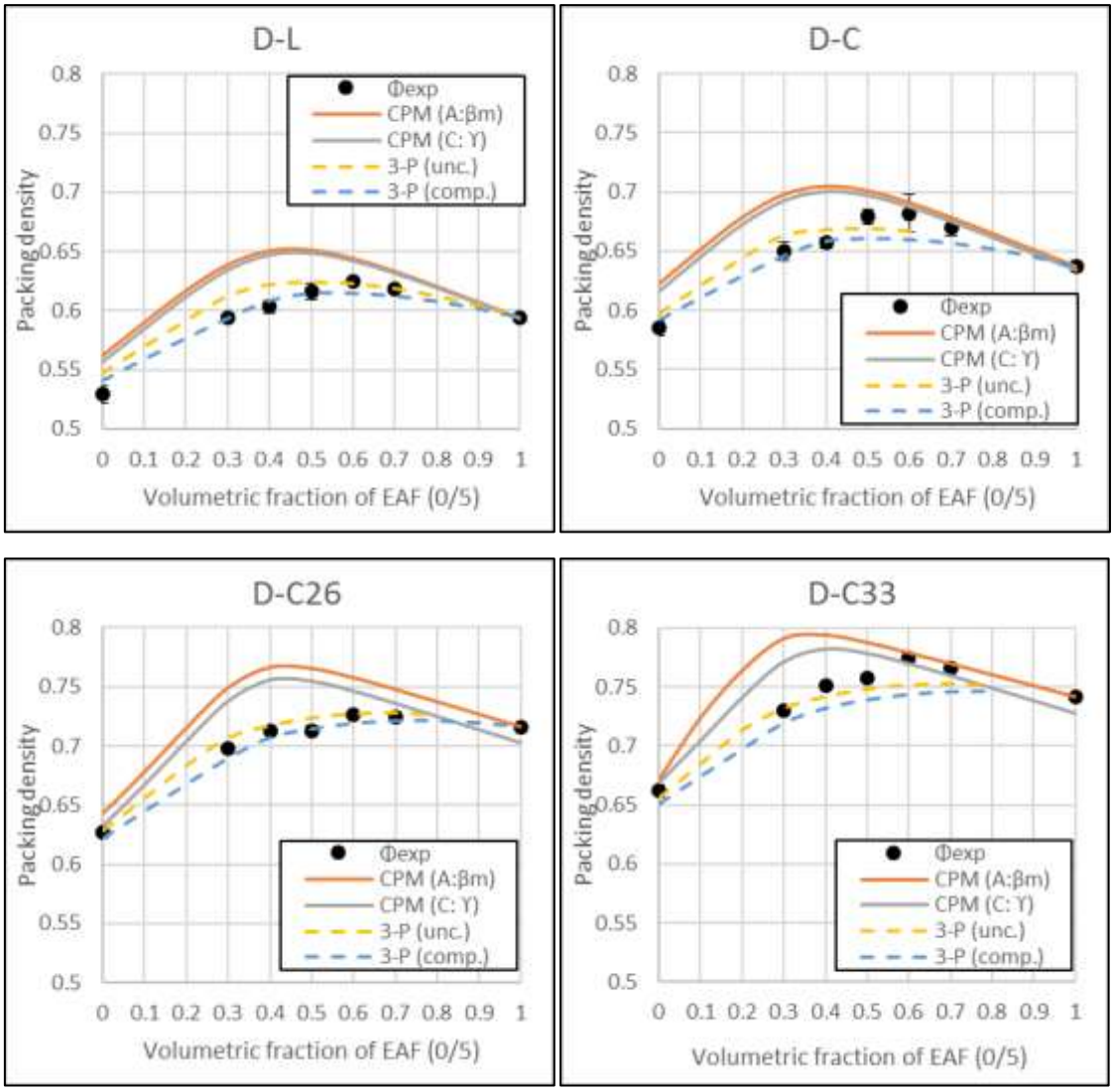

Fig. 4.45. PD of ternary mixtures (0.4EC:0.6EM):EF.

Finally, two quaternary mixtures of EAF aggregates mixed with the NL (0/2) fraction were compared with both theoretical models. As can be seen in Fig. 4.46 and Fig. 4.47, the CPM model significantly overestimated the PD of mixtures with additions of natural fine fractions, and the discrepancies between the experimental and the theoretical PD were especially large. In contrast, the PD was underestimated by the 3-P model, although it showed better fits with the actual PD. These observations may be explained by the 3-P model that accounts for the wedding effect between particles or the reduction of the PD when complete layers of fine particles cannot be formed, because some gaps between coarse particles are too narrow and when fine particles are entrapped at the gaps between the coarse aggregates. The inclusion of this interparticle effect explains the greater accuracy of the predictions of the 3-P model when predicting the PD of the EAF aggregates.

According to the CPM model, the maximum PD was reached after the addition of ±50% fine aggregate to the initial mixture. However, when the 3-P model was applied, the

maximum PD was obtained after the addition of ±50% fine aggregate to the initial mixture for the D-L and the D-C compaction methods and the addition of ±40% for the D-C26 and the D-C33 compaction methods.

In terms of model accuracy, the packing densities predicted by the CPM for the binary mixtures of EAF showed a maximum deviation from the experimental values of 6.2%. In addition, this error slightly increased when ternary and quaternary mixtures were assessed, as the model overestimated the experimental values.

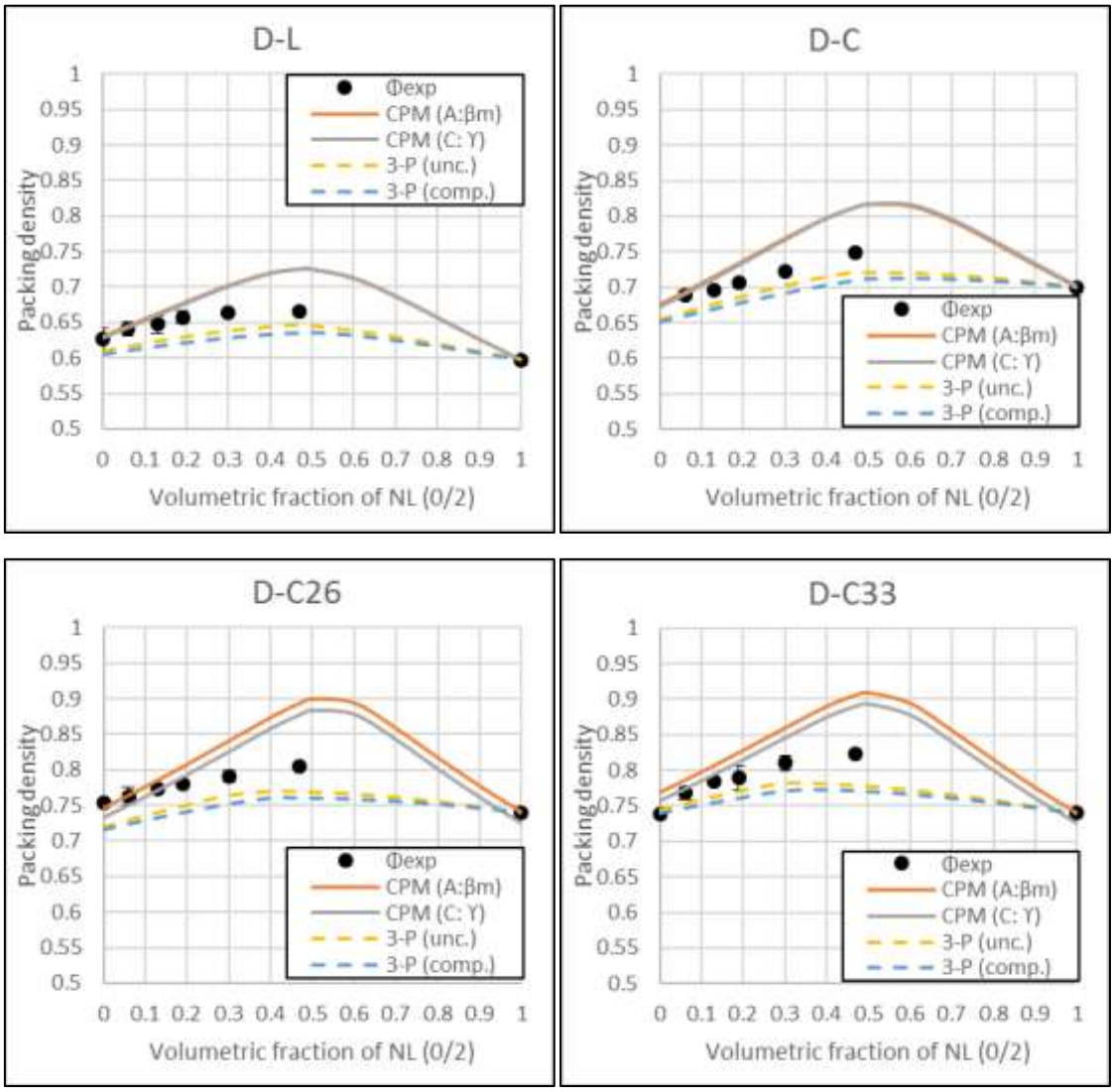

Fig. 4.46. PD of quaternary mixtures ((0.2EC:0.8EM):0.7EF):NF2

In contrast, better agreement was found for the 3-P model. The predicted values presented maximum errors of 5.3% in the worst case and mean errors below 1.4% for the binary mixture of EAF. In addition, maximum errors of 4.3% and mean errors lower than 2.1% can be found for ternary mixtures of EAF. For quaternary mixtures, although the maximum error was 5.8% when the uncompacted parameter for angular aggregate was applied, the accuracy of the 3-P model was lower, and the PD was underestimated.

Neither method has been used to design EAF aggregate mixtures. If the experimental results are compared to the error found by the other above-mentioned authors, it can be said that the 3-P model is suitable for predicting the PD of EAF aggregates, regardless of the compaction method applied for a wide size distribution and taking into account the mean diameter of each fraction that is considered for this thesis. However, the interaction parameters and the compaction index of the CPM should be investigated, to extend its usability to aggregate fractions with wider distribution sizes and alternative aggregates such as EAF.

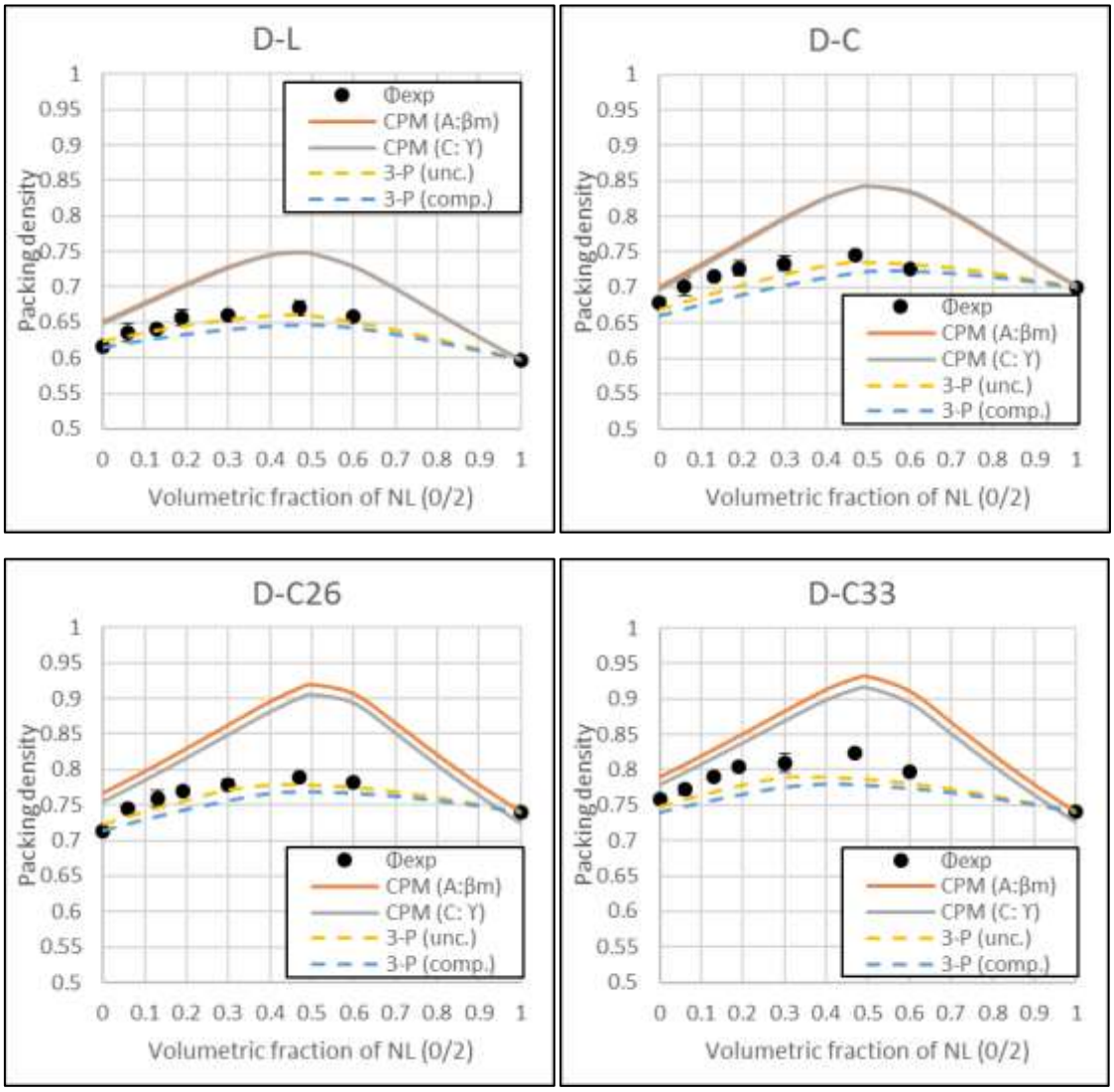

Fig. 4.47. PD of quaternary mixtures ((0.4EC:0.6EM):0.5EF):NF2

In a second approach, both the CPM and the 3-P model were applied to predict the aggregate proportion with the highest PD, as previously shown for the NL aggregates. The results are shown in Table 4.34.

According to the CPM, the maximum PD was obtained for the ((0.5EC:0.5EM):0.4EF):0.5NF2 mixture regardless of the compaction method. However, the absolute value of the PD was very close (less than -0.001 unit) for two binary mixtures (0.5EC:0.5EM and 0.4EC:0.6EM) under all the scenarios and the same may be said of the NL aggregates. There were therefore several aggregate proportions that were very close to the experimental maximum PD.

The optimal proportions predicted by both models for the EAF aggregates were very different. The mixtures predicted by the 3-P model as optimal had a low content of coarse aggregate (EAF (11/22)) and proportions higher than 0.7 by volume of fine aggregates (NL (0/2) + EAF (0/5)). However, the binary mixtures of EC:EM had a threshold point (±0.6 by volume of medium fraction), after which the difference in the PD was practically negligible (deviation ±0.003), although the maximum was obtained after larger additions of the medium fraction. Therefore, if the threshold value is considered as the optimal value for enhancing the concrete properties (as the coarse aggregate adds strength to hardened concrete making it an important factor), then the highest aggregate proportion predicted by the 3-P model will range between 0.5EC:0.5EM and 0.4EC:0.6EM for binary mixtures with additions ranging between 0.5 and 0.6 of EF and approximately 0.4 of NF.

Table 4.34. Optimal granular proportion of EAF aggregates according to discrete models.

Model	D-L					D-C				
	Volumetric proportion				PD	Volumetric proportion				PD
	NL (0/2)	EAF (0/5)	EAF (4/11)	EAF (11/22)		NL (0/2)	EAF (0/5)	EAF (4/11)	EAF (11/22)	
CPM $A:\beta_m$	0.4	0.24	0.18	0.18	0.755	0.5	0.2	0.15	0.15	0.85
CPM $C:\gamma$	0.5	0.2	0.15	0.15	0.753	0.5	0.2	0.15	0.15	0.839
3-P (unc.)	0.4	0.3	0.18	0.12	0.66	0.5	0.25	0.175	0.075	0.734
3-P (comp.)	0.5	0.25	0.15	0.1	0.647	0.6	0.24	0.144	0.016	0.716
Model	**D-C26**					**D-C33**				
	Volumetric proportion				PD	Volumetric proportion				PD
	NL (0/2)	EAF (0/5)	EAF (4/11)	EAF (11/22)		NL (0/2)	EAF (0/5)	EAF (4/11)	EAF (11/22)	
CPM $A:\beta_m$	0.5	0.2	0.15	0.15	0.925	0.5	0.2	0.15	0.15	0.937
CPM $C:\gamma$	0.5	0.2	0.15	0.15	0.914	0.5	0.2	0.15	0.15	0.922
3-P (unc.)	0.4	0.42	0.126	0.054	0.76	0.3	0.49	0.147	0.063	0.782
3-P (comp.)	0.4	0.48	0.096	0.024	0.758	0.4	0.36	0.192	0.048	0.775

4.5 Conclusions

The packing densities of both EAF and NL aggregate have shown differences even though they have similar grain size distributions and have followed the same compaction

process. The EAFS (4/11) presented higher PD than NL (4/11) and the EAFS (11/22) presented lower PD than NL (11/22). These differences were probably associated with surface texture and aggregate shape, which in turn simply depended on whether the fractions were either crushed, or crushed and screened. However, further research is still needed to confirm the physical factors that can affect the PD.

NL and EAF aggregates are more sensitive to the compaction method than the rounded aggregate, as observed from the PD values of the different aggregate morphologies and granular size distribution.

Comparing the compactness (F) of the coarse and the medium fractions of NL and EAF, it can be observed that both fractions are equally sensitive, despite morphological differences. In addition, the fine fractions are also more sensitive to the packing method, due to the agglomeration effect produced by the interparticle forces of the finer particles that can only be resolved by applying high levels of compaction energy.

It can be also seen for cement packing, since wet methods are needed to measure the PD, overlooking the Van der Waals forces. It is therefore important to consider the compaction methods, because aggregate with different particle shapes and granular size distributions will show different behaviours under the same compaction process.

The PD test performed on rounded aggregate mixtures showed similar or even lower packing values when the energy of the compaction process was increased (D-C26 to D-C33 method). These values have been explained in two ways: on the one hand, because the maximum packing for rounded aggregates was obtained at low compaction energies, due to their spherical, smooth surfaces that facilitate compaction; and, on the other hand, because the segregation effect at this vibration frequency occurred when the aggregate size ratio was lower than 0.20. The PD of the NL and EAF aggregate mixtures increased when higher compaction energy was applied.

The binary mixes of coarse and medium aggregate fractions needed a higher volumetric proportion of EAF (4/11) than the NL mixtures to reach the aggregate proportion with the highest PD, due to the high PD of the EAF (4/11). In addition, although the size ratios of both mixtures were similar, the PD of the coarse fraction of EAF can be increased up to 17% in comparison with the 11% that can be achieved with the NL aggregates, due to the higher PD of the EAF (4/11).

In the case of the ternary mixtures of coarse, medium and fine fractions, the PD values achieved with the NL aggregates were notably higher than those obtained with the EAF mixtures (maximum close to 0.84 for NL mixtures compared to 0.77 for EAF mixtures at D-C33), as the EAF (0/5) fraction has a lower content of fine particles (higher size ratio). Therefore, the NL (0/2) fraction is needed to obtain mixtures with a PD close to 0.84.

The mixtures of NL and EAF showed slightly different PD values when coarse and medium aggregate fractions were varied within the range previously under

consideration. Therefore, both the coarse and the medium aggregate fractions can be combined within a range of values without affecting the maximum PD. However, it was also observed that a lower fine content was required for mixtures with a higher content of coarse aggregate. In addition, the maximum PD with the wet-packing methods required a reduced fine content in comparison with the dry methods. This lower fine content may be taken into account in concrete mix design, as mixtures with high fines content require more water to achieve the required workability and therefore the hardening properties can be detrimental, if the amount of cement is not increased to maintain an adequate W/C ratio.

In the determination of the optimal aggregate mix design by means of ideal distribution curves, the predicted aggregate mix was within the range of experimental results with the highest PD. However, ideal curves are not in accordance with the experimental results for the EAF aggregates, as a higher volumetric fraction of the medium fraction (EAF (4/11)) was required to reach the maximum experimental PD (0.4EC:0.6EM vs 0.6EC:0.4EM). Therefore, other methods should be used for EAF that consider the PD and, therefore, the shape of each aggregate fraction, to achieve optimal aggregate packing.

Although, the suitability of CPM and the 3-P model for predicting aggregate mix PD has only been tested in the literature for fractions with narrow particle-size distributions, the model in this thesis has been applied to the commercial aggregate fraction with wider particle-size distributions. In addition, the extended 3-P model for multicomponent mixtures that had only been tested before in ternary mixtures for spherical particles, was also applied for limestone crushed aggregates and EAF aggregates. In view of the results, both the CPM model and the 3-P model produced accurate predictions of the packing densities for binary mixes of NL and EAF. However, the 3-P model showed higher accuracy for the ternary and the quaternary mixtures, regardless of the compaction method applied to determine the PD of each individual fraction (D-L, D-C, D-26 and D-33).

4.6 References

Bala, M., Zentar, R. and Boustingorry, P. (2019) 'Parameter determination of the Compressible Packing Model (CPM) for concrete application', *Pwder Technology*. Elsevier B.V, p. 107941. doi: 10.1016/j.meatsci.2019.107941.

BS-812 (1975) 'Determination of the Angularity Number of the given Aggregate Sample'.

Cai, W. (2017) *Effect of Particle Packing on Flow Property and Strength of Concrete Mortar*, *Iowa State University Capstones, Theses and Dissertations*. Available at: https://lib.dr.iastate.edu/etd/15271.

Fennis, S. A. A. M. (2009) *Design of Ecological Concrete by Particle Packing Optimization*.

Delf University of Tecnhology.

Fuller, W. B. and Thompson, S. E. (1907) 'The laws of proportioning concrete', *ASCE J.Transport*, 59, pp. 67–143.

Funk, J. E., Dinger, D. R. and Funk, J. E. J. (1980) 'Caol Grinding and Particle Size Distribution Studies for Coal-Water Slurries at High Solids Content', *Final Report, Empire State Electric Energy Research Corporation (ESEERCO)*. New York.

Ghasemi, Y. (2017) *Aggregates in Concrete Mix Design*. Luleå University of Technology.

Kwan, A. K. H., Chan, K. W. and Wong, V. (2013) 'A 3-parameter particle packing model incorporating the wedging effect', *Powder Technology*. Elsevier B.V., 237, pp. 172–179. doi: 10.1016/j.powtec.2013.01.043.

Kwan, A. K. H. and Li, L. G. (2012) 'Combined effects of water film thickness and paste film thickness on rheology of mortar', *Materials and Structures*, 45(9), pp. 1359–1374. doi: 10.1617/s11527-012-9837-y.

Kwan, A. K. H., Wong, V. and Fung, W. W. S. (2015) 'A 3-parameter packing density model for angular rock aggregate particles', *Powder Technology*. Elsevier B.V., 274, pp. 154–162. doi: 10.1016/j.powtec.2014.12.054.

de Larrard, F. (1999) *Concrete Mixture Proportioning*. E & FN SPON.

Lecomte, A. (2006) 'The measurement of real and virtual packing density of soft grains', *Materials and Structures/Materiaux et Constructions*, 39(285), pp. 63–80. doi: 10.1617/s11527-005-9029-0.

Li, L. G. and Kwan, A. K. H. (2014) 'Packing density of concrete mix under dry and wet conditions', *Powder Technology*, 253, pp. 514–521. doi: 10.1016/j.powtec.2013.12.020.

Li, L. G., Lin, C. J., Chen, G. M., Kwan, A. K. H. and Jiang, T. (2017) 'Effects of packing on compressive behaviour of recycled aggregate concrete', *Construction and Building Materials*, 157(December), pp. 757–777. doi: 10.1016/j.conbuildmat.2017.09.097.

Mangulkar, M. N. and Jamkar, S. S. (2013) 'Review of Particle Packing Theories Used For Concrete Mix Proportioning', 4(5), pp. 143–148.

Manso, J., Hernández, D., Losanez, M. and Gonzalez, J. (2011) 'Design and Elaboration of Concrete Mixes Using Steelmaking Slags', *ACI Materials Journal*, 108, p. 673.

Martín-Morales, M., Sánchez-Roldán, Z., Zamorano, M. and Valverde-Palacios, I. (2013) 'Métodos granulométricos en la caracterización del árido reciclado para su uso en hormigón estructural', *Materiales de Construcción*, 63(310), pp. 235–249. doi: 10.3989/mc.2013.mc.06511.

Moutassem, F. (2016) 'Assessment of Packing Density Models and Optimizing Concrete Mixtures', *International Journal of Civil, Mechanical and Energy Science (IJCMES)*, 2(4), pp. 2455–5304. Available at: www.ijcmes.com.

Pradhan, S., Kumar, S. and Barai, S. V (2017) 'Recycled aggregate concrete: Particle Packing Method (PPM) of mix design approach', *Construction and Building Materials*. Elsevier Ltd, 152, pp. 269–284. doi: 10.1016/j.conbuildmat.2017.06.171.

Rached, M., Fowler, D. and Kpehler, E. (2010) 'Use of aggregates to reduce cement

content in concrete', *2nd International Conference on Sustainable Construction Materials and Technologies*, pp. 179–189.

Roquier, G. (2016) 'The 4-parameter Compressible Packing Model (CPM) for sustainable concrete', in *Stratergies for Sustainable Concrete Structures (SSCS2015)*. Available at: https://hal.archives-ouvertes.fr/hal-01279904v2.

Shekarchi, M., Libre, N. A. and Mousavi, S. M. (2010) 'Verification of wet and dry packing methods with experimental data', in *Proceedings of FraMCoS-7*, pp. 1322–1327.

Thomas, C., Rosales, J., Polanco, J. A. and Agrela, F. (2019) *7. Steel slags*, *New Trends in Eco-efficient and Recycled Concrete*. Elsevier Ltd. doi: 10.1016/B978-0-08-102480-5.00007-5.

UNE-EN 1097-3 (1999) 'Ensayos para determinar las propiedades mecánicas y físicas de los áridos. Parte 3: Determinación de la densidad aparente y la porosidad.'

UNE-EN 1097-6 (2014) 'Ensayos para determinar las propiedades mecánicas y físicas de los áridos. Parte 6: Determinación de la densidad de partículas y la absorción de agua'.

UNE-EN 13043 (2003) 'Áridos para mezclas bituminosas y tratamientos superficiales de carreteras, aeropuertos y otras zonas pavimentadas'.

UNE-EN 196-6 (2019) 'Métodos de ensayo de cementos Parte 6: Determinación de la finura'.

UNE-EN 933-1 (2012) 'Ensayos para determinar las propiedades geométricas de los áridos Parte 1: Determinación de la granulometría de las partículas.'

UNE 80103 (2013) 'Métodos de ensayo de cmentos. Ensayos Físicos. Determinación de la densidad real'.

Wong, H. H. C. and Kwan, A. K. H. (2008) 'Packing density of cementitious materials: Part 1-measurement using a wet packing method', *Materials and Structures/Materiaux et Constructions*, 41(4), pp. 689–701. doi: 10.1617/s11527-007-9274-5.

Wong, V. (2015) *A 3-Parameter particle packing model for spherical and non-spherical particles*. The University of Hong Kong.

Yepes, V. (2014) 'Equipos de compactación superficial'. Valencia: Apuntes de la Universitat Politècnica de València, Ref. 187. Available at: https://victoryepes.blogs.upv.es/tag/compactabilidad/.

Yousuf, S., Sanchez, L. F. M. and Shammeh, S. A. (2019) 'The use of particle packing models (PPMs) to design structural low cement concrete as an alternative for construction industry', *Journal of Building Engineering*. Elsevier Ltd, 25(October 2018), p. 100815. doi: 10.1016/j.jobe.2019.100815.

Yu, A. B., Bridgwater, J. and Burbidge, A. (1997) 'On the modelling of the packing of fine particles', *Powder Technology*, 92(3), pp. 185–194. doi: 10.1016/S0032-5910(97)03219-1.

5

Concrete mix design through granular compacity

CONTENT

5 Concrete mix design through granular compacity 187

5.1 Introduction 187

5.2 Methodology and materials 188

5.2.1 Overall methodological approach 188

5.2.2 Materials 190

5.2.3 Determination of aggregate specific surface area 190

5.2.4 Cement-paste characterization 191

5.2.5 Concrete mix design and characterization techniques 192

5.3 Determination of cement-paste content 198

5.4 Effect of packing density on cement-paste compressive strength and workability 201

5.5 Compressive strength and dry aggregate compacity of NL aggregate concretes 203

5.6 Funk and Dinger curves for cement-content reduction in concrete mix design 210

5.7 Effect of paste content on different aggregate proportions 215

5.8 Conclusions 221

5.9 References 222

5 Concrete mix design

In chapter 5, the results of the experimental investigation on both the fresh and the hardened performance of Natural Limestone (NL) aggregate concrete and Electric Arc Furnace (EAF) aggregate concrete, designed with highly compacted aggregate structures, will be presented. Based on the results of chapter 4, the concrete-mix design through PPMs will be discussed and several concrete mixes will be designed, considering different scenarios, to determine the extent to which the cement may be reduced in compacted concrete mixtures and the effect of reduced amounts of cement on concrete workability and compressive strength.

5.1 Introduction

Concrete mix design using Particle Packing Methods (PPMs) minimizes voids within the aggregates and reduces the binder content of the concrete, which enhances both its hardened-state properties and its durability, as well as its environmental and economic impacts. However, the placeability of concrete is also determined by its workability. A highly compacted aggregate skeleton will probably result in a less workable mix that is difficult to pour and to shape for a given volume of cement paste and W/C ratio, limiting its application to highly compacted concretes such as roller-compacted concrete and certain precast concretes.

As previously mentioned in chapter 2, recent research has proposed different approaches to concrete mix design through PPMs. They range from methods based on the particle packing of aggregate or the entire solid content (including the cement) and adding an excess of cement paste or water, to enhance concrete workability, to approaches that combine the Packing Density (PD) of solid components with thickness layer theories, to find the factors that may affect the rheology of the cementitious compounds, so as to optimize the cementitious mix. Most of these approaches will be discussed below.

As the effect of aggregate PD on compressive strength and workability is not totally clear, especially for concrete designed with recovered material aggregates with such a peculiar morphology as EAF, several concrete formulations with a range of high aggregate packing densities were analysed.

The aim of this chapter will be to design NL and EAF aggregate concretes with reduced amounts of cement using PPMs, without significantly compromising their performance. With that aim in mind, the following partial goals are proposed:

- To analyse the ideal aggregate proportions and their influence on the hardened and fresh properties of NL and EAF aggregate concrete with different amounts of cement paste.
- To verify the applicability of the Funk and Dinger curves to concrete mix design with lower cement content.
- To validate the aggregate proportion with the highest PD predicted by discrete PPMs (CPM and 3-P), to obtain sustainable concrete mix designs.

5.2 Methodology and materials

5.2.1 Overall methodological approach

The methodology used to obtain concrete with a reduced amount of cement was applied to two types of concrete, designed on the basis of the compacted aggregate mix described in chapter 4:

- Concrete made with NL aggregates, using three size fractions: 12/22 mm, 4/12 mm, and 0/4 mm
- Concrete made with EAF aggregates, using four size fractions: 12/22 mm, 4/12 mm, 0/5 mm, and 0/2 mm. In this mixture the first three fractions of EAF aggregates were combined with the 0/2 mm fraction of NL. This fraction is required to adjust the grading curve of the EAF, as recommended by other researchers (Manso et al. 2011; Arribas et al. 2014; San-José et al. 2014; Fuente-Alonso et al. 2017; Santamaría et al. 2020).

First, the different approaches to concrete mix design through PPMs that are available in the literature were discussed and analysed, to gain a better understanding of how the paste content can be determined by the aggregate PD.

Then, the compressive strength and the consistency of the cement pastes with higher packing densities were analysed, to understand the effect of cement PD on both the fresh and the hardened properties.

Finally, 17 concrete mixes (11 with NL aggregates and 6 with EAF aggregates) were manufactured and characterized according to the methodology detailed below (see Table 5.1). The study of these concrete mixes was divided as follow:

- Four NL aggregate concretes were manufactured, each containing the same cement content and W/C ratio, but with different proportions of aggregate and, therefore, each with a different PD in the dry state. The aim was to analyse the effect of PD on compressive strength and workability, by isolating the effect of the cement-paste content.
- Six concrete mixes (three with NL aggregates and three with EAF aggregate) were designed, based on the Funk and Dinger grading curve, by using three different

q parameters, which modify the fines content of the mix, and thereby the cement amount. These tests were conducted for two purposes. On the one hand, to validate the use of this model for reducing the amount of cement in concrete mixtures and, on the other hand, to compare both the in-hard and in-fresh concrete properties with mixes containing similar aggregate proportions, but differing amounts of cement-paste. In addition, the compressive strength and workability of these mixtures will be compared with the properties obtained in concrete with a higher aggregate PD, as the most compacted EAF aggregate proportion showed no correspondence to the proportion predicted by the optimal curves methods (see chapter 4, conclusions). From the six mixes that were designed, only 5 were finally manufactured as one design referred to over 330 kg/m^3 of cement, a long way off the objective of reducing the cement content and designing more sustainable concrete.

- Eight concrete mixes (four with NL aggregates and four with EAF aggregate) were designed with two different aggregate proportions and two volumes of cement paste. On the one hand, the aggregate proportion with the highest experimentally obtained PD was selected and, on the other hand the aggregate proportion predicted by the discrete PPMs (CPM and 3-P) was selected. In addition, both concretes were manufactured with a reduced content of cement paste, 23% Paste Volume (PV) and with a more typical volume paste, 28% (approximately 300 kg of cement per cubic meter of concrete), to compare the effect of cement paste content on the compressive strength and the workability properties of the concrete.

Table 5.1. Manufactured concrete mixes.

Test series	Nº of concrete produced		W/C	Volume of cement paste	Aggregate proportion
	NL	EAF			
1	4	-	0.62	Constant	Variable. Selected from the experimentally obtained range of maximum PD.
2	3	2	0.55	Variable. Cement amount selected by Funk and Dinger curves for different q parameter	Constant
3	4	4	0.55	Variable. Two options: Reduced paste volume: 23% Conventional paste volume[18]: 28%	Variable. Two options: Maximum PD obtained experimentally Maximum obtained through PPMs

[18] Paste volume in line with benchmark concrete 300-320 kg cement per cubic meter of concrete.

5.2.2 Materials

CEM II/A-M (V-L) 42.5 R was used to perform both the cement pastes and the concrete specimens.

The Natural Limestone (NL) aggregate and the Electric Arc Furnace (EAF) aggregate, both characterized in chapter 4, were separately added to the two concrete mixes:

- Concrete made with NL aggregates:
  - NL (12/22)
  - NL (4/12)
  - NL (0/4)
- Concrete made with EAF aggregates:
  - EAF (12/22)
  - EAF (4/12)
  - EAF (0/5)
  - NL (0/2)

The specific surface area of each aggregate fraction was also included in the tests described in this chapter.

5.2.3 Determination of aggregate specific surface area

The Specific Surface Area (SSA) of each aggregate fraction was calculated, in accordance with the method proposed by Ghasemi (Ghasemi, Cwirzen, *et al.* 2018; Ghasemi, Rajczakowska, *et al.* 2018), which assumes uniform shaped particles (by considering the platonic solids geometries), applied to the particle size distribution. Although, the method was tested for fine aggregates and particles, here it was extended to all granular sizes as it is well-know that fine particles are the main responsible of the specific surface area. Therefore, the possible deviation of the coarse aggregate specific surface area will be practically neglected. As Ghasemi proposed, the SSA of the crushed aggregate, calculated on the assumption of a cubic shape, presented good agreement with the X-ray microtomography test. Although the EAF aggregates are expected to have larger SSA than NL, due to their cavernous structure, specific data on their real SSA were not found, so the NL and EAF aggregate shapes were therefore both assumed to be in the form of a geometric cube (see Table 5.2).

Note that if the tetrahedroid shape of the EAF aggregate can be assumed, due to its cavernous surface, then its SSA will be higher (see Table 5.3).

Table 5.2. SSA of each aggregate fraction considered cubic in shape.

Aggregate fraction	SSA (cm^2/g)	SSA (cm^2/cm^3)
NL (12/22)	3.3	8.8
NL (4/12)	35.7	94.2

Aggregate fraction	SSA (cm^2/g)	SSA (cm^2/cm^3)
NL (0/4)	143.7	385.4
EAF (12/22)	2.4	8.4
EAF (4/12)	8.4	29.5
EAF (0/5)	48.3	171.5
NL (0/2)	162.6	435.8

Table 5.3. SSA of EAF aggregate considered tetrahedroid in shape.

Aggregate fraction	SSA (cm^2/g)	SSA (cm^2/cm^3)
EAF (12/22)	4.7	16.4
EAF (4/12)	16.6	58.0
EAF (0/5)	95.1	337.5
NL (0/2)	320	857.6

5.2.4 Cement-paste characterization

Some of the cement pastes were prepared, as detailed in Chapter 4, to analyse the effect of their cement PD on both their fresh and their hardened properties, to determine their maximum PD under wet conditions and for their characterization in terms of their workability and their compressive and flexural strength. For this purpose, six specimens (10x10x60mm) were manufactured for six pastes with W/C ratios close to the maximum PD. The moulds were filled and tamped down with 60 strokes on a compaction table. The specimens were demoulded after 24 hours in the wet chamber and cured in water until the date of testing (7 days).

5.2.4.1 Mixing process

The cement pastes were mixed following the process described in chapter 4 to obtain the maximum packing of the cement.

Fig. 5.1. Cementitious material mixer.

5.2.4.2 Fresh density

The fresh density of each cement paste was measured, as described in chapter 4.

5.2.4.3 Slump test

Standard UNE-EN 1015-3:2000 (UNE-EN 1015-3 2000), used to determine the consistency of mortars on the shaking table, was adapted to determine the consistency of the cement pastes. The cement paste was poured in two layers (each layer was tamped down ten times) into a mould (60 mm in height, internal diameter: base 100 mm - top 70 mm) located at the centre of a circular table. The excess cement paste was removed from the top of the mould with the palette knife. Having removed the mould, the table was jolted 15 times at a rate of one jolt per second. The diameter of the spread of the cement paste was measured with callipers in two directions, at right angles to each other, and both measurements were noted.

Fig. 5.2. Consistency test for cement paste.

5.2.4.4 Compressive strength and flexural strength

Compressive and flexural strength tests were performed with an AUTOTEST 200/10-SW hydraulic press, equipped with a specific clamp for 1×1×6 cm prismatic specimens.

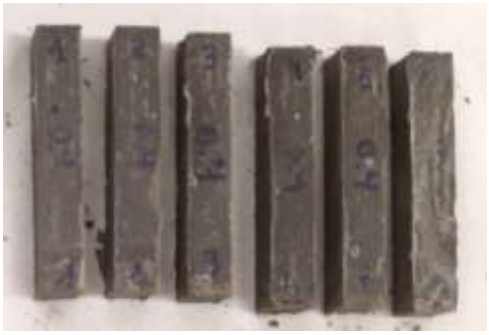

Fig. 5.3. Cement paste specimens.

5.2.5 Concrete mix design and characterization techniques

5.2.5.1 Concrete mix design

All the concretes were designed following the known absolute volume method (see eq. 5.1). Air content was fixed at 2% according to the ACI 211.1 method (ACI 2002) for a maximum aggregate size of 20 mm and the total concrete volume was assumed to be 1 m^3.

No admixtures were used, with the aim of isolating the effect of the aggregate proportion on the hardened and fresh concrete properties. Since chemical admixtures increase the complexity of the particle packing and the flow behaviour of the concrete, they likewise complicate any comparison of the concretes made with different types of admixtures and dosages. As no admixtures were added, the W/C ratio was established between 0.6 and 0.55, within the limits established by the Spanish structural concrete instruction EHE-08 (EHE 2008) for a normal exposure class.

$$1\ m^3 of\ concrete = V_{CA} + V_{MA} + V_{FA} + V_c + V_w + V_{air} \quad 5.1$$

The water content was adjusted by considering the water absorption levels of the aggregates. As is well known, the time that passes from the kneading of the concrete to its compaction in the mould, in the laboratory, is insufficient for the total absorption of water by the aggregates. Consequently, the absorption kinetics of the aggregates were considered by reference to the data in the literature, to add the appropriate amount of water, thereby preventing any unintended rise in the W/C ratio.

Thus, an absorption rate of 70% of total absorption during the first 15 minutes was considered for the NL aggregates (Alhozaimy 2009), while an absorption rate of 80% was considered for the EAF aggregates (Lam *et al.* 2018).

The humidity of the aggregates was measured at the beginning of the experiments and was practically zero. As the aggregates were stored in the warehouse, the moisture of the aggregates was considered constant during the experimental period.

Table 5.4. List of concrete characterization tests.

Test	State	Standard employed	Dimension of the specimen	Curing days
Aggregate packing density	Dry mix			-
Granular packing density	Dry and wet mix			-
Fresh density	Fresh concrete	EN 12350-6		-
Slump	Fresh concrete	EN 12350-2	Abrams cone: 20x10x30 cm	-
Air content in fresh state	Fresh concrete	EN 12350-7	8 l	-
Compressive strength	Hard concrete	EN 12390-3	Cube: 10x10x10 cm	7 and 28

5.2.5.2 Mixing process

A concrete mixer with a vertical axis and a central shaft (Heavy Duty Forced-Action Mixer XM 2/650) was used for the mixing process, following the procedure indicated below:

- Introduce aggregate constituents
- Dry mix for 60 seconds
- Measure the dry-packing density of the aggregate
- Add cement
- Dry mix for 60 seconds

- Measure the dry-packing density of the granular mixture
- Add 3/4 of the water
- Wet mix for 1 minute
- Add the rest of the water
- Wet mix for 4 minutes

Fig. 5.4. Concrete mixing.

5.2.5.3 Dry packing

The dry-packing density of the aggregates and cement was calculated from their bulk density (UNE-EN 1097-3 1999) using a tamping rod, and following the D-C compaction method procedure explained in chapter 4, a 4.79 l cylinder was used.

Fig. 5.5. Cylindrical mould.

5.2.5.4 Wet packing

The solid concentration of the concrete (solid concentration of the aggregates and aggregates + cement (θ_{a+c})) in the fresh state was calculated from the fresh density, according to the method proposed by (Wong & Kwan 2008). The equations were as follows:

$$V_s = \frac{M}{(\rho_w u_w + \rho_{a1} r_{a1} + \rho_{a2} r_{a2} + \rho_{a3} r_{a3} + \rho_c r_c)} \quad 5.2$$

$$V_w = u_w \cdot V_s \quad 5.3$$

$$\theta_{a+c} = \frac{V_s}{V} \quad 5.4$$

where, V_s is the solid volume; V is the container volume; ρ_w is the density of water; ρ_{a1}, ρ_{a2}, and ρ_{a3} are the densities of the different aggregate fractions; and, ρ_c is the density of the cement. In addition, r_{a1}, r_{a2}, and r_{a3} are the volumetric fractions of the aggregates to the total of solid materials, and u_w is the water-to-solid (W/S) ratio by volume.

The voids ratio (u) and the air ratio (u_a) may be also determined:

$$u = (V - V_s)/V_s \quad 5.5$$

$$u_a = (V - V_s - V_w)/V_s \quad 5.6$$

The voids content (ε) is filled by water and air therefore, the air content (ε_a) and water content (ε_w) may be calculated:

$$\varepsilon = 1 - \theta_{a+c} \quad 5.7$$

$$\varepsilon = \varepsilon_w + \varepsilon_a \quad 5.8$$

$$\varepsilon_w = \frac{V_w}{V} \quad 5.9$$

$$\varepsilon_a = \frac{V - V_s - V_w}{V} \quad 5.10$$

5.2.5.5 Fresh density

The bulk density of concrete is the mass of freshly mixed concrete required to fill the container of a unit volume. The bulk density of concrete reflects the capacity of concrete to function for structural support, water and solute movement, and durability. This method helps to calculate the yield of concrete per cubic meter.

The test was carried out according to the EN 12350-6 standard (UNE-EN 12350-6 2009). A cylindrical mould was filled with freshly mixed concrete and compacted using a tamping rod. The exterior surface of the cylinder was smartly tapped 10 to 15 times or until no large bubbles of air appeared on the surface of the compacted layer.

After consolidation of the concrete, the top surface was struck-off and finished smoothly with a flat cover plate, taking great care to level off the measure, so that it was filled to the brim. All excess concrete was then cleaned off the exterior of the mould that was filled with concrete, which was then weighed.

5.2.5.6 Slump

The concrete slump test measures the consistency of fresh concrete before it sets. It is performed to check the workability of freshly made concrete, and therefore the ease with which concrete flows. It can also be used as an indicator of an improperly mixed batch.

The test (UNE-EN 12350-2 2009) is popular, due to the simplicity of both the apparatus in use and the procedure that is followed. It was performed using a cone-shape metal mould known as a slump cone or Abrams cone, which is open at both ends and has handles attached to each side. It typically has internal diameters of 100 and 200 millimetres at the top and at the bottom, respectively, and a height of 305 millimetres. It was filled with fresh concrete in three stages and each layer was tamped 25 times with a 600 mm long bullet-nosed metal dowel. The mould was carefully lifted upwards in a vertical direction, so as not to disturb the concrete cone. The slump of the concrete was measured, by measuring the distance from the top of the slumped concrete to the level of the top of the slump cone.

Fig. 5.6. Slump test with Abrams cone.

5.2.5.7 Air content of fresh concrete

The air content of the concrete is fundamental, to guarantee the durability of the concrete under freezing and thawing conditions, in addition the workability is also improved in air-entrained concretes. However, strength can be affected due to the higher porosity of the hardened concrete.

From the methods that are available to determine the air content of concrete, the pressure gauge method in EN 12350-7 was selected (UNE-EN 12350-7 2010). The pressure test is based on Boyle's law, which states that the volume occupied by air is proportional to the applied pressure. The test consists of filling a sealed cylinder with a sample of concrete in three layers and tamping down each layer with a tamping rod. The exterior surface of the cylinder was smartly tapped 10 to 15 times or until no large bubbles of air appeared on the surface of the compacted layer. The cylinder was then filled to the brim, and the cover clamped over the cylinder. The assembly was filled with water that expelled any air through a valve. Having closed the valve, an air pump was used to raise the internal pressure. As the pressure was raised, the concrete became compressed and when the pressure reached a constant value, the air content reading was noted.

The concrete used in this test was discarded as water was added during the test.

Fig. 5.7. Air entrainment meter, 8 l capacity.

The air content was also indirectly determined from the fresh density of concrete and the specific density of all the concrete components, with the method proposed by (Wong & Kwan 2008) (see eq. 5.10). Air content errors of up to 1% by volume of concrete are reported for this method, as the additivity assumption can apply to the composition of the concrete mix and the free water content in the concrete mix is dependent on aggregate absorption levels. In addition, slight material density variations and errors for the mass of fresh concrete may have a significant effect on indirect measurements of the air content.

5.2.5.8 Compressive strength

Cubic specimens of 100x100x100 mm dimensions were manufactured to measure compression strengths as per standard UNE-EN 1015-3:2000 (UNE-EN 1015-3 2000). Three specimens were manufactured for each age (7 and 28 days). The specimens were demoulded after 24 hours, having been cured in the wet chamber until the date of testing.

Fig. 5.8. Casting of concrete specimens.

Fig. 5.9. Compressive strength test.

5.3 Determination of cement-paste content

The prediction of the cement paste content through the PPM models is not an easy task. Although, the aim of the PPM applied to concrete mix design is to predict the most densely packed granular mix, in order to reduce the voids, different approaches to obtaining the optimal proportion of the concrete components through PPM can be found in the literature.

The most widespread theoretical system is that the voids between packed aggregates will be filled by cement paste (Sunayana & Barai 2017; Pradhan *et al.* 2017) and an excess of paste will be needed to provide the required workability. Along these lines, a concrete mix design guide was proposed by ACI (ACI 211.6T 2014). In the ACI method, both the paste and the air volume are calculated from the void content of the optimal aggregate mix and the minimum volume of paste-to-air spacing that is selected from previously proposed values, depending on the angularity of aggregates and the slump (0 to 200mm of self-compacting concrete (SCC)). Thus, the minimum paste content will be higher for high angularity aggregates. The optimal aggregate mix is obtained with the power curve (0.45) adjustment and its PD is measured through the dry-rodded bulk density, according to ASTM C29. Aggregate shape is not therefore considered in the aggregate proportion, but it is considered for the required volume of paste. However, Fennis (Fennis 2009) considered both the PD of all the solid particles (including supplementary cementitious materials (SCMs) and cement) and the voids that are filled by water and admixtures, achieving the required workability by adding extra water. In contrast, Ng *et al.* (Ng *et al.* 2016) proposed the three-tier mix design method on the basis of the PD and the film thickness theories. According to their method, the paste (water, admixtures and particles lower than 0.75 µm) is firstly optimized with the wet-packing method, then the mortar (particles finer than 1.2 mm) and finally the concrete, as they considered that the voids left by the coarse aggregates will be filled with mortar and the voids between the fine aggregates will be filled with paste. They therefore focused on finding the

optimum film thickness of water, paste, and mortar, in order to meet the strength and workability requirements of the concrete, rather than simply focusing on maximizing the PD.

All these methods present their various advantages and limitations.

In the first approach, the highest PD aggregate mix (or the range of high PD aggregate mixes when a maximum is not clear) can be easily obtained by PPMs, reducing the experimental tests. From the results of the suitability of PPMs for the proportioning of NL and EAF aggregates obtained in chapter 4, the 3-parameter packing model was found to be the most accurate. However, once the volume voids to be filled by paste are known, some difficulties arise.

- The volume of voids (total volume minus the PD) will depend on the compaction method that is applied. The PD of the aggregate mixture is not the same when the aggregate is compacted simply by pouring or by vibrating and compression, nor when it is compacted by dry or wet methods (see chapter 4). Therefore, the optimal paste amount will not only depend on the concrete workability that is required, but will also depend on the compaction methods, to measure the PD of each aggregate fraction, and to manufacture the concrete specimens. Hence, experimental trials are required, to establish the paste volume to fill the voids and to provide the desired workability.
- W/C has to be selected by other methods such as standard recommendations and compressive strength models, which will mainly depend on the W/C ratio.

In an application of the second approach, Fennis developed the CIPM model (Compressible Interaction Packing Model), to accurately predict not only the PD of particles larger than 1 mm but also the PD of particles finer than 1 mm (including cementitious materials). Thus, once the solid proportion with the highest PD is known, only water needs to be added to fill the voids, and the excess quantity of water to be added will depend on a cement separation factor, related to the desired compressive strength and workability. However, this method presents the following drawbacks:

- The CIPM suitability has been only validated for a mono-size fraction of aggregates. The commercially available aggregate fractions should therefore be graded, in order to measure the PD of narrow granular size distributions, which is unfeasible on an industrial scale. Furthermore, wet methods must be performed, to obtain the PD of cementitious material and finer particles. In addition, the CIPM is a complex model which was calibrated for a specific admixture, so Fennis recommended calibration of the model for other admixtures. However, the difficulty of obtaining the maximum PD of all the solids of the concrete mixture in a simple and reliable way complicates the implementation of this approach.

- The strength prediction based on the cement spacing factor was only tested for a type of cement and admixtures and other types of binders will probably behave differently.

A third approach that has recently caught the attention of the research community is based on the premise that PD and layer thickness theories must be combined (Li *et al.* 2017; Ng *et al.* 2016; Ghasemi *et al.* 2019a), to optimize mixtures of cementitious materials. The reasoning is that an increased PD of a cementitious mixture will not always be beneficial for the total water demand. As the PD increases the required amount of water to fill the voids, the remaining voids will decrease, but the amount of water needed for the onset of flow will increase, because of the higher solid specific surface of the mix (Ghasemi *et al.* 2019a). Although most of these studies focused on mortars, Li *et al.* (Li & Kwan 2013) found a relationship between Water Film Thickness (WFT) and Paste Film Thickness (PFT) and concrete properties. They developed two graphics for concrete mix design showing concrete strength and concrete flows vs WFT and PFT. However, these graphs are probably affected by the properties of the concrete ingredients and the type of admixture and cannot be widely employed to design concrete mixtures. At present, research on this approach is focused on determining the relationship between the physical parameter of the solid particles and the thickness layer of the water, paste or mortar. Some of the drawbacks of this approach are as follows:

- Measurement of the WFT, PFT and Mortar Film Thickness (MFT) will depend on the measure of the Specific Surface Area (SSA) of particles and other assumptions, making it difficult to compare absolute results with those of other authors.
- The maximum PD of solid particles must be measured by experimental wet methods. This process is laborious as several mixtures with different water amounts must be performed, to find the minimum water required by the mix to be totally compacted.

From among the different approaches to determine the cement paste content, the first method was preferred, due to its simplicity. However, a combination of the first and the third approach could produce a suitable method for sustainable concrete mix design. In this thesis, different quantities of NL and EAF aggregate concrete have been analysed, to explore the relationship between aggregate PD and aggregate combination vs compressive strength and workability.

5.4 Effect of packing density on cement-paste compressive strength and workability

In this section the effect of cement PD or solid concentration, θ, on both the fresh and the hardened properties of the cement pastes was analysed. Table 5.5 shows the workability, compressive strength, and flexural strength of the cement pastes made with CEM II 42.5R. No admixtures were added to minimize the variables affecting the properties of the cement paste.

Table 5.5. Properties of the cement pastes at different W/C ratios.

V_w/V_c	W/C	ρ_{bulk} (kg/m³)	Solid concentration θ	Mini slump (mm)	Compressive strength 7d (MPa)	Flexural strength 7d (MPa)
1.42	0.47	1825	0.414	-	-	-
1.20	0.40	1915	0.457	249	-	-
1.10	0.37	1948	0.476	235	-	-
1.00	0.33	2017	0.505	176	60.8	12.7
0.90	0.30	2071	0.532	151	-	-
0.85	0.28	2066	0.538	138	66.1	10.7
0.80	0.27	2081	0.549	127	-	-
0.75	0.25	2069	0.553	107	67.0	13.7
0.70	0.23	2047	0.554	100	70.8	12.0
0.60	0.20	1679	0.467	100	52.1	9.2

As shown in Table 5.5 and Fig. 5.10, the higher PD corresponds to the highest compressive strength. This result was expected, since a higher PD of cement and binder meant fewer available voids to be filled by water, lowering the W/C ratios, and thereby enhancing compressive strength and durability (Ng *et al.* 2016). The results are in line with other research that assessed the PD and compressive strength of cement pastes made of CEM I 52.5R and silica fume (Van Der Putten *et al.* 2017).

Both parameters, solid concentration and compressive strength tend to increase when the W/C ratio decreases up to a W/C threshold value (0.20). Then, both parameters decrease. The PD of the cement paste will decrease, if the volume of water is insufficient to reach the saturation state of the mix, as the air will be entrapped in the remaining voids. The compressive strength may moreover be affected by two additional aspects:

- Insufficient water for complete hydration of the cement.
- Rough paste that it is difficult to place with an applied compaction method (compaction table), resulting in a specimen with significant voids.

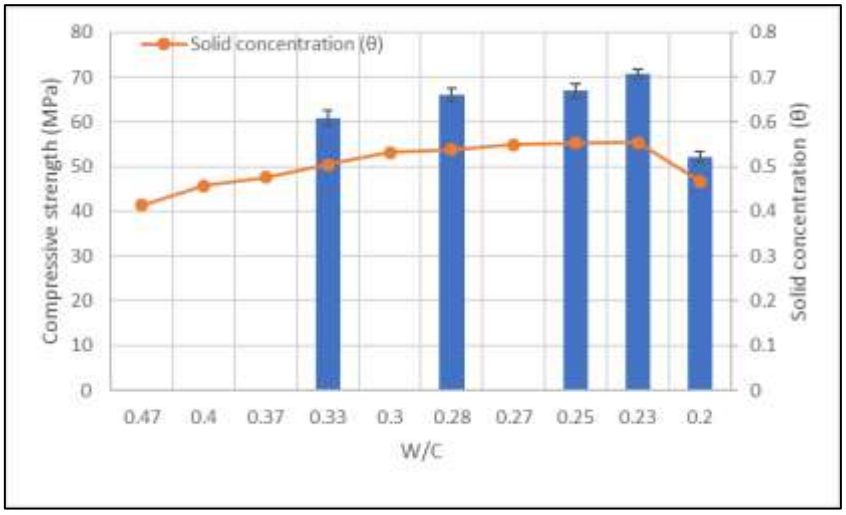

Fig. 5.10. Compressive strength of CEM II 42.5R.

Regarding the consistency of the cement paste, as the W/C ratio is reduced, the cone will decrease and the solid concentration will increase, as may be seen from Table 5.5. However, a point will be reached where the slump is minimum (since the average diameter obtained from the slurry will be the same as that of the mold), which is known as onset of flow paste. In this case, it will correspond with the minimum water demand of the mix to reach the onset of flow (Ghasemi *et al.* 2019b).

Ghasemi (Ghasemi *et al.* 2019b) proposed that the water content of a paste could be understood as three separate quantities, in order to control paste workability: the water that fills the voids between cement particles, the excess water that the mixture needs to reach the onset of flow, and a relative excess of available paste for increasing the relative slump (see Fig. 5.11).

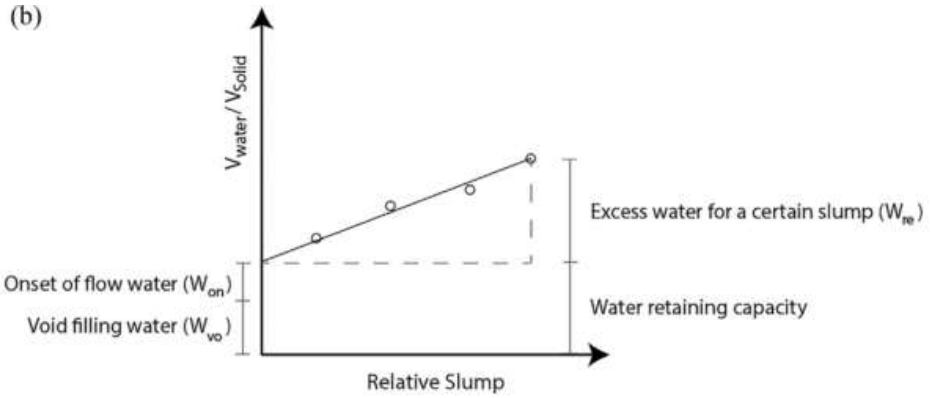

Fig. 5.11. Schematic diagram of the relationship between relative slump and the water-to-solid ratio (Ghasemi et al. 2019b).

Following this statement, the relative slump, calculated according to eq. 5.11 (Ghasemi *et al.* 2019b), was represented in Fig. 5.12 to analyse the effect of the Vw/Vc and solid concentration. According to Fig. 5.12, a Vw/Vc of 0.70 is needed for the paste to flow, coinciding with the maximum PD of cement (0.554). Therefore, at the point where the

paste exceeded the minimum water content at the onset of flow, both the water content and the PD showed a linear, but opposite trend with respect to the relative slump.

$$\Gamma = \left[\frac{d_1 + d_2}{2}/d_0\right]^2 - 1 \qquad 5.11$$

where d_1 and d_2 are the diameter of the spread of the cement paste, measured with callipers in two directions. d_0 is the diameter of the mould.

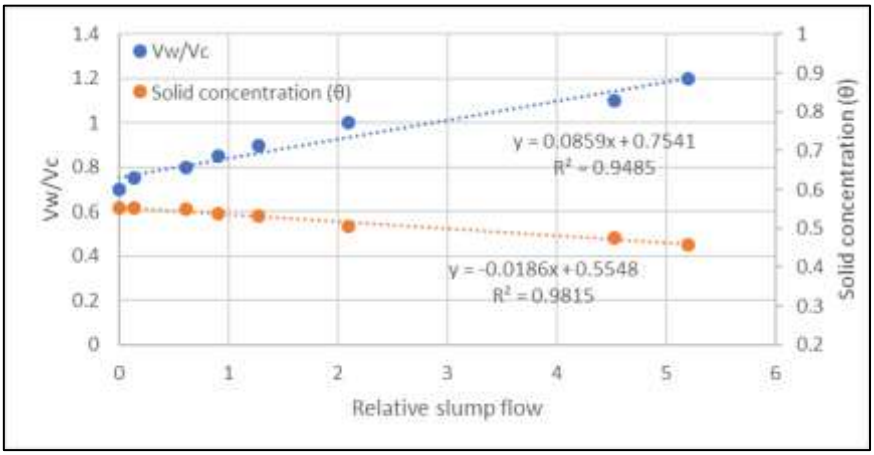

Fig. 5.12. Relationship between relative slump and Vw/Vc ratio and solid concentration.

The paste with the highest PD presents the maximum compressive strength, but its workability is null since it coincides with the onset of flow of the paste. Thus, at a given workability, the most compacted cement paste will require the greatest amount of water since its specific solid surface will be greater, and therefore the amount of excess water to increase flowability will also be greater.

5.5 Compressive strength and dry aggregate compacity of NL aggregate concretes

With the aim of understanding the effect of packing density on the properties of conventional concrete mixes and how to design the concrete mix through PD values, the analysis was firstly focused on the NL aggregate.

Four NL aggregate concretes with different aggregate proportions and therefore different dry-packing densities were designed, to analyse the influence on the compressive strength and the workability of the concrete. The cement content and the W/C ratio were kept constant (300 kg/m^3 and W/C=0.62), to assess the effect of aggregate PD for a given cement paste content, considering the cement as part of the paste that will fill the voids between the aggregates.

The aggregate mixes were established on the basis of the PD results obtained in chapter 4 (see Table 5.6):

- NL-(47:53):41→ Optimal aggregate mix according to the Fuller curve.
- NL-(60:40):50→ Experimentally optimal mixture for concrete mix design, considering the deviations from the experimental PD tests.
- NL-(50:50):50→ Mixture with the highest PD in the experimental test, in line with the predicted aggregate ratio according to the 3-parameter packing model.
- NL-(40:60):60→ Mixture with the highest experimental PD, if the second-degree polynomial curves are considered valid for the packing model.

The aggregate mix proportion and the experimental PD are detailed in Table 5.6. Fig. 5.13 shows the granular size distribution of the concrete mixes.

Table 5.6. Packing densities of each aggregate mixture in the dry state.

Mix ID	Experimental PD (%)			
	D-L	D-C	D-C26	D-C33
NL-(47:53):41	65	71.2	80.0	82.3
NL-(60:40):50	66.2	72.3	78.6	83.9
NL-(50:50):50	66.7	74.6	81.4	84.8
NL-(40:60):60	68.0	75.5	82.0	85.1

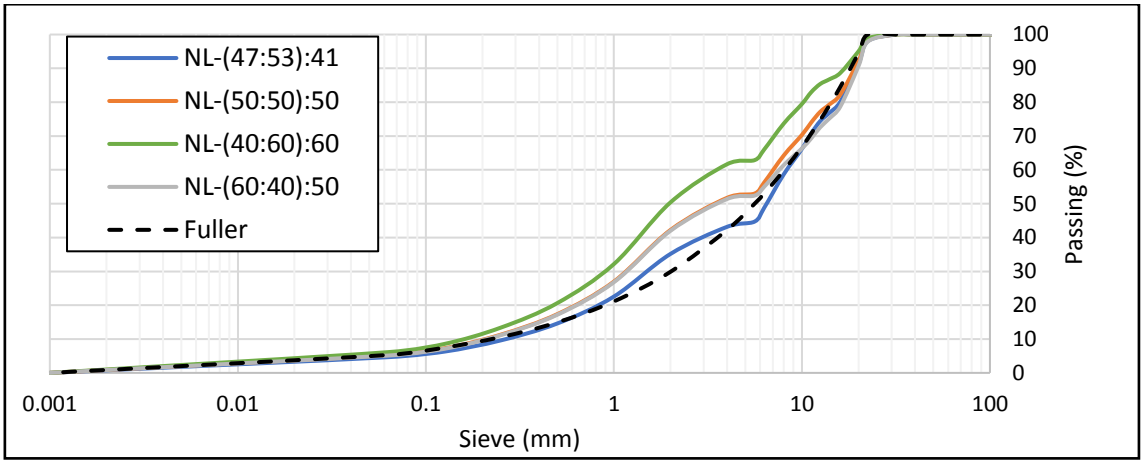

Fig. 5.13. Granular size distribution of concrete mixes.

The concretes were designed according to the volumetric method (see eq. 5.1). The air content was set at 2% at the starting point. W/C=0.5 was considered for the mix design, although additional water was added up until W/C=0.62 during the mixing process, to obtain workable mixtures. Hence, the cement content was reduced from 300 to 290 (kg/m^3) as a higher volume of concrete was obtained. Water content was adapted by considering aggregate absorption levels, as mentioned in the methodology.

The direct and the indirect measurement methods yielded significantly different levels of entrained air in the fresh concrete. Although the highly accurate direct (pressure) method resulted in a higher air content that was in line with the expected air content of concrete without an air-entrainment agent (0.6-2.5%) (de Larrard 1999), the less

accurate indirect method can also be used to compare the mixtures, as both follow the same trend.

Table 5.7. Concrete mixtures at W/C=0.62 and paste volume 27.5% (PV).

	NL-(47:53):41	NL-(60:40):50	NL-(50:50):50	NL-(40:60):60
Vol. (%) NL (0/4)	41	50	50	60
Vol. (%) NL (4/12)	31	20	25	24
Vol. (%) NL (12/22)	28	30	25	16
CEM II 42.5R (kg/m^3)	290	290	290	290
W_{free} (kg/m^3)	180	180	180	180
W_{abs} (kg/m^3)	10.6	11.1	10.7	11.3
V_{paste} (%)	27.5	27.5	27.5	27.5
Theoretical density (kg/m^3)	2373	2362	2375	2387
Properties				
Bulk density (kg/m^3)	2378	2349	2355	2370
Air content (direct method) (%)	1.9	2.1	2.3	2.4
Air content (indirect method) (%)	0.8	1.7	1.8	1.9
Solid concentration (%)	81.1	81.2	80.3	81.3
Aggregate concentration (%)	71.4	71.5	70.7	71.5
Slump (mm)	120	90	80	25
Compressive strength 7d (MPa)	32.1±1.18	32.4±0.98	32.8±1.0	31.6±0.51
Compressive strength 28d (MPa)	42.2±0.38	40.2±1.5	39.4±2.25	37.8±0.55
Aggregate SSA (cm^2/cm^3)	189	222	218	256
Total SSA (cm^2/ cm^3)	1650	1685	1675	1730

The PD of the concrete mixes varied between 3% and 6% for the same compaction process in the dry state (see Table 5.6). However, when the aggregate concentrations of the concrete mixes were calculated, hardly any differences were observed. One probable explanation is that the four concrete mixes were designed for the same volume of paste, without considering the quantity of voids remaining between the aggregates. Hence, even though on their own the aggregates were likely to achieve a higher PD, the volume of paste prevents this from happening. In other words, the paste would limit the compaction of the aggregates.

The results of the compressive strength and workability are presented in Fig. 5.14. Some photographs of the air content and the Abrams cones of the concrete produced in this stage were included in Fig. 5.15. In the same graph, the aggregate PD in the dry state and the aggregate concentration of the concrete mix were represented, to analyse their effects. The following observations may be noted:

- The compressive strength at 7-days remained constant for all the mixes under study, regardless of the aggregate proportion.

- The compressive strength at 28-days was slightly higher for the mixes with a lower PD in the dry state. The concrete mix with higher amounts of fine aggregate (NL-(40:60):60) presented lower compressive strengths (11% lower than the mix with the highest strength NL-(47:53):41). However, the four concrete mixes have very similar compressive strengths, so it cannot be guaranteed that the PD in the dry state has any effect on it (see Fig. 5.14).
  In view of the results, mixtures with higher aggregate volumes of larger size aggregate could have a greater effect on the compressive strength than the aggregate mixture with the highest PD in the dry state. The literature shows some evidence of the benefits of adding higher coarse-aggregate concentrations (Zarauskas *et al.* 2017), although an opposite effect also exists, in so far as larger aggregates tend to form weaker transition zones containing more micro-cracks. Therefore, one effective approach may be to use PPMs to find an optimal aggregate mix, always within the maximum packing plateau, which presents the highest volume of coarse aggregate.
- The workability of the four concrete mixes differed significantly. Although the concrete mix with the highest dry PD had the lowest workability, there was no evidence that workability was affected by the PD factor, as the aggregate concentration remained constant in all the concrete mixes. In addition, NL-(40:60):60 contained the largest amount of fine aggregate and consequently the highest specific surface area of aggregate, which leads us to expect that a larger amount of cement paste will be necessary to surround the aggregate, in order for the concrete mix to start flowing.

In Fig. 5.16 and Fig. 5.17, the workability of the mixes with aggregate sizes below 0.063 mm was compared, as many authors have claimed in the literature that such small sizes should be considered as part of the paste (ACI 211.6T 2014; Ng *et al.* 2016). The Spanish structural concrete instruction EHE-08 (EHE 2008) recommends a content of particles below 0.063 mm in concrete aggregate of 10% for limestone aggregates and <6% for other aggregates. As may be observed in Fig. 5.16, the slump decreased as the volume of particles lower than 0.063 mm increased, which indicates that workability is mainly affected by the fines content of the concrete mixture, by a given volume of paste, and by the W/C ratio. In Fig. 5.17, the relation is shown between workability, particle contents below 0.063 mm, and the aggregate SSA, revealing the same trend, and a good adjustment in the linear regression.

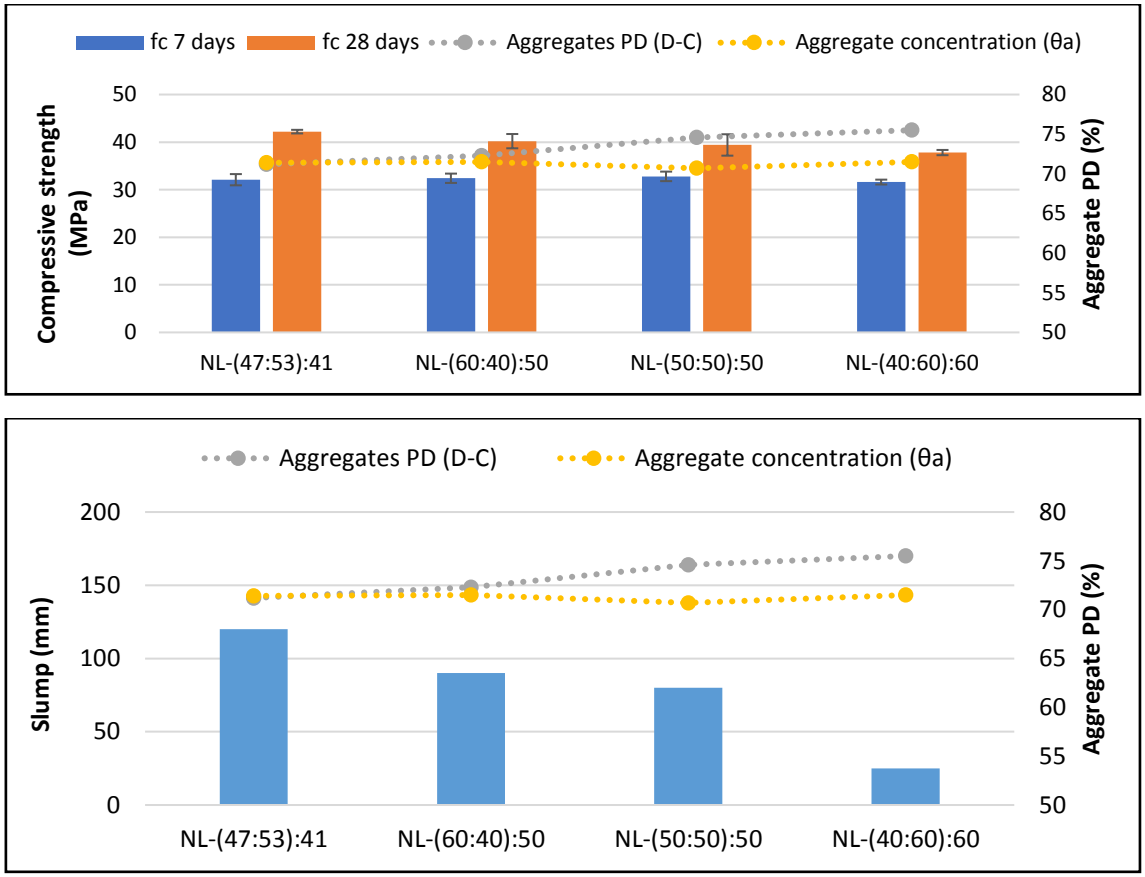

Fig. 5.14. PD effect on compressive strength and workability of concrete.

NL-(47:53):41

NL-(60:40):50

NL-(40:60):60

NL-(50:50):50

Fig. 5.15. Slump and air content of the concrete mixes.

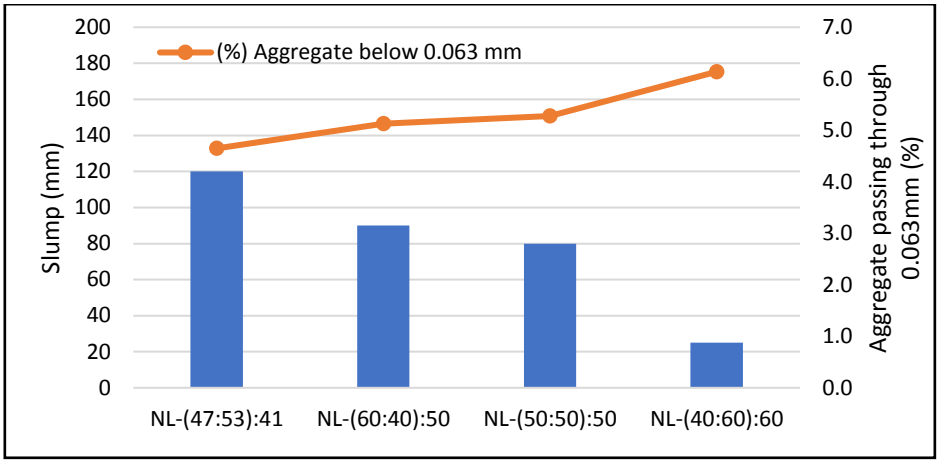

Fig. 5.16. Effect of the fine content on concrete workability.

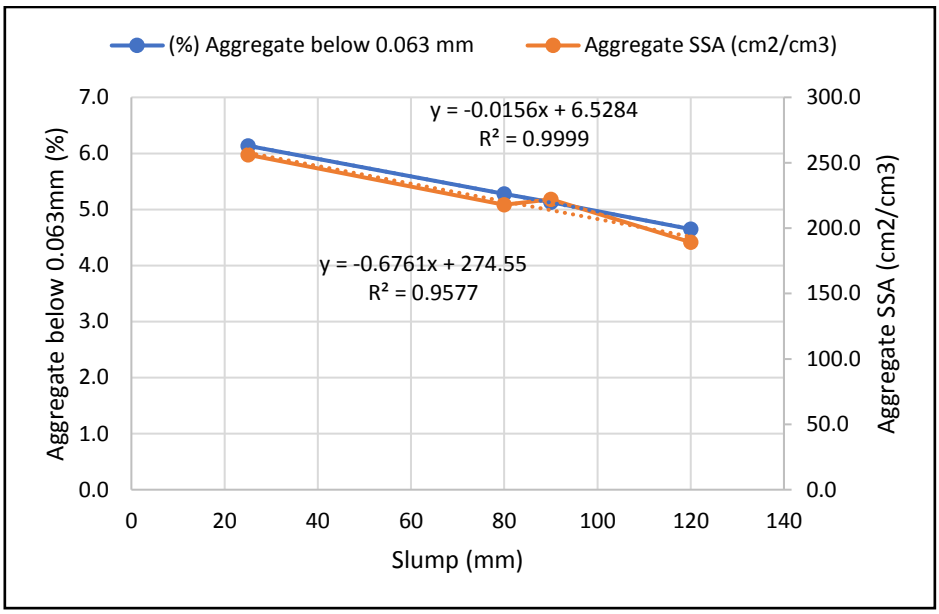

Fig. 5.17. Relationship between slump and fine aggregate content for a given paste volume.

Finally, with a view to assessing the usefulness of the dry PD measures for concrete mix design, the theoretical volume of paste required to fill the voids remaining between the aggregate and the excess paste added to achieve a PV of 27.5% for each concrete mix were detailed in Table 5.8.

The PD measured through the compacted method by rodding D-C was chosen as a starting point. Thus, the required paste content to fill the aggregate voids and the excess of cement paste was calculated as follows:

$$Cement\ paste\ to\ fill\ voids\ (\%) = 100 - PD_{D-C}(\%) - V_{air}(\%) \qquad 5.12$$

$$Excess\ of\ cement\ paste\ (\%) = 27.5 - rquired\ cement\ paste(\%) \qquad 5.13$$

As can be observed in Table 5.8, a larger volume of excess paste was added to the concrete mixes of lower workability. An addition that can be explained by following the

argument that Ghasemi (Ghasemi *et al.* 2019b) proposed when analysing mortar flow with PD and layer thickness theories. He divided the paste amount that was needed to reach the point of mortar flow onset into two components (see Fig. 5.18) in similar way as Fig. 5.11.

- Void filling paste, P_{vo}, obtained through the aggregate PD.
- Onset of flow paste, P_{on}, which depends on the aggregate morphology, SSA and surface-wetting.

The first component, P_{vo}, is easy to calculate through the PD of the particles and the PPMs, such that the aggregates with a higher PD will lead to a lower paste content. However, the second component depends on the aggregate morphology and the total SSA. Hence, although a mix with a higher content of fine aggregate will lead to a lower volume of voids to be filled with paste (high PD), an increased amount of water will be needed to cover the particle surfaces and to arrive at the onset of flow of the paste. The theory of filling the remaining voids between the compacted aggregates and adding a preset excess amount of cement paste, depending on the angularity factor of the aggregates and the desired workability, as recommend by the ACI method (ACI 211.6T 2014), is only valid for the concrete mixes with a specific granular size distribution. Other parameters combined with PD should be considered, to achieve the optimal aggregate proportion to concrete mix design.

Note also that the PD depends on the compaction process and the differences between the aggregates from the compaction process and the concrete compaction process must be considered.

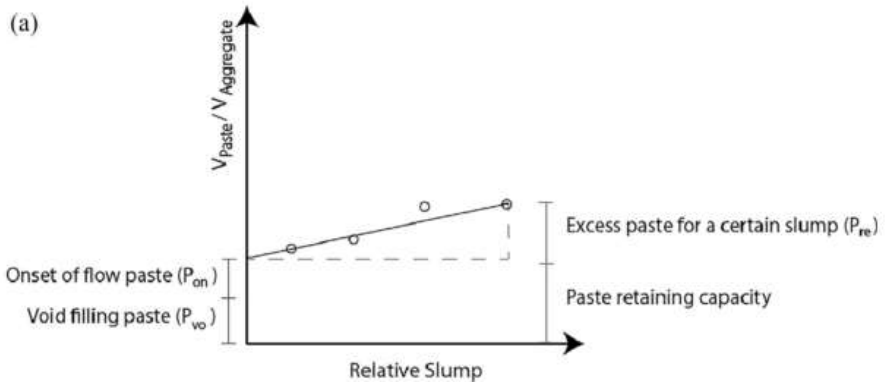

Fig. 5.18. Schematic diagram of the relationship between relative slump and paste to aggregate ratio (Ghasemi et al. 2019b).

Table 5.8. Cement paste required to achieve the highest concrete compacity.

	NL-(47:53):41	NL-(60:40):50	NL-(50:50):50	NL-(40:60):60
Cement paste to fill voids (%)	26.8	25.7	23.4	22.5
Excess of cement paste (%)	0.7	1.8	4.1	5
Increment of cement paste (%)	2.5	6.5	14.9	18.2

5.6 Funk and Dinger curves for cement-content reduction in concrete mix design

Although the ideal curves were not in agreement with the prediction of the highest PD aggregate EAF mix (see Chap 4, section 4.4.2), in this section, the behaviour of the concrete mixes designed with the Funk and Dinger curves will be discussed, in order to reduce the cement content. This method was selected, because it has the advantage of estimating not only the aggregate proportions, but also the overall concrete solids including the cement. Thus, the concrete mix for a given W/C ratio can be obtained automatically. In fact, in a recent paper (Yousuf *et al.* 2019), the authors observed that this method (also called the Alfred model) can reduce the cement content of concrete mixtures designed with the ACI method, while retaining remarkable performance levels.

Following Yousuf *et al.* (Yousuf *et al.* 2019), three *q* factors (0.31; 0.33 and 0.37) were selected, which will vary the amount of fines within the mix and that are close to the factor that is widely considered to predict the maximum PD. In this thesis, they determine the granular composition (including cement) of the concretes made with NL aggregates and those made with EAF aggregates. Thus, the paste volume of the concrete will be varied, to analyse its effects on the concrete properties.

The aggregate fractions commercially available in the Basque Country were directly used, without modifying their granulometry, for a better adjustment to the Funk and Dinger curves, so as to validate this model as a possible solution on both a laboratory and an industrial scale. The grading curves for the thee q values have previously been presented in chapter 4 (sections 4.4.1 and 4.4.2).

The concretes were designed following the known absolute volume method (see eq.5.1). The W/C ratio was fixed at 0.55. Air content was fixed at 2% and the total concrete volume was estimated at 1 m^3. The water content was adjusted by considering the water absorption of the aggregates, as detailed in the methodology. The volumetric proportions of each concrete-mix component are detailed in ***Table 4.29*** and ***Table 4.32***.

During the mixing process of the concretes, some difficulties arose over the manufacture of the concretes designed with a q factor of 0.37 for the two types of aggregate concrete. Due to the low quantity of cement, an inconsistent and very dry mixture was obtained, which could not be homogeneously placed within the moulds. Hence, the q factor was decreased until the cement content was sufficient to manufacture the specimens (q=0.33 for NL concretes and q=0.35 for EAF concretes).

In addition, due to the differences found in cement consumption, the manufacture of the EAF-$q_{0.31}$ was discarded, as a cement content of above 300 kg/m^3 was recorded for the EAF-$q_{0.33,}$ at some distance from the objectives of this thesis.

Table 5.9. Optimal granular proportion of NL aggregates by ideal curves.

Method	Volumetric proportion (%)			
	CEM II	NL (0/4)	NL (4/11)	NL (11/22)
Funk and Dinger $q_{0.29}$	13%	46%	24%	16%
Funk and Dinger $q_{0.31}$	11%	46%	26%	17%
Funk and Dinger $q_{0.33}$	10%	45%	27%	18%
Funk and Dinger $q_{0.37}$	7%	44%	29%	20%

Table 5.10. Optimal granular proportion of EAF aggregates by the ideal curves.

Method	Volumetric proportion (%)				
	CEM II	NL (0/2)	EAF (0/5)	EAF (4/11)	EAF (11/22)
Funk and Dinger $q_{0.31}$	14%	19%	29%	18%	21%
Funk and Dinger $q_{0.33}$	12%	18%	30%	19%	22%
Funk and Dinger $q_{0.35}$	11%	12%	32%	20%	24%
Funk and Dinger $q_{0.37}$	10%	15%	31%	20%	24%

Table 5.11. As can be observed in relation to the q parameters, the Funk and Dinger curve predictions pointed to a higher cement content for the EAF concrete. A prediction in line with the literature that has remarked upon the higher quantities of cement paste needed to fill the cavernous morphology of the EAF aggregates, in order to reach the required levels of concrete workability (Thomas et al. 2019; Santamaría et al. 2017; Santamaría et al. 2018; Arribas et al. 2015). However, the aggregate morphology is not considered in the Funk and Dinger curve. Consequently, the cement volume predicted for the model will depend only on the granular size distribution of the aggregates and the cement and the adjustment to the optimum curve.

The optimum granular proportion of NL aggregate concrete according to the curve has a higher fine aggregate content, below 0.063 mm, than the EAF aggregate concrete, possibly related to the higher amount of cement for EAF concrete mixtures.

Table 5.11. Concrete mixtures designed with the Funk and Dinger curves at W/C=0.55.

	NL-$q_{0.29}$	NL-$q_{0.31}$	NL-$q_{0.33}$	EAF-$q_{0.33}$	EAF-$q_{0.35}$
Vol. (%) NL (0/4)	53%	52%	50%		
Vol. (%) NL (4/12)	28%	29%	30%		
Vol. (%) NL (12/22)	19%	19%	20%		
Vol. (%) NL (0/2)				20%	14%
Vol. (%) EAF (0/5)				34%	36%
Vol. (%) EAF (4/12)				21%	23%
Vol. (%) EAF (12/22)				25%	27%
CEM II 42.5R (kg/m^3)	306	270	252	326	267
W_{free} (kg/m^3)	168	149	139	179	147
W_{abs} (kg/m^3)	11.1	11.6	11.8	31.2	37.2
V_{paste} (%)	27	23.9	22.3	29	23.6

	NL-$q_{0.29}$	NL-$q_{0.31}$	NL-$q_{0.33}$	EAF-$q_{0.33}$	EAF-$q_{0.35}$
Aggregate below 0.063 mm (%)	5.5	5.4	5.2	3.4	3.0
Properties					
Theoretical density (kg/m^3)	2379	2409	2423	2850	2961
Bulk density (kg/m^3)	2397	2385	2445	2864	2935
Hardened density (kg/m^3)	2487	2484	2412	2974	3049
Air content (direct method) (%)	-	-	-	2	2.5
Air content (indirect method) (%)	0.8	2.5	0.6	0.6	1.6
PD $_{D-C}$ aggregates (%)	75.8	75.4	75	74.3	74.9
PD $_{D-C}$ aggregates + cement (%)	76.1	76	76.4	76.3	76.5
Solid concentration (%)	82.2	82.7	85.3	81.4	83.7
Aggregate concentration (%)	71.8	73.8	76.8	70.3	74.7
Slump (mm)	40	10	10	160	15
Compressive strength 7d (MPa)	35.4±1.9	32.6±0.6	29.38±1.9	31.9±0.8	38.15±0.3
Compressive strength 28d (MPa)	42.79±0.6	38.54±0.7	40.66±2.5	45.36±1.8	44.17±3.4
Aggregate SSA (cm^2/cm^3)	227	223	214	154	142
Total SSA (cm^2/ cm^3)	1756	1539	1429	1815	1449

Some pictures of the Abrams cones of the concrete mixes are shown in Fig. 5.20 and Fig. 5.21.

The results of the compressive strength and workability are presented in Fig. 5.19. In the same graph, the aggregate PD in the dry state and the aggregate concentration in the concrete mix is represented, to analyse its effect on concrete with different volumes of paste. The following observations can be noted:

- The PD in the dry state was practically the same for both types of concrete (NL and EAF), as the variation of the q-factor mainly affected the content of fines below 1 mm, therefore the variations in the proportion of aggregates were almost negligible.
- The aggregate concentration decreased as the volume of cement paste increased (lower q-factors). Hence, the cement paste content was mainly responsible for the aggregate concentrations within the concrete mix.
- The 7-day compressive strength of the NL aggregate concretes decreased, as the cement content decreased. However, at 28 days the cement paste content was seen not to have such a relevant effect and the higher difference was found between the NL-$q_{0.29}$ and the NL-$q_{0.31}$ concrete mixes (approx. 10%).
- The 7-day compressive strength of the EAF aggregate concretes increased as the cement content decreased. However, at 28 days the compressive strength remained the same, regardless of the cement content in the concrete mix.
- The EAF aggregate concretes presented compressive strengths between 6 and 17% higher than the NL aggregate concrete.

- The slump of the NL aggregate concretes was practically zero, until a volume of paste of 27% was added (NL-$q_{0.31}$). In addition, higher dispersion in compressive strength was appreciated for the concrete with a low cement content (NL-$q_{0.33}$: 252 kg/m^3). As was expected, the concrete mix with the highest aggregate concentrations presented the lowest workability, but also contained the lowest amount of cement paste.
- The EAF aggregate concretes presented slumps with greater differences than the slumps of the NL aggregate concretes, as a higher amount of cement was needed to fit the concrete mix to the Funk and Dinger curve with a q factor of 0.33. A concrete volume of at least 23.6% was needed for a similar onset of flow to the NL aggregate concretes.

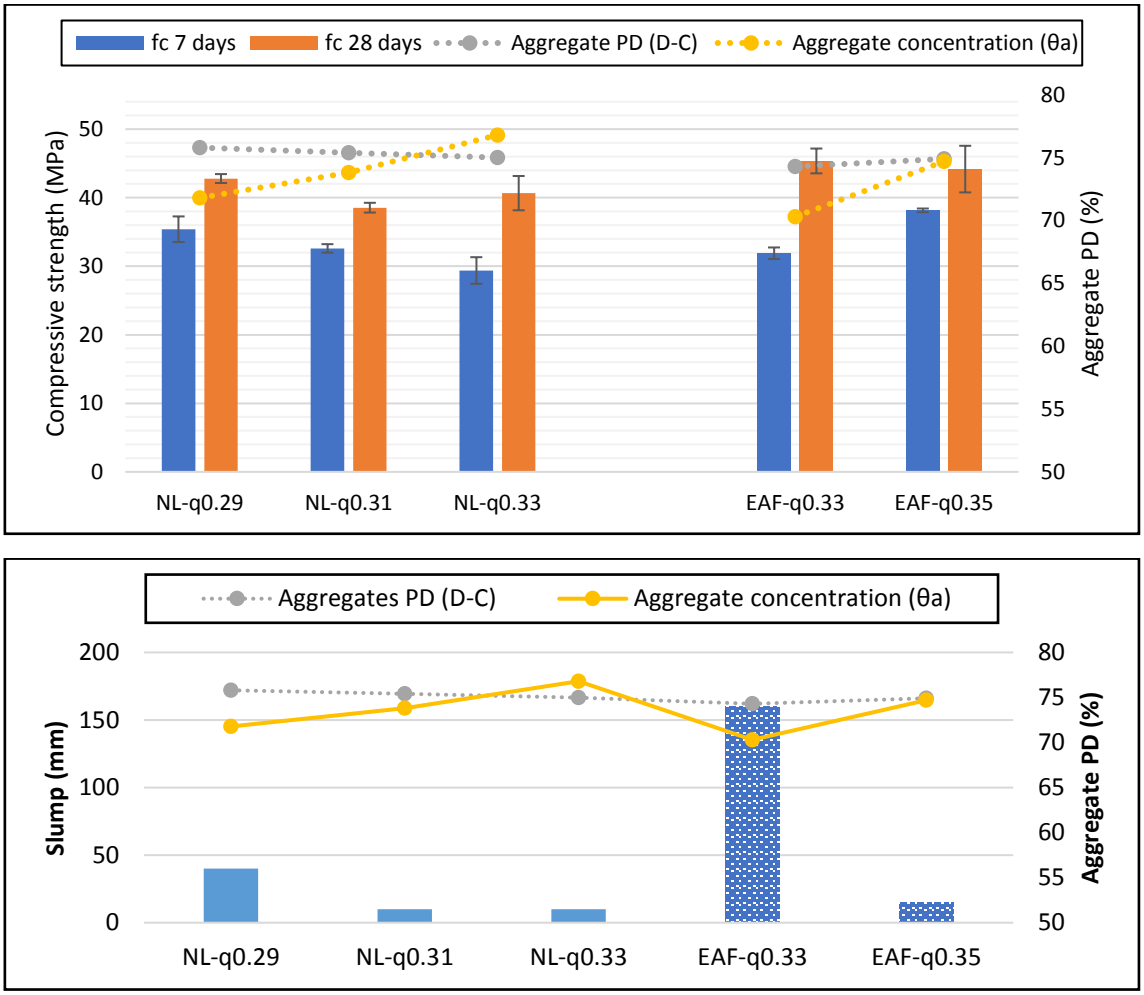

Fig. 5.19. PD effect on compressive strength and workability.

NL-$q_{0.29}$ NL-$q_{0.31}$ NL-$q_{0.33}$

Fig. 5.20. Slump of the NL aggregate concrete mixes.

EAF-$q_{0.31}$ EAF-$q_{0.35}$

Fig. 5.21. Slump of the EAF aggregate concrete mixes.

In view of the results, the Funk and Dinger method appears to be suitable for concrete mix design with reduced amounts of cement and good compressive strength. However, as can be observed in Table 4.29, the q parameter, used to obtain the mix with the lowest content of cement, will depend on the size distribution of the aggregates and their shape. A reduction of the q parameter from 0.37 to 0.35 was sufficient to manufacture the EAF aggregate concrete in the pre-set compaction conditions, but the q parameter must be reduced from 0.37 to 0.33, for the NL aggregate concrete. Therefore, additional concrete trials are recommended.

If the theoretical volume of paste required to fill the remaining voids between the aggregate is considered, according to both 5.12 and 5.13 (see Table 5.12), then the amount of paste to fill the voids of mix NL-$q_{0.33}$ will be insufficient. In addition, only 0.5% of excess volume paste was added to the EAF-$q_{0.35}$. Considering this fact, the PD measure of the dry aggregates with the D-C method could be an indicator of the minimum paste content to be added to the concrete mix and it could be combined with the selection of the optimal q factor. This simple test, which can be carried out on a reduced sample of aggregate, could help with the selection of the optimum q value, to reduce the amount of cement as much as possible without any need for concrete trials.

Table 5.12. Cement paste required to achieve the highest concrete compacity.

	NL-$q_{0.29}$	NL-$q_{0.31}$	NL-$q_{0.33}$	EAF-$q_{0.33}$	EAF-$q_{0.35}$
Volume of cement paste (%)	27	23.9	22.3	29	23.6
Cement paste to fill voids (%)	22.2	22.6	23	23.7	23.1
Excess of cement paste (%)	4.8	1.3	-0.7	5.3	0.5
Increment of cement paste (%)	17.8%	5.4%	-3.1%	18.3%	2.1%

5.7 Effect of paste content on different aggregate proportions

In this section, aggregate proportions were established, on the one hand, according to the experimental values obtained and, on the other hand, according to the CPM, in order to test the influence of aggregate dosages on the two types of concretes. In addition, two mixtures were prepared for each aggregate combination with two different paste contents (V_1: 23% and V_2: 28%), to analyse the possible variations in the properties of the concrete.

The selected aggregate volumetric proportion for both types of concrete, NL and EAF are shown in Table 5.13 and Table 5.14, respectively. As the experimental PD of the NL aggregates was similar to the CPM prediction, the aggregate proportion predicted by the 3-CPM model was selected. Although the absolute maximum PD was found for a volume proportion of 50% of NL (0/4), the aggregate mix with 40% of NL (0/4) was very close and considering that sand is more expensive than the other aggregates, an amount of 40% was selected.

Table 5.13. Volumetric proportions of NL aggregate concretes

Method	Mix ID	Volumetric proportion (%)		
		NL (0/4)	NL (4/11)	NL (11/22)
Experimental PD	E-NL	45	22	33
3-P model	3-P-NL	40	30	30

Table 5.14. Volumetric proportions of EAF aggregate concretes

Method	Mix ID	Volumetric proportion (%)			
		NL (0/2)	EAF (0/4)	EAF (4/11)	EAF (11/22)
Experimental PD	E-EAF	20	40	24	16
CPM	CPM-EAF	45	22	16.5	16.5

Fig. 5.22 shows the granular size distribution of each concrete mix and its corresponding Fuller curve. As can be observed, the EAF aggregate concrete mixes (E-EAF and CPM-EAF) are far from fitting the Fuller curve, which appears not to be a suitable technique for EAF aggregate proportioning.

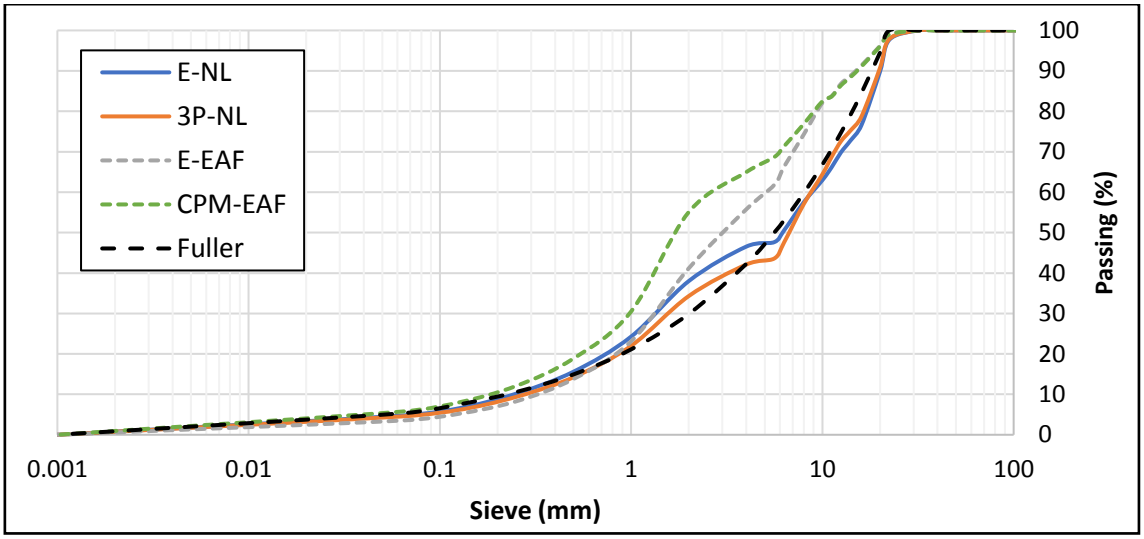

Fig. 5.22. Granular size distribution of aggregates for each concrete mix.

Table 5.15. Concrete mix design of NL aggregate concretes.

	E-NL-V_1	**E-NL-V_2**	**3-P-NL-V_1**	**3-P-NL-V_2**
Vol. (%) NL (0/4)	45%	45%	40%	40%
Vol. (%) NL (4/12)	22%	22%	30%	30%
Vol. (%) NL (12/22)	33%	33%	30%	30%
CEM II 42.5R (kg/m^3)	260	317	260	317
W_{free} (kg/m^3)	143	174	143	174
W_{abs} (kg/m^3)	10.6	9.9	11	10.3
V_{paste} (%)	23	28	23	28
Aggregate below 0.063 mm (%)	4.7	4.7	4.5	4.5
Properties				
Theoretical density (kg/m^3)	2418	2371	2416	2370
Bulk density (kg/m^3)	2426	2401	2441	2422
Hardened density (kg/m^3)	2509	2492	2526	2501
Air content (direct method) (%)				
Air content (indirect method) (%)	1.2	0.3	0.5	-0.6
PD $_{D\text{-}C}$ aggregates (%)	71.6	71.5	71.4	71.6
PD $_{D\text{-}C}$ aggregates + cement (%)	75.2	75.8	75.5	75.9
Solid concentration (%)	84.4	82	85	82.8
Aggregate concentration (%)	71.6	71.5	71.4	71.6
Slump (mm)	15	80	15	150
Compressive strength 7d (MPa)	39.1±0.45	36.9±0.23	38.5±1.66	35.7±
Compressive strength 28d (MPa)	48.7±0.29	45.5±0.97	42.3±0.92	39.8±0.4
Aggregate SSA (cm^2/cm^3)	197	197	185	185
Total SSA (cm^2/ cm^3)	1460	1794	1450	1784

Table 5.16. Concrete mix design of EAF aggregate concretes

	E-EAF-V_1	**E-EAF-V_2**	**CPM-EAF-V_1**	**CPM-EAF-V_2**
Vol. (%) EAF (0/5)	40%	40%	22%	22%
Vol. (%) EAF (4/12)	24%	24%	17%	17%
Vol. (%) EAF (12/22)	16%	16%	17%	17%
Vol. (%) NL (0/2)	20%	20%	45%	45%
CEM II 42.5R (kg/m^3)	260	317	260	317
W_{free} (kg/m^3)	143	174	143	174
W_{abs} (kg/m^3)	34.3	32	33.6	31.4
V_{paste} (%)	23	28	23	28
Aggregate below 0.063 mm (%)	25.6	30.5	27.3	32.0
Properties				
Theoretical density (kg/m^3)	23	28	23	28
Bulk density (kg/m^3)	2952	2870	2791	2719
Hardened density (kg/m^3)	2907	2850	2727	2702
Air content (direct method) (%)				
Air content (indirect method) (%)	2.3	1.5	3	1.4
PD $_{D\text{-}C}$ aggregates (%)	72	72.1	74	74
PD $_{D\text{-}C}$ aggregates + cement (%)	74.1	75	75.4	74.8
Solid concentration (%)	83.4	81	82.8	81
Aggregate concentration (%)	74.7	70.3	74.2	70.4
Slump (mm)	0	150	15	40
Compressive strength 7d (MPa)	39.5±1.22	40.3±0.58	37±1.08	34.2±0.1
Compressive strength 28d (MPa)	51.9±1.0	53.1±1.1	47±1.1	41.6±0.7
Aggregate SSA (cm^2/cm^3)	164	164	240	240
Total SSA (cm^2/ cm^3)	1431	1766	1499	1832

The results of compressive strength and workability are presented in Fig. 5.23 and Fig. 5.24. The following observations may be noted:

- The PD in the dry state was practically the same for the NL concrete mixes. However, the CPM-EAF mixes presented a slightly higher PD in the dry state than the E-EAF mixes, showing that the hierarchy applied to obtain the maximum experimental PD (see methodology chapter 4) will not always lead to the aggregate mix with the highest PD. It can also be seen that EAF aggregate mixtures have a slightly higher PD than NL.

  Additionally, the aggregate concentrations were practically the same for both aggregates when the same paste amount was added, and any differences will probably be due to the air content, rather than the aggregate PD.
- The increase in paste volume of the NL-aggregate concretes appeared not to have such a significant effect on compressive strength at 7-days and at 28-days. Although slightly higher values of compressive strength were obtained for

concretes with lower cement paste volumes and higher aggregate concentrations, differences of only 6-8% were found.

- Comparing the E-NL and the 3-P-NL mixtures with different aggregate proportions, no difference in compressive strength was observed after 7 days. However, the compressive strength of the E-NL mix at 28 days was ±15% higher than the 3-P-NL mix, regardless of the cement paste content.
- A similar behaviour was observed for the compressive strength of the EAF mixes. The increase in the paste volume appears not to have such a significant effect on the 7-day and the 28-day compressive strengths for the E-EAF mixes. However, the 28-day compressive strength of the CPM-EAF decreased by ±13% for the mixture with the highest volume of cement paste (CPM-EAF-V_2).
- Slightly higher compressive strengths were observed for the E-EAF mixes in a comparison of the E-EAF and the CPM-EAF mixtures with different aggregate proportions, after 7 days. In addition, the compressive strength at 28 days of the E-EAF mix was ±10% higher for the mixes with 23% cement paste (E-EAF-V_1 vs CPM-EAF- V_1), and up to 27% higher for the mix with 28% cement paste by volume (E-EAF-V_2 vs CPM-EAF- V_2).
- The EAF aggregate concretes presented compressive strengths that were between 6 and 16% higher than the NL aggregate concretes.
- The slump of all the concrete mixes designed with a cement paste volume of 23% was practically zero. However, as expected, when a higher paste content was added to the concrete, the evolution of workability depended on the proportion of aggregates and, especially, on the specific surface of the aggregates (see ***Fig. 5.25***). For a given volume of cement paste, the workability of the concrete mixes increased as the SSA of the aggregates decreased, because more paste was needed for the workability of the mix.

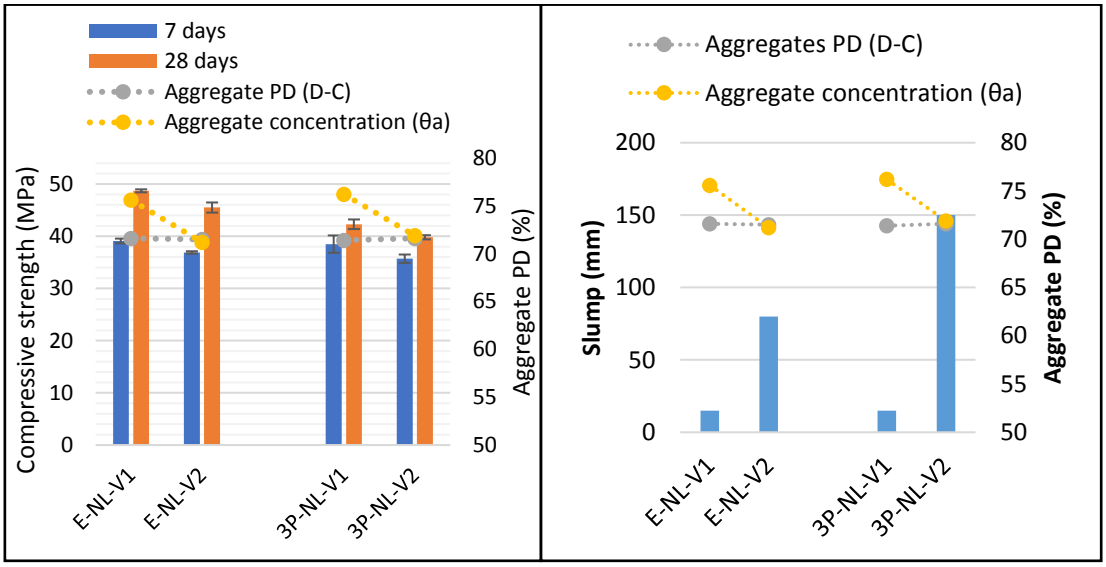

Fig. 5.23. PD effect on compressive strength and workability. NL aggregate concrete.

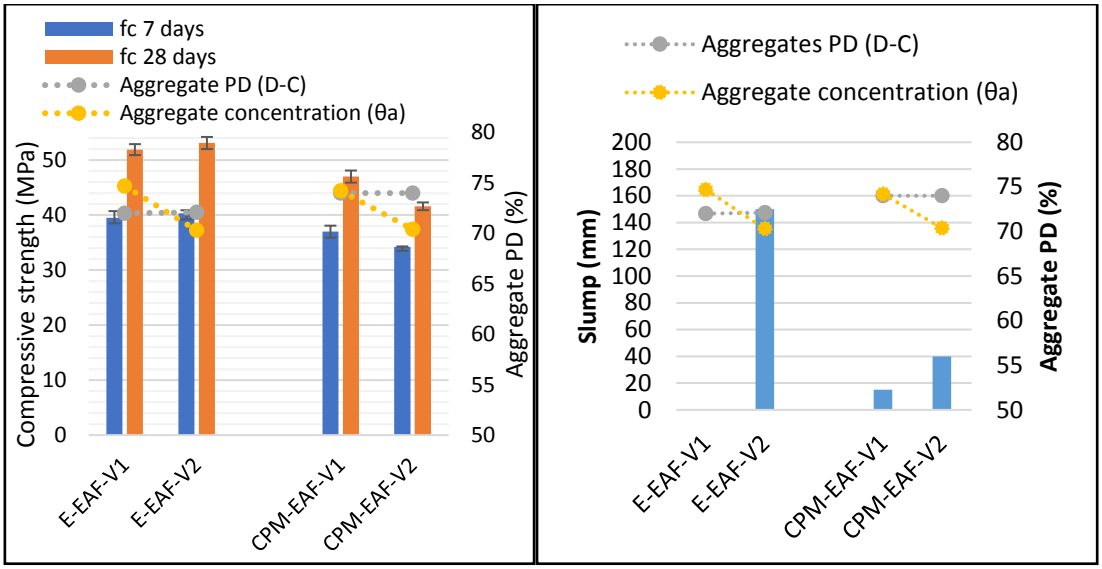

Fig. 5.24. PD effect on compressive strength and workability. EAF aggregate concretes.

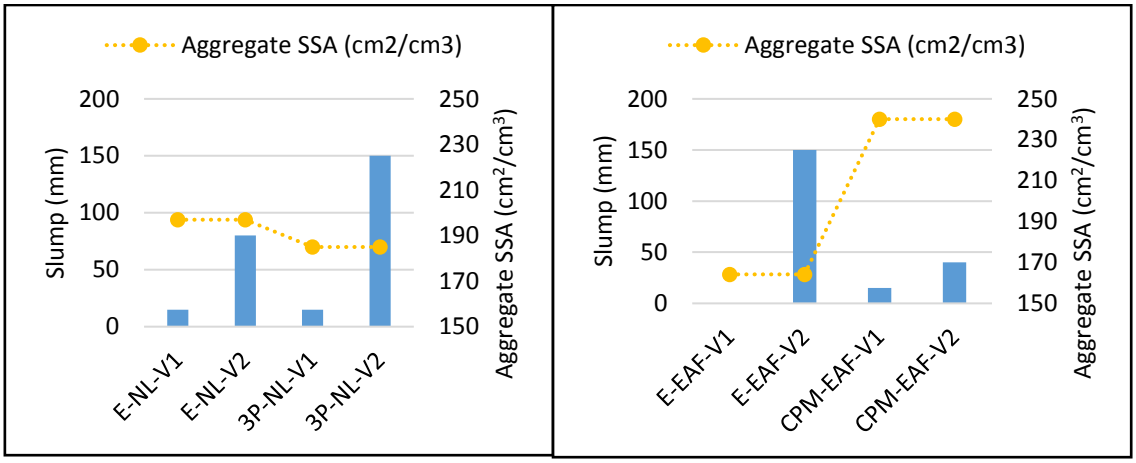

Fig. 5.25. Aggregate SSA effect on concrete workability.

The aggregate proportions for both types of concrete (NL and EAF) showed the highest compressive strength, according to the experimental results for aggregate PD. It should be noted that the experimental aggregate proportion was selected from a range of aggregate mixes with a similar PD, prioritising a higher content of the larger aggregates. Therefore, the same rule should be further applied and analysed to the Particle Packing Method (PPM) models, specially the 3-P model, as it yielded the most suitable predictions of the aggregate proportion with the highest PD, both for the NL and for the EAFS aggregate, in order to select the optimal aggregate proportion.

This way of selecting the optimal proportion of aggregates also has the advantage of reducing the specific solid surface of the aggregates, reducing the demand for cement paste in the concrete mix to obtain the desired workability.

Concerning the relationship between the coarse aggregate in the mix and the compressive strength conflicting views can be found in literature. Mehta and Monteiro (Mehta & Monteiro 2014) indicate that increase the maximum size of coarse aggregate can provide two opposites effects on the compressive strength of concrete. On the one hand, the concrete mix will require less water than those contained smaller aggregate. On the other hand, the transition zone between the larger aggregates and the matrix will be weaker containing more microcracks. Therefore, a compromising solution should be established. In addition, they indicate that there not exists a clear relationship between the porosity of concrete and the compressive strength as there also exist presence of micro-crack in the transition zone between coarse aggregate and the matrix. Conversely, Montoya et al. (Jimenez-Montoya et al. 2000) claim that a the larger the aggregate size the grater compressive strength.

A comparison of the concrete mixtures with lower amounts of cement (approx. 23% of PV), designed with the Funk and Dinger curves, and the concrete mixtures designed with maximum PD and PPMs, showed compressive strength increments of up to 20% for both the NL and the EAF concretes.

E-NL-V1

E-NL-V2

3-P-NL-V1

3-P-NL-V2

Fig. 5.26. Slump of NL aggregate concrete mixes

E-EAF-V1

E-EAF-V2

CPM-EAF-V1

CPM-EAF-V2

Fig. 5.27. Slump of EAF aggregate concrete mixes

5.8 Conclusions

As regards the cement pastes, the highest concentration of cement corresponds to the highest compressive strength. However, the mini slump at this point is minimal as there is insufficient water to lubricate the cement particles. In addition, the maximum PD of the cement corresponded to the minimum water demand of CEMII 42.5R for the mixture at its onset of flow. Therefore, the higher concentration of cementitious material appears suitable for the design of high-strength cement pastes.

Although it is believed that a high PD will have a positive influence on the concrete strength, the difference in the PD of the aggregates selected from the range of the most compacted aggregate mixtures in the dry state appeared irrelevant in the compressive strength at 7 and 28 days of the NL aggregate concrete mixtures. However, the higher content of coarse aggregates by volume in the concrete mix appeared to have a greater influence. Therefore, the optimal aggregate mix may be selected by using the PPMs and by maximising the coarse aggregate fraction within the maximum packing plateau. There was likewise no evidence that workability was affected by the dry PD of the aggregate.

However, the workability of the NL aggregate concrete was inversely proportional to the fines content of the aggregates and, consequently, to the SSA for a given volume of paste and W/C ratio. Therefore, a concrete mix with a higher compressive strength could be

provided, by maximizing the coarse aggregate fraction in terms of PPM and lowering the water demand to achieve the desired workability.

The prediction of the optimal cement paste content of concrete through the dry PD of the aggregates and a pre-determined volume of excess paste depending on the angularity factor of the aggregates is only valid for aggregate mixes designed with optimal grading curves and not for maximum packing aggregate mixes, as the SSA of the mix also influences the cement paste demand.

The Funk and Dinger curve appears to be a suitable option to formulate NL aggregate concrete and EAF aggregate concrete mixes with reduced amounts of cement without reducing the concrete compressive strength. However, the q parameter to obtain the concrete mix with minimum cement will depend on the aggregates and cement grading and its shape and should therefore be previously calibrated.

The proportion of aggregates for both types of concrete (NL and EAF) showed the highest compressive strength, according to the experimental aggregate PD results. Hence, the selection of the optimal aggregate mix within the range of the higher PD and the maximization of the coarse aggregate fraction appeared to be valid to obtain concrete with a low amount of cement and a high compressive strength. It should be highlighted that the granular size distribution of the EAF aggregate concretes with the highest compressive strength hardly fitted the optimal curves at all, so the discrete PPMs (specially the 3-particle packing model) therefore appear to be promising tools for the design of concretes with recovered aggregates that have a particular shape and surface texture.

Both the NL and the EAF aggregate concretes with reduced volumes of cement paste (cement amount of approx. 260 kg/m^3) can be produced without a lower compressive strength at 28 days, compared with concretes containing paste volumes of 28% (approx. 317 kg of cement per cubic meter).

All the concrete mixes that have been manufactured with a low cement content presented a dry consistency, according to the Spanish structural concrete instruction EHE-08 (EHE 2008). They will therefore require higher compaction energies when placed and their applicability will be limited to precast concrete or roller-compacted concrete. Further research will be needed to extend their range of application and to validate the design methods for concretes that incorporate admixtures for greater workability.

5.9 References

ACI (2002) ‘Standard Practice for Selecting Proportions for Normal , Heavyweight , and Mass Concrete (ACI 211.1-91)’, *ACI Manual of Concrete Practice, Part 1*, (Reapproved), pp. 1–38.

ACI 211.6T (2014) 'Aggregate suspension mixture proportioning method'.

Alhozaimy, A. M. (2009) 'Effect of absorption of limestone aggregates on strength and slump loss of concrete', *Cement and Concrete Composites*. Elsevier Ltd, 31(7), pp. 470–473. doi: 10.1016/j.cemconcomp.2009.04.010.

Arribas, I., Santamaría, A., Ruiz, E., Ortega-López, V. and Manso, J. M. (2015) 'Electric arc furnace slag and its use in hydraulic concrete', *Construction and Building Materials*. Elsevier Ltd, 90, pp. 68–79. doi: 10.1016/j.conbuildmat.2015.05.003.

Arribas, I., Vegas, I., San-José, J. T. and Manso, J. M. (2014) 'Durability Studies on Steelmaking Slag Concretes', *Materials and Design*, 63, pp. 168–176.

EHE (2008) 'Instrucción de Hormigón Estructural (EHE-08)'. Available at: https://www.fomento.gob.es/organos-colegiados/mas-organos-colegiados/comision-permanente-del-hormigon/cph/instrucciones/ehe-08-version-en-castellano.

Fennis, S. A. A. M. (2009) *Design of Ecological Concrete by Particle Packing Optimization*. Delf University of Tecnhology.

Fuente-Alonso, J. A., Ortega-López, V., Skaf, M., Aragón, Á. and San-José, J. T. (2017) 'Performance of fiber-reinforced EAF slag concrete for use in pavements', *Construction and Building Materials*, 149, pp. 629–638. doi: 10.1016/j.conbuildmat.2017.05.174.

Ghasemi, Y., Cwirzen, A. and Emborg, M. (2018) 'Estimation of specific surface area of particles based on size distribution curve', *Magazine of Concrete Research*, 70(10), pp. 533–540.

Ghasemi, Y., Emborg, M. and Cwirzen, A. (2019a) 'Effect of water film thickness on the flow in conventional mortars and concrete', *Materials and Structures*. Springer Netherlands, 52(3), pp. 1–15. doi: 10.1617/s11527-019-1362-9.

Ghasemi, Y., Emborg, M. and Cwirzen, A. (2019b) 'Exploring the relation between the flow of mortar and specific surface area of its constituents', *Construction and Building Materials*. Elsevier Ltd, 211, pp. 492–501. doi: 10.1016/j.conbuildmat.2019.03.260.

Ghasemi, Y., Rajczakowska, M. and Cwirzen, A. (2018) 'Shape-dependent calculation of specific surface area of aggregates versus X-ray microtomography', *Magazine of Concrete Research*. doi: 10.1680/jmacr.18.00121.

Jimenez-Montoya, P., García-Meseguer, A. and Morán Cabré, F. (2000) *El hormigón armado. 14ª edición basada en la EHE ajustada al Código Modelo y al Eurocódigo.* Ed. Gustavo Gil, S.A.

Lam, M. N. T., Jaritngam, S. and Le, D. H. (2018) 'EAF slag aggregate in roller-compacted concrete pavement: Effects of delay in compaction', *Sustainability*, 10(4), pp. 1–14. doi: 10.3390/su10041122.

de Larrard, F. (1999) *Concrete Mixture Proportioning*. E & FN SPON.

Li, J., Chen, Y. and Wan, C. (2017) 'A mix-design method for lightweight aggregate self-compacting concrete based on packing and mortar film thickness theories', *Construction and Building Materials*. Elsevier Ltd, 157, pp. 621–634. doi: 10.1016/j.conbuildmat.2017.09.141.

Li, L. G. and Kwan, A. K. H. (2013) 'Concrete mix design based on water film thickness and paste film thickness', *Cement and Concrete Composites*. Elsevier Ltd, 39, pp. 33–42. doi: 10.1016/j.cemconcomp.2013.03.021.

Manso, J., Hernández, D., Losanez, M. and Gonzalez, J. (2011) 'Design and Elaboration of Concrete Mixes Using Steelmaking Slags', *ACI Materials Journal*, 108, p. 673.

Mehta, P. and Monteiro, P. J. (2014) *Concrete microstructure, properties, and materials*. Ed. McGraw-Hill Education Book.

Ng, P., Kwan, A. K. H. and Li, L. G. (2016) 'Packing and film thickness theories for the mix design of high-performance concrete', *Zhejiang University-SCIENCE A (Applied Physics & Engineering) ISSN*, 17(10), pp. 759–781.

Pradhan, S., Kumar, S. and Barai, S. V (2017) 'Recycled aggregate concrete: Particle Packing Method (PPM) of mix design approach', *Construction and Building Materials*. Elsevier Ltd, 152, pp. 269–284. doi: 10.1016/j.conbuildmat.2017.06.171.

Van Der Putten, J., Dils, J., Minne, P., Boel, V. and De Schutter, G. (2017) 'Determination of packing profiles for the verification of the compressible packing model in case of UHPC pastes', *Materials and Structures/Materiaux et Constructions*. Springer Netherlands, 50(2), pp. 1–14. doi: 10.1617/s11527-016-0986-2.

San-José, J. T., Vegas, I., Arribas, I. and Marcos, I. (2014) 'The performance of steel-making slag concretes in the hardened state', *Materials and Design*, 60, pp. 612–619. doi: 10.1016/j.matdes.2014.04.030.

Santamaría, A., Orbe, A., José, J. T. S. and González, J. J. (2018) 'A study on the durability of structural concrete incorporating electric steelmaking slags', 161, pp. 94–111.

Santamaría, A., Orbe, A., Losañez, M. M., Skaf, M., Ortega-lopez, V. and González, J. J. (2017) 'Self-compacting concrete incorporating electric arc-furnace steelmaking slag as aggregate', 115, pp. 179–193.

Santamaría, A., Ortega-López, V., Skaf, M., Chica, J. A. and Manso, J. M. (2020) 'The study of properties and behavior of self compacting concrete containing Electric Arc Furnace Slag (EAFS) as aggregate', *Ain Shams Engineering Journal*, 11(xxxx), pp. 1–13. doi: 10.1016/j.asej.2019.10.001.

Sunayana, S. and Barai, S. V (2017) 'Recycled aggregate concrete incorporating fly ash : Comparative study on particle packing and conventional method', *Construction and Building Materials*. Elsevier Ltd, 156, pp. 376–386. doi: 10.1016/j.conbuildmat.2017.08.132.

Thomas, C., Rosales, J., Polanco, J. A. and Agrela, F. (2019) *7. Steel slags*, *New Trends in Eco-efficient and Recycled Concrete*. Elsevier Ltd. doi: 10.1016/B978-0-08-102480-5.00007-5.

UNE-EN 1015-3 (2000) 'Métodos de ensayo para morteros de albañilería. Parte 3: Determinación de la consistencia del mortero fresco por la mesa de sacudidas'.

UNE-EN 1097-3 (1999) 'Ensayos para determinar las propiedades mecánicas y físicas de los áridos. Parte 3: Determinación de la densidad aparente y la porosidad.'

UNE-EN 12350-2 (2009) 'Ensayos de hormigón fresco. Parte 2: Ensayo de asentamiento'.

UNE-EN 12350-6 (2009) 'Ensayos de hormigón fresco. Parte 6: Determinación de la densidad'.

UNE-EN 12350-7 (2010) 'Ensayos de hormigón fresco. Parte 7: Determinación del contenido de aire. Métodos de presión'.

Wong, H. H. C. and Kwan, A. K. H. (2008) 'Packing density of cementitious materials: Part 1-measurement using a wet packing method', *Materials and Structures/Materiaux et Constructions*, 41(4), pp. 689–701. doi: 10.1617/s11527-007-9274-5.

Yousuf, S., Sanchez, L. F. M. and Shammeh, S. A. (2019) 'The use of particle packing models (PPMs) to design structural low cement concrete as an alternative for construction industry', *Journal of Building Engineering*. Elsevier Ltd, 25(October 2018), p. 100815. doi: 10.1016/j.jobe.2019.100815.

Zarauskas, L., Skripkiunas, G. and Girskas, G. (2017) 'Influence of Aggregate Granulometry on Air Content in Concrete Mixture and Freezing-Thawing Resistance of Concrete', *Procedia Engineering*. Elsevier B.V., 172, pp. 1278–1285. doi: 10.1016/j.proeng.2017.02.153.